Preparation and Characterisation of New Efficient Conjugated Polymers for Photovoltaic Applications

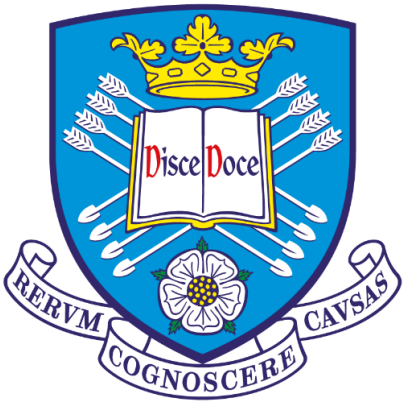

The University Of Sheffield.

A thesis submitted in partial fulfilment of the requirements for the degree of Doctor of Philosophy

By

Bader Mohammed A. Altayeb

Department of Chemistry

March 2019

Declaration

I hereby declare that this thesis is submitted for the degree of doctorate of philosophy (PhD) at the University of Sheffield, having been submitted for no other degree. It records the research carried out at the University of Sheffield from March 2015 to March 2019. It is entirely my original work, unless where referenced.

Signed …….

Date …….

Acknowledgements

First of all, I would like to take this opportunity to express my deepest appreciation and sincere gratitude to my supervisor Dr Ahmed Iraqi, for his continuous guidance, advices and support, throughout my PhD study and his help for the write up of this thesis.

Furthermore, I would also like to acknowledge and thank all my laboratory colleagues and staff in Chemistry department for crucial role in easing things for me in the department, especially Heather Grievson, Simon Thorpe, Rob Hanson, Nick Smith and the others.

All thanks go to my mother for her support and payers for me. I also would not forget to thank my brothers and sisters for their support.

Special thanks go to my beloved wife and daughter for their support and continuous encouragements throughout the past challenging years of my PhD study. I would not have done it without them in my life.

Abstract

Strong demand for clean, renewable sources of energy has led researchers to examine every area for alternative renewable resources. Solar energy is the only renewable source that has the potential to satisfy the world's large and increasing energy demand. The Earth receives enough solar irradiation in one hour to fulfil the world's energy needs for one year. Commercially available solar cells based on inorganic materials dominate photovoltaic (PV) technologies. However, these have drawbacks such as high production costs and environmental concerns. Therefore, organic photovoltaic cells (OPVs) have shown promising potential as they show advantages over their inorganic counterparts. These include: high absorption coefficients; better operation at lower light-intensity levels; flexible substrates; and low-cost production. Bulk heterojunction (BHJ) architecture has been frequently applied to fabricate the active layer in polymer-based solar devices. Previous studies have shown that BHJ solar cells fabricated from polymers that consist of an electron-rich donor unit and an electron-deficient acceptor monomer in an alternate donor-acceptor (D-A) arrangement result in a higher power conversion efficiency (PCE). Therefore, designing conjugated polymers that consist of alternating donor-acceptor units is a promising strategy to produce high-efficiency BHJ solar cells.

In this study, we report the synthesis of a series of conjugated polymers that consist of alternating difluoro-quinoxaline or thieno[3,4-c]pyrrole-4,6-dione (TPD) or 2,1,3-benzothiadiazole-5,6-dicarboxylic imide (BDI) units as electron acceptors with two well-known electron-donor segments. These were phenanthro[9,10-b]quinoxaline and 9,10-dialkoxy-phenanthreneunits, which were prepared *via* Suzuki cross-coupling using palladium-catalysed cross-coupling reactions. The synthesis yielded a family of conjugated polymers with low optical band gaps. The purity and structure of each of the monomers were confirmed by ^{1}H-NMR, ^{13}C-NMR, elemental analysis and mass spectrometry. All synthesised polymers in this project were purified *via* Soxhlet extraction and their structures were verified by elemental analysis and ^{1}H-NMR spectroscopy. The optical, electrochemical and thermal properties of all the resulting conjugated polymers were determined by various techniques such as ultraviolet-visible spectroscopy (UV-Vis), thermal gravimetric analysis (TGA), cyclic voltammetry (CV) and X-ray diffraction (XRD), to examine their suitability

for application in OPV devices. All synthesised polymers exhibited optical band gaps ranging between 1.68 eV and 2.05 eV.

Table of contents

Declaration i
Acknowledgements ii
Abstract iii
Table of contents v
List of Figures x
List of Schemes xii
List of Tables xiv
List of Equations xv
List of abbreviations xvi
Chapter 1: Introduction 1
1. Introduction 2
1.1 Photovoltaic Cells 2
1.2. Background and Development 3
1.3. Principle of Operation of Organic Solar Cells 5
1.4. Architecture of Organic Solar Cells 7
1.4.1. Single Layer Organic Photovoltaic Cells 7
1.4.2. Bilayer Organic Photovoltaic Cells 8
1.4.3. Bulk Heterojunction Photovoltaic Cells 9
1.5. Characteristics of organic photovoltaic cells 10
1.5.1. Open-Circuit Voltage (V_{oc}) 11
1.5.2. Short-Circuit Current (J_{sc}) 11
1.5.3. Fill Factor (FF) 12
1.6. Conjugated Polymers 12
1.6.1. Background 12
1.7. The Electronic Structure of Conjugated Polymers 14
1.8. The Band Gap of Conjugated Polymers 15
1.9. Engineering of Band Gap in Conjugated Polymers 17
1.10. Solubility of Conjugated Polymers 19
1.11. Synthesis of Conjugated Polymers 20
1.11.1. Preparation Methods of Conjugated Polymers 20
1.11.1.1. Suzuki Cross-Coupling 20
1.11.1.2. Stille Cross-Coupling 22
1.12. Materials used in organic solar cells 23

1.12.1. Phenanthrene-based Conjugated Polymers 23
1.12.2. Fullerenes (Electron-Accepting Materials) 28
1.13. Project Aims 31
1.14. References 33
Chapter 2: Phenanthrene-Difluoro-Quinoxaline, Donor-Acceptor Polymers for OPV applications 40
Abstract 41
2.1. Introduction 42
2.2. Results and Discussion 45
2.2.1. Synthesis of Monomers for the Quinoxaline-based Copolymers P1, P2, P3 and P4 45
2.2.1.1. Synthesis of Electron Acceptor Monomers (9) and (21) 48
2.2.1.2 Synthesis of the Electron Donor Monomers (16) and (19): 60
2.2.2. Synthesis of Fluorinated Quinoxaline-based Alternating Copolymers P1, P2, P3 and P4 . 71
2.2.3. Analysis by UV-Visible absorption spectroscopy 74
2.2.4. Analysis by Cyclic Voltammetry 76
2.2.5. Study of Thermal Properties 79
2.2.6. Studies of the Molecular Structures 80
2.3. Conclusion 82
2.4. References 84
Chapter 3: Phenanthrene-Thieno[3,4-C]Pyrrole-4,6-Dione Based Polymers for OPV applications 87
Abstract 88
3.1. Introduction 89
3.2. Results and Discussion 92
3.2.1. Synthesis of Monomers for the Thienopyrroledione- based Copolymers P5, P6, P7 and P8 92
3.2.1.1. Synthesis of the electron acceptor monomers (31) and (33). 95
3.2.2. Synthesis of the series of TPD-based-alternating copolymers P5, P6, P7 and P8 100
3.2.3. Analysis by UV-Visible absorption spectroscopy 102
3.2.4. Analysis by Cyclic Voltammetry 106
3.2.5. Study of Thermal Properties 108
3.2.6. Studies of the Polymers' Molecular Structures 109
3.3. Conclusion 111
3.4. References 113
Chapter 4: Phenanthrene-2,1,3-Benzothiadiazole-5,6-Dicarboxylic Imide, Donor-Acceptor Polymers for OPV applications 115

Abstract 116
4.1 Introduction 117
4.2. Results and Discussion 121
4.2.1. Synthesis of Monomers for the BDI based Copolymers P9 and P10 121
4.2.2. Synthesis of BDI-based alternating copolymers P9 and P10 122
4.2.3. UV-Visible absorption spectroscopy analysis 123
4.2.4. Cyclic Voltammetry analysis 126
4.2.5. Study of Thermal Properties 128
4.2.6. Studies of Molecular Structure 129
4.3. Conclusion 131
4.4. References 132
Chapter 5: Conclusions and Future Work 134
5.1. Conclusions 135
5.2. Future work 137
Chapter 6: Experimental 139
6.1. Materials 140
6.2. Analytical Techniques Used for Measurements 140
6.2.1. Nuclear magnetic resonance spectra (NMR) 140
6.2.2. Thin layer chromatography (TLC) 140
6.2.3. Elemental analysis 140
6.2.4. Melting point 140
6.2.5. Gel permeation chromatography analysis 141
6.2.6. Cyclic voltammetry 141
6.2.7. UV-Visible absorption spectroscopy analysis 141
6.2.8. Thermogravimetric analysis 141
6.2.9. Powder X-ray diffraction analysis 142
6.3. Preparation of Monomers 142
6.3.1. Synthesis of 1,4-dimethylpiperazine-2,3-dione (1)[1] 142
6.3.2. Synthesis of 1-Bromo-3-(octyloxy) benzene (2)[2] 142
6.3.3. Synthesis of 1,2-bis(3-(octyloxy)phenyl)ethane-1,2-dione (3)[3] 143
6.3.4. Synthesis of 5,6-difluoro[c][1,2,5]thiadiazole (4)[4] 144
6.3.5. Synthesis of 5,6-difluoro-4,7-diiodo-benzo[1,2,5]thiadiazole (5)[4] 145
6.3.6. Synthesis of 5,6-difluoro-4,7-bis(4,2-thienyl)-2,1,3-benzothaidiazole (6)[5] 145
6.3.7. Synthesis of 1,2-diamino-3,6-di(2-thienyl)-4,5-difluorobenzene (7) and 2,3-Bis(3-(octyloxy)phenyl)-5,8-di(2-thienyl)-6,7-difluoroquinoxaline (8)[3,6] 146

6.3.8. Synthesis of 2,3-bis(3-(octyloxy)phenyl)-6,7-difluoro-5,8-bis(5-bromo-2-thienyl)quinoxaline (9)[3] 147
6.3.9. Synthesis of 2,7-dibromophenanthrene-9,10-dione (10)[7] 148
6.3.10. Synthesis of bromo-2-hexyldecane (11)[8] 149
6.3.11. Synthesis of 1,2 bis-(2-hexyldecyloxy) benzene (12)[9] 150
6.3.12. Synthesis of 1,2-dinitro-4,5-bis(2-hexyldecyloxy)benzene (13)[9] 150
6.3.13. Synthesis of 1,2-diamine-4,5-bis(2-hexyldecyloxy)benzene (14)[10] 151
6.3.14. Synthesis of 2,7-dibromo-11,12-bis-(2-hexyldecyloxy)-phenanthro[9,10-b]quinoxaline(15)[11] 152
6.3.15. Synthesis of 2,7- bis-(4,4,5,5-tetramethyl-1,3,2-dioxaborolan-2-yl)-11,12-bis-(2-hexyldecyloxy)-phenanthro[9,10-b]quinoxaline (16)[12] 153
6.3.16. Synthesis of 5-bromomethylundecane (17)[8] 154
6.3.17. Synthesis of 2,7-dibromo-9,10-bis-(2-butyl-octyloxy) phenanthrene (18)[13] 154
6.3.18. Synthesis of 2,7- bis-(4,4,5,5-tetramethyl-1,3,2-dioxaborolan-2-yl)-9,10-bis-(2-butyl-octyloxy)-phenanthrene (19)[12] 155
6.3.19. Synthesis of 2,3-Bis(3-(octyloxy)phenyl)-6,7-difluoro-5,8-bis((2,2′-bithiophene)-5-yl)quinoxaline (20)[5] 156
6.3.20. Synthesis of 2,3-bis(3-(octyloxy)phenyl)-6,7-difluoro-5,8-bis(5-bromo-(2,2'-bithiophene)-5-yl)quinoxaline (21)[3] 157
6.3.21. Synthesis of 1-bromo-3,7-dimethyloctane (22)[8] 158
6.3.22. Synthesis of N-(3,7-dimethyloctyl)phthalimide (23)[14] 158
6.3.23. Synthesis of 3,7-dimethyloctan-1-amine (24)[14] 159
6.3.24. Synthesis of 3-ethyl-4-methyl-2-aminothiophene-3,4-dicarboxylate (25)[15] 160
6.3.25. Synthesis of thiophene-3,4-dicarboxylic acid (26)[16] 161
6.3.26. Synthesis of 2,5-dibromothiophene-3,4-dicarboxylic acid (27)[17] 162
6.3.27. Synthesis of 4,6-dibromothieno[3,4-c]furan-1,3-dione (28)[18] 162
6.3.28. Synthesis of 1,3-dibromo-5-(3,7-dimethyloctyl)-4H-thieno[3,4-c]pyrrole-4,6(5H)-dione (29)[19] 163
6.3.29. Synthesis of 1,3-bis(thiophen-2-yl)-5-(3,7-dimethyloctyl)-4H-thieno[3,4-c]pyrrole-4,6(5H)-dione (30)[20,21] 164
6.3.30. Synthesis of 1,3-bis(5-bromo-thiophen-2-yl)-5-(3,7-dimethyloctyl)-4H-thieno[3,4-c]pyrrole-4,6(5H)-dione (31)[20] 165
6.3.31. Synthesis of 1,3-bis([2,2'-bithiophen]-5-yl)-5-(3,7-dimethyloctyl)-4H-thieno[3,4-c]pyrrole-4,6(5H)-dione (32)[20] 166
6.3.32. Synthesis of 1,3-bis(5'-bromo-[2,2'-bithiophen]-5-yl)-5-(3,7-dimethyloctyl)-4H-thieno[3,4-c]pyrrole-4,6(5H)-dione (33)[20] 167
6.3.33. 4,7-di(5-bromo-thien-2-yl)-2,1,3-benzothiadiazole-5,6-N-octyl-dicarboxylic imide (A) 168
6.4. Preparation of the Polymers 168

6.4.1. Poly [11,12-bis-(2-hexyl-decyloxy)-phenanthro[9,10-b]quinoxaline-(2,7-di-yl)-alt-(2,3-Bis(3-(octyloxy)phenyl)-6,7-difluoro-5,8-bis(2-thienyl)quinoxaline)-5,5-(di-yl)] (P1)[22] 168

6.4.2. Poly[9,10-bis-(2-butyl-octyloxy)-2,7-phenanthrene-alt-[2,3-Bis(3-(octyloxy)phenyl)-6,7-difluoro-5,8-bis(2-thienyl)quinoxaline]-5,5-(di-yl)] (P2)[22] 169

6.4.3. Poly[[11,12-bis-(2-hexyl-decyloxy)-phenanthro[9,10-b]quinoxaline]- (2,7-di-yl)-alt-[2,3-Bis(3-(octyloxy)phenyl)-6,7-difluoro-5,8-bis-(2,2'-bithiophene)-5-yl)quinoxaline]-5,5-(di-yl)] (P3)[22] 170

6.4.4. Poly[9,10-bis-(2-butyl-octyloxy)-2,7-phenanthrene-alt-[2,3-Bis(3-(octyloxy)phenyl)-6,7-difluoro-5,8-bis-(2,2'-bithiophene)-5-yl)quinoxaline]-5,5-(di-yl)] (P4)[22] 170

6.4.5. Poly[[11,12-bis-(2-hexyl-decyloxy)-phenanthro[9,10-b]quinoxaline]- (2,7-di-yl)-alt-[1,3-bis(thiophen-2-yl)-5-(3,7-dimethyloctyl)-4H-thieno[3,4-c]pyrrole-4,6(5H)-dione]-5,5-(di-yl)] (P5)[22] 171

6.4.6. Poly[9,10-bis(2-butyl-octyloxy)-2,7-phenanthrene-alt-[1,3-bis(thiophen-2-yl)-5-(3,7-dimethyloctyl)-4H-thieno[3,4-c]pyrrole-4,6(5H)-dione]-5,5-(di-yl)] (P6)[22] 171

6.4.7. Poly[[11,12-bis-(2-hexyl-decyloxy)-phenanthro[9,10-b]quinoxaline]- (2,7-di-yl)-alt-[1,3-bis([2,2'-bithiophen]-5-yl)-5-(3,7-dimethyloctyl)-4H-thieno[3,4-c]pyrrole-4,6(5H)-dione]-5,5-(di-yl)] (P7)[22] 172

6.4.8. Poly[9,10-bis(2-butyl-octyloxy)-2,7-phenanthrene-alt-[1,3-bis([2,2'-bithiophen]-5-yl)-5-(3,7-dimethyloctyl)-4H-thieno[3,4-c]pyrrole-4,6(5H)-dione]-5,5-(di-yl)] (P8)[22] 172

6.4.9. Poly[[11,12-bis-(2-hexyl-decyloxy)-phenanthro[9,10-b]quinoxaline]- (2,7-di-yl)-alt-[4',7'-bis(2-thienyl)-2',1',3'-benzothiadiazole-5,6-N-octyl-dicarboxylic imide]-5,5-(di-yl)] (P9)[22] 173

6.4.9. Poly[9,10-bis(2-butyl-octyloxy)-2,7-phenanthrene–alt-[4',7'-bis(2-thienyl)-2',1',3'-benzothiadiazole-5,6-N-octyl-dicarboxylic-imide]-5,5-(di-yl)] (P10)[22] 173

6.5. Reference 175

Chapter 7: Supplementary Information 177

List of Figures

Figure 1.1. Illustration of some differences in the physical properties between (a) organic solar cells, and (b) inorganic solar cells. 3
Figure 1.2. Structures of some electron-acceptor materials, such as fullerene derivative (PCBM) and perylenediimide derivative (PDI). 4
Figure 1.3. Structures of some conjugated polymers widely used in organic solar cells as electron-donors, such as poly(3-hexylthiophene) (P3HT) and poly(p-phenylene vinylene) (PPV). 5
Figure 1.4. Stages of the operation of organic solar cells. 6
Figure 1.5. Structure of single-layer organic photovoltaic cell. 7
Figure 1.6. Structure of bilayer organic photovoltaic cells. 9
Figure 1.7. Structure of bulk heterojunction photovoltaic cells. 10
Figure 1.8. Current-voltage (J-V) curve of an organic photovoltaic device under illuminated conditions. P_{abs} is the absolute power point and P_{max} is the maximum power point. 11
Figure 1.9. Polyacetylene. 13
Figure 1.10. Chemical structures of some conjugated polymers. 14
Figure 1.11. Formation of σ-bonds and π-bonds by overlapping orbitals. 14
Figure 1.12. Diagram of molecular orbitals illustrating overlap of two 2p atomic orbitals for the formation of π-bonding and π*-antibonding molecular orbitals. 15
Figure 1.13. Diagram of band gaps in metals, semiconductors and insulators. 16
Figure 1.14. The effect of increased conjugation on E_g in conjugated polymers.[75] 16
Figure 1.15. Formation of new energy levels by copolymerisation of electron-donor monomer with electron-acceptor monomer. 18
Figure 1.16. (a) Illustration of energy levels of aromatic and quinoidal resonance structures. (b) The aromatic and quinoidal resonance structures of PITN. 19
Figure 1.17. Non-covalent interactions along a conjugated polymer backbone.[81] 19
Figure 1.18. The resonance hybrid structures of phenanthrene and the position of the K-region.[110] 24
Figure 1.19. (a) Oxidation of 9,10-positions of phenanthrene. (b) Extension of the conjugated system in phenanthrene to produce phenanthro[9,10-b]quinoxaline. 25
Figure 1.20. Schematic representation of $PN_{40}DPP$ synthesised by Jo and co-workers. 25
Figure 1.21. Schematic representation of P1 to P6 synthesised by Kim *et al*. 26
Figure 1.22. Polymer structures of PA1 and PA2 synthesised by Kim and co-workers. 26
Figure 1.23. Structural representation of a phenanthrene derivative, phenanthro[9,10-b]quinoxaline. 27
Figure 1.24. The different linking positions in the phenanthro[9,10-b]quinoxaline moiety. 27
Figure 1.25. Polymer structures of PBDT-DBPz and PBDT-DTDBPz. 28
Figure 1.26. Schematic of the process of electron transfer from the donor P3HT to the acceptor $PC_{61}BM$ and exciton dissociation. 29
Figure 1.27. Structural representation of fullerene derivatives (a) $PC_{61}BM$ and (b) $PC_{71}BM$. 30

Figure 2.1b. Aromatic and quinoidal structures of (a) benzothiadiazole and (b) quinoxaline acceptor units.[10] 43
Figure 2.2. Polymer structures of PPQP and PPQM synthesised by Park and co-workers.[13] 43
Figure 2.3. Polymer structures of PTQTI-F and PTQTI synthesised by Dang and co-workers.[15] 44
Figure 2.4. ^{1}H-NMR spectrum of (9) in $CDCl_3$. 56
Figure 2.5. ^{1}H-NMR spectrum of compound (21) in $CDCl_3$. 59

Figure 2.6. ^{1}H-NMR spectrum for compound (16) in $CDCl_3$. 67
Figure 2.7. ^{1}H-NMR spectrum of compound (19) in $CDCl_3$. 71
Figure 2.8. Normalised absorption spectra of P1, P2, P3 and P4 in: (a) chloroform solutions; and (b) thin films. 76
Figure 2.9. Cyclic voltammograms of P1, P2, P3 and P4 78
Figure 2.10. Polymer structures of PBDTT-TQ and PBDTT-BTQ synthesised by Dang and co-workers.[6] 78
Figure 2.11. Thermogravimetric analysis of P1, P2, P3 and P4 carried out at a heating rate of 10^{o}C min^{-1} and under an inert nitrogen atmosphere. 80
Figure 2.12. PXRD patterns of polymers P1, P2, P3 and P4. 81

Figure 3.1. Polymer structure of PBDT-TPD synthesised by Leclerc and co-workers.[8] 90
Figure 3.2. Polymer structure of PDTS-TPD-C8 synthesised by Chu *et al.* and co-workers.[12] 91
Figure 3. 3. Polymer structure of PBDT-TPD synthesised by Clément and co-workers.[9] 91
Figure 3.4. ^{1}H-NMR spectrum of compound (31) in $CDCl_3$. 99
Figure 3. 5. ^{1}H-NMR spectrum of compound (33) in $CDCl_3$. 99
Figure 3.6. Polymer structures of PTA-TPD(O), PTA-TPD(DMO) and PTA-TPD(BP), synthesised by Cartwright and co-workers.[21] 104
Figure 3.7. Normalised absorption spectra of P5, P6, P7 and P8 in 105
Figure 3.8. Cyclic voltammograms of P5, P6, P7 and P8. 106
Figure 3.9. Thermogravimetric analysis of P5, P6, P7 and P8 carried out at a heating rate of 109
Figure 3.10. PXRD patterns of polymers P5, P6, P7 and P8. 110

Figure 4.1. Polymer structures of PBnDT-DTffBT (PCEs of 7.2 per cent) and PDTG-TPD (PCEs of 7.3 per cent).[12,22] 118
Figure 4.2. Examples of various 2,1,3-benzothiadiazole derivatives, with the alterations in the 5- and 6-positions.[20] 119
Figure 4.3. Polymer structures of PDI-BDTT and PDI-BDTO synthesised by Wang and co-workers.[9] 120
Figure 4.4. Polymer structures of P(BTI-F) and P(BTI-B) synthesised by Li and co-workers.[24] 120
Figure 4.5. Polymer structures of BBTI-1 and BBTI-2 synthesised by Nielsen and co-workers.[20] 121
Figure 4.6. Polymers P9 and P10. 123
Figure 4.7. Normalised absorption spectra of P9 and P10 in: 126
Figure 4.8. Cyclic voltammograms of P9 and P10. 128
Figure 4.9. Thermogravimetric analysis of P9 and P10 carried out at a heating rate of 10 ^{o}C min^{-1} and under an inert nitrogen atmosphere. 129
Figure 4.10. PXRD patterns for polymers P9 and P10. 130

Figure 5.1. Schematic representations of modified P9 and P10 that should be investigated. 137
Figure 5.2 Schematic representations of suggested conjugated polymers with different types of alkyl chains. 138

List of Schemes

Scheme 1.1. Suzuki cross-coupling reaction. 21
Scheme 1.2. Mechanism of Suzuki cross-coupling reaction. 21
Scheme 1.3. Stille cross-coupling reaction 22
Scheme 1.4. Mechanism of Stille cross-coupling reaction. 22

Scheme 2.1. Monomers (9), (16) and (19) that are used to prepare P1 and P2. 46
Scheme 2.2. Monomers (21), (16) and (19) that are used to prepare P3 and P4. 47
Scheme 2.3. The synthetic route to produce monomer 2,3-bis-(3-(octyloxy)phenyl)-6,7-difluoro-5,8-bis(5-bromo-2-thienyl)quinoxaline (9). 48
Scheme 2.4. The suggested mechanism for the ring closure of compound (1). 49
Scheme 2.5. The mechanism of production of compound (2). 50
Scheme 2.6. The suggested mechanism for the ring closure of compound (4). 52
Scheme 2.7. The suggested mechanism for production of compound (5). 53
Scheme 2.8. Mechanism of production of compound (8). 55
Scheme 2.9. Mechanism of reaction to produce compound (9). 57
Scheme 2.10. The synthetic route to production of monomer 2,3-bis(3-(octyloxy)phenyl)-6,7-difluoro-5,8-bis(5-bromo-(2,2'-bithiophene)-5-yl)quinoxaline (21). 58
Scheme 2.11. The synthetic route for monomer 2,7- bis-(4,4,5,5-tetramethyl-1,3,2-dioxaborolan-2-yl)-11,12-bis-(2-hexyldecyloxy)- phenanthro[9,10-b]quinoxaline (16). 60
Scheme 2.12. Mechanism of synthesis of compound (11). 62
Scheme 2.13. Mechanism of synthesis of compound (13). 63
Scheme 2.14. Mechanism of production of compound 14. 65
Scheme 2.15. The synthetic route for production of monomer 2,7-bis-(4,4,5,5-tetramethyl-1,3,2-dioxaborolan-2-yl)-9,10-bis-(2-butyl-octyloxy)-phenanthrene (19). 68
Scheme 2.16. Mechanism for the formation of the dihydroxyl groups in compound (18). 69
Scheme 2.17. Mechanism of attachment of the alkyl groups in compound (18). 70
Scheme 2.18. Polymers P1, P2, P3 and P4. Explanations of their synthesis are included in this chapter. 74

Scheme 3.1. The preparation of P5 and P6 from monomers (31), (16) and (19). 92
Scheme 3.2. Preparation method for P7 and P8 from monomers (33), (16) and (19). 93
Scheme 3.3. The synthetic route for production of monomer 1,3-bis(5-bromo-thiophen-2-yl)-5-(3,7-dimethyloctyl)-4H-thieno[3,4-c]pyrrole-4,6(5H)-dione (31). 94
Scheme 3.4. The synthetic route for production of monomer 1,3-bis(5'-bromo-[2,2'-bithiophen]-5-yl)-5-(3,7-dimethyloctyl)-4H-thieno[3,4-c]pyrrole-4,6(5H)-dione (33). 95
Scheme 3.5. Suggested mechanism for the formation of compound (25). 96
Scheme 3.6. Mechanism of production of compound (26). 97
Scheme 3.7. Mechanism of production of compound (29). 98
Scheme 3.8. Polymers P5, P6, P7 and P8 whose synthesis is discussed in this chapter. 101

Scheme 4.1. Monomers (A), (16) and (19) used to prepare P9 and P10..... 122

List of Tables

Table 2.1. GPC analysis of P1, P2, P3 and P4 74
Table 2.2. Optical data of polymers P1, P2, P3 and P4 74
Table 2.3. Electrochemical properties of P1, P2, P3 and P4 77
Table 2.4. Thermal Properties of P1, P2, P3 and P4 79

Table 3.1 GPC analysis of P5, P6, P7 and P8 101
Table 3.2. Optical data of polymers P5, P6, P7 and P8 102
Table 3.3. Electrochemical properties of P5, P6, P7 and P8 106
Table 3.4. Thermal Properties of P5, P6, P7 and P8 108

Table 4.1. GPC analysis of P9 and P10 123
Table 4.2. Optical data of polymers P9 and P10 124
Table 4.3. Electrochemical properties of P9 and P10 127
Table 4.4. Thermal properties of P9 and P10. 128

List of Equations

Equation 1.1. The required energy of photons for excitation, where E_{photon} is the absorbed photons' energy, c is the speed of light, h is Planck's constant and λ_{photon} is the wavelength of incident light.[29] . 5
Equation 1.2. Equation to calculate the PCE in organic solar cells. P_{in} is the power density of incident light. 11
Equation 1.3. Formula used to determine the FF of OPV devices. 12

Equation 2.1. Formation of I_2^+ cation owing to oxidation of iodine by SO_3. 53
Equation 2.2. Formation of the nitronium ion. 63
Equation 2.3. Decomposition of ammonium formate to produce hydrogen gas. 64
Equation 2.4. Formation of sodium bisulphite. 69
Equation 2.5. Formula used to determine HOMO and LUMO energy levels. 76

List of abbreviations

A	**Electron-Acceptor**
Acetone-d_6	**Deuterated acetone**
Ar	**Argon gas**
AM	**Air Mass**
BHJ	**Bulk Heterojunction**
br	**Broad peak (NMR)**
bm	**Broad multiplet (NMR)**
bs	**Broad singlet (NMR)**
b	**Broad (NMR)**
CB	**Conduction Band**
$CDCl_3$	**Deuterated Chloroform**
$C_2D_2Cl_4$	**Deuterated 1,1,2,2-Tetrachlorethan**
CV	**Cyclic voltammetry**
D-A	**Donor-Acceptor**
D	**Electron donor**
d	**Doublet (NMR)**
dd	**Doublet of doublet (NMR)**
DCM	**Dichloromethane**
DMF	**N,N-Dimethylformamide**
DMSO	**Dimethylsulfoxide**
DP	**DP Degree of polymerization**
$E_{g\ (opt)}$	**Optical band gap**
$E_{g\ (elec)}$	**Electrochemical band gap**
eV	**Electron Volt**
Et_3N	**Triethylamine**
Fc	**Ferrocene**
GPC	**Gel Permeation Chromatography**
Hz	**Hertz**
HOMO	**Highest Occupied Molecular Orbital**
ICT	**Intramolecular charge transfer**
ITO	**Indium Tin Oxide**

J	**Coupling constant (NMR)**
JSC	**Short Circuit Voltage**
J-V	**Current-Voltage**
LUMO	**Lowest Unoccupied Molecular Orbital**
Lambda max (λ_{max})	**Maximum absorption wavelength**
MS	**Mass spectrometry**
m/z	**Mass to charge ratio (MS)**
m	**Multiplet (NMR)**
Mn	**Number-average molecular weight**
Mw	**Weight-average molecular weight**
MOT	**Molecular Orbital Theory**
M.p	**Melting Point**
NBS	**N-Bromosuccinimide**
NMR	**Nuclear Magnetic Resonance**
OSC	**Organic Solar Cell**
OPV	**Organic Photovoltaic**
PCE	**Power Conversion Efficiency**
PDI	**Polydispersity Index**
P3HT	**Poly(3-hexylthiophene)**
$PC_{70}BM$	**Phenyl-C70-Butyric Acid Methyl Ester**
ppm	**Part per million**
$P(o\text{-}tol)_3$	**Tris(ortho-methoxyphenyl)phosphine**
s	**Singlet (NMR)**
T_d	**Onset of Decomposition**
t	**Triplet (NMR)**
TGA	**Thermogravimetric analysis**
THF	**Tetrahydrofuran**
TPD	**Thieno[3,4-c]pyrrole-4,6-dione**
UV-vis	**Ultra-Violet-visible spectroscopy**
V	**Volt**
V_{oc}	**Open circuit voltage**
VB	**Valence Band**
XRD	**X-ray diffraction**

Chapter 1: Introduction

1. Introduction

1.1 Photovoltaic Cells

The collection of radiant energy emitted by the sun, through photovoltaic technology, is one technique available to reduce the negative effects of atmospheric emissions into the environment, and it addresses the increasing demand for a clean, renewable source of energy. The Earth receives a massive amount of solar irradiation, approximately 3.9×10^{24} joules (J) every year.[1] Enough solar irradiation hits the Earth in one hour to meet a year's demand, since the consumption of energy in 2004 was 4.7×10^{20} J.[1] Thus, if an area of 100 kilometres (km) x 100 km, in a region of high solar insolation such as deserts, was covered with solar cells rated at a PCE of 15 per cent, it could fulfil the electricity demand of the United States.[2] In addition, the cost of generating this energy would be lower than the operational cost of currently used energy technologies, and there would be no detrimental effects on the environment from their use. Solar cells are considered to be an effective method to solve the issue of the greenhouse effect, which is still increasing owing to the high demand for energy. Currently, less than 0.1 per cent of global energy consumption is harvested from PV cells. About 90 per cent of these cells employ crystalline silicon wafer-based technology: nine per cent consist of thin-film solar panels, and only the remaining one per cent consist of organic solar cells (OSCs).[3,4] Inorganic solar cells based on silicon achieve PCEs of between eight and 25 per cent,[5,6,7] yet this advantage is offset by disadvantages that limit their extensive production and usage. The main disadvantages of silicon solar-cell panels are: the high cost of the manufacturing process; the toxicity of the materials used in these devices; and the need for non-renewable energy during their production, which leads to additional emissions and detrimental effects on the environment.[8,9]

Therefore, researchers are focusing their efforts on OSCs, which can overcome some of the disadvantages of their inorganic counterparts. Fabrication of the active layer in OSCs from organic polymers reduces the cost of manufacturing the cells, improves their flexibility and enhances the operation of the cells at low light intensities. Moreover, many techniques are available for large-scale production of the cells, for example, vacuum thermal evaporation and polymer solution casting.[10,11]

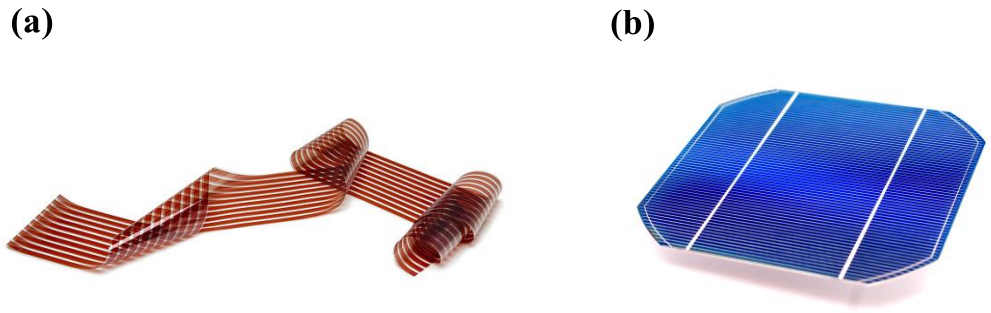

Figure 1.1. Illustration of some differences in the physical properties between (a) organic solar cells, and (b) inorganic solar cells.

1.2. Background and Development

French scientist Edmond Becquerel in 1839 was the first to observe the PV effect. He generated electric current by illuminating two platinum electrodes coated with light-sensitive material such as silver chloride immersed in an acidic solution that acted as an electrolyte.[12] In 1877, Smith and Adams reported that they had observed the photoconductive effect in a solid-state system by using a selenium bar.[13] Pochettino in 1906 and Volmer in 1913 observed the photoconductive effect in anthracene.[14,15] After this, researchers turned their attention to materials with photoconductive properties, but not those with PV properties, until 1959. Then, Kallmann and Pope observed the generation of photovoltage when they used five-micrometre (μm) single crystals of an organic material, such as anthracene, sandwiched between two identical electrodes in a solution of sodium chloride, after illuminating it on one side.[16] Seven years later, studies reported by Geacintov, Pope and Kallman showed that the PV effect was also observed in single crystals of tetracene sandwiched between two chambers of distilled water.[17] In 1958, Kearns and Calvin made the first PV device by using porphyrins and magnesium phthalocyanines sandwiched between two metallic conductors as electrodes. This resulted in a photovoltage of 200 milliVolts (mV).[18]

In 1975, physical chemist Ching W. Tang attempted to simulate the photosynthesis process that occurred in plants by using chlorophyll-a pigments that were extracted from spinach. He was successful, but with poor PCE of less than 0.01 per cent.[19] However, Tang's studies produced a breakthrough in 1986 when he reported the first bilayer heterojunction PV device, which consisted of a derivative of perylene diimide as an n-type organic semiconductor layer, and a derivative of phthalocyanine as a p-type organic semiconductor layer.[20]

Through the 1980s, there were many attempts to fabricate single-layer cells by using conjugated polymers such as polyacetylene and polythiophene. However, they produced low efficiencies of less than 0.01 per cent.[21] In 1992 Sariciftci *et al.* discovered that, by exciting a conducting polymer such as polyphenylene vinylene with light, an electron was transferred by photoinduction onto the buckminsterfullerene C_{60} molecule, which therefore behaved as an acceptor of electrons.[22] This breakthrough contributed to the development of polymer-fullerenes as D-A arrangements in PV cells, and led to heterojunction PV devices.[23] Wide ranges of acceptors, such as fullerene and perylene diimide derivatives (Figure 1.2), were employed to enhance the efficiency of heterojunction PV cells.

The bulk heterojunction (BHJ) architecture of solar cells was first introduced by Heeger and co-workers in 1995.[24] Yu *et al*. explained the main concept of BHJs: in order to improve the efficiency of solar cells, the interfacial area between donor and acceptor was required to be decreased, by using a mixture of donor and acceptor.[24]

The control of the nanostructural morphology of the active layers in BHJs is difficult, but plays a critical role in the performance of solar cells. For instance, ordered and disordered BHJs, and molecular heterojunctions, were used in 2001 by Ramos *et al.* in PV cells.[25]

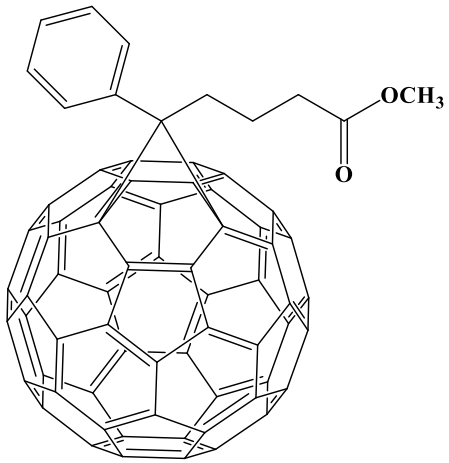

PCBM

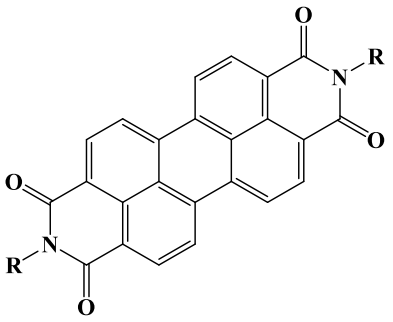

PDIs

Figure 1.2. Structures of some electron-acceptor materials, such as fullerene derivative (PCBM) and perylenediimide derivative (PDI).

In general, conjugated polymers in OSCs, such as those shown in Figure 1.3, are required to achieve two main stages: absorption of light to create electron-hole pairs (charge carriers),

and transport of these charge carriers. These two properties are connected with delocalisation of π-electrons, leading to the semiconducting behaviour of organic materials.[26]

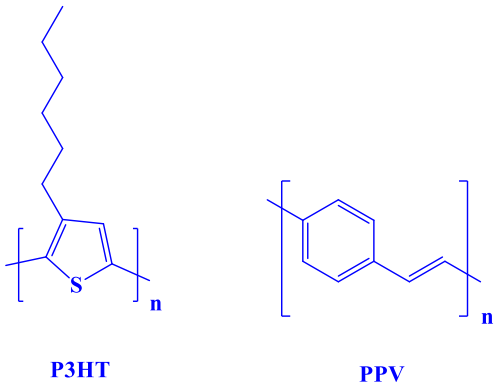

Figure 1.3. Structures of some conjugated polymers widely used in organic solar cells as electron-donors, such as poly(3-hexylthiophene) (P3HT) and poly(p-phenylene vinylene) (PPV).

1.3. Principle of Operation of Organic Solar Cells

The principle of converting sunlight directly to generate electricity through solar cells relies on four main stages:

The first is the ***absorption of light***, which depends on the band-gap energy (E_g) of the conjugated polymers that make up the active layers in OPV cells.[26] The photons of the absorbed incident light must have greater energy than the band-gap energy. This photoexcitation enables the excitation of electrons so that they move from the highest occupied molecular orbital (HOMO) to the lowest unoccupied molecular orbital (LUMO), leaving behind holes in the valence band (VB). This leads to the formation of electron-hole pairs, which are formed in organic semiconductors and are called excitons characterised by a certain binding energy (E_b).[8,27,28]

$$E_{photon} = c \,.\, h \,/\, \lambda_{photon} \geq E_g$$

Equation 1.1. The required energy of photons for excitation, where E_{photon} is the absorbed photons' energy, c is the speed of light, h is Planck's constant and λ_{photon} is the wavelength of incident light.[29]

The next stage is ***diffusion of the charges.*** The excitons, held together by coulombic forces, diffuse to the interfacial area between the electron-donors (conjugated polymers) and electron-acceptors (fullerene derivatives). Excitons have a short lifetime, therefore the diffusion length of excitons before they deactivate to the ground state in conducting polymers

is of the order of five nanometres (nm) to 20 nm.[30,31,32] This can be addressed by employing a BHJ morphology that increases the interfacial area between the donor and acceptor to optimise the exciton diffusion. However, if an exciton is generated far from the diffusion length, it decays, causing low quantum efficiencies.[33]

The third stage is ***dissociation.*** When the excitons reach the interfacial area, they are separated to produce free charge carriers, owing to the electrical field generated by the difference in work functions of the two electrodes.[34,35] It is hypothesised that the offset energy needed to facilitate the separation of the excitons is 0.3 electron Volts (eV) between the LUMO of the donor (conjugated polymers) and of the acceptor (fullerene derivatives).[36]

The final stage is ***charge collection,*** in which photocurrent and photovoltage are generated.[28,37] During this phase, the holes (positive-charge carriers) travel to the anode, which is commonly a transparent conducting material with high work function, such as indium tin oxide (ITO). The electrons (negative-charge carriers) travel to the cathode which has a low work function. This is a metal electrode such as aluminium (Al). The process is shown in Figure 1.4.[35]

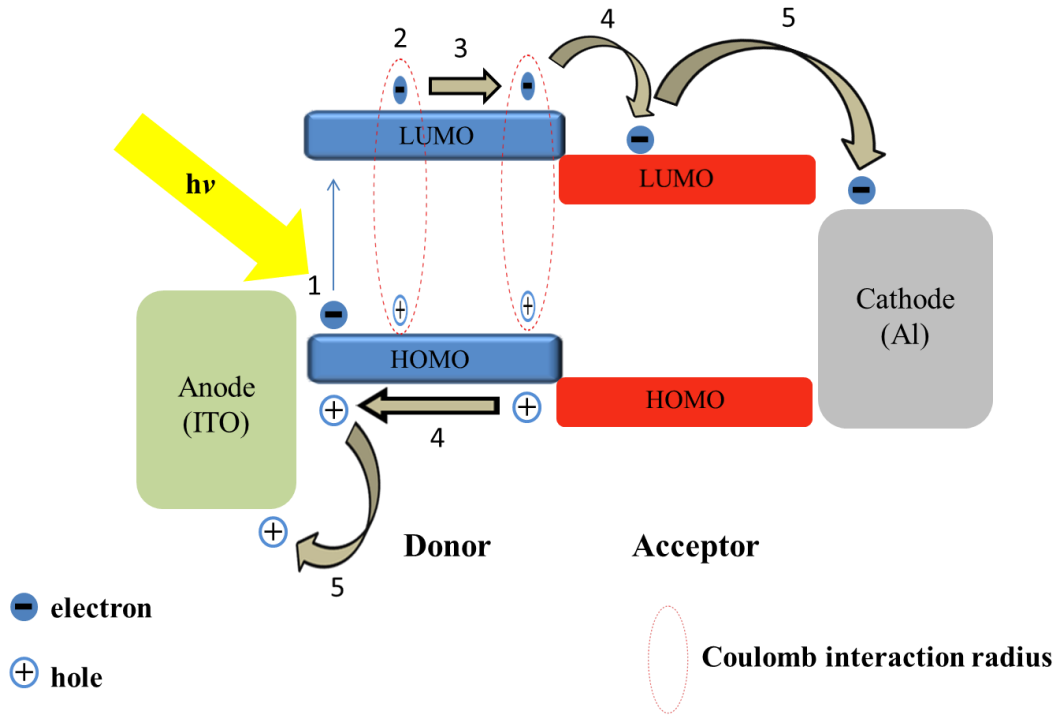

Figure 1.4. Stages of the operation of organic solar cells.

1.4. Architecture of Organic Solar Cells

1.4.1. Single Layer Organic Photovoltaic Cells

This type of solar cell contains a single active layer of organic electronic material sandwiched between two electrodes.[38] The cathode is made commonly of a layer of metal with a low work function, such as aluminium or calcium, which is evaporated onto the organic layer. The anode, which is usually a transparent conducting material with a high work function, such as ITO, is coated onto the glass substrate. The driving force of the electrical field in the organic active layer, generated by the difference in work functions between the two electrodes, should separate the excitons by attracting electrons to the cathode (the positive electrode) and holes to the anode (the negative electrode).[38,39] However, this type of solar cell shows unsatisfactory PCEs of between 10^{-1} per cent and 10^{-3} per cent, owing to poor dissociation of excitons because most carry no electrical charge and therefore are unaffected by the electric field.[40] Consequently, very few excitons are separated into electron-hole pairs, and instead they deactivate to the ground state without reaching the corresponding electrodes (Figure 1.5).[32] This issue can be addressed through the addition of a second layer of material to enhance the performance and charge separation.[32,40]

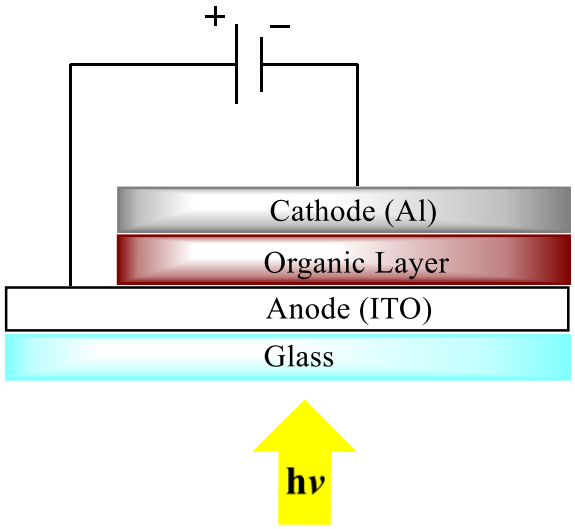

Figure 1.5. Structure of single-layer organic photovoltaic cell.

1.4.2. Bilayer Organic Photovoltaic Cells

This type of solar cell contains two active layers: an electron donor layer (p-type semiconductor) and an electron-acceptor layer (n-type semiconductor) between conductive electrodes.[37] The layers are stacked on top of each other to create a planar interfacial area for exciton dissociation.[41] The electron donor and acceptor layers have different properties, such as ionisation potentials (I_p) and electron affinities (E_A), in order to generate a strong electric field at the interfacial area to dissociate the excitons to free charges. This is shown in Figure 1.6.[41,42] Tang *et al*. reported the first bilayer solar cells, which contained phthalocyanine as the electron-donor layer and a perylene derivative as the electron-acceptor layer. This arrangement produced a PCE of approximately one per cent.[20,43]

The advantage of these solar cells is the ability of the excitons to diffuse to the interfacial area and then dissociate into free charge carriers. Electrons are then transported through the acceptor and holes are transported through the donor to the corresponding electrodes. This prevents the excitons from deactivating to the ground state in the conducting polymer.[39] However, the drawback of this type is the diffusion length of the excitons. Only excitons that are formed within diffusion lengths of between four nm and 20 nm can diffuse to the interfacial area and then dissociate into free charge carriers.[44,45] Excitons that form outside this range of diffusion length recombine and deactivate to the ground state, due to their short lifetime of typically less than one nanosecond (ns). Therefore, the efficiency of this type is low.[46] Bilayer cells can be prepared through sequential thermal deposition of two materials or through solution casting. PCEs in this type, for example copper phthalocyanine/C_{60}, can reach approximately 4.2 per cent.[47]

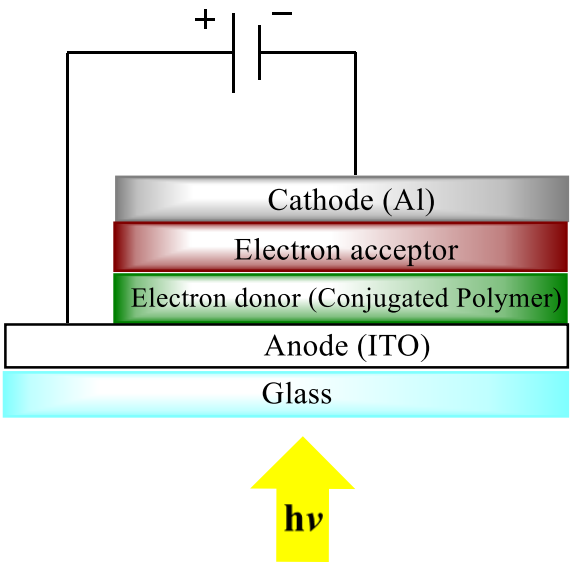

Figure 1.6. Structure of bilayer organic photovoltaic cells.

1.4.3. Bulk Heterojunction Photovoltaic Cells

In this type of solar cell, the active layers are blended to form a homogeneous mixture of the electron-donor and electron-acceptor in a bulk volume as first reported by Yu *et al*.[24] This increases the interfacial area between the donor and acceptor, and creates a morphology with interpenetrating nanoscale networks that enables more excitons than in the former designs to diffuse to the interfacial area and to be dissociated into free charge carriers at the D-A interface (Figure 1.7). The interpenetrating network offers the advantage that excitons have less distance to travel to reach the D-A interface, so the production of charge carriers is increased.[48] In addition, the homogeneous network affords passage for the charge carriers to be transported and collected by the corresponding electrodes.[49] Hence, this type of solar cell overcomes the problem of the limited interfacial area and recombination of excitons in bilayer cells.[50] The film thickness of the active layer can be increased up to 100 nm, which results in greater absorption of light and therefore increases the number of excitons formed to be separated into free charge carriers.[37, 45]

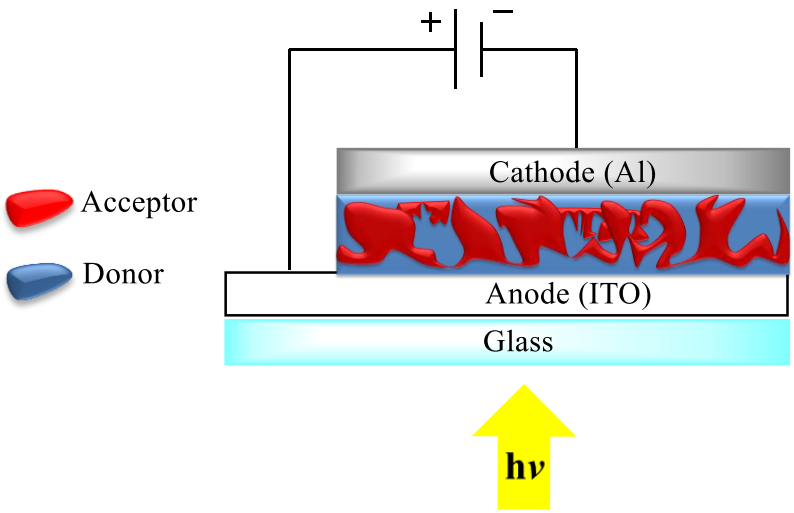

Figure 1.7. Structure of bulk heterojunction photovoltaic cells.

The active layer in BHJ cells is fabricated by casting a solution of an electron-donor, a conjugated polymer, blended with an electron-acceptor, a fullerene derivative.[39] Other factors need to be considered in order to improve PCEs in BHJ cells. These are: the adjustment of the blending ratio between the conjugated polymer and the fullerene derivative in the active layer; the enhancement of the morphology of the active layer during the manufacture through solvent-casting or spin-coating techniques; and employing conjugated polymers which show high thermal stability, which is necessary to prevent aggregation during the annealing process.[51,52,53]

1.5. Characteristics of organic photovoltaic cells

Three essential parameters need to be taken into account to acquire the highest PCEs in BHJ devices based on conjugated polymers: short-circuit current (J_{sc}), open-circuit voltage (V_{oc}) and fill factor (FF).[49,54,55] These parameters are given from the curve of current against voltage (J-V) for the organic PV device under illumination, as illustrated in Figure 1.8. Equation 1.2 is utilised to determine the PCE (η) in solar cells.

$$\eta = \frac{V_{oc} \times J_{sc} \times FF}{P_{in}}$$

Equation 1.2. Equation to calculate the PCE in organic solar cells. P_{in} is the power density of incident light.

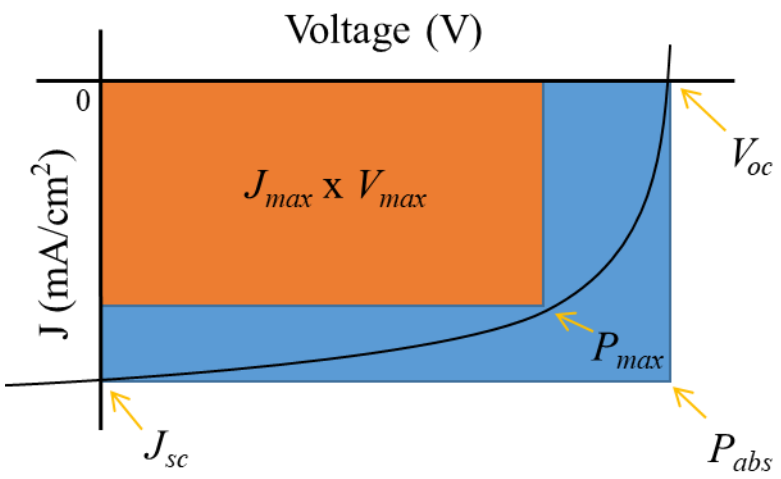

Figure 1.8. Current-voltage (J-V) curve of an organic photovoltaic device under illuminated conditions. P_{abs} is the absolute power point and P_{max} is the maximum power point.

1.5.1. Open-Circuit Voltage (V_{oc})

The V_{oc} in a PV cell is the maximum voltage produced without current flow within the device. The difference between the energy level of the HOMO in the electron-donor material (conjugated polymer) and the energy level of the LUMO in the electron-acceptor material (fullerene derivative) shows a proportional relationship with the V_{oc}.[49] Gadisa *et al.* and Scharber *et al.* observed a linear inverse correlation between the HOMO energy levels and the V_{oc}.[36,56] In theory, the lower the HOMO energy levels of the conjugated polymer, the higher the value of V_{oc}. However, the LUMO energy levels of the conjugated polymer have also to be taken into consideration. HOMO levels can be reduced only to the minimum point at which 0.3 eV can be maintained between the LUMO level of the electron-donor and the LUMO energy level of the electron-acceptor, in order to sustain efficient exciton separation.[39,54] In addition, the morphology of the active layer can have an impact on the V_{oc} value.[49,57]

1.5.2. Short-Circuit Current (J_{sc})

The J_{sc} represents the maximum electrical current produced by a BHJ cell when no voltage is applied across the device.[58] The amount of absorbed light generated and the number of charge carriers collected during solar illumination are responsible for the J_{sc}.[59] Therefore, the J_{sc} is restricted theoretically by the number of excitons formed within the period of solar illumination in excitonic solar cells.[54] To increase the number of excitons, the active layer

used in fabricated BHJ devices is required to absorb light from the visible and near-IR regions of the solar spectrum. Conjugated polymers with low band gaps have the ability to absorb more light and consequently improve the J_{sc}. However, the synthesis of low band-gap conjugated polymers requires an increase in the HOMO energy level, which decreases the V_{oc}. Therefore, the ideal compromise to obtain the best combination of J_{sc} and V_{oc} requires the design of a conjugated polymer with a band gap of 1.5 eV, a HOMO level at -5.4 eV and a LUMO level no lower than -3.9 eV.[36,60] Furthermore, the J_{sc} is sensitive to the nanoscale morphology of the active layer in fabricated BHJ devices. Several parameters must be taken into consideration during the preparation of the active layer, such as the casting solvent, spin-speed, substrate temperature and the deposition method to control the final morphology.[61,62]

1.5.3. Fill Factor (FF)

The FF is the ratio of the maximum power that can be obtained from a PV device to its V_{oc} and J_{sc}. The method of calculation is shown in Equation 1.3. The FF is a measure of the number of charge carriers that can reach the electrodes in a PV device.

$$FF = \frac{P_{max}}{P_{abs}} = \frac{P_{max}}{V_{oc} \times J_{SC}}$$

Equation 1.3. Formula used to determine the FF of OPV devices.

The ideal value for the FF (100 per cent) can be identified by a rectangular J–V curve. However, in practice the FF cannot reach this ideal, even in inorganic PV devices, which have higher PCEs than OSCs. The maximum FF that can be obtained in OPV devices ranges between 50 per cent and 70 per cent, while it is approximately 90 per cent in inorganic counterparts.[63] The FF is influenced by other parameters including the morphology of the active layer which, when it is optimised, improves charge dissociation and transport of free charge carriers. The area of the solar-cell device and the efficiency of the electrodes in the collection of free charge carriers can also affect the FF.[63,64,65]

1.6. Conjugated Polymers

1.6.1. Background

Conjugated polymers, also known as conducting polymers, are large organic molecules with alternating single and double bonds between carbon atoms. This structure can produce delocalised π-electrons, which are responsible for the polymers' electronic and optical

properties.[66] The simplest form of conjugated polymer, polyacetylene, was first prepared in 1958 by Natta as an air-sensitive, black powder,[67] but not much activity was recorded until a thin film of polyacetylene was prepared by Shirakawa in 1975.[68] The following year, Shirakawa discovered that polyacetylene could reach a conductivity level of 10^{-3} Siemens per centimetre after it was doped reductively or oxidatively, in order to delocalise the double bonds along the backbone polymer chain (Figure 1.9). In 2000 the Nobel Prize for Chemistry was awarded to Shirakawa, Heeger and MacDiarmid for this discovery.[69] These materials offer a combination of the properties of metals and plastics, including conductivity, flexibility, optical activity and processability.[70]

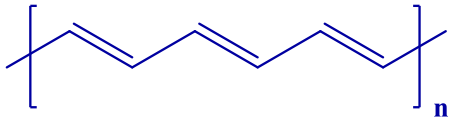

Trans-polyacetylene

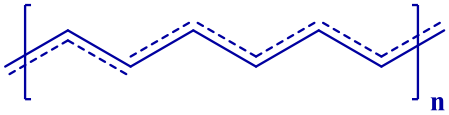

Doped-polyacetylene

Figure 1.9. Polyacetylene.

Since the discovery of polyacetylene, the research of conjugated polymers has increased significantly, and many conjugated polymers have been synthesised and developed for several applications that depend on their properties. These include solar cells (PV cells), field-effect transistors (FET) and light-emitting diodes (LEDs). Additionally, methods for the synthesis of conjugated polymers have been investigated and improved. Some common semiconducting polymers are illustrated in Figure 1.10.[71]

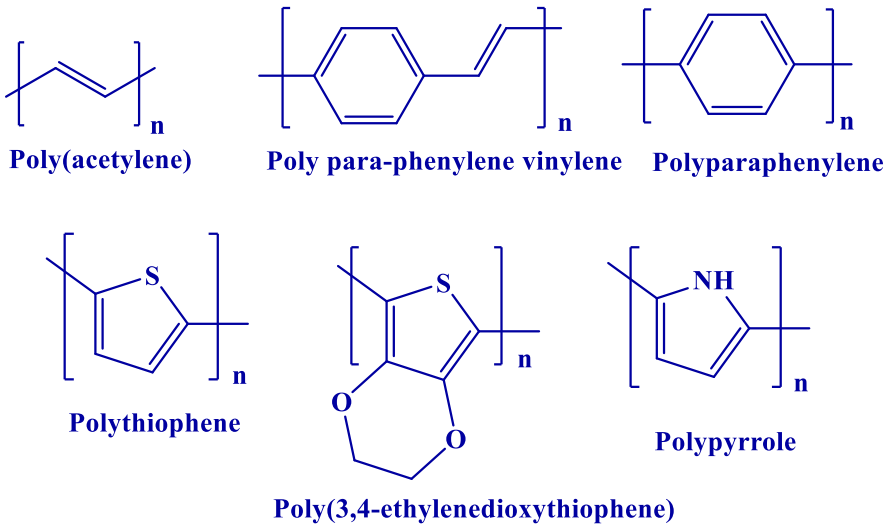

Figure 1.10. Chemical structures of some conjugated polymers.

1.7. The Electronic Structure of Conjugated Polymers

The molecular orbital (MO) theory explains the ways in which the optoelectronic properties of organic semiconducting materials can be manipulated. Organic macromolecules with alternating single and double bonds between their carbon atoms contain hybridised 2s and 2p orbitals, which produce three sp^2 hybrid orbitals. Two of these hybrid orbitals are positioned between two neighbouring carbon atoms and form σ-bonds, while the third forms σ-bonds between carbon and hydrogen atoms or other substituents.[72] The remaining p_z orbital, which is perpendicular to the sp^2 hybrid orbitals, interacts and overlaps with the p_z orbitals in the neighbouring atoms to form a π-bond, in which the electrons are delocalised along the chain of the polymer. The chemical structure of trans-polyacetylene shown in Figure 1.11 is an illustration.[73]

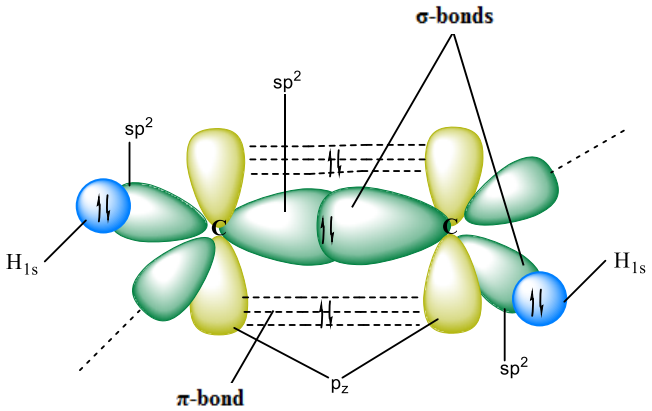

Figure 1.11. Formation of σ-bonds and π-bonds by overlapping orbitals.

1.8. The Band Gap of Conjugated Polymers

According to MO theory, p_z orbitals interact and overlap with other p_z orbitals from neighbouring atoms to form π-molecular orbitals. These are divided into occupied orbitals that have low energy, known as π-bonding orbitals, and unoccupied orbitals that have higher energy than the original atomic orbitals, known as π*-antibonding orbitals. The band-gap energy (E_g) is the energy difference measured in electron Volts (eV) between the highest occupied molecular orbitals (HOMO) and the lowest unoccupied molecular orbitals (LUMO).

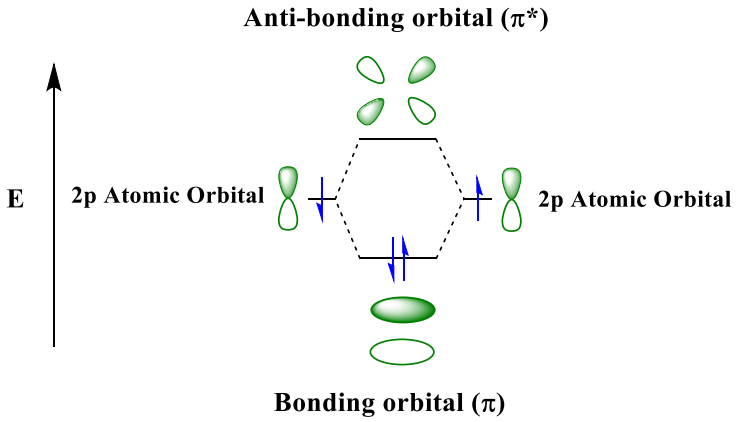

Figure 1.12. Diagram of molecular orbitals illustrating overlap of two 2p atomic orbitals for the formation of π-bonding and π*-antibonding molecular orbitals.

In monomers, the band gaps between the HOMO and LUMO orbitals are large compared with those of conjugated polymers. This is because conjugated polymers have more π-molecular orbitals. As the polymer chain grows longer through the polymerisation process, the discrete energy levels of the HOMO merge into a band called the valence band, (VB), which forms the fully occupied π-band. Similarly, the discrete energy levels of the LUMO merge into a band called the conduction band, (CB), which forms the empty π*-band. This is illustrated in Figure 1.13.[74,75]

As the number of units with π-molecular orbitals along the polymer chain is increased, the band gap between the HOMO and LUMO energy levels decreases accordingly, and therefore the conductivity of the conjugated polymer increases.[75,76] Once the E_g in a conjugated polymer is infinitely small, the polymer will act as a metallic conductor. Conductive polymers or intrinsically conducting polymers are produced without the need for a doping process.[65,73]

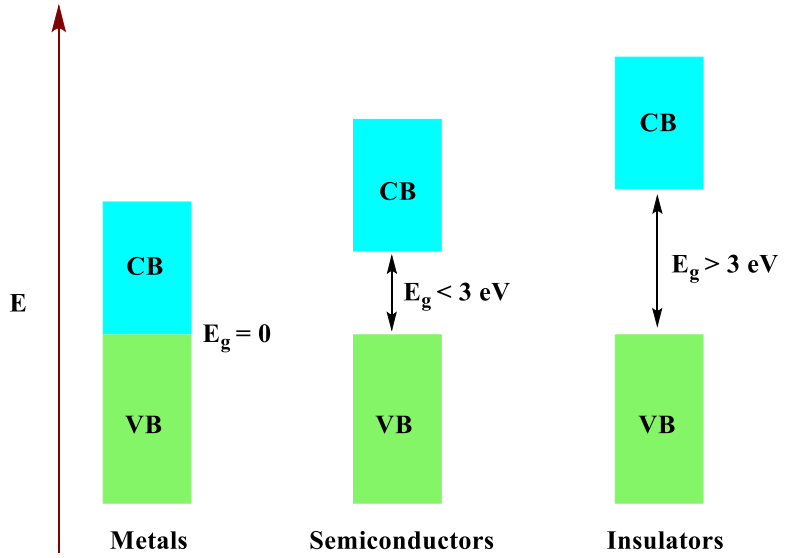

Figure 1.13. Diagram of band gaps in metals, semiconductors and insulators.

However, all synthesised conjugated polymers contain band gaps that are too large for them to be considered as intrinsic semiconductors. This is because the electrons in the valence band require energy to jump to the conduction band.[76] This energy can be supplied by, for example, light photons or heat. The energy band parameters comprising E_g, electron affinity (EA) and ionisation potential (IP) vary from one polymer to another.[71,77]

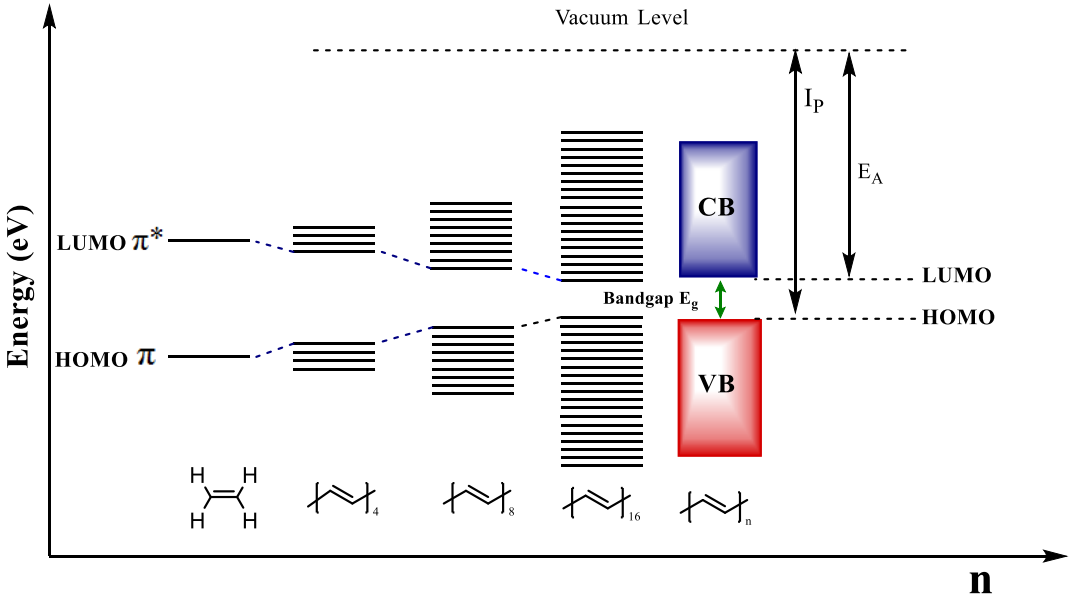

Figure 1.14. The effect of increased conjugation on E_g in conjugated polymers.[75]

Therefore, the band gap in conjugated polymers plays a significant role in the materials' electronic and optical properties, such as light absorption and conductivity. The band-gap energy can be measured by the absorption of ultraviolet-visible light by the conjugated polymer. It is essential to synthesise and develop conjugated polymers that can absorb long-wavelength light in the near-infrared region, to obtain a low band gap of approximately 1.5 eV in the near-infrared spectrum.[69]

1.9. Engineering of Band Gap in Conjugated Polymers

The maximum photon-flux density of the incident solar spectrum is situated between 400 nm and 1100 nm, which corresponds to energy levels of between 3.01 eV and 1.3 eV.[78] Thus, for conjugated polymers to absorb sufficient incident solar radiation, they require the optimum size of band gap. For instance, a conjugated polymer with a band gap of 1.1 eV has the ability to harvest approximately 77 per cent of the incident solar radiation.[38]

However, the band gap must fulfil certain conditions. It cannot be too narrow, since the energy offset of 0.3 eV between the LUMO levels of the polymer and fullerene derivative must be retained for efficient exciton separation. This then sets a limit for the reduction of HOMO energy levels to retain this energy offset. However, an offset energy that is greater than 0.3 eV leads to a loss of potential photovoltage.[36,79]

Therefore, there are two main approaches to the design of conjugated polymers to obtain polymers that combine the harvesting of near-infrared, long-wavelength light with improved electron delocalisation along the backbone of the polymers.

The first strategy is through the copolymerisation of an electron-rich monomer (known as an electron donor) with an electron-deficient monomer (known as the electron acceptor) in an alternating arrangement. This D-A, or push-pull, arrangement allows the electron-deficient moieties to pull π-electrons from the electron-rich moieties.[39] This results in the formation of a mesomeric structure (D-A $\rightarrow$ $D^{+}=A^{-}$) in which the bond length is similar throughout the structure and therefore electron delocalisation is increased.[39] In addition, the enhanced intramolecular charge transfer (ICT) between the HOMO levels of the donor and the LUMO levels of the acceptor contributes to the narrowing of the optical band gap within the conjugated polymer.[39]

MO theory illustrates the way in which the band gap is decreased in D-A polymers. It is shown in Figure 1.15. The HOMO energy levels of the donor and acceptor units interact with each other to create two new HOMO levels. In the same way, two new LUMO levels are formed by the interaction of the LUMO levels of the donor and acceptor units within the D-A polymer.[6,39] The new hybridised levels form a lower LUMO level and higher HOMO level than those observed in a standard conjugated polymer, leading to a band-gap reduction in the D-A copolymer.

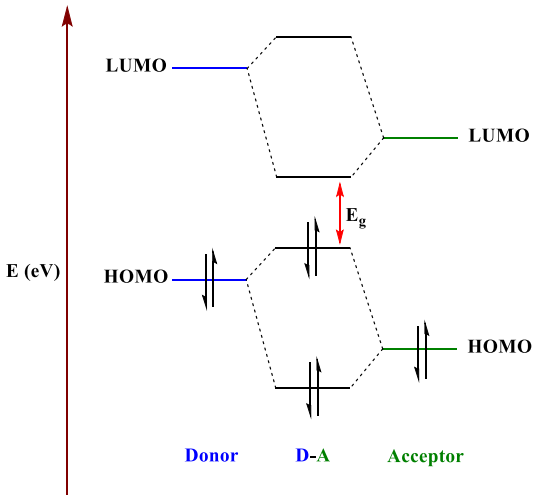

Figure 1.15. Formation of new energy levels by copolymerisation of electron-donor monomer with electron-acceptor monomer.

The second approach produces a similar effect to that observed in the mesomeric D-A structure. This method involves formation of opposing resonance structures that have a great impact on the conjugated polymer with lower band gap.[39,80] Two resonance structures, aromatic and quinoidal, can be formed. The quinoidal form has narrower band gaps than the aromatic form, since it is energetically less stable. This has been attributed to the destruction of the aromaticity as the molecule adopts a quinoid structure and hence loses stabilisation energy, as shown in Figure 1.16(a).[39,80] For example, the aromatic resonance energy of thiophene (1.26 eV) is lower than that of benzene (1.56 eV).[39] Therefore, polyisothianaphthene (PITN) exhibits a significant quinoidal character, as a result of the destruction of the aromatic configuration and the adoption of the quinoidal structure. Consequently, PITN shows a narrow band-gap of 1.0 eV (Figure 1.16.(b)).[39]

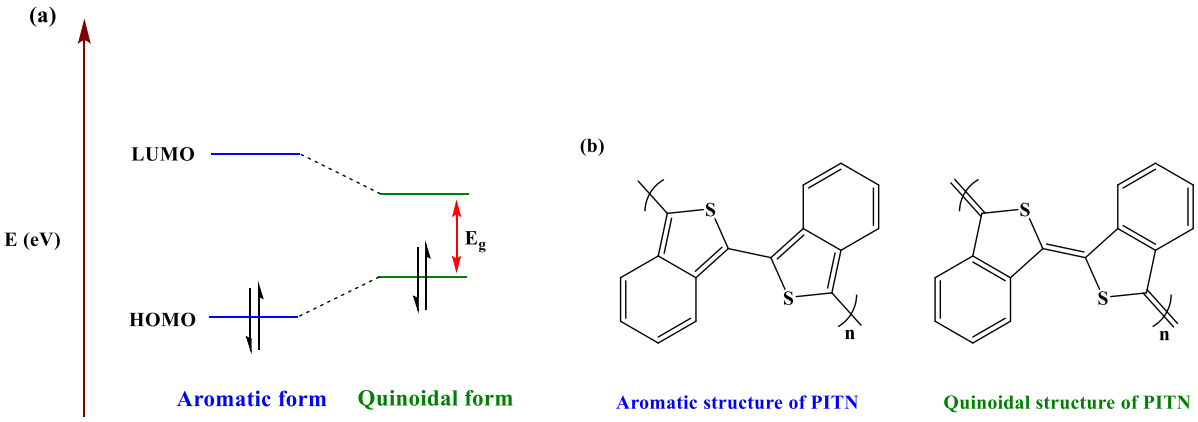

Figure 1.16. (a) Illustration of energy levels of aromatic and quinoidal resonance structures. (b) The aromatic and quinoidal resonance structures of PITN.

Incorporation of electron-donating or electron-withdrawing substituents into the backbone of conjugated polymers enables energy band gaps to be tuned. For instance, the introduction of a fluorine atom, which is the smallest electron-withdrawing group with electronegativity of 4.0, can contribute to improved oxidative and thermal stability of the conjugated polymer. It also results in enhanced molecular order throughout the non-covalent interactions between atoms on neighbouring aromatics and the fluorine atoms, as shown in Figure 1.17. This improves planarity of the polymer backbone, which can be helpful to enhance π-π stacking.[81,82]

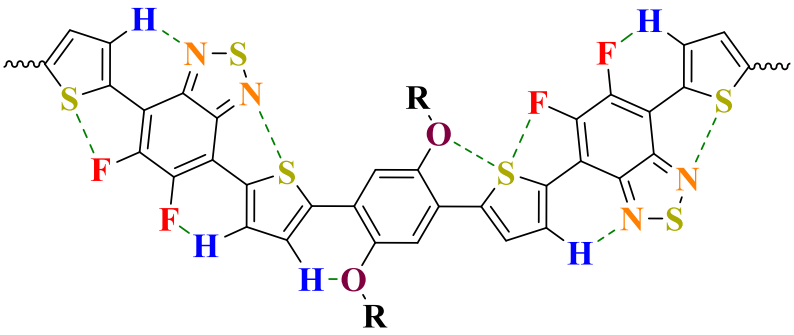

Figure 1.17. Non-covalent interactions along a conjugated polymer backbone.[81]

1.10. Solubility of Conjugated Polymers

Solubility plays an important role in the processability of the resulting conjugated polymer. Some essential aspects control the degree of solubility of the final conjugated polymer, such as: the degree of polymerisation, the structural rigidity of the backbone, the type of substituents and the length of the aliphatic side chain. Therefore, in order to achieve a

processable polymer that dissolves in common organic solvents at room temperature, the introduction of side chains along the backbone can promote both the solubility and processability. In addition, incorporation of side chains can increase the molecular weight of the resulting polymer. The attachment of side chains can also affect the intermolecular interactions and optimise the morphology of the active layer in PV devices.[83] Furthermore, solubility in organic solvents can be increased more effectively through the incorporation of branched alkyl chains rather than through the use of their analogous linear alkyl chains. The use of branched chains in turn leads to a reduction of the π–π stacking, and hence to promotion of the solubility and processability of the conjugated polymers.[6,39] However, poor anchoring of the side chains can be detrimental to the performance of PV devices, as this may create a steric hindrance that distorts the conjugated backbone.[83,84] This results in an increase of the polymer band gap and a corresponding decrease in the optical and electronic properties of the conjugated polymer. Moreover, incorporation of bulky insulating side chains can disturb the π-π stacking of polymer backbones and result in deterioration of the charge-carrier mobility. Consequently, the length and conformation of side chains must be considered carefully, owing to their large impact on the PV properties of the synthesised conjugated polymers.[85]

1.11. Synthesis of Conjugated Polymers

1.11.1. Preparation Methods of Conjugated Polymers

Many methods have been developed for the synthesis and polymerisation of conjugated polymers. Since the polymerisation of polyacetylene, many researchers have focused on the manufacture of conjugated polymers with novel electronic and optical properties.[86] The main feature of these new polymers is the carbon-carbon bond link between the aromatic repeating units, as in, for example, polythiophene or polyparaphenylene (Figure 1.10).[87,88] This thesis focuses on the two most common and important routes taken to synthesise these conjugated polymers: Suzuki cross-coupling and Stille cross-coupling.

1.11.1.1. Suzuki Cross-Coupling

There is widespread interest in this polymerisation method. It involves palladium-catalysed cross coupling between aryl halides and organoboronic acids or esters in the presence of a base such as sodium hydroxide (NaOH) as shown in Scheme 1.1. The purpose of this method is to activate the boron atom, which is required to improve the organic ligand polarisation and to facilitate transmetallation. The advantages of this methodology compared with other cross-

coupling reactions are: ease of preparation; the stability of the boronic acids or ester derivatives in the presence of heat, moisture and air; and their low toxicity.[89,90,91]

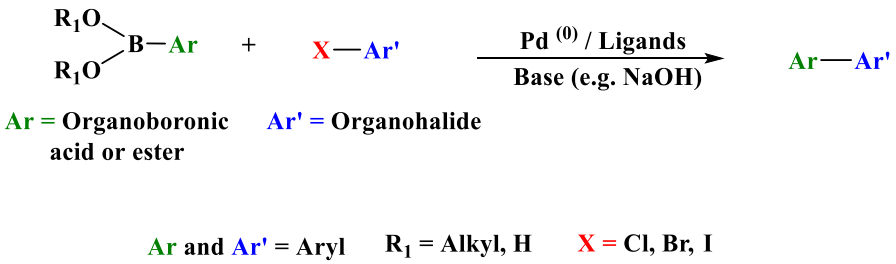

Scheme 1.1. Suzuki cross-coupling reaction.

Scheme 1.2 illustrates the mechanism of the Suzuki cross-coupling reaction:

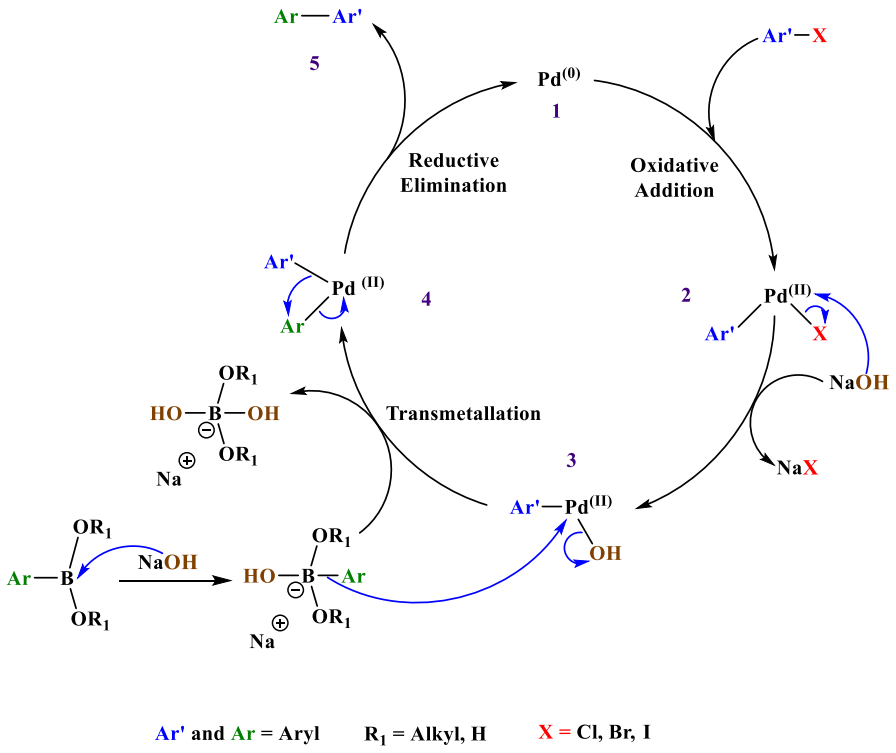

Scheme 1.2. Mechanism of Suzuki cross-coupling reaction.

The first step is the oxidative addition of aryl halide **[1]** to the palladium (0) catalyst to produce a palladium (II) complex **[2]**. Then the halide group in the complex is replaced by a hydroxide group from the base to produce an aryl palladium (II) complex **[3]**. After that, organoboronic acid or ester reacts with the aryl palladium (II) complex to produce intermediate palladium (II) **[4]**. In the transmetallation step, the boron atom in the organoboronic acid or ester is activated by reacting with a base, which increases the

nucleophilic nature of its aryl group. This facilitates the transmetallation reaction. The final step is the reductive elimination of the intermediate palladium (II) **[4]** to form the desired coupling product **[5]**, and the catalytic cycle of the palladium (0) catalyst is repeated with other aryl halides to yield desired compounds.[92]

1.11.1.2. Stille Cross-Coupling

This chemical reaction is used widely for polymerisation, owing to its versatility and tolerance when used with different functional groups,[93] particularly in the formation of sp^2 hybridised C-C bonds. It involves the coupling of organostannane compounds with a variety of organic electrophiles, such as aryl halides, in the presence of a palladium-catalyst (Scheme 1.3).[94] Although this preparation route produces conjugated polymers in high yields, the high toxicity of trialkylstannane compounds is a disadvantage of this method.[93,95,96]

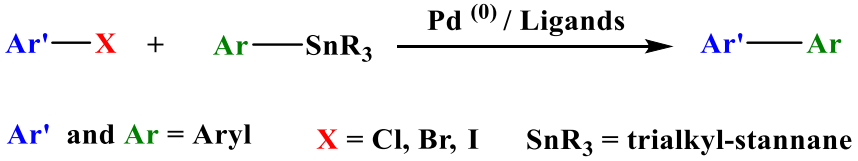

Scheme 1.3. Stille cross-coupling reaction

Scheme 1.4 illustrates the mechanism of the Stille cross-coupling reaction:

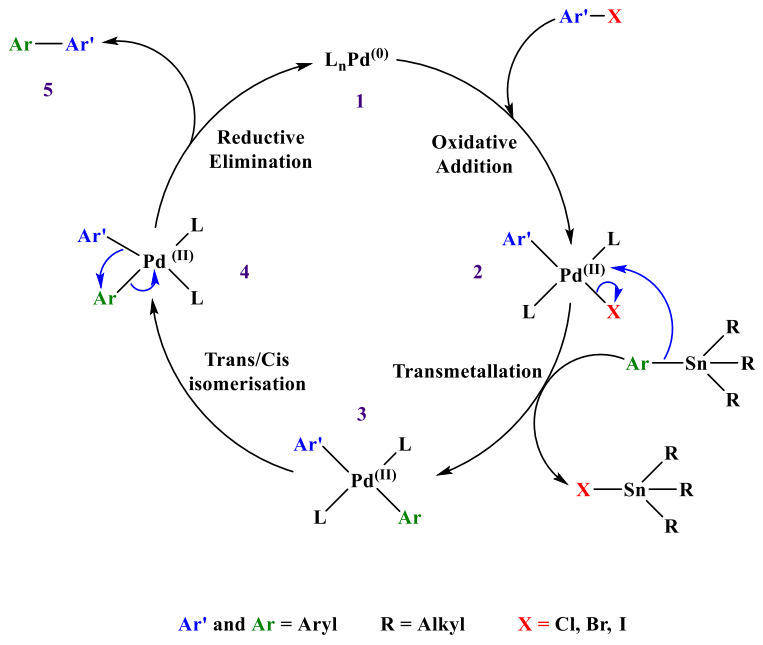

Scheme 1.4. Mechanism of Stille cross-coupling reaction.

Stille coupling, introduced by Stille,[94,97] is a four-step catalytic cycle: oxidative addition of the palladium catalyst into the aryl halide to produce an organopalladium (II) complex **[2]**; transmetallation of the organopalladium complex to produce a trans-intermediate, which is the more stable intermediate **[3]**[94]; trans- to cis-isomerisation to form a complex **[4]**; and reductive elimination of the palladium complex, leading to the formation of a C-C bond between aryl groups **[5]**.[94]

1.12. Materials used in organic solar cells

1.12.1. Phenanthrene-based Conjugated Polymers

Phenanthrene and its derivatives are considered to be among the most versatile building blocks to form electronic and optoelectronic devices, owing to their ability to extend the π-conjugated systems.[98-100] Phenanthrene is familiar as a polycyclic aromatic hydrocarbon. These molecules consist of three fused benzene rings, such as naphthalene, anthracene and pyrene.[99] Phenanthrene was discovered in 1872 in coal-tar by Ostermayer and Fittig, and almost simultaneously by G1aser.[101] It is an isomer of linear anthracene, but, because of its curved structure, it possesses higher thermal stability and greater resonance energy than anthracene and is, therefore, more stable and less likely to be affected by photochemical degradation when exposed to air compared with other aromatic compounds such as pentacenes.[99,102,103] Moreover, the phenanthrene moiety has a high degree of structural rigidity and planarity, so it can easily form strong π-π stacking, which can increase charge-carrier mobilities.[99,104,105] Phenanthrene has been used widely in the manufacture of dyes, explosives and for the synthesis of medicinal drugs.[106] In addition, it has been utilised as a core component in the development of organic LEDs and in organic FETs.[102,103,107] Phenanthrene is a tricyclic aromatic hydrocarbon, which can perform electrophilic aromatic substitution reactions. Moreover, an addition reaction can occur at the double bond positioned between carbons 9 and 10, a part of the molecule also known as the K-region (Figure 1.18).[108] This is supported by examination of the resonance structures, which demonstrate a strong olefinic character.[109,110]

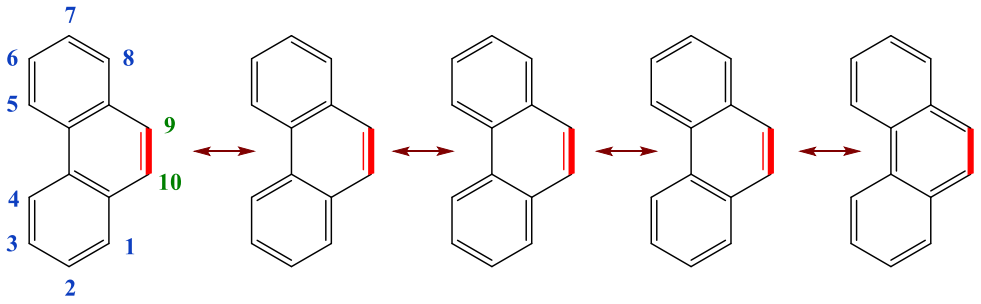

Figure 1.18. The resonance hybrid structures of phenanthrene and the position of the K-region.[110]

The positions 9 and 10, or the K-region, of the phenanthrene unit have been extensively investigated, due to their ability to extend the π-conjugated system through the functionalisation of a variety of aromatic building blocks.[111-114] Moreover, the 9 and 10 positions of phenanthrene can be easily functionalised with alkoxy groups to enhance the solubility of the resulting polymers without affecting the conjugation system, as well as to improve the electron density along the polymer chains.[99,105,113,114] In addition, the advantage of employing phenanthrene is that positions 2 and 7 are open linkage positions for the polymer without hindrance from side substituents, since phenanthrene and its derivatives do not have substituents on the 3 and 6 positions. This reduces the steric hindrance between neighbouring units.[105]

Several methods are used widely to synthesise 9,10-phenanthrenedione or 9,10-phenanthrenequinone. The benefit of using dicarbonylated phenanthrene is that it provides access to numerous types of chemical reactions that have a significant role in organic synthesis, such as condensation and electrophilic aromatic substitution. This enables the preparation of desirable and reactive starting materials.[115,116] The compound 9,10-phenanthrenequinone can be obtained by the oxidation of phenanthrene with chromium trioxide (CrO_3) in glacial acetic acid or sulphuric acid with a yield of approximately 80 per cent.[117,118] This method is shown in Figure 1.19. Another method involves the reaction of phenanthrene with bromochromate in the presence of cetyltrimethylammonium bromochromate (CTMABC) under microwave irradiation for 20 minutes with a yield of 85 per cent.[119]

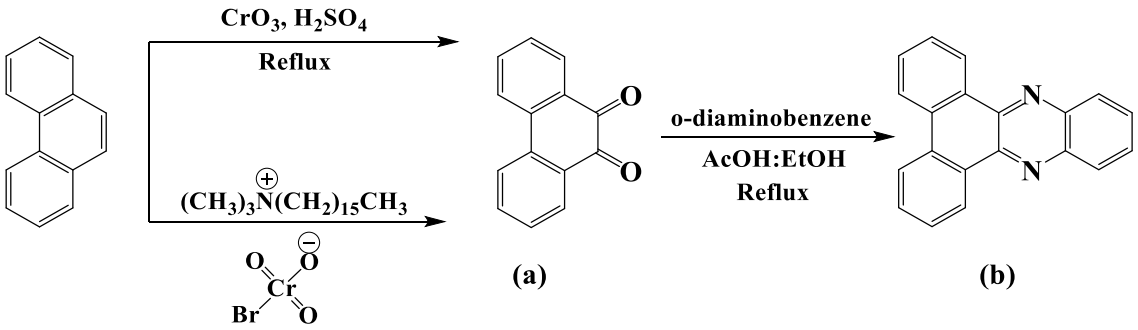

Figure 1.19. (a) Oxidation of 9,10-positions of phenanthrene. (b) Extension of the conjugated system in phenanthrene to produce phenanthro[9,10-b]quinoxaline.

When phenanthrene and its derivatives are utilised in conjugated polymers as electron-donating building blocks, they are likely to achieve high V_{oc}, owing to their high oxidation potential compared with the commonly used thiophene derivatives.[98,99,120] This is due to their polycyclic aromatic structures.

In a study reported by Jo and co-workers, the copolymer $PN_{40}DPP$ was synthesised by the copolymerisation of 9,10-dialkoxyphenanthrene and diketopyrrolopyrrole (DPP) units. It demonstrated a low optical band gap of 1.65 eV in film states. The resulting conjugated polymer when blended with phenyl-C_{61}-butyric acid methyl ester ($PC_{61}BM$) exhibited a high V_{oc} of 0.68 V–0.70 V with PCE of 1.19 per cent (Figure 1.20).[105]

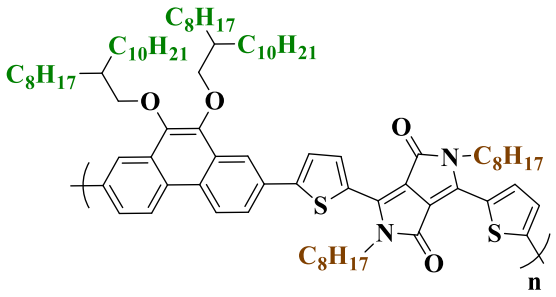

Figure 1.20. Schematic representation of $PN_{40}DPP$ synthesised by Jo and co-workers.

Kim *et al.* studied the synthesis of a series of narrow band-gap conjugated copolymers for organic BHJ solar cells. These copolymers consisted of phenanthrene as an electron-donor copolymerised with DPP units and blended with PCBM (Figure 1.21). Positions 9 and 10 of phenanthrene were functionalised with different solubilising groups.[99] All polymers showed low optical band gaps of about 1.6 eV and deep HOMO energy levels of -5.14 eV to -5.25 eV. The best performance was observed from P4, with the highest molecular weight of 66.5 kg

mol^{-1}, which achieved a high open-circuit voltage of about 0.79 V, and delivered a PCE of 2.73 per cent.

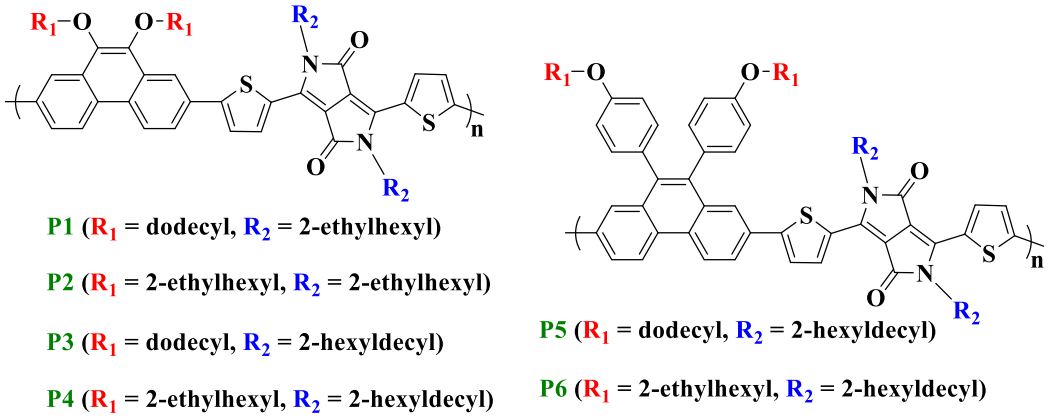

Figure 1.21. Schematic representation of P1 to P6 synthesised by Kim *et al*.

In another study conducted by Kim *et al.*, D-A copolymers were reported that were based on phenanthrene and DPP units. These are shown in Figure 1.22 as **PA1** and **PA2.**[121] Both **PA1** and **PA2** displayed narrow optical band gaps of 1.63 eV.[121] However, **PA1** showed slightly lower-lying HOMO energy levels with a value of -5.22 eV compared with those in **PA2**, which showed a value of -5.12 eV. The BHJ devices that were fabricated with **PA1** and **PA2** with $PC_{71}BM$ demonstrated enhanced PCEs of 5.3 per cent and 4.8 per cent, with V_{oc} of 0.72 V and 0.68 V, respectively.[121]

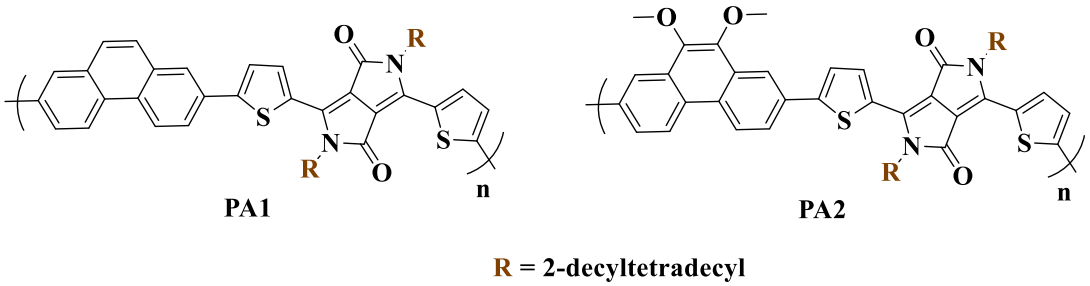

Figure 1.22. Polymer structures of PA1 and PA2 synthesised by Kim and co-workers.

Li *et al.* carried out a study that employed the phenanthrene derivative phenanthro[9,10-b]quinoxaline (Figure 1.23). The study demonstrated the use of different linking positions in phenanthro[9,10-b]quinoxaline when it was used as the electron-accepting unit, with carbazole as the electron-donating unit, to synthesise two new D-A copolymers **PCT-10,13-BPz** and **PCT-2,7-BPz** as shown in Figure 1.24.[122] Although **PCT-2,7-BPz** showed

significantly higher molecular weight and lower HOMO levels than **PCT-10,13-BPz**, the optical band gap of **PCT-10,13-BPz** (1.94 eV) **was** lower than that of **PCT-2,7-BPz** (2.38 eV).[122] This was attributed to the more stable quinoid structure formed by **PCT-10,13-BPz** compared with **PCT-2,7-BPz.**[49,122,123] However, **PCT-10,13-BPz** exhibited a higher PCE than **PCT-2,7-BPz**, with PCEs of 4.31 per cent and 0.64 per cent, respectively, when fabricated into BHJ solar devices using $PC_{71}BM$ as the acceptor.[122]

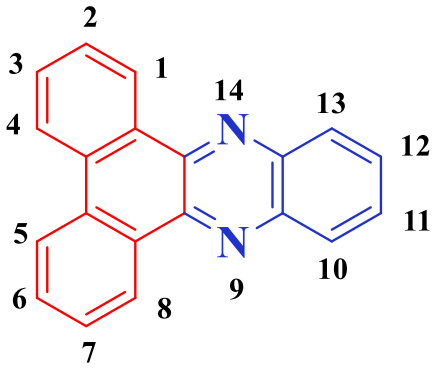

Figure 1.23. Structural representation of a phenanthrene derivative, phenanthro[9,10-b]quinoxaline.

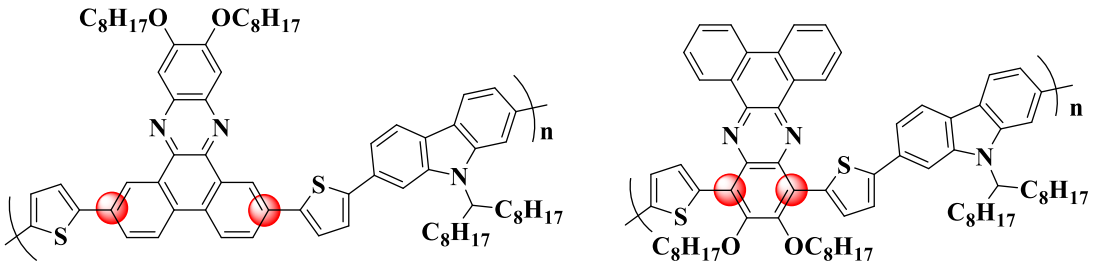

Figure 1.24. The different linking positions in the phenanthro[9,10-b]quinoxaline moiety.

In a different study, Li and co-workers investigated the effect of incorporation of thiophene spacer units when synthesising two new low band-gap D-A copolymers, based on benzodithiophene (BDT) as the donor unit and phenanthro[9,10-b]quinoxaline as the acceptor unit, to yield **PBDT-DBPz** and **PBDT-DTDBPz** (Figure 1.25).[124] **PBDT-DTDBPz** displayed considerably higher molecular weight of 221.93 kg mol^{-1}, when compared with that of **PBDT-DBPz** (5.26 kg $mol^{-1)}$.[124] The thiophene spacer units reduced the steric hindrance between the donor and acceptor moieties, enabling further polymerisation and hence higher molecular weight of **PBDT-DTDBPz**. Moreover, the introduction of thiophene spacer units

extended the conjugation system and therefore lowered the optical band gap. Thus, **PBDT-DTDBPz** showed a narrower band gap of 1.70 eV compared with **PBDT-DBPz**, which showed a band gap of 1.83 eV.[124] A PCE of 4.75 per cent was achieved for **PBDT-DTDBPz** when fabricated into BHJ solar devices using $PC_{71}BM$ as the acceptor. This was significantly greater than the PCE of 0.46 per cent for **PBDT-DBPz** when fabricated into BHJ devices under the same conditions.[124]

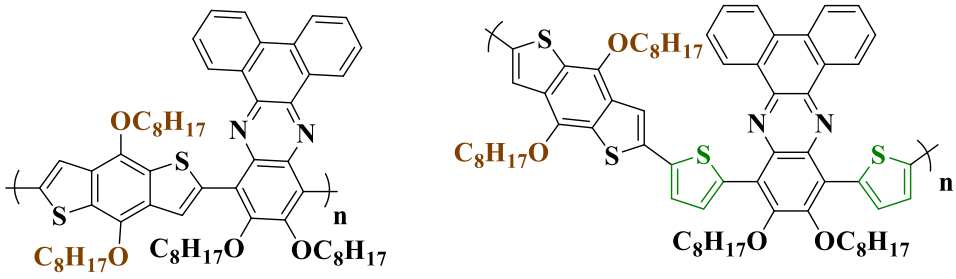

PBDT-DBPz **PBDT-DTDBPz**

Figure 1.25. Polymer structures of PBDT-DBPz and PBDT-DTDBPz.

1.12.2. Fullerenes (Electron-Accepting Materials)

The development of OPV cells has mainly focused on the design of conjugated polymers. However, fullerene and its derivatives are commonly utilised as electron acceptors in BHJ devices, as a result of their ability to accept and transport electrons.[39,125,126] When a conjugated polymer (donor) is blended with fullerene derivatives (acceptor), non-reversing behaviour occurs, owing to the charge transport properties of the donor and acceptor. Therefore, current is conducted in one direction, creating a basic diode.

Buckminsterfullerene (C_{60}) has been recognised as an ideal electron-accepting material for applications in OPV cells. Sariciftci *et al.* first reported photoinduced electron transfer (PET) from a conjugated polymer on to buckminsterfullerene as shown in Figure 1.26.[33] PET occurs on a time scale of femtoseconds, which is much quicker than the radiative decay process of photoexcitation that is responsible for decreasing PCE in OPV devices. The quicker the electron transfer is between the interfacial area and fullerene molecules, the lower the rate of recombination, and therefore, the higher the total PCE in the OSCs.[49,127,128] However, one of the main drawbacks of buckminsterfullerene is its poor solubility in common organic solvents. This prevents its use in low-cost solution-processing techniques. Thus, in 1995 Hemmelen *et al.* attached solubilising groups to buckminsterfullerene to produce [6,6]phenyl-C_{61}-butyric acid methyl ester ($PC_{61}BM$), as shown in Figure 1.27.(a).This has become the most electron-

accepting material used in BHJ solar cells.[24,49,129] $PC_{61}BM$ possesses higher electron affinity and electron mobility than C_{60}, but relatively low LUMO energy levels, which may constrain the current density J_{sc} value in PV devices. In addition, it limits the energy levels that can be accepted in electron-donating materials in order to obtain a high value of V_{oc}.[125] Another drawback of fullerene derivatives is their lack of absorption in the visible and near-IR regions of the solar spectrum due to their symmetrical structures, which prevent low-energy transitions.[39] However, PCEs in BHJ devices can be enhanced by substituting $PC_{61}BM$ with its higher fullerene analogue $PC_{71}BM$ (Figure 1.27.(b)). This analogue has a less symmetrical structure than C_{60}, and consequently, light absorption is increased in the visible spectrum, enabling higher optical transitions and higher current densities J_{sc}.[125,130]

The tuning of the LUMO energy levels of fullerenes compared with those of conjugated polymers to reduce thermalisation losses is considered to be challenging.[125] He *et al.* reported a new use of indene-C_{60} bis-adduct ($IC_{60}BA$) and indene-C_{70} bis-adduct ($IC_{70}BA$), which are other fullerene derivatives that display several advantages in comparison with $PC_{61}BM$ and $PC_{71}BM$, such as: stronger light absorption in the visible region, higher-lying LUMO levels, ease of preparation and enhanced solubility. Use of these has considerably improved the V_{oc} and PCE in PV devices.[131,132]

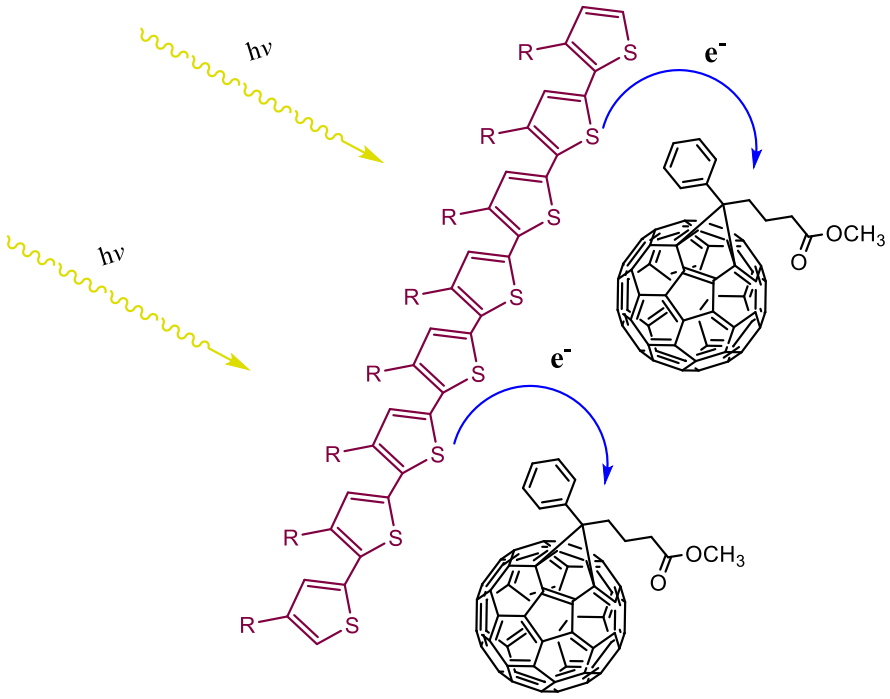

Figure 1.26. Schematic of the process of electron transfer from the donor P3HT to the acceptor $PC_{61}BM$ and exciton dissociation.

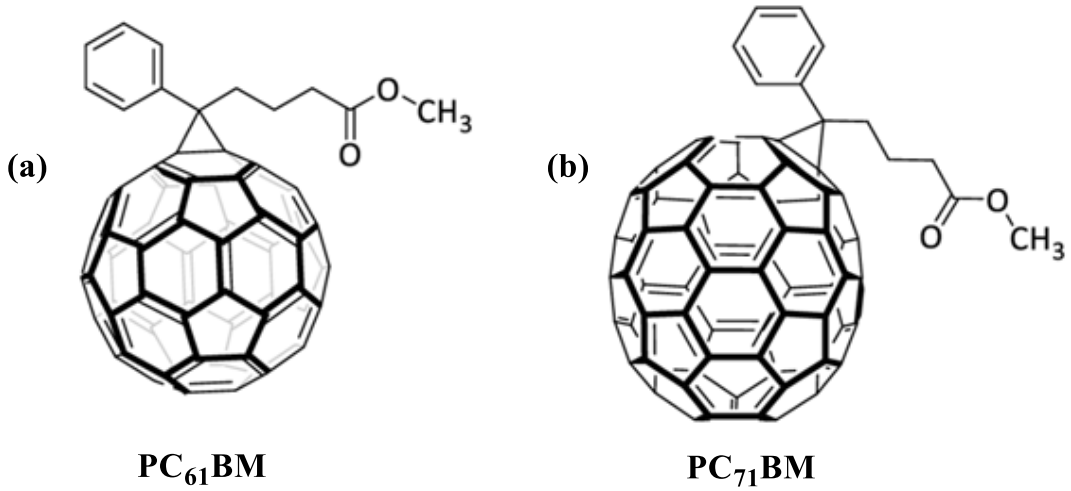

$PC_{61}BM$ **$PC_{71}BM$**

Figure 1.27. Structural representation of fullerene derivatives (a) $PC_{61}BM$ and (b) $PC_{71}BM$.

1.13. Project Aims

BHJ solar cells show increasingly promising developments and results. Currently, many studies aim to prepare effective conjugated polymers and to control and improve the active-layer morphology. The layer has a conjugated polymer as the electron-donor and fullerene derivatives as molecular electron acceptors. Researchers focus on the development of conjugated polymers with low energy band gaps that are able to absorb a large part of the sun's light spectrum. This enables quantitative exciton dissociation and good charge-carrier mobility.

Therefore, the aim of this project is to synthesise and design a range of conjugated polymers suitable for PV applications, with low band gaps, extended absorption in the visible and infrared regions of the spectrum, and high molecular weights. The D-A, or push-pull, arrangement is used for the synthesis of a new series of conjugated polymers *via* palladium-catalysed Suzuki cross-coupling reactions. In this thesis, 9,10-dialkoxy-phenanthrene and its derivative, phenanthro[9,10-b]quinoxaline, are mainly used as the electron donors in D-A copolymers. The 2,7-positions are employed as linkage positions along the conjugated polymer backbone.

Chapter 2 describes the synthesis of four new alternating copolymers that consist of difluoro-quinoxaline as the electron-acceptor and 9,10-dialkoxy-phenanthrene and its derivative phenanthro[9,10-b]quinoxaline as electron donors. Few studies discovered during this study have reported alternating structures of phenanthrene derivatives with quinoxaline. Therefore, this study evaluates the suitability of utilising phenanthrene derivatives as donor units in these polymers, and determines their influence on the optical, electrochemical and thermal properties of the resulting polymers.

The quinoxaline unit as an electron acceptor provides promising conjugated polymers with narrow band gaps. An acceptor with substituents of two fluorine atoms in positions 6 and 7 of the quinoxaline unit is tested to investigate the effects of lowering the HOMO energy levels. Two different alkoxyl substituents are incorporated to donor and acceptor moieties to achieve good solubility in many organic solvents at room temperature. In addition, a number of thienyl units are flanked between the donor-acceptor units along the polymer chains to increase the conjugation and to tune finely the optical and electronic properties of the resulting polymers.

In Chapter 3, a series of narrow band-gap copolymers that use thieno[3,4-c]pyrrole-4,6-dione (TPD) as an acceptor are synthesised and alternated with 9,10-dialkoxy-phenanthreneand its derivative, phenanthro[9,10-b]quinoxaline, as donor moieties, to improve the optical and electronic properties of conjugated polymers for application in PV devices. TPD has a highly compact planar structure that shows a high degree of symmetry and strong electron-withdrawing properties. This improves electron delocalisation along polymer chains, which lowers the band gap of the resulting copolymers and promotes their hole mobility. Moreover, the nitrogen of the imide group in the TPD unit can be functionalised by anchoring various solubilising groups to improve solubility and to increase the molecular weight of the resulting polymers. Furthermore, the conjugation system will be extended by incorporation of a number of thiophene units, in order to study their effect on the electrochemical, thermal and optical properties of the resulting polymers in the solid state and to compare the results with those of their analogous copolymers.

Chapter 4 presents the synthesis and characterisation of two new narrow band-gap alternating copolymers, comprising 2,1,3-benzothiadiazole-5,6-dicarboxylic imide (BDI) as the acceptor, alternating with 9,10-dialkoxy-phenanthreneand its derivative, phenanthro[9,10-b]quinoxaline, as donor moieties. BDI exhibits strength as an electron-deficient unit since it possesses the advantageous properties of both the dicarboxylic imide group from TPD and the planar benzothiadiazole (BT) unit. The exploitation of these characteristics will enable the synthesis of narrow band-gap copolymers with deep HOMO energy levels. In addition, the nitrogen of the imide group can be functionalised by the attachment of various solubilising groups to enhance the solubility of the resulting polymers. This aids in the understanding and evaluation of the effects of incorporating 9,10-dialkoxy-phenanthreneand its derivative, phenanthro[9,10-b]quinoxaline, as donor moieties, and the study also examines their influence on the optical, thermal and electrochemical properties of the resultant polymers.

1.14. References

(1) Ameri, T.; Dennler, G.; Lungenschmied, C.; Brabec, C. J. Organic tandem solar cells: A review.

(2) Shaheen, S. E.; Ginley, D. S.; Jabbour, G. E. J. M. b. Organic-based photovoltaics: toward low-cost power generation. 2005, *30* (1), 10.

(3) Jäger-Waldau, A. J. R.; Reviews, S. E. Photovoltaics and renewable energies in Europe. 2007, *11* (7), 1414.

(4) Sopian, K.; Cheow, S.; Zaidi, S. AIP Conference Proceedings, 2017; p 020004.

(5) Jayawardena, K. I.; Rozanski, L. J.; Mills, C. A.; Beliatis, M. J.; Nismy, N. A.; Silva, S. R. P. J. N. 'Inorganics-in-Organics': recent developments and outlook for 4G polymer solar cells. 2013, *5* (18), 8411.

(6) Lu, L.; Zheng, T.; Wu, Q.; Schneider, A. M.; Zhao, D.; Yu, L. J. C. r. Recent advances in bulk heterojunction polymer solar cells. 2015, *115* (23), 12666.

(7) Green, M. A.; Emery, K.; Hishikawa, Y.; Warta, W. J. P. i. p. r.; applications. Solar cell efficiency tables (version 37). 2011, *19* (1), 84.

(8) Gregg, B. A.; ACS Publications, 2003.

(9) Green, M. J. P. P. R. A. MA Green, K. Emery, Y. Hishikawa, W. Warta, and ED Dunlop, Solar cell efficiency tables (Version 45), Prog. Photovolt: Res. Appl. 23, 805 (2015). 2015, *23*, 805.

(10) Bundgaard, E.; Krebs, F. C. J. S. E. M.; Cells, S. Low band gap polymers for organic photovoltaics. 2007, *91* (11), 954.

(11) Myers, J. D.; Xue, J. J. P. R. Organic semiconductors and their applications in photovoltaic devices. 2012, *52* (1), 1.

(12) Becquerel, A. J. C. A. S. P. Photoelctrochemical effect. 1839, *14*.

(13) Adams, W. G.; Day, R. E. J. P. o. t. R. S. o. L. V. The action of light on selenium. 1877, *25* (171-178), 113.

(14) Pochettino, A.; Sella, A. J. A. L. R. Photoelectric behavior of anthracene. 1906, *15*, 355.

(15) Volmer, M. J. A. P. The different photoelectrical occurrences on anthracene, their connections to each other, to fluorescence and dianthracene formation. 1913, *40* (4), 775.

(16) Kallmann, H.; Pope, M. J. T. J. o. C. P. Photovoltaic effect in organic crystals. 1959, *30* (2), 585.

(17) Geacintov, N.; Pope, M.; Kallmann, H. J. T. J. o. C. P. Photogeneration of charge carriers in tetracene. 1966, *45* (7), 2639.

(18) Kearns, D.; Calvin, M. J. T. J. o. c. p. Photovoltaic effect and photoconductivity in laminated organic systems. 1958, *29* (4), 950.

(19) Tang, C. W.; Albrecht, A. C. J. T. J. o. c. p. Photovoltaic effects of metal–chlorophyll-a–metal sandwich cells. 1975, *62* (6), 2139.

(20) Tang, C. W. J. A. P. L. Two-layer organic photovoltaic cell. 1986, *48* (2), 183.

(21) Glenis, S.; Tourillon, G.; Garnier, F. J. T. S. F. Influence of the doping on the photovoltaic properties of thin films of poly-3-methylthiophene. 1986, *139* (3), 221.

(22) Sariciftci, N. S.; Smilowitz, L.; Heeger, A. J.; Wudl, F. J. S. Photoinduced electron transfer from a conducting polymer to buckminsterfullerene. 1992, *258* (5087), 1474.

(23) Sariciftci, N.; Braun, D.; Zhang, C.; Srdanov, V.; Heeger, A.; Stucky, G.; Wudl, F. J. A. p. l. Semiconducting polymer-buckminsterfullerene heterojunctions: Diodes, photodiodes, and photovoltaic cells. 1993, *62* (6), 585.

(24) Yu, G.; Gao, J.; Hummelen, J. C.; Wudl, F.; Heeger, A. J. J. S. Polymer photovoltaic cells: enhanced efficiencies via a network of internal donor-acceptor heterojunctions. 1995, *270* (5243), 1789.
(25) Ramos, A.; Rispens, M.; van Duren, J. J. J. A. C. S. Hummelen JC and Janssen RAJ. 2001, *2001*, 123.
(26) McEvoy, A.; Markvart, T.; Castañer, L.; Castaner, L. *Practical Handbook of Photovoltaics: Fundamentals and Applications*; Elsevier Science, 2012.
(27) Knupfer, M. J. A. P. A. Exciton binding energies in organic semiconductors. 2003, *77* (5), 623.
(28) Su, Y.-W.; Lan, S.-C.; Wei, K.-H. J. M. T. Organic photovoltaics. 2012, *15* (12), 554.
(29) Nakamura, J. *Image Sensors and Signal Processing for Digital Still Cameras*; CRC Press, 2017.
(30) Bakhshi, A.; Bhalla, G. Electrically conducting polymers: Materials of the twentyfirst century. 2004.
(31) Marks, R.; Halls, J.; Bradley, D.; Friend, R.; Holmes, A. J. J. o. P. C. M. The photovoltaic response in poly (p-phenylene vinylene) thin-film devices. 1994, *6* (7), 1379.
(32) Hoppe, H.; Sariciftci, N. S. J. J. o. M. C. Morphology of polymer/fullerene bulk heterojunction solar cells. 2006, *16* (1), 45.
(33) Sariciftci, N.; Hebger, A. J. I. J. o. M. P. B. Reversible, metastable, ultrafast photoinduced electron transfer from semiconducting polymers to buckminsterfullerene and in the corresponding donor/acceptor heterojunctions. 1994, *8* (03), 237.
(34) Deibel, C.; Strobel, T.; Dyakonov, V. J. A. m. Role of the charge transfer state in organic donor–acceptor solar cells. 2010, *22* (37), 4097.
(35) Yu, G.; Heeger, A. J. J. J. o. A. P. Charge separation and photovoltaic conversion in polymer composites with internal donor/acceptor heterojunctions. 1995, *78* (7), 4510.
(36) Scharber, M. C.; Mühlbacher, D.; Koppe, M.; Denk, P.; Waldauf, C.; Heeger, A. J.; Brabec, C. J. J. A. m. Design rules for donors in bulk-heterojunction solar cells—Towards 10% energy-conversion efficiency. 2006, *18* (6), 789.
(37) Hoppe, H.; Sariciftci, N. S. J. J. o. m. r. Organic solar cells: An overview. 2004, *19* (7), 1924.
(38) Nunzi, J.-M. J. C. R. P. Organic photovoltaic materials and devices. 2002, *3* (4), 523.
(39) Cheng, Y.-J.; Yang, S.-H.; Hsu, C.-S. J. C. r. Synthesis of conjugated polymers for organic solar cell applications. 2009, *109* (11), 5868.
(40) Nelson, J. J. C. O. i. S. S.; Science, M. Organic photovoltaic films. 2002, *6* (1), 87.
(41) Spanggaard, H.; Krebs, F. C. J. S. E. M.; Cells, S. A brief history of the development of organic and polymeric photovoltaics. 2004, *83* (2-3), 125.
(42) Peumans, P.; Yakimov, A.; Forrest, S. R. J. J. o. A. P. Small molecular weight organic thin-film photodetectors and solar cells. 2003, *93* (7), 3693.
(43) Coakley, K. M.; McGehee, M. D. J. C. o. m. Conjugated polymer photovoltaic cells. 2004, *16* (23), 4533.
(44) Halls, J.; Pichler, K.; Friend, R.; Moratti, S.; Holmes, A. J. S. m. Exciton dissociation at a poly (p-phenylenevinylene)/C60 heterojunction. 1996, *77* (1-3), 277.
(45) Günes, S.; Neugebauer, H.; Sariciftci, N. S. J. C. r. Conjugated polymer-based organic solar cells. 2007, *107* (4), 1324.
(46) Winder, C.; Sariciftci, N. S. J. J. o. M. C. Low bandgap polymers for photon harvesting in bulk heterojunction solar cells. 2004, *14* (7), 1077.
(47) Xue, J.; Uchida, S.; Rand, B. P.; Forrest, S. R. J. A. P. L. 4.2% efficient organic photovoltaic cells with low series resistances. 2004, *84* (16), 3013.

(48) Graupner, W.; Leising, G.; Lanzani, G.; Nisoli, M.; De Silvestri, S.; Scherf, U. J. P. r. l. Femtosecond relaxation of photoexcitations in a poly (para-phenylene)-type ladder polymer. 1996, *76* (5), 847.
(49) Zhou, H.; Yang, L.; You, W. J. M. Rational design of high performance conjugated polymers for organic solar cells. 2012, *45* (2), 607.
(50) Tessler, N.; Denton, G.; Friend, R. J. N. Lasing from conjugated-polymer microcavities. 1996, *382* (6593), 695.
(51) Bartelt, J. A.; Beiley, Z. M.; Hoke, E. T.; Mateker, W. R.; Douglas, J. D.; Collins, B. A.; Tumbleston, J. R.; Graham, K. R.; Amassian, A.; Ade, H. J. A. E. M. The importance of fullerene percolation in the mixed regions of polymer–fullerene bulk heterojunction solar cells. 2013, *3* (3), 364.
(52) Liu, Y.; Zhao, J.; Li, Z.; Mu, C.; Ma, W.; Hu, H.; Jiang, K.; Lin, H.; Ade, H.; Yan, H. J. N. c. Aggregation and morphology control enables multiple cases of high-efficiency polymer solar cells. 2014, *5*, 5293.
(53) Ma, W.; Yang, C.; Gong, X.; Lee, K.; Heeger, A. J. J. A. F. M. Thermally stable, efficient polymer solar cells with nanoscale control of the interpenetrating network morphology. 2005, *15* (10), 1617.
(54) Zhou, H.; Yang, L.; Stoneking, S.; You, W. J. A. a. m.; interfaces. A weak donor−strong acceptor strategy to design ideal polymers for organic solar cells. 2010, *2* (5), 1377.
(55) He, Z.; Zhong, C.; Huang, X.; Wong, W. Y.; Wu, H.; Chen, L.; Su, S.; Cao, Y. J. A. M. Simultaneous enhancement of open-circuit voltage, short-circuit current density, and fill factor in polymer solar cells. 2011, *23* (40), 4636.
(56) Inganäs, O.; Svensson, M.; Zhang, F.; Gadisa, A.; Persson, N.-K.; Wang, X.; Andersson, M. J. A. P. A. Low bandgap alternating polyfluorene copolymers in plastic photodiodes and solar cells. 2004, *79* (1), 31.
(57) Brabec, C. J. J. S. e. m.; cells, s. Organic photovoltaics: technology and market. 2004, *83* (2-3), 273.
(58) Haruk, A.; Mativetsky, J. J. I. j. o. m. s. Supramolecular approaches to nanoscale morphological control in organic solar cells. 2015, *16* (6), 13381.
(59) Kim, F. S.; Ren, G.; Jenekhe, S. A. J. C. o. M. One-dimensional nanostructures of π-conjugated molecular systems: assembly, properties, and applications from photovoltaics, sensors, and nanophotonics to nanoelectronics. 2010, *23* (3), 682.
(60) Soci, C.; Hwang, I. W.; Moses, D.; Zhu, Z.; Waller, D.; Gaudiana, R.; Brabec, C. J.; Heeger, A. J. J. A. F. M. Photoconductivity of a low-bandgap conjugated polymer. 2007, *17* (4), 632.
(61) Arias, A.; MacKenzie, J.; Stevenson, R.; Halls, J.; Inbasekaran, M.; Woo, E.; Richards, D.; Friend, R. J. M. Photovoltaic performance and morphology of polyfluorene blends: a combined microscopic and photovoltaic investigation. 2001, *34* (17), 6005.
(62) Gadisa, A.; Svensson, M.; Andersson, M. R.; Inganäs, O. J. A. P. L. Correlation between oxidation potential and open-circuit voltage of composite solar cells based on blends of polythiophenes/fullerene derivative. 2004, *84* (9), 1609.
(63) Qi, B.; Wang, J. J. P. C. C. P. Fill factor in organic solar cells. 2013, *15* (23), 8972.
(64) Jeong, W. I.; Lee, J.; Park, S. Y.; Kang, J. W.; Kim, J. J. J. A. F. M. Reduction of collection efficiency of charge carriers with increasing cell size in polymer bulk heterojunction solar cells. 2011, *21* (2), 343.
(65) Gupta, D.; Bag, M.; Narayan, K. J. A. P. L. Area dependent efficiency of organic solar cells. 2008, *93* (16), 384.

(66) Friend, R. J. P.; Chemistry, A. Conjugated polymers. New materials for optoelectronic devices. 2001, *73* (3), 425.
(67) Natta, G.; Mazzanti, G.; Corradini, P. J. S. F., Mat. Nat., Rend. Atti Accad. Naz. Lincei, Cl. 1958, *25* (3).
(68) Ito, T.; Shirakawa, H.; Ikeda, S. J. J. o. p. s. p. c. e. Simultaneous polymerization and formation of polyacetylene film on the surface of concentrated soluble Ziegler-type catalyst solution. 1974, *12* (1), 11.
(69) Skotheim, T.; Reynolds, J.; CRC Press, Boca Raton, 2007.
(70) Heeger, A. J.; ACS Publications, 2001.
(71) Salzner, U.; Lagowski, J.; Pickup, P.; Poirier, R. J. S. M. Comparison of geometries and electronic structures of polyacetylene, polyborole, polycyclopentadiene, polypyrrole, polyfuran, polysilole, polyphosphole, polythiophene, polyselenophene and polytellurophene. 1998, *96* (3), 177.
(72) Barrow, G.; Chap.
(73) Reddinger, J. L.; Reynolds, J. R. In *Radical Polymerisation Polyelectrolytes*; Springer, 1999.
(74) Pron, A.; Rannou, P. J. P. i. p. s. Processible conjugated polymers: from organic semiconductors to organic metals and superconductors. 2002, *27* (1), 135.
(75) Ajayaghosh, A. J. C. S. R. Donor–acceptor type low band gap polymers: polysquaraines and related systems. 2003, *32* (4), 181.
(76) Roncali, J. J. C. r. Synthetic principles for bandgap control in linear π-conjugated systems. 1997, *97* (1), 173.
(77) Strobl, G. J. L. N. P. The physics of polymers—Concepts for understanding their structures and behaviors. 2007, *714* (1), 87.
(78) Ritchie, R. J. P. Modelling photosynthetic photon flux density and maximum potential gross photosynthesis. 2010, *48* (4), 596.
(79) Koster, L.; Mihailetchi, V.; Blom, P. J. A. P. L. Ultimate efficiency of polymer/fullerene bulk heterojunction solar cells. 2006, *88* (9), 093511.
(80) Roncali, J. J. M. R. C. Molecular engineering of the band gap of π-conjugated systems: Facing technological applications. 2007, *28* (17), 1761.
(81) Nguyen, T. L.; Choi, H.; Ko, S.-J.; Uddin, M. A.; Walker, B.; Yum, S.; Jeong, J.-E.; Yun, M.; Shin, T.; Hwang, S. J. E.et al. Semi-crystalline photovoltaic polymers with efficiency exceeding 9% in a∼ 300 nm thick conventional single-cell device. 2014, *7* (9), 3040.
(82) Lee, W.; Choi, H.; Hwang, S.; Kim, J. Y.; Woo, H. Y. J. C. A. E. J. Efficient Conventional-and Inverted-Type Photovoltaic Cells Using a Planar Alternating Polythiophene Copolymer. 2012, *18* (9), 2551.
(83) Gadisa, A.; Oosterbaan, W. D.; Vandewal, K.; Bolsée, J. C.; Bertho, S.; D'Haen, J.; Lutsen, L.; Vanderzande, D.; Manca, J. V. J. A. F. M. Effect of Alkyl Side-Chain Length on Photovoltaic Properties of Poly (3-alkylthiophene)/PCBM Bulk Heterojunctions. 2009, *19* (20), 3300.
(84) Wang, E.; Wang, M.; Wang, L.; Duan, C.; Zhang, J.; Cai, W.; He, C.; Wu, H.; Cao, Y. J. M. Donor polymers containing benzothiadiazole and four thiophene rings in their repeating units with improved photovoltaic performance. 2009, *42* (13), 4410.
(85) Yang, L.; Zhou, H.; You, W. J. T. J. o. P. C. C. Quantitatively analyzing the influence of side chains on photovoltaic properties of polymer− fullerene solar cells. 2010, *114* (39), 16793.
(86) Chandrasekhar, P. *Conducting Polymers, Fundamentals and Applications: A Practical Approach*; Springer US, 1999.
(87) Sakamoto, J.; Rehahn, M.; Schlüter, A.; WILEY-VCH, Weinheim, 2010.

(88) Leclerc, M.; Morin, J. F. *Design and Synthesis of Conjugated Polymers*; Wiley, 2010.
(89) Miyaura, N.; Suzuki, A. J. C. r. Palladium-catalyzed cross-coupling reactions of organoboron compounds. 1995, *95* (7), 2457.
(90) Miura, Y.; Oka, H.; Morita, M. J. M. Syntheses and Characterization of Poly (1, 3-phenylene-2-amino-1, 3-phenylene) s and Dimer and Tetramer Model Compounds. 1998, *31* (7), 2041.
(91) Littke, A. F.; Dai, C.; Fu, G. C. J. J. o. t. A. C. S. Versatile catalysts for the Suzuki cross-coupling of arylboronic acids with aryl and vinyl halides and triflates under mild conditions. 2000, *122* (17), 4020.
(92) Suzuki, A. J. P.; chemistry, a. Organoboron compounds in new synthetic reactions. 1985, *57* (12), 1749.
(93) Farina, V.; Krishnamurthy, V.; Scott, W. J. J. O. r. The Stille Reaction. 2004.
(94) Casado, A. L.; Espinet, P.; Gallego, A. M. J. J. o. t. A. C. S. Mechanism of the Stille reaction. 2. Couplings of aryl triflates with vinyltributyltin. Observation of intermediates. A more comprehensive scheme. 2000, *122* (48), 11771.
(95) Hassan, J.; Sevignon, M.; Gozzi, C.; Schulz, E.; Lemaire, M. J. C. R. Aryl− aryl bond formation one century after the discovery of the Ullmann reaction. 2002, *102* (5), 1359.
(96) Bao, Z.; Chan, W.; Yu, L. J. C. o. m. Synthesis of conjugated polymer by the stille coupling reaction. 1993, *5* (1), 2.
(97) Milstein, D.; Stille, J. K. A General, Selective, and Facile Method for Ketone Synthesis from Acid Chlorides and Organotin Compounds Catalyzed by Palladium. J. Am. Chem. Soc. 1978, 100 (11), 3636–3638.
(98) Yang, C.; Scheiber, H.; List, E. J.; Jacob, J.; Müllen, K. J. M. Poly (2, 7-phenanthrylene) s and Poly (3, 6-phenanthrylene) s as Polyphenylene and Poly (phenylenevinylene) Analogues. 2006, *39* (16), 5213.
(99) Kim, Y.-A.; Hwang, K.-I.; Kang, M.; Kim, N.-K.; Jang, S.-y.; Kim, I.-B.; Kim, J.; Kim, D.-Y. J. O. E. Effect of side chains on phenanthrene based DA type copolymers for polymer solar cells. 2017, *44*, 238.
(100) Hanemann, T.; Böhm, J.; Honnef, K.; Ritzhaupt-Kleissl, E.; Haußelt, J. Polymer/Phenanthrene-Derivative Host-Guest Systems: Rheological, Optical and Thermal Properties. 2007, *292* (3), 285.
(101) Schoental, R.; Clar, E. *Polycyclic Hydrocarbons*; Springer Berlin Heidelberg, 2013.
(102) Qi, H.; Chen, Y.-H.; Cheng, C.-H.; Bard, A. J. Electrochemistry and Electrogenerated Chemiluminescence of Three Phenanthrene Derivatives, Enhancement of Radical Stability, and Electrogenerated Chemiluminescence Efficiency by Substituent Groups. J. Am. Chem. Soc. 2013, 135 (24), 9041–9049.
(103) Schreivogel, A.; Sieger, M.; Baro, A.; Laschat, S. J. H. C. A. Synthesis and Redox Behavior of Novel 9, 10-Diphenylphenanthrenes. 2010, *93* (10), 1912.
(104) Hepworth, J.; Waring, D.; Waring, M.; John Wiley and Sons, New York, 2003.
(105) Jo, M. Y.; Bae, J. H.; Lim, G. E.; Ha, Y. E.; Katz, H. E.; Kim, J. H. J. S. M. Photovoltaic properties of low band gap polymer based on phenanthrene and diketopyrrolopyrrole. 2013, *176*, 41.
(106) Zhang, Y.; Huang, L.; Wang, C.; Gao, D.; Zuo, Z. J. C. Phenanthrene exposure produces cardiac defects during embryo development of zebrafish (Danio rerio) through activation of MMP-9. 2013, *93* (6), 1168.
(107) Nayak, M. K. J. J. o. P.; Chemistry, P. A. Synthesis, characterization and optical properties of aryl and diaryl substituted phenanthroimidazoles. 2012, *241*, 26.

(108) Ozaki, K.; Kawasumi, K.; Shibata, M.; Ito, H.; Itami, K. One-shot K-region-selective annulative π-extension for nanographene synthesis and functionalization. *Nature Communications* 2015, *6*, 6251.
(109) Schmitt, W. J.; Moriconi, E. J.; O'Connor, W. F. J. J. o. t. A. C. S. The Ozonolysis of Phenanthrene1. 1955, *77* (21), 5640.
(110) de Azeredo, S. O. F.; Figueroa-Villar, J. D. J. W. J. o. P.; Sciences, P. Phenanthrene derivatives for synthesis and applications in medicinal chemistry: a review. 2014, *3* (11).
(111) Raouafi, S.; Aloui, F.; Raouafi, A.; Hassine, B. B. J. C. R. C. Synthesis and characterization of phenanthrene derivatives for optoelectronic applications. 2017, *20* (7), 697.
(112) Dadsetani, M.; Ebrahimian, A.; Nejatipour, H. J. M. S. i. S. P. Phase transition and related electronic and optical properties of crystalline phenanthrene: An ab initio investigation. 2015, *34*, 236.
(113) Bouzayani, B.; Ben Salem, R.; Soulé, J. F.; Doucet, H. J. E. J. o. O. C. Synthesis of C9, C10-Diheteroarylated Phenanthrenes via Palladium-Catalyzed C–H Bond Activation. 2018, *2018* (44), 6092.
(114) Grisorio, R.; Suranna, G. P.; Mastrorilli, P.; Nobile, C. F. J. O. l. A versatile synthesis for new 9, 10-bis (4-alkoxyphenyl)-2, 7-diiodophenanthrenes: useful precursors for conjugated polymers. 2007, *9* (16), 3149.
(115) Arora, K.; Verma, S.; Joshi, R.; Pardasani, P.; Pardasani, R. Synthesis, configurational analysis and antimicrobial activity of imidazolidinone, thiazolidinone and isoxazolone derivatives of 9, 10-phenanthrenequinone. 2011.
(116) Bhatt, M. J. T. Quinone studies—I: Evidence for a new type of substitution reaction of phenanthrene-9, 10-quinone derivatives. 1964, *20* (4), 803.
(117) Guédouar, H.; Aloui, F.; Moussa, S.; Marrot, J.; Hassine, B. B. J. T. L. Synthesis and characterization of new heptacyclic helicenes. 2014, *55* (45), 6167.
(118) Guédouar, H.; Aloui, F.; Beltifa, A.; Mansour, H. B.; Hassine, B. B. J. C. R. C. Synthesis and characterization of phenanthrene derivatives with anticancer property against human colon and epithelial cancer cell lines. 2017, *20* (8), 841.
(119) Mohammadi, M. K. J. O. J. o. S. T.; Applications. Microwave-Assisted Oxidation of Organic Compounds with Cetyltrimethylammonium Chlorochromate. 2013, *2* (03), 87.
(120) Boden, B. N.; Jardine, K. J.; Leung, A. C.; MacLachlan, M. J. J. O. l. Tetraalkoxyphenanthrene: a new precursor for luminescent conjugated polymers. 2006, *8* (9), 1855.
(121) Kim, Y.-A.; Kang, M.; Jeon, Y.-J.; Hwang, K.; Kim, Y.-J.; Jang, S.-Y.; Kim, I.-B.; Kwon, G.; Kim, D.-Y. J. J. o. M. C. C. Structure–property relationship of D–A type copolymers based on phenanthrene and naphthalene units for organic electronics. 2017, *5* (39), 10332.
(122) Li, S.; He, Z.; Yu, J.; Zhong, A.; Tang, R.; Wu, H.; Qin, J.; Li, Z. J. J. o. M. C. How the linkage positions affect the performance of bulk-heterojunction polymer solar cells. 2012, *22* (25), 12523.
(123) Brédas, J.; Thémans, B.; Fripiat, J.; André, J.; Chance, R. J. P. R. B. Highly conducting polyparaphenylene, polypyrrole, and polythiophene chains: An ab initio study of the geometry and electronic-structure modifications upon doping. 1984, *29* (12), 6761.
(124) Li, S.; Zhao, B.; He, Z.; Yu, J.; Zhong, A.; Tang, R.; Wu, H.; Li, Q.; Qin, J.; Li, Z. J. J. o. M. C. A. Synthesis, characterization and photovoltaic performances of D–A

copolymers based on BDT and DBPz: the largely improved performance caused by additional thiophene blocks. 2013, *1* (14), 4508.
(125) Mazzio, K. A.; Luscombe, C. K. J. C. S. R. The future of organic photovoltaics. 2014, *44* (1), 78.
(126) Brabec, C. J.; Gowrisanker, S.; Halls, J. J.; Laird, D.; Jia, S.; Williams, S. P. J. A. M. Polymer–fullerene bulk-heterojunction solar cells. 2010, *22* (34), 3839.
(127) Wang, G.; Swensen, J.; Moses, D.; Heeger, A. J. J. J. o. a. p. Increased mobility from regioregular poly (3-hexylthiophene) field-effect transistors. 2003, *93* (10), 6137.
(128) Brabec, C. J.; Zerza, G.; Cerullo, G.; De Silvestri, S.; Luzzati, S.; Hummelen, J. C.; Sariciftci, S. J. C. P. L. Tracing photoinduced electron transfer process in conjugated polymer/fullerene bulk heterojunctions in real time. 2001, *340* (3-4), 232.
(129) Hummelen, J. C.; Knight, B. W.; LePeq, F.; Wudl, F.; Yao, J.; Wilkins, C. L. J. T. J. o. O. C. Preparation and characterization of fulleroid and methanofullerene derivatives. 1995, *60* (3), 532.
(130) Wienk, M. M.; Kroon, J. M.; Verhees, W. J.; Knol, J.; Hummelen, J. C.; van Hal, P. A.; Janssen, R. A. J. A. C. I. E. Efficient methano [70] fullerene/MDMO-PPV bulk heterojunction photovoltaic cells. 2003, *42* (29), 3371.
(131) He, Y.; Chen, H.-Y.; Hou, J.; Li, Y. J. J. o. t. A. C. S. Indene− C60 bisadduct: a new acceptor for high-performance polymer solar cells. 2010, *132* (4), 1377.
(132) He, Y.; Zhao, G.; Peng, B.; Li, Y. J. A. F. M. High-Yield Synthesis and Electrochemical and Photovoltaic Properties of Indene-C70 Bisadduct. 2010, *20* (19), 3383.

Chapter 2: Phenanthrene-Difluoro-Quinoxaline, Donor-Acceptor Polymers for OPV applications

Abstract

P1, **P2**, **P3** and **P4** are four new donor-acceptor conjugated copolymers, synthesised *via* Suzuki cross-coupling. **P1** and **P3** consist of alternating quinoxaline repeating units as electron acceptors, with phenanthro[9,10-b]quinoxaline units as electron donor, while **P2** and **P4** consist of alternating quinoxaline units with phenanthrene-9,10-dialkoxy. These copolymers are designed by taking into consideration some parameters that affect the electrical and optical properties of conjugated polymers. The acceptor has substituents of two fluorine atoms in the positions 6 and 7 of the quinoxaline unit to investigate the effects of deepening the HOMO energy levels. Two different alkoxyl substituents are incorporated to the donor moieties to produce good solubility in many organic solvents at room temperature. In addition, a number of thienyl units are attached between the donor-acceptor units along the polymer chains to increase the conjugation system. The report also presents the results of the synthesis of the monomers and copolymers, as well as the data collected from UV-Vis, CV analysis and TGA for the synthesised copolymers. **P1** and **P2** exhibit similar optical band gaps with values of 1.97 eV and 1.98 eV respectively. **P3** and **P4** display narrower optical band gaps than **P1** and **P2** with values of 1.80 eV and 1.83 eV respectively, due to the extension of the conjugation system by the addition of thiophene units to **P3** and **P4**. The HOMO level of **P2** is the deepest with a value of -5.57 eV. **P2** has reduced conjugation compared with the others, leading to a wider electrochemical band gap with a value of 1.99 eV. All the polymers show good thermal stability with decomposition temperatures in excess of 330 ˚C, which is sufficient for the requirements of OSC applications.

2.1. Introduction

Conjugated polymers show promise as constituents of OPVs due to their advantages compared with inorganic PV cells. These are: ease of fabrication, high absorption coefficients, reduced toxicity of materials, flexible substrates and low-cost production.[1] Research and development of BHJ solar cells have drawn attention to the synthesis of conjugated polymers as electron donors and fullerene derivatives as electron acceptors. The PCEs of OPVs have improved to reach more than 10 per cent,[2] due to the tunability of conjugated polymers and the enhancement of the morphology of the active layers of BHJ solar cells.[3]

Previous studies have shown that BHJ solar cells fabricated from polymers consisting of an electron-rich donor unit and an electron-deficient acceptor monomer in an arrangement of D-A results in higher PCEs.[4] This is a consequence of hybridisation between the donor HOMO and acceptor LUMO, which results in a reduction of the band gap.[5] This D-A arrangement improves ICT along the polymer backbone chain, and hence promotes mobility of charge carriers. In addition, this arrangement enables the conjugated polymers to harvest large numbers of photons from the whole solar spectrum.[5]

Quinoxaline units are widely used in polymer solar cells (PSCs), which show PCEs of up to six per cent.[6] In a recent study, Zhao *et al.* reported the synthesis of a copolymer based on two fluorine-substituted quinoxaline derivatives, abbreviated as **PBDTT-DFTQ** (Figure 2.1.a.), which showed an enhanced PCE of 7.76 per cent.[7] Since the quinoxaline units show strong electron-withdrawing characteristics, the high PCE is due to the two symmetrical, unsaturated electronegative nitrogen atoms.[8,9,9] The use of quinoxaline units maintains a quinoidal, planar structure, which extends the π-electron system across the polymer and results in a reduced band gap.[10] This is illustrated in Figure 2.1.b.

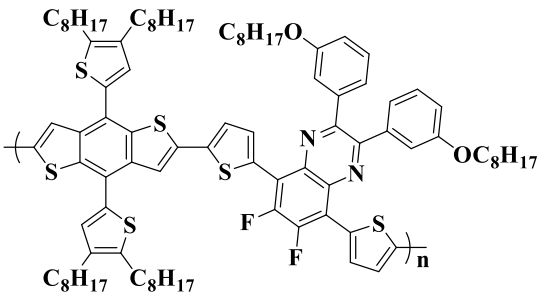

Figure 2.1a. Polymer structures of PBDTT-DFTQ synthesised by Zhao and co-workers.

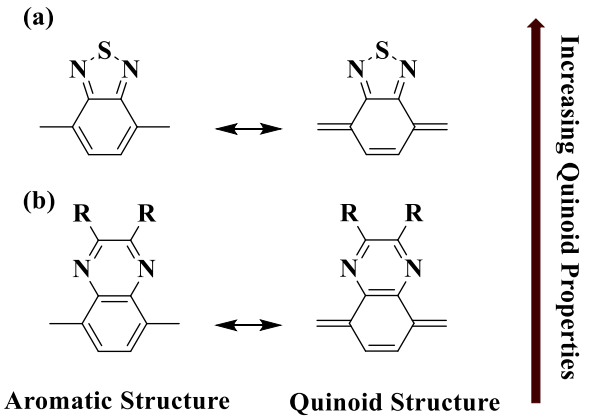

Figure 2.1b. Aromatic and quinoidal structures of (a) benzothiadiazole and (b) quinoxaline acceptor units.[10]

However, some polymers based on quinoxaline units display low PCEs owing to their low solubility and relatively low molecular weights.[11] An approach is possible to promote the solubility of the copolymers in organic solvents by the introduction of solubilising side chains such as long flexible alkoxy or alkyl chains to the quinoxaline unit. However, the addition of side chains may cause steric interactions that can affect the planar structure of the polymer backbone, thus altering the electrochemical and optical properties of the D-A polymers.[12]

A study by Park *et al.* showed the impact of the positions of solubilising groups in polymers, and their effects on their optical and electrochemical properties in PV cells.[13] The researchers synthesised polymers with an octyloxy solubilising group in various positions. One polymer with the side chain attached in the *para*-position was named **PPQP**, while the other with the side chain attached in the *meta*-position was named **PQPM** (Figure 2.2).[13]

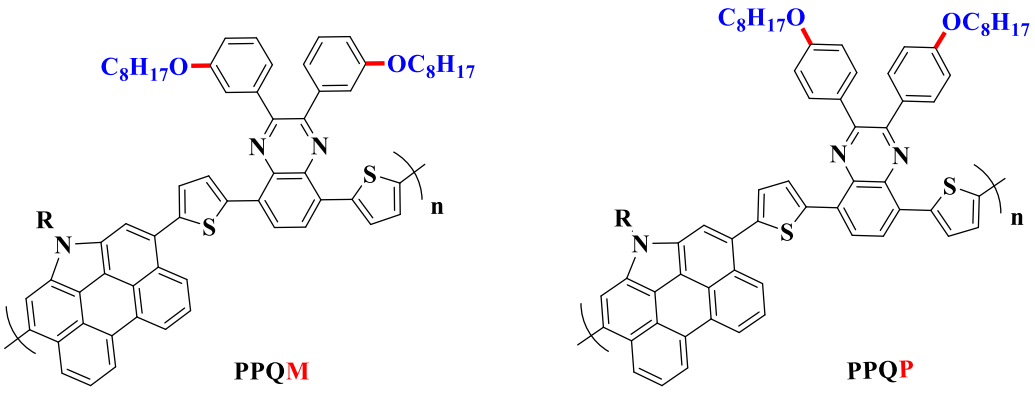

Figure 2.2. Polymer structures of PPQP and PPQM synthesised by Park and co-workers.[13]

PPQM exhibited a narrower optical band gap and lower HOMO energy level when compared with **PPQP**. This is due to the position of the octyloxy side chains on the quinoxaline units.[13] Park *et al.* theorised that the introduction of the solubilising groups in the *meta*-position decreased the electron density of the quinoxaline and therefore drove the quinoxaline moiety towards greater electron deficiency and stronger electron acceptance, which led to a higher PCE of the polymer.[13]

The PCE of these polymers can also be improved through the introduction of additional electron-withdrawing groups such as fluorine atoms to the quinoxaline units. This enables reduction of the HOMO energy levels of the polymers, and this is understood to increase the V_{oc}, which leads to a higher PCE.[14]

Dang *et al.* studied the influence of fluorine substitution of the quinoxaline units on the PV properties of polymers.[15] The polymers **PTQTI** and **PTQTI-F,** in which fluorine atoms were substituted for hydrogen atoms, were prepared. Their structures are shown in Figure 2.3.

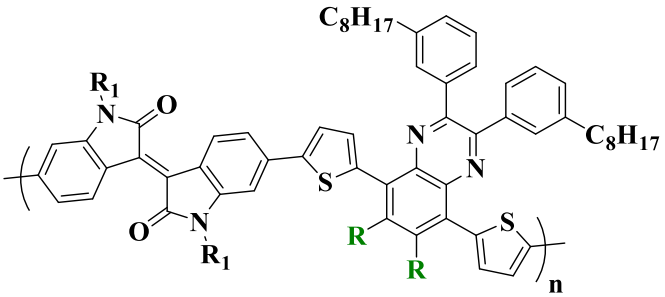

PTQTI-F; R = F

PTQTI; R = H

Figure 2.3. Polymer structures of PTQTI-F and PTQTI synthesised by Dang and co-workers.[15]

The fluorinated polymer **PTQTI-F** showed a lower HOMO energy level of -5.90 eV when compared with its non-fluorinated analogue polymer **PTQTI**, which showed a HOMO energy level of -5.80 eV.[15] This resulted in improved PV performance within BHJ solar cells. Dang *et al.* hypothesised that this behaviour could be attributed to the incorporation of fluorine atoms on the quinoxaline unit.

In this study, we report the synthesis of a series of conjugated polymers that consist of alternating quinoxaline units and two frequently used donor segments: phenanthro[9,10-b]quinoxaline and 9,10-dialkoxy-phenanthreneunits. The two copolymers produced are: poly

[11,12-bis-(2-hexyl-decyloxy)-phenanthro[9,10-b]quinoxaline(2,7-di-yl)-alt-(2,3-bis(3-(octyloxy)phenyl)-6,7-difluoro-5,8-bis(2-thienyl)quinoxaline)-5,5-(di-yl)] (**P1**) and poly [9,10-bis-(2-butyl-octyloxy)-2,7-phenanthrene-alt-[2,3-bis(3-(octyloxy)phenyl)-6,7-difluoro-5,8-bis(2-thienyl)quinoxaline]-5,5-(di-yl)] (**P2**). The monomers used are shown in Scheme 2.1.

In addition, the conjugation within the copolymers is extended by the attachment of bithiophene units to the electron-acceptor units to reduce the optical band gap and any steric hindrance. The polymers produced in this case are: poly [[11,12-bis-(2-hexyl-decyloxy)-phenanthro[9,10-b]quinoxaline]-(2,7-di-yl)-alt-[2,3-bis(3-(octyloxy)phenyl)-6,7-difluoro-5,8-bis-(2,2'-bithiophene)-5-yl)quinoxaline]5,5-(di-yl)] (**P3**) and poly [9,10-bis-(2-butyl-octyloxy)-2,7-phenanthrene-alt-[2,3-bis(3-(octyloxy)phenyl)-6,7-difluoro-5,8-bis-(2,2'-bithiophene)-5-yl)quinoxaline]-5,5-(di-yl)] (**P4**). The monomers used are shown in Scheme 2.2.

The backbone of the quinoxaline-based copolymer behaves as a D-A system, owing to the electron deficiency of the quinoxaline units. The introduction of side chains to the quinoxaline units promotes the solubility of the copolymers and facilitates polymer characterisation. It also improves PV device fabrication.

The hypothesis is that phenanthrene-based copolymers improve the absorption of light across the spectrum and the hole transport property. Phenanthro[9,10-b]quinoxaline is a promising unit for the construction of high-efficiency copolymer donor materials, due to the planarity of the structure and the efficient hole mobility suitable for electronic energy levels. The effects of the different donor segments on the electrochemical, optical and PV characteristics of the resulting quinoxaline-based copolymers are investigated.

2.2. Results and Discussion

2.2.1. Synthesis of Monomers for the Quinoxaline-based Copolymers P1, P2, P3 and P4

Scheme 2.1 shows the required monomers to prepare polymers **P1** and **P2**. The 2,3-bis-(3-(octyloxy)phenyl)-6,7-difluoro-5,8-bis(5-bromo-2-thienyl)quinoxaline **(9)**, 2,7- bis-(4,4,5,5-tetramethyl-1,3,2-dioxaborolan-2-yl)-11,12-bis-(2-hexyldecyloxy)-phenanthrene-quinoxaline **(16)** and 2,7-bis-(4,4,5,5-tetramethyl-1,3,2-dioxaborolan-2-yl)-9,10-bis-(2-butyl-octyloxy)-phenanthrene **(19)** were synthesised successfully in good yields. The purities and structures were confirmed using ^{1}H nuclear magnetic resonance spectrometry (NMR), ^{13}C NMR, mass

spectrometry and elemental analysis. Compound **(9)** was used as an electron acceptor, and compounds **(16)** and **(19)** were used as electron-donor units to prepare polymers **P1** and **P2** respectively. The synthetic routes for the preparation of compounds **(9)**, **(16)** and **(19)** are shown in Schemes 2.3, 2.11 and 2.15 respectively.

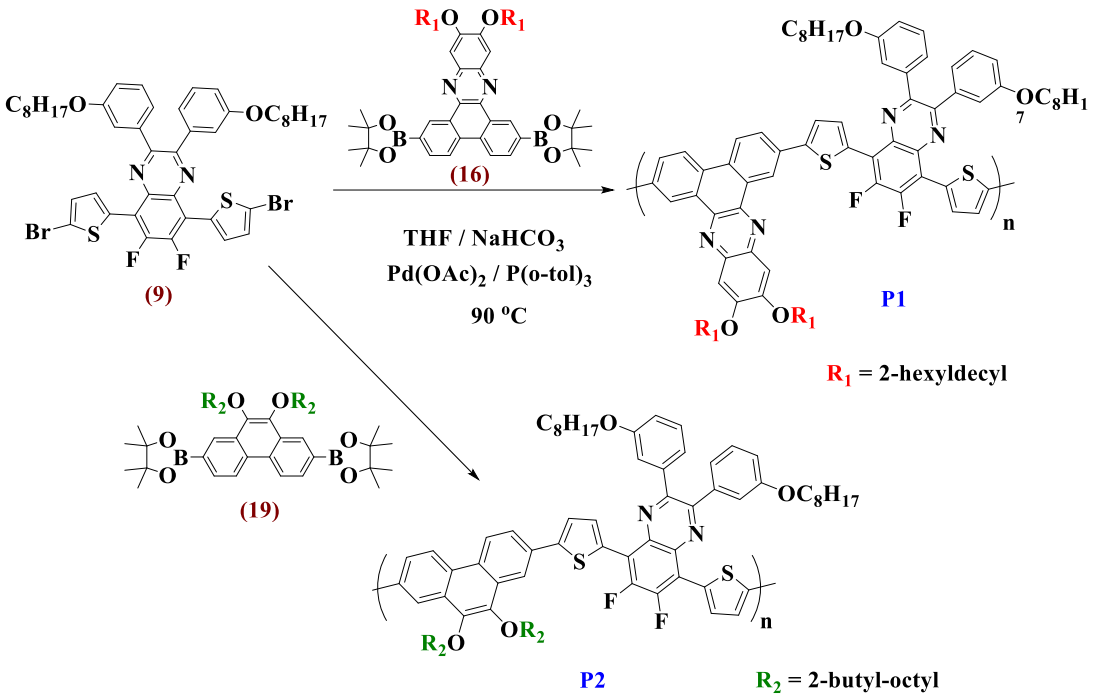

Scheme 2.1. Monomers (9), (16) and (19) that are used to prepare P1 and P2.

Scheme 2.2 shows the required monomers to prepare polymers **P3** and **P4**. The 2,3-bis-(3-(octyloxy)phenyl)-6,7-difluoro-5,8-bis(5-bromo-2-thienyl)quinoxaline **(21)**, compound **(16)** and compound **(19)** were prepared in good yields. The purities and their structures were confirmed. Compound **(21)** was used as an electron acceptor, and compounds **(16)** and **(19)** were used as electron-donor units to prepare polymers **P3** and **P4** respectively. The synthetic route for preparing compound **(21)** is shown in Scheme 2.10.

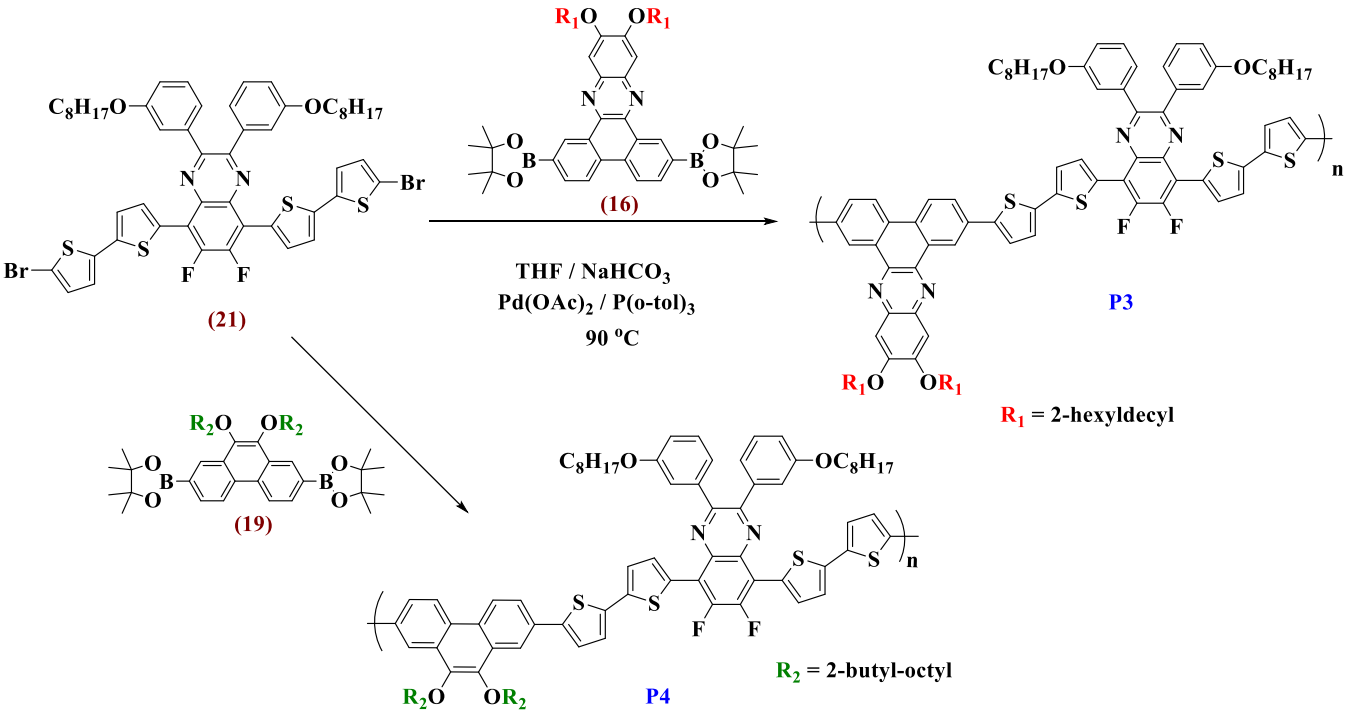

Scheme 2.2. Monomers (21), (16) and (19) that are used to prepare P3 and P4.

2.2.1.1. Synthesis of Electron Acceptor Monomers (9) and (21)

The synthetic steps for production of monomer **(9)** are depicted in Scheme 2.3.

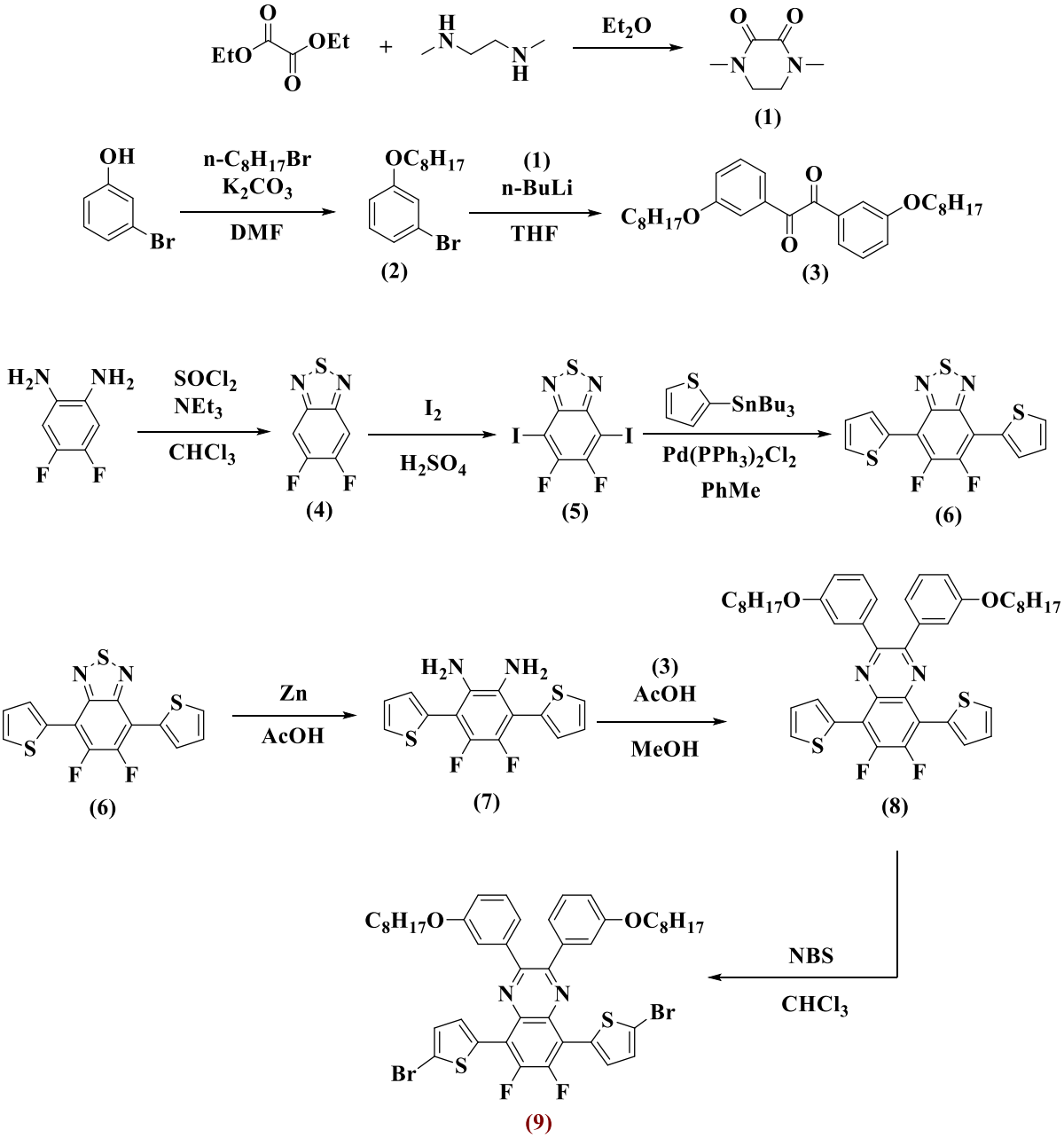

Scheme 2.3. The synthetic route to produce monomer 2,3-bis-(3-(octyloxy)phenyl)-6,7-difluoro-5,8-bis(5-bromo-2-thienyl)quinoxaline (9).

The reaction shown below is the first step in the synthetic route towards the preparation of monomer **(9)**:

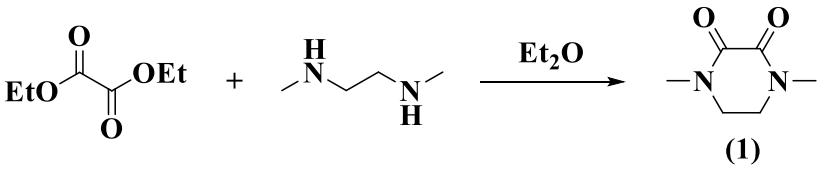

The 1,4-dimethylpiperazine-2,3-dione **(1)** was prepared *via* a procedure modified from that carried out by Ulrich *et al.*[16] The product was obtained as white needle-shaped crystals with 92 per cent yield. The structure of the product was identified by ^{1}H NMR and ^{13}C NMR. The mass spectrum for **(1)** showed a peak at 142, which was in agreement with the desired structure. The ^{1}H NMR spectrum displayed the protons of N-CH_3 and CH_2 groups as singlet peaks at 3.10 ppm and 3.58 ppm respectively. This indicated that compound **(1)** was prepared successfully. The suggested mechanism for the ring closure of compound **(1)** is shown in Scheme 2.4.

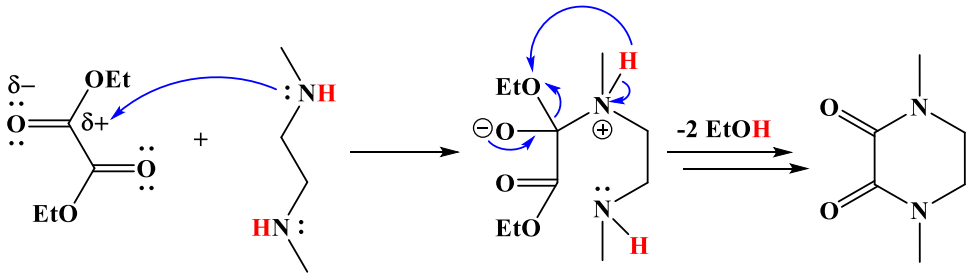

Scheme 2.4. The suggested mechanism for the ring closure of compound (1).

The reaction resulted from pericyclic reaction of a charge-transfer complex between the di-ester and the diamine, which pre-oriented the reactants from trans-conformation into their cis-conformation and enabled the lone pairs on the nucleophilic diamine to attack the carbonyl carbon atoms one at time to produce a six-membered ring with two heteroatoms and eventually the targeted product **(1)**.[16]

Then, 1-bromo-3-(octyloxy)benzene **(2)** was synthesised according to the procedure used by Zhang *et al.*:[17]

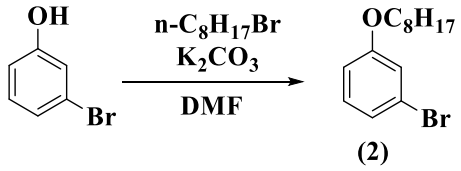

The desired product was obtained as colourless oil with a yield of 65 per cent. The purification of the product was performed by column chromatography. The product showed a single spot on thin-layer chromatography (TLC) using petroleum ether as solvent. The reaction followed the Williamson reaction mechanism of nucleophilic substitution (S_N2). This mechanism consists of two steps as shown in Scheme 2.5.

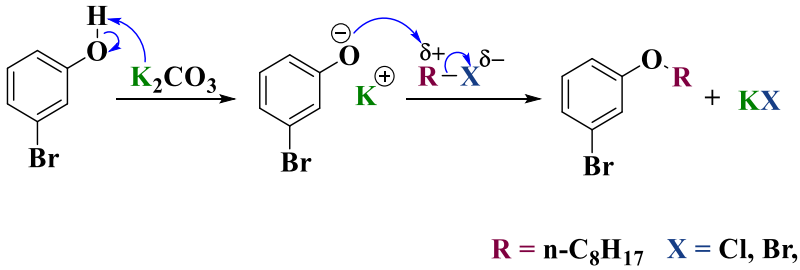

Scheme 2.5. The mechanism of production of compound (2).

The first step towards the desired compound was a deprotonation of the hydroxyl groups using a base such as potassium carbonate (K_2CO_3) to create a phenoxide ion, which in turn attacked the 1-bromooctane as a nucleophile to produce the desired product. The purity and the structure of the product **(2)** were confirmed by ^{1}H NMR, ^{13}C NMR, elemental analysis and mass spectrometry. The mass spectrum displayed the main mass at 284 (M+), which was in agreement with the desired compound. The ^{1}H NMR showed the protons of the OCH_2 and CH_3 groups as triplet peaks at 3.95 ppm and 0.91 ppm respectively, and the proton of the OH group at 5.35 ppm had disappeared.

After that, 1,2-bis(3-(octyloxy)phenyl)ethane-1,2-dione **(3)** was synthesised according to a procedure modified from that used by Mammo *et al.*,[18] by reacting compounds **(1)** and **(2)** in the presence of n-butyllithium solution as shown below:

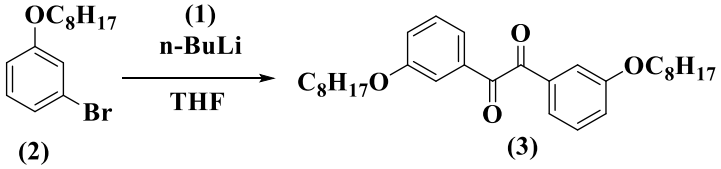

The product was obtained as a white solid with 60 per cent yield. The purification of the product was performed by precipitation in cold methanol. The purity of the product was confirmed by gas chromatography-mass spectrometry and elemental analysis. The structure was identified by ^{1}H NMR and ^{13}C NMR. The mass spectrum for compound **(3)** showed a peak at 466 as expected.

Moving on to the next reaction, 5,6-difluoro-benzo[1,2,5]thiadiazole **(4)** was synthesised according to the procedure by Wang *et al*.[19]

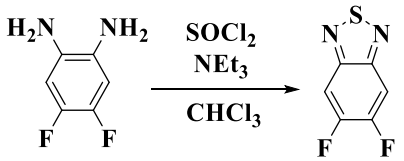

(4)

Compound **(4)** was obtained as an ivory-white solid at 60 per cent yield. The purification of the product was performed by column chromatography. All analytical results verified that product **(4)** was prepared successfully. The mass spectra showed a main integer mass at 172.0 as expected. Elemental analysis produced these results: C, 42.06; H, 1.19; N, 16.54; S, 18.54. These figures were in agreement with the calculated percentages. The ^{1}H NMR spectrum identified the product with a main distinct signal equal to intensity. The proton signal assigned to the aromatic ring system appeared at δ 7.78 ppm and was a triplet due to coupling with the nearby fluorine.

The suggested mechanism for the ring closure of compound **(4)** is shown below in Scheme 2.6.

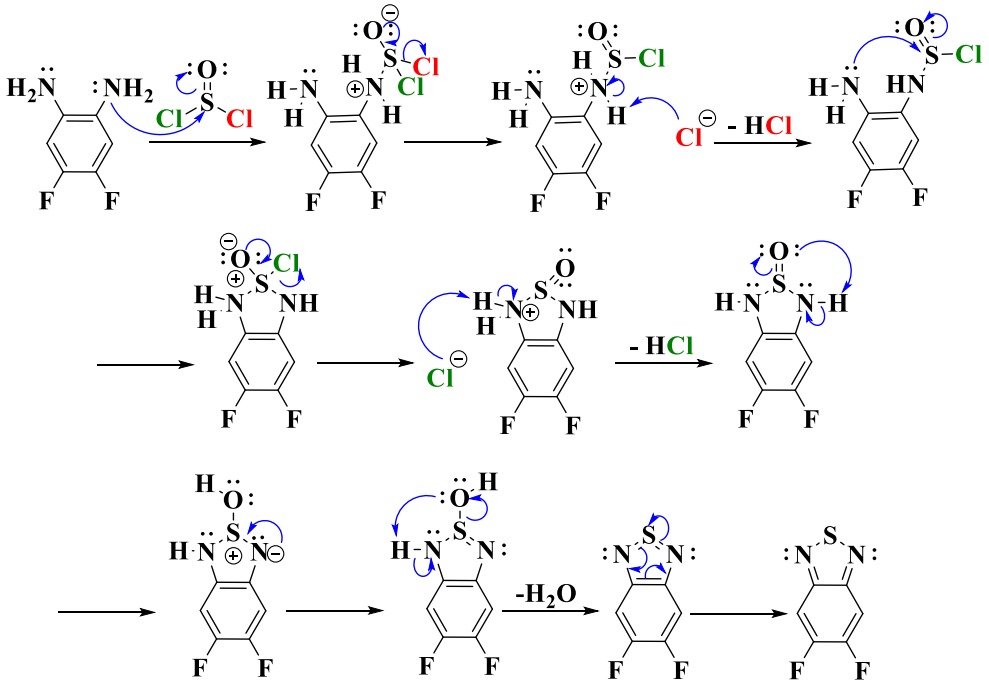

Scheme 2.6. The suggested mechanism for the ring closure of compound (4).

The nitrogen lone pairs on the amine groups act as nucleophiles and attack the sulphur of the thionyl chloride. Then hydrogen chloride is removed. The same steps occur at the other lone pair in the amine group, thus closing the ring. During the final step, the target product is formed after a water molecule is eliminated from the product by the action of hydrogen chloride, followed by electronic re-arrangement to form the product **(4)**.

Iodination of compound **(4)** then results in production of 5,6-difluoro-4,7-diiodo-benzo[1,2,5]thiadiazole **(5):**

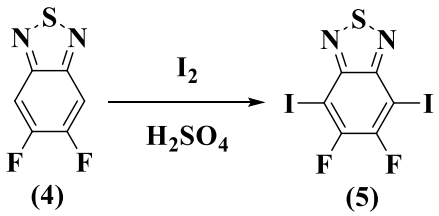

Compound **(5)** was prepared using the Wang *et al* procedure.[19] The crude compound was recrystallised using ethanol to give the desired product as cream crystals in a good yield (92 per cent). The reaction was prepared in the presence of fuming sulphuric acid as catalyst at room temperature. The sulphur trioxide (SO_3) group oxidised iodine to form the $\mathbf{I^+_2}$ cation, which increased the electrophilic activity of the iodine as shown in Equation 2.1.[20]

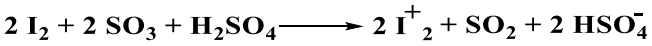

Equation 2.1. Formation of I_2^+ cation owing to oxidation of iodine by SO_3.

A lack of proton peaks in the aromatic region of the ^{1}H-NMR spectrum showed that all hydrogen atoms had been substituted by iodine atoms. The purity of the desired product **(5)** was confirmed through elemental analysis. The mass spectrum exhibited a main mass peak at 424, as expected. The suggested steps of the reaction follow the electrophilic aromatic substitution mechanism as illustrated in Scheme 2.7 below:

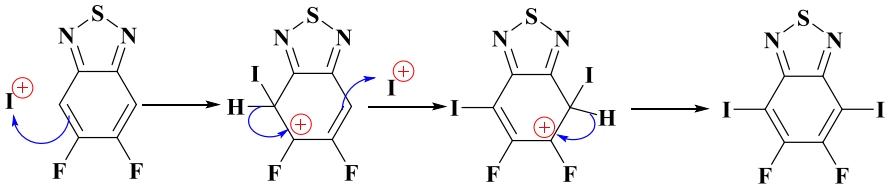

Scheme 2.7. The suggested mechanism for production of compound (5).

Electrophilic substitution of protons on the benzene ring is suggested as the reaction mechanism. Position 4 on the benzene ring attacks the iodine cation, producing an intermediate with a positive charge, which loses a proton in order to become more stable. The previous step is repeated with the proton in position 7 on the benzene ring, followed by electronic re-arrangement to produce product **(5)**.

Compound **(5)** was used to prepare compound **(6)**, which was synthesised *via* the Stille coupling reaction.[21] This coupling is a versatile form of carbon-carbon bond formation, and occurs between aryl halides and aryl stannanes in the presence of a palladium catalyst. The reaction requires one equivalent of the dihalide compound to react with two equivalents of the organostannyl compound as illustrated below.

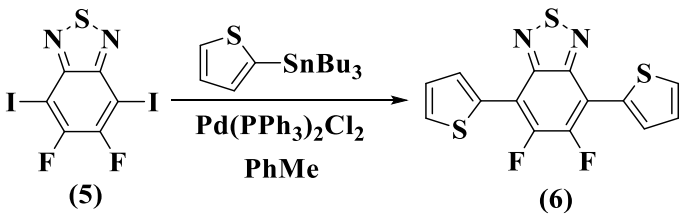

The compound 5,6-difluoro-4,7-bis(4,2-thienyl)-2,1,3-benzothiadiazole **(6)** was prepared using a procedure modified from that carried out by Zhou.[22] Compound **(6)** was obtained as

orange crystals in 90 per cent yield. The purification of the product was performed by precipitation in methanol. The purity was confirmed by a single peak by gas chromatography-mass spectrometry at 336. The ^{1}H NMR spectrum showed three signals in the aromatic region at δ 8.32 ppm, 7.63 ppm and 7.29 ppm. These signals were assigned to the protons on the thiophene ring system, and could be compared with the signal obtained from compound **(5)**, which showed no signal in this region as it had no protons in the aromatic region.

The mechanism of the Stille reaction is similar to the mechanism described in Chapter 1.[23]

Compound **(6)** was first reduced to 1,2-diamino-3,6-di(2-thienyl)-4,5-difluorobenzene **(7)** through the reaction shown below:

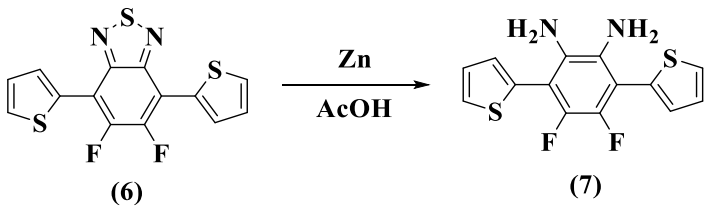

(6) **(7)**

Compound **(7)** was synthesised according to a procedure modified from that used by Tsubata.[24] The product was obtained as an orange solid with 80 per cent yield. The product **(7)** was unstable to oxidation: it was used straight after dry filtration for the next reaction without any further purification.

The next step involved a cyclocondensation reaction between compounds **(3)** and **(7)** to synthesise 2,3-bis(3-(octyloxy)phenyl)-5,8-di(2-thienyl)-6,7-difluoroquinoxaline **(8)** as follows:

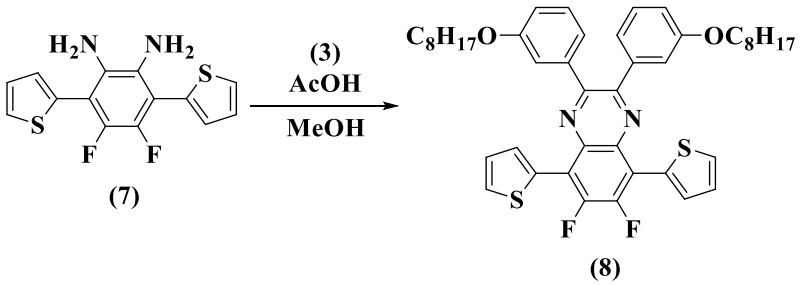

(7) **(8)**

Compound **(8)** was prepared *via* a procedure modified from that carried out by Robinson *et al*.[25] The product was obtained as a bright yellow solid with 50 per cent yield. Compound **(8)** was characterised by a number of techniques: ^{1}H NMR spectroscopy, elemental analysis and mass spectrometry. The mass spectrum for **(8)** showed a peak at 738 as expected, and this indicated that compound **(8)** had been prepared successfully.

The suggested reaction mechanism follows that of acid-catalysed condensation reactions as shown in Scheme 2.8.

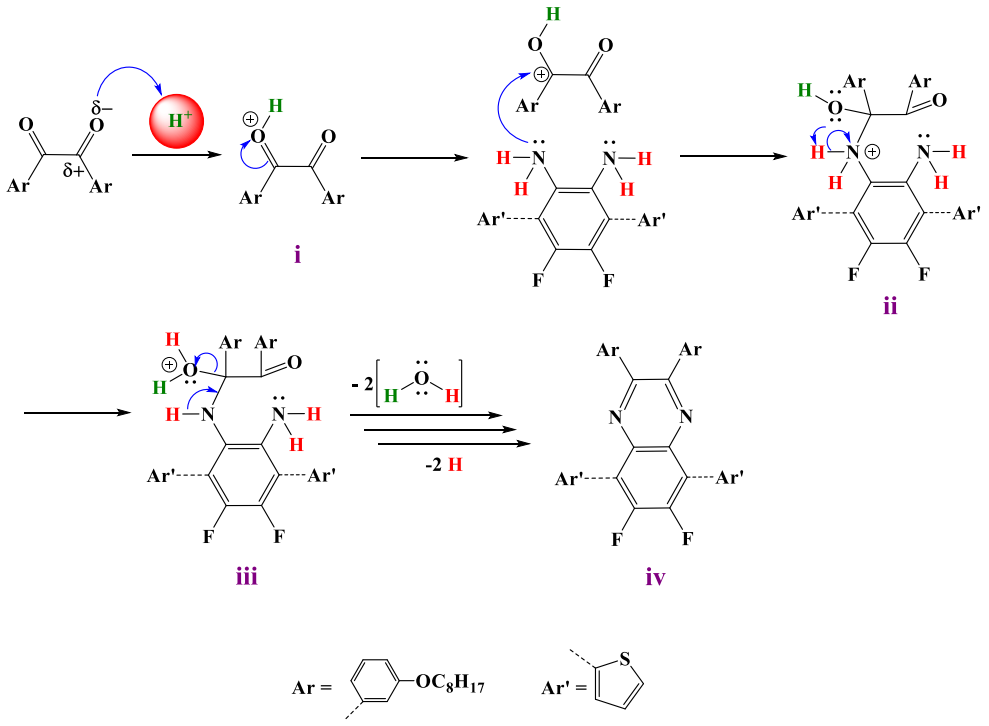

Scheme 2.8. Mechanism of production of compound (8).

First, a 1,2-dicarbonyl group coordinates with the acid sites from acetic acid **(i).** This is followed by a nucleophilic attack by lone pairs of the diamine on the carbonyl group to deliver intermediate **(ii)**, then a dehydration step produces a carbo-cation intermediate **(iii)** and finally deportation of hydrogen leads to the targeted quinoxaline product **(iv)**.[25]

Finally, bromination of both positions 5 on the thiophene rings produces monomer 2,3-bis(3-(octyloxy)phenyl)-6,7-difluoro-5,8-bis(5-bromo-2-thienyl) quinoxaline **(9)** as shown below:

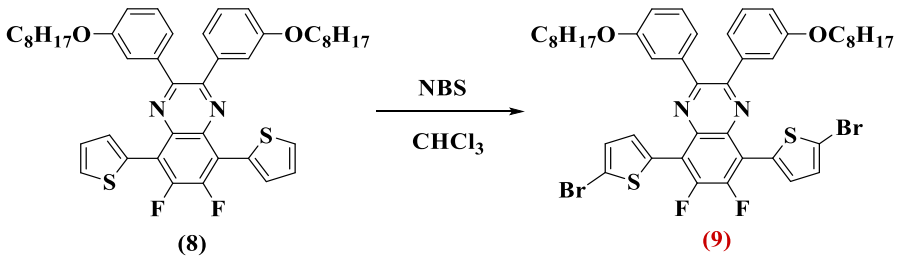

Compound **(9)** was prepared *via* a procedure modified from that carried out by Takahashi *et al*.[26] The product was obtained as an orange solid with 85 per cent yield. Purification was performed by recrystallisation in isopropanol. The purity of the product was confirmed by gas chromatography-mass spectrometry. Peaks were observed at 894, 896 and 898 owing to the presence of bromine isotopes ^{81}Br and ^{79}Br. The ^{1}H NMR spectrum showed that two protons had disappeared from the aromatic region. These were understood to be protons assigned to the thiophene ring system, and peaks for these protons could be observed in the spectrum for compound **(8)**. This was an indication that bromination of compound **(9)** had been successful.

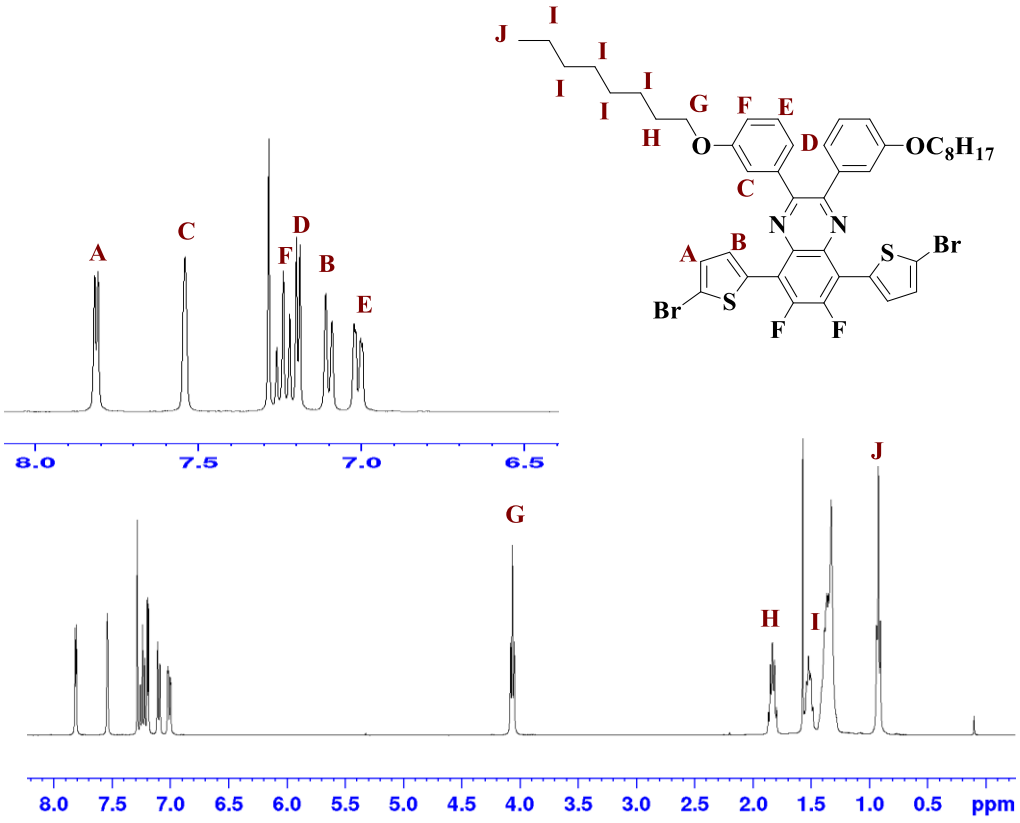

Figure 2.4. ^{1}H-NMR spectrum of (9) in $CDCl_3$.

The reaction mechanism follows an electrophilic aromatic substitution shown below in Scheme 2.9.

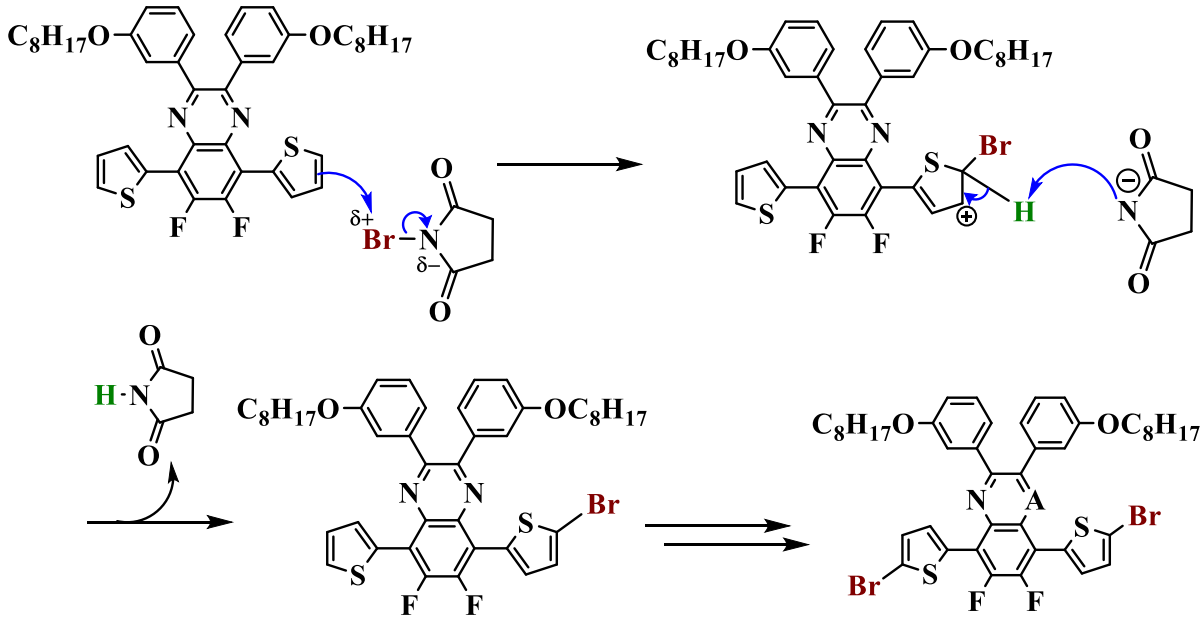

Scheme 2.9. Mechanism of reaction to produce compound (9).

The resonance effect of the thiophene ring makes position 5 more nucleophilic. The N-bromosuccinimide (NBS) molecule shows a difference in electronegativity between the oxygen and nitrogen atoms on one side and the bromine atom on the other, making the bromine atom partially positive. Consequently, the thiophene ring attacks the bromine cation. The succinimide anion deprotonates the thiophene ring, yielding the brominated ring. The previous steps are repeated on other thiophene rings to produce the end product **(9)**.

The steps in the synthesis of monomer **(21)** are depicted in Scheme 2.10.

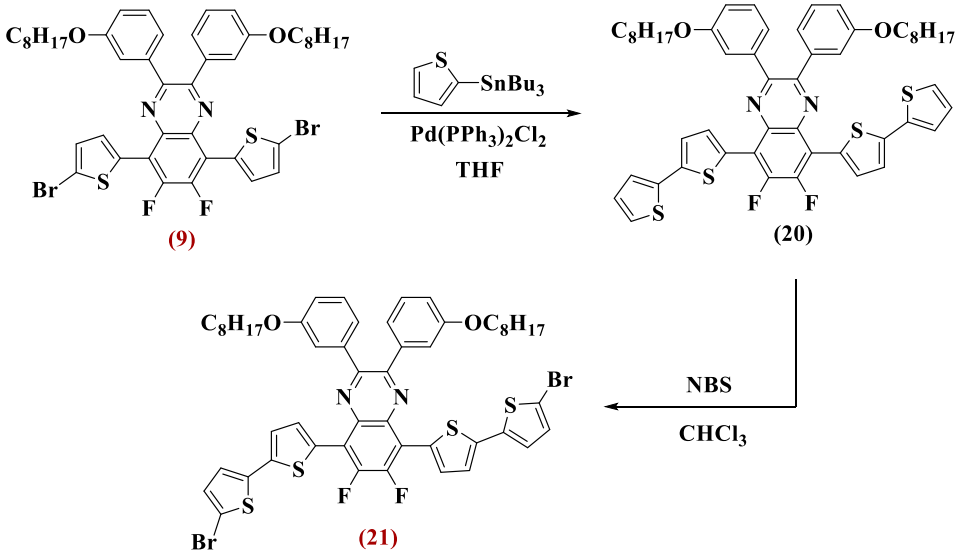

Scheme 2.10. The synthetic route to production of monomer 2,3-bis(3-(octyloxy)phenyl)-6,7-difluoro-5,8-bis(5-bromo-(2,2'-bithiophene)-5-yl)quinoxaline (21).

Compound **(9)** was used to synthesise 2,3-bis(3-(octyloxy)phenyl)-6,7-difluoro-5,8-bis((2,2′-bithiophene)-5-yl)quinoxaline **(20)**, according to the same procedure used to prepare compound **(6).**

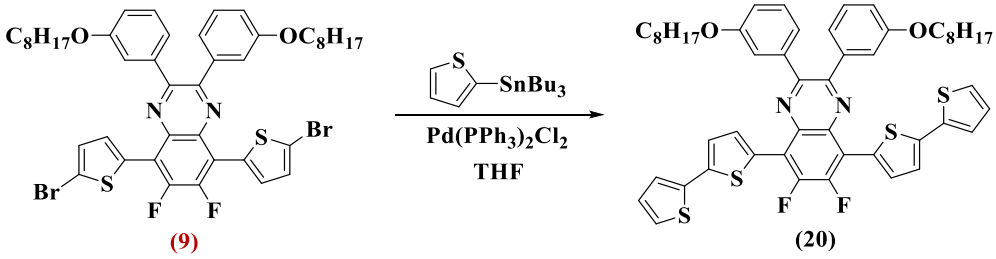

Compound **(20)** was obtained as dark-orange crystals at a 73 per cent yield. Purification was performed by precipitation in methanol. The purity was confirmed by a single peak seen in gas chromatography-mass spectrometry at 902.

The reaction mechanism follows that of Stille coupling, which was explained in the preparation of compound **(6)**.[21]

Lastly, both positions 5 on the thiophene rings were brominated to obtain monomer **(21)**.

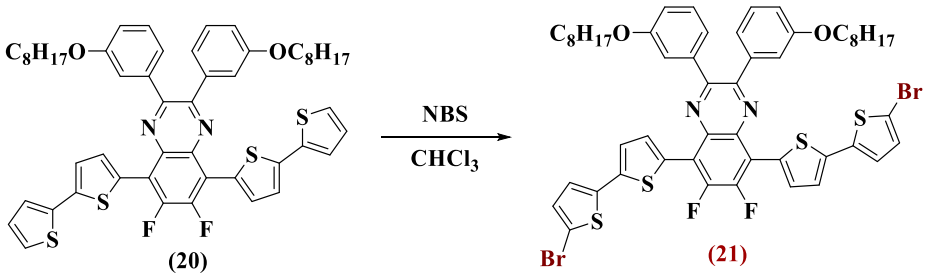

Compound **(21)** was prepared *via* a procedure modified from that carried out by Takahashi *et al.*[26] The product was obtained as dark-red crystals with 93 per cent yield. The purification was performed by recrystallisation in methanol. The purity of the product was confirmed by gas chromatography-mass spectrometry and elemental analysis. The structure of the product was identified by ^{1}H NMR and ^{13}C NMR. The mass spectrum for **(21)** showed peaks at 1058, 1060 and 1062 due to the presence of the bromine isotopes ^{81}Br and ^{79}Br. The ^{1}H NMR spectrum displayed in Figure 2.5 showed that peaks assigned to two protons on the thiophene ring system in the aromatic region had disappeared when compared with compound **(8)**. This suggested that bromination of compound **(21)** had been successful.

The reaction follows the same molecular electrophilic substitution mechanism as that shown for compound **(9)**.

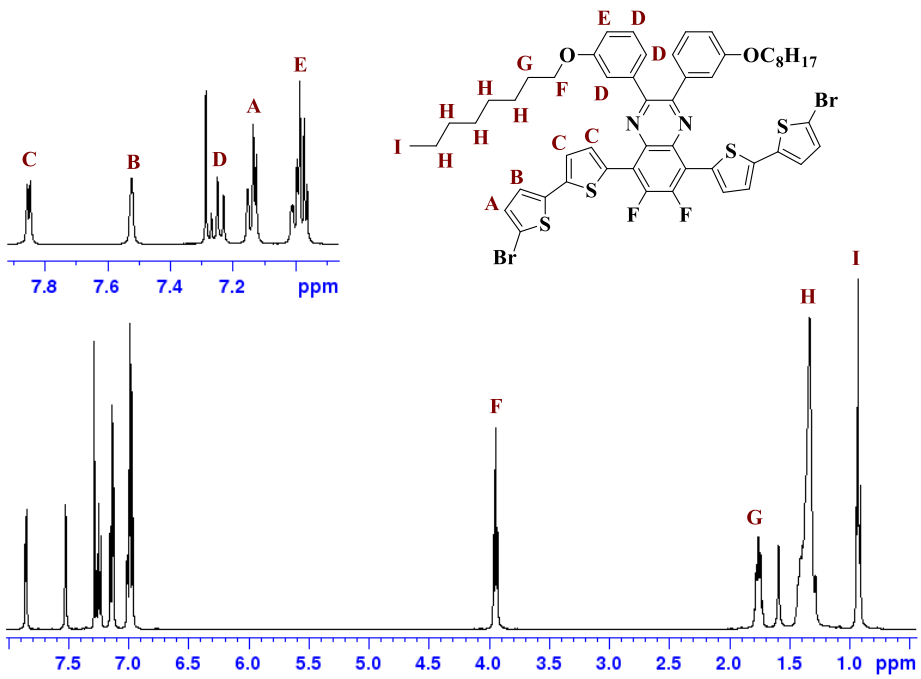

Figure 2.5. ^{1}H-NMR spectrum of compound (21) in $CDCl_3$.

2.2.1.2 Synthesis of the Electron Donor Monomers (16) and (19):

The synthetic steps for production of monomer **(16)** are depicted in Scheme 2.11.

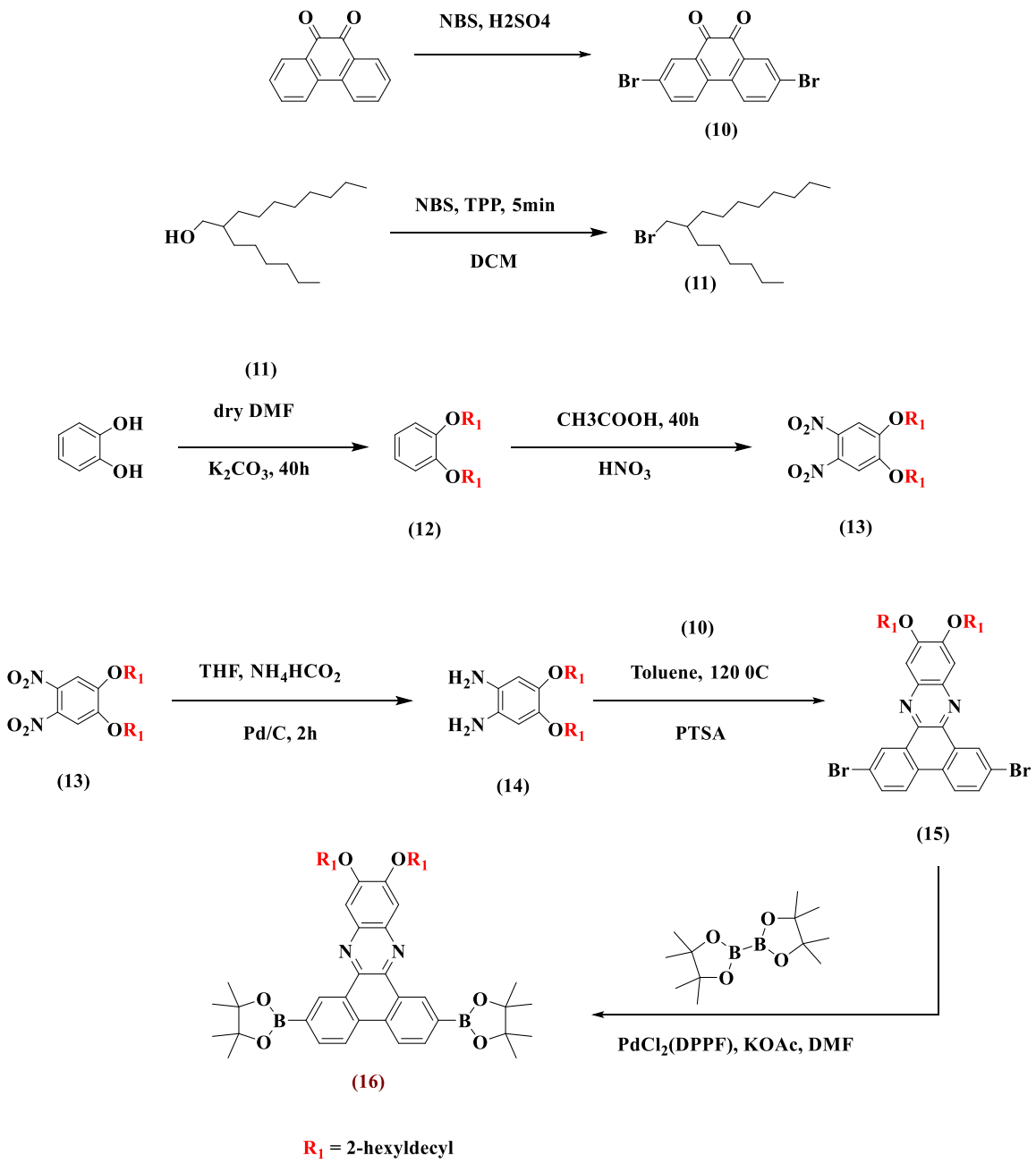

Scheme 2.11. The synthetic route for monomer 2,7- bis-(4,4,5,5-tetramethyl-1,3,2-dioxaborolan-2-yl)-11,12-bis-(2-hexyldecyloxy)- phenanthro[9,10-b]quinoxaline (16).

The compound 2,7-dibromophenanthrene-9,10-dione **(10)** was synthesised according to a procedure modified from that used by Wang *et al*.[19] It is shown below.

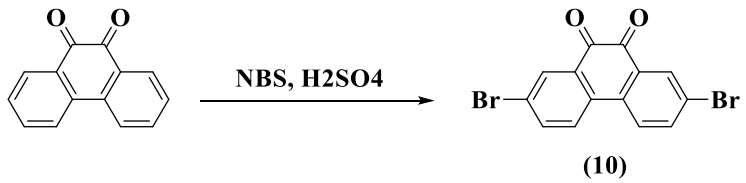

(10)

The product was obtained as deep-orange needle-shaped crystals with 60 per cent yield. The purity of the product was confirmed by gas chromatography-mass spectrometry and elemental analysis. The mass spectrum for compound **(10)** showed peaks at 363, 365 and 367 due to the presence of bromine isotopes (^{81}Br and ^{79}Br).

The reaction follows the same molecular electrophilic substitution mechanism as that shown for compound **(9)**.

Bromo-2-hexyldecane **(11)** was then synthesised according to a procedure modified from that used by Lee *et al*.[27] and shown below.

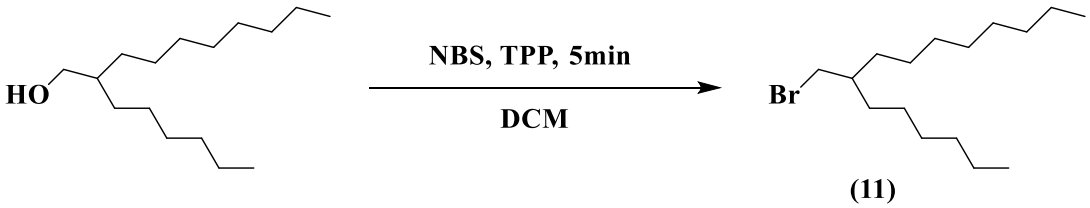

(11)

Bromo-2-hexyldecane **(11)** was obtained from commercially available 7-hydroxymethylpentadecane as a colourless liquid with 98 per cent yield. The purity of the product was confirmed by gas chromatography-mass spectrometry and elemental analysis. The structure of the product was identified by ^{1}H NMR and ^{13}C NMR. The mass spectrum for compound **(11)** showed peaks at 304 and 306. The suggested mechanism of the bromination reaction was described by Denton[28] and is outlined in Scheme 2.12. It follows a nucleophilic substitution mechanism by a S_N2 mechanism.[28]

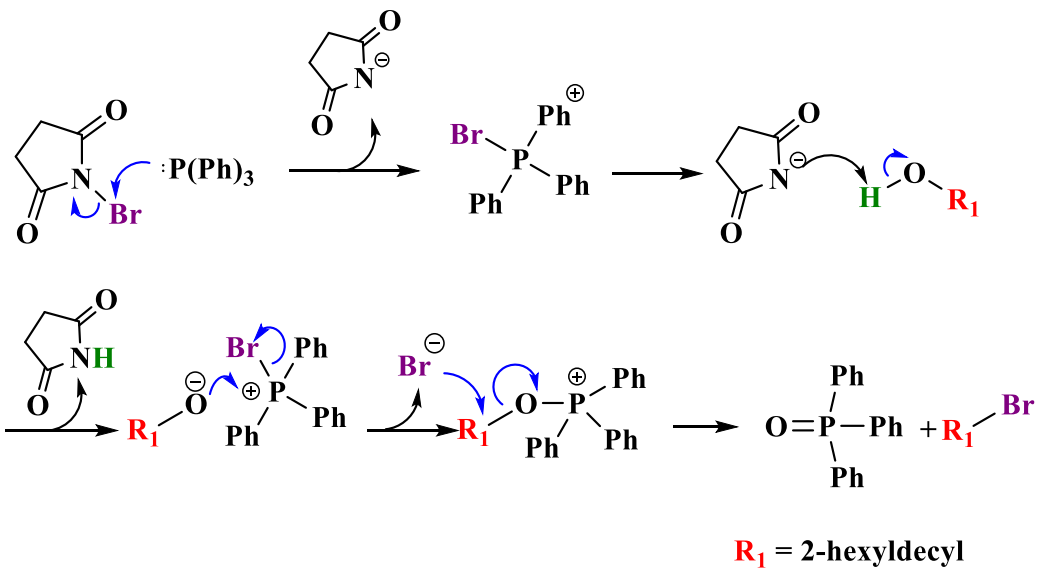

Scheme 2.12. Mechanism of synthesis of compound (11).

Compound **(11)** was reacted with commercially available catechol to prepare 1,2 bis-(2-hexyldecyloxy) benzene **(12)**, as shown below.

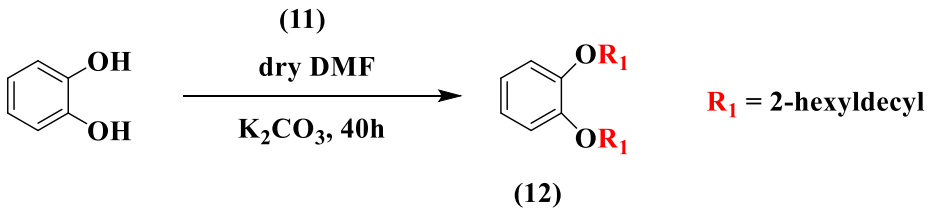

Compound **(12)** was synthesised according to the procedure developed by Zhang *et al.*[17] The product was obtained as colourless oil with 67 per cent yield. Purification was performed using column chromatography by passing first petroleum ether to eliminate the residue of the alkyl group, and then a second wash produced the pure product. The purity and the structure of the product **(12)** were confirmed by ^{1}H NMR, ^{13}C NMR, elemental analysis and mass spectrometry. The mass spectrum showed the main mass at 558, in agreement with the target structure of compound **(12)**. The ^{1}H-NMR spectrum indicated the presence of the protons of OCH_2 and CH_3 as triplet peaks positioned at 3.88 ppm and 0.90 ppm respectively.

The Williamson reaction mechanism follows that of nucleophilic substitution (S_N2), which is the same mechanism as that shown for compound **(2)**.

The next reaction was the nitration of compound **(12)** resulting in 1,2-dinitro-4,5-bis(2-hexyldecyloxy)benzene **(13).** The reaction is shown below.

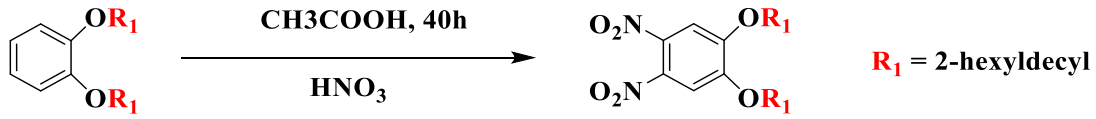

(12) **(13)**

Compound **(13)** was synthesised according to a procedure by Sessler.[29] The product was obtained as a yellow oil with 96 per cent yield. The purity and structure of the product **(13)** were confirmed by ^{1}H NMR, ^{13}C NMR, elemental analysis and mass spectrometry.

The reaction follows the electrophilic aromatic substitution mechanism. It comprises two steps: the first involves the formation of nitronium ion as an electrophile, as shown in Equation 2.2 below:

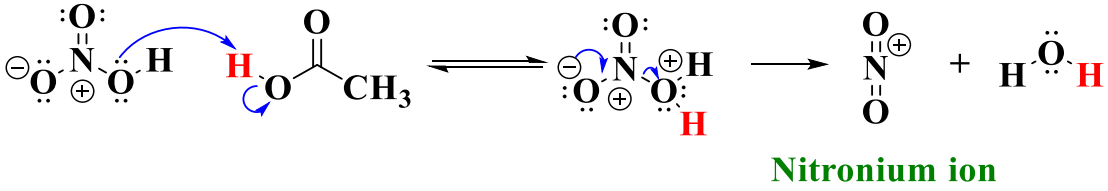

Equation 2.2. Formation of the nitronium ion.

In the second step, the π-electrons in the aromatic ring act as nucleophiles and attack the positively charged electrophile (the nitronium ion) as shown below. The second step repeats to yield the desired product:

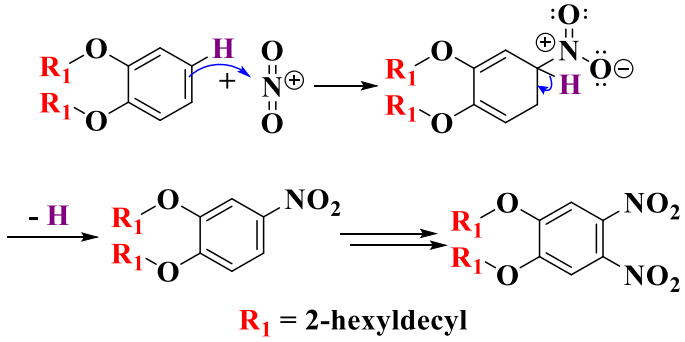

Scheme 2.13. Mechanism of synthesis of compound (13).

The ^{1}H-NMR spectrum illustrates a singlet peak at 7.30 ppm, which corresponds to only two aromatic protons. The mass spectrum shows the main mass at 648, which is in agreement with the structure of the product **(13)**.

Compound **(13)** was then reduced by using ammonium formate as a reducing agent to form 1,2-diamine-4,5-bis(2-hexyldecyloxy)benzene **(14)**, as shown below:

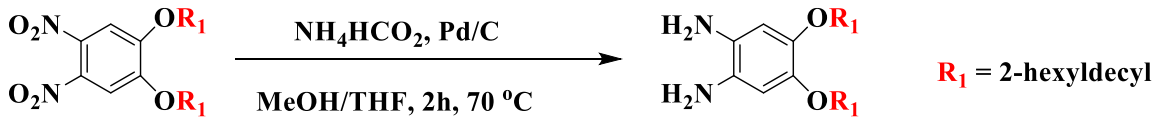

(13) **(14)**

Compound **(14)** was synthesised according to a procedure modified from that used by Ram *et al*.[30] The reaction was carried out in dry tetrahydrofuran at 70˚C for two hours in the presence of 10 per cent palladium on activated carbon (Pd/C). The nitro groups on the benzene ring were reduced by ammonium formate in the presence of methanol. The product was obtained as a colourless oil. The product **(14)** was unstable to oxidation, and was used straight after dry filtration under argon for the next reaction without any further purification.

The mechanism of the reaction involves the reduction of the nitro group. This involves two steps. The first is the decomposition of ammonium formate in the presence of Pd/C, and this catalytic decomposition of ammonium formate in the absence of water leads to the formation of carbon dioxide, ammonia and hydrogen gas as described in Equation 2.3 below.[31,32, 32, 33]

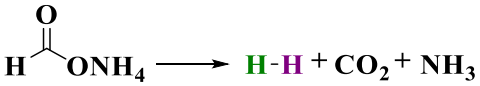

Equation 2.3. Decomposition of ammonium formate to produce hydrogen gas.

The second step is the adsorption of the hydrogen gas on to the surface of the palladium metal, from where it reacts with and reduces the aromatic nitro groups to amines by the elimination of water molecules as shown in Scheme 2.14.[34]

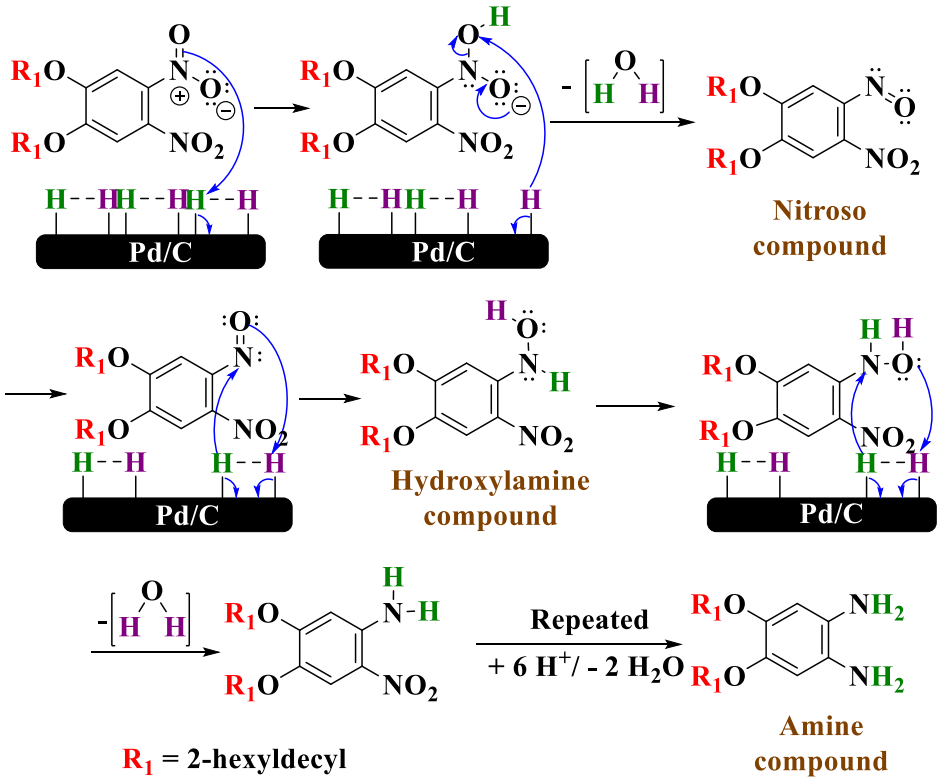

Scheme 2.14. Mechanism of production of compound 14.

A cyclocondensation reaction follows with the compound **(10)** to obtain 2,7-dibromo-bis-(2-hexyldecyloxy) quinoxalino phenanthrene **(15)**. This reaction is shown below.

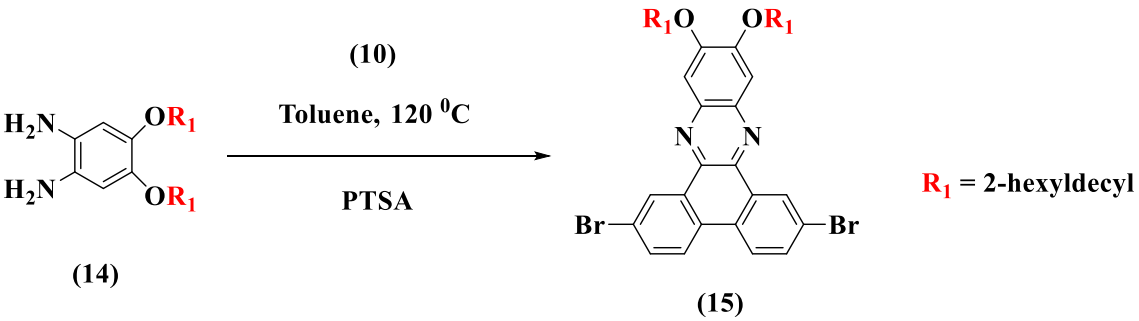

Compound **(15)** was synthesised according to a procedure modified from that used by Robinson *et al.*[25] The product was obtained as a thick yellow oil with 61 per cent yield. The product was purified by column chromatography using petroleum ether and toluene (10:2) as the eluent. The purity of the product was confirmed by gas chromatography-mass spectrometry and elemental analysis. The structure of the product was identified by ^{1}H NMR and ^{13}C NMR. The mass spectrum for compound **(15)** showed a main peak at 919 ($M+H^{+}$) which is in agreement with the proposed structure. The suggested reaction mechanism is

similar to that of acid-catalysed condensation reactions as shown previously for compound **(8)**.

Lastly, compound **(15)** was boronated using bis(pinacolato)diboron to produce 2,7- bis-(4,4,5,5-tetramethyl-1,3,2-dioxaborolan-2-yl)-11,12-bis-(2-hexyldecyloxy)-dibenzo[a,c]phenazine **(16)**. The equation for the reaction is shown below.

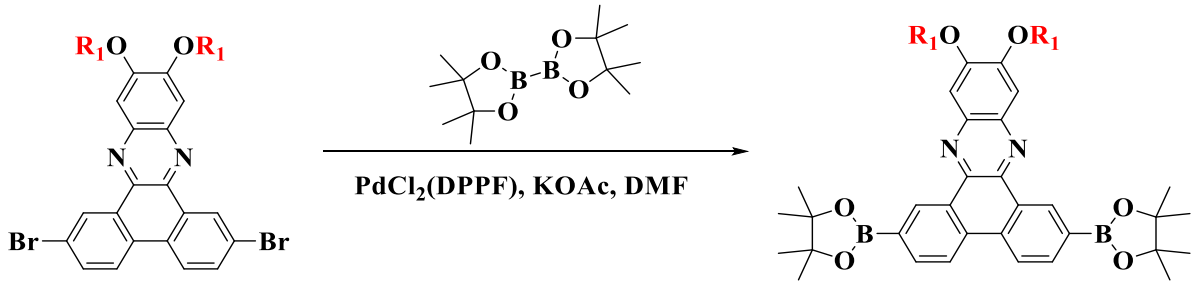

(15) **(16)**

Compound **(16)** was synthesised according to a procedure modified from that used by Brunner.[35] The product was obtained as a dark-green thick oil with 78 per cent yield. The product was purified by precipitation from methanol, which had been passed through basic alumina to remove the acidic protons. The purity of the product was confirmed by gas chromatography-mass spectrometry and elemental analysis. The structure of the product was identified by ^{1}H NMR and ^{13}C NMR. The mass spectrum for compound **(16)** showed peaks at 1011, 1012 and 1013 due to the presence of the boron isotopes ^{10}B and ^{11}B. The ^{1}H NMR is shown in Figure 2.6. It showed a single peak at 1.47 ppm, which corresponded to 24 protons of the methyl groups in the boronic ester. This was an indication that the brominated compound **(15)** had been converted to boronic ester compound **(16)**. The reaction follows the mechanism of Suzuki cross-coupling, which is similar to the mechanism described in Chapter 1.

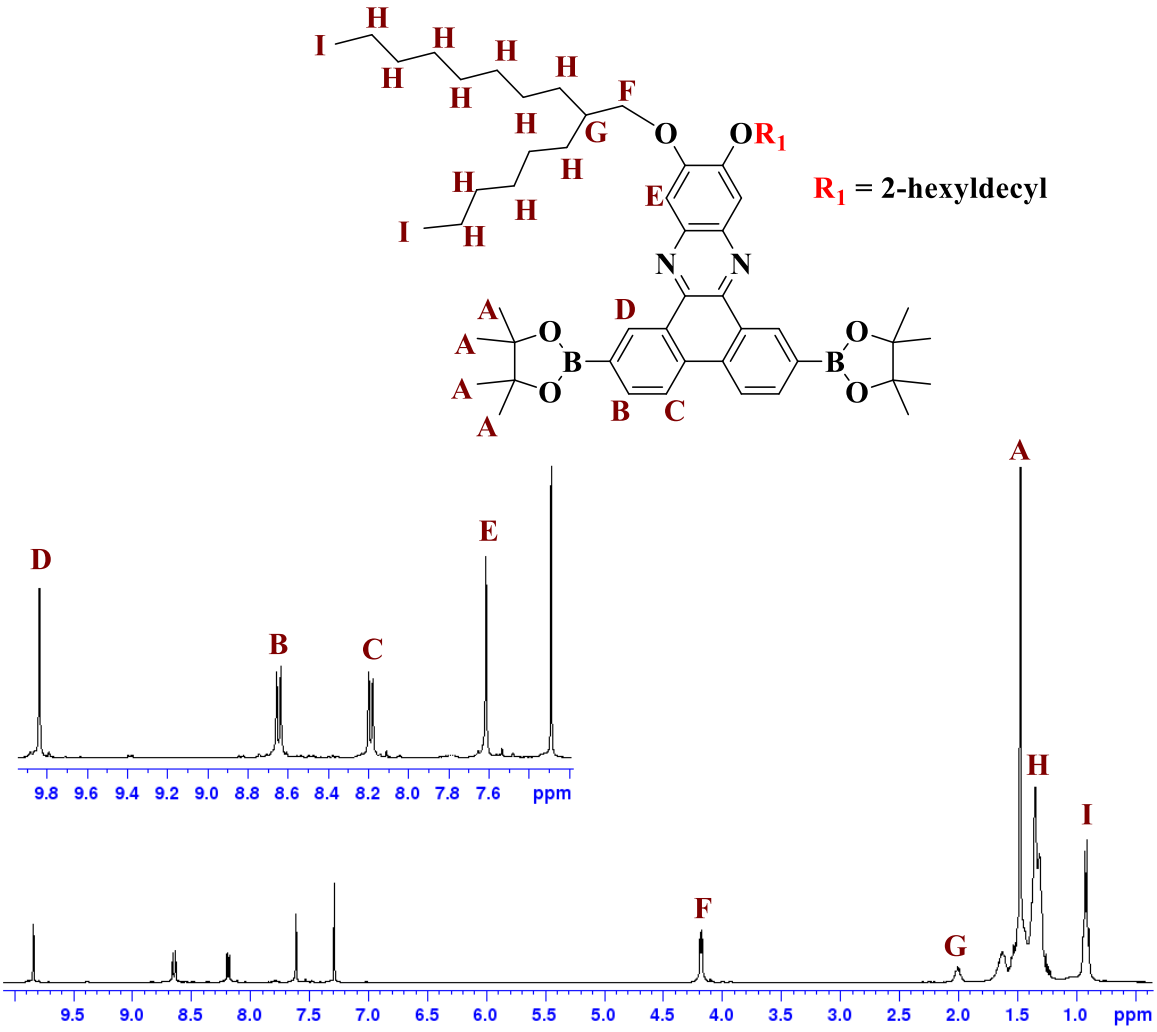

Figure 2.6. ^{1}H-NMR spectrum for compound (16) in $CDCl_3$.

The synthetic steps for production of monomer **(19)** are illustrated in Scheme 2.15.

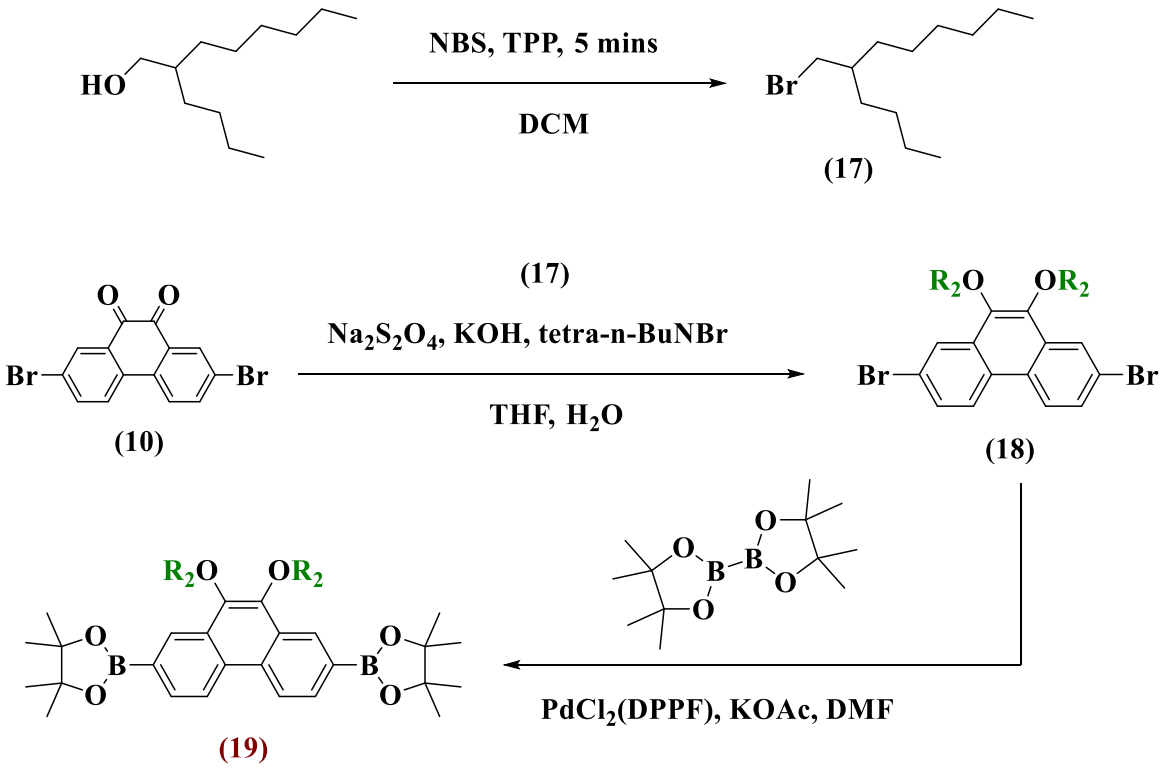

Scheme 2.15. The synthetic route for production of monomer 2,7-bis-(4,4,5,5-tetramethyl-1,3,2-dioxaborolan-2-yl)-9,10-bis-(2-butyl-octyloxy)-phenanthrene (19).

To produce compound **(17)**, the hydroxy group on 2-butyl-1-octanol was brominated to produce 5-bromomethylundecane **(17)**, as shown below:

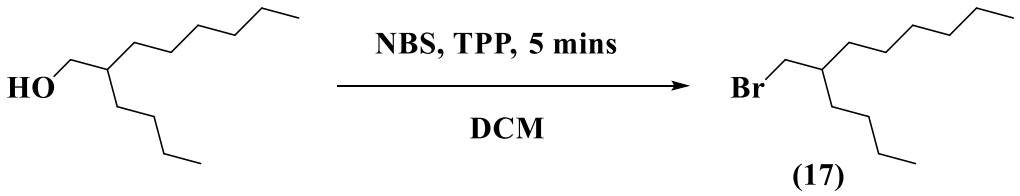

This synthesis followed a procedure modified from that used by Lee *et al.*[27] The product was obtained as a colourless liquid with 84.5 per cent yield. The purity of the product was confirmed by gas chromatography-mass spectrometry and elemental analysis. The structure of the product was identified by ^{1}H NMR and ^{13}C NMR. The mass spectrum for compound **(17)** showed peaks at 248 and 250. The reaction mechanism follows the bromination reaction as described by Denton, which is the same mechanism as shown for compound **(11)**.[28]

The next step involved the reduction of the diketone groups on compound **(10)** to produce dihydroxyl groups, followed by the attachment of compound **(17)** to form 2,7-dibromo-9,10-bis-(2-butyl-octyloxy)-phenanthrene **(18)** as illustrated below.

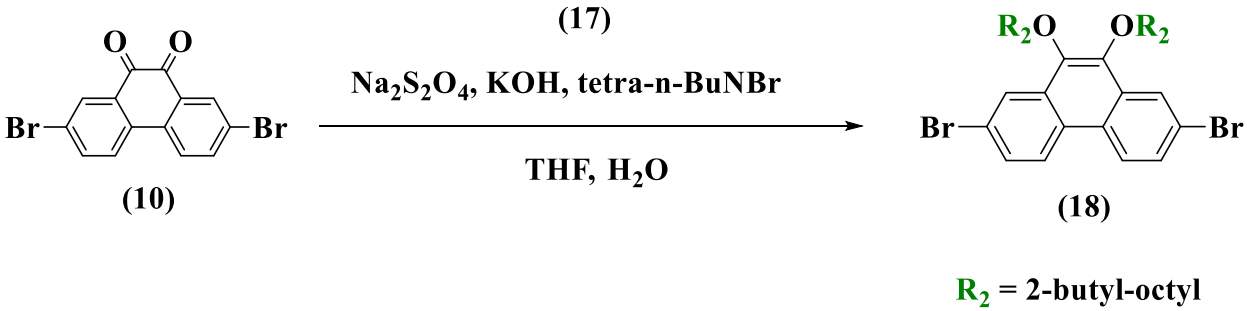

Compound **(18)** was synthesised according to a procedure modified from that used by Chen *et al.*[36,37] The product was obtained as a yellow oil with 60.4 per cent yield. The resultant oil was purified *via* column chromatography, first by passing only petroleum ether to eliminate the residue of the alkyl group. Pure product was obtained as the third spot.

The suggested reaction mechanism follows the molecular nucleophilic substitution S_N2.[36] This mechanism consists of two steps. The first is the reaction of sodium dithionite with water to form sodium bisulphite, as shown in Equation 2.4.

Equation 2.4. Formation of sodium bisulphite.

The sodium bisulphite acts as a nucleophile and attacks the carbons in the carbonyl groups of the diketones to convert them to dihydroxyl groups as shown in Scheme 2.16.

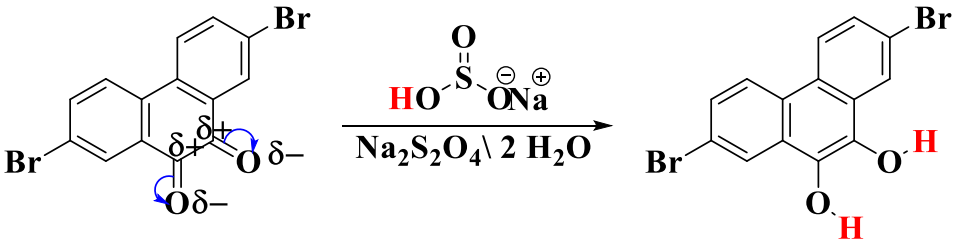

Scheme 2.16. Mechanism for the formation of the dihydroxyl groups in compound (18).

The second step is a deprotonation of the dihydroxyl groups by the base potassium hydroxide to form phenoxide ions, which attack 5-bromomethylundecane **(17)** as nucleophiles to form the desired product as shown in Scheme 2.17.

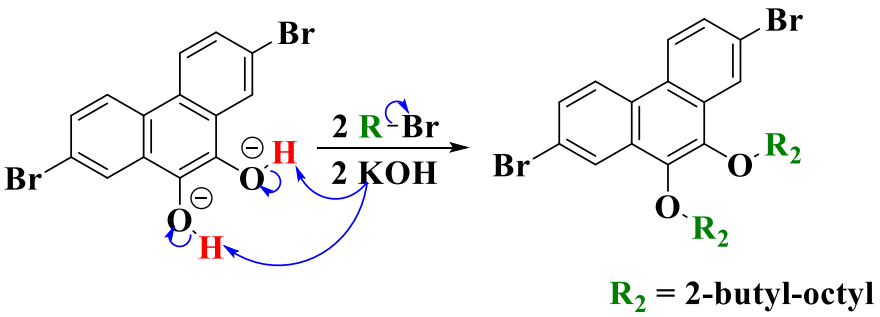

Scheme 2.17. Mechanism of attachment of the alkyl groups in compound (18).

The purity of the product was confirmed by gas chromatography-mass spectrometry and elemental analysis. The structure of the product was identified by ^{1}H NMR and ^{13}C NMR. The mass spectrum for compound **(18)** showed peaks at 702, 704 and 706, due to the presence of bromine isotopes ^{81}Br and ^{79}Br. This was in agreement with the proposed structure of compound **(18)**. The ^{1}H NMR indicated the presence of the protons of the OCH_2 and CH_3 groups as doublet peaks at 4.1 ppm and as triplet at 0.94 ppm, respectively.

Lastly, compound **(18)** was boronated using bis(pinacolato)diboron to produce2,7-bis-(4,4,5,5-tetramethyl-1,3,2-dioxaborolan-2-yl)-9,10-bis-(2-butyl-octyloxy)phenanthrene **(19)**. The equation is shown below.

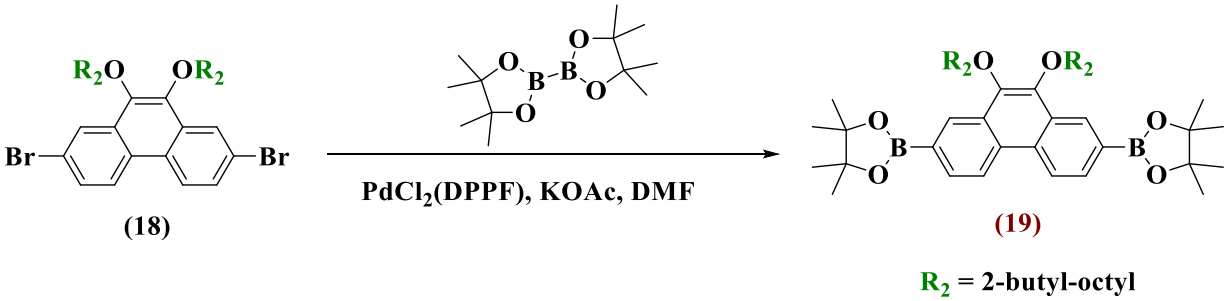

Compound **(19)** was synthesised according to a procedure modified from that used by Brunner.[35] The product was obtained as a dark-brown oil with 75 per cent yield. The product was purified by precipitation from methanol, which had been passed through basic alumina to remove the acidic protons. The purity of the product was confirmed by gas chromatography-mass spectrometry and elemental analysis. The structure of the product was identified by ^{1}H

NMR and ^{13}C NMR. The mass spectrum for compound **(19)** showed peaks at 796, 798 and 800 due to the presence of boron isotopes (^{10}B and ^{11}B). The ^{1}H NMR showed a singlet peak at 1.41 ppm, which corresponded to 24 protons of the methyl groups in the boronic ester. This was an indication that the brominated compound **(18)** had been converted to the boronic ester compound **(19)**. The reaction follows the mechanism of Suzuki cross-coupling, which was described in Chapter 1.

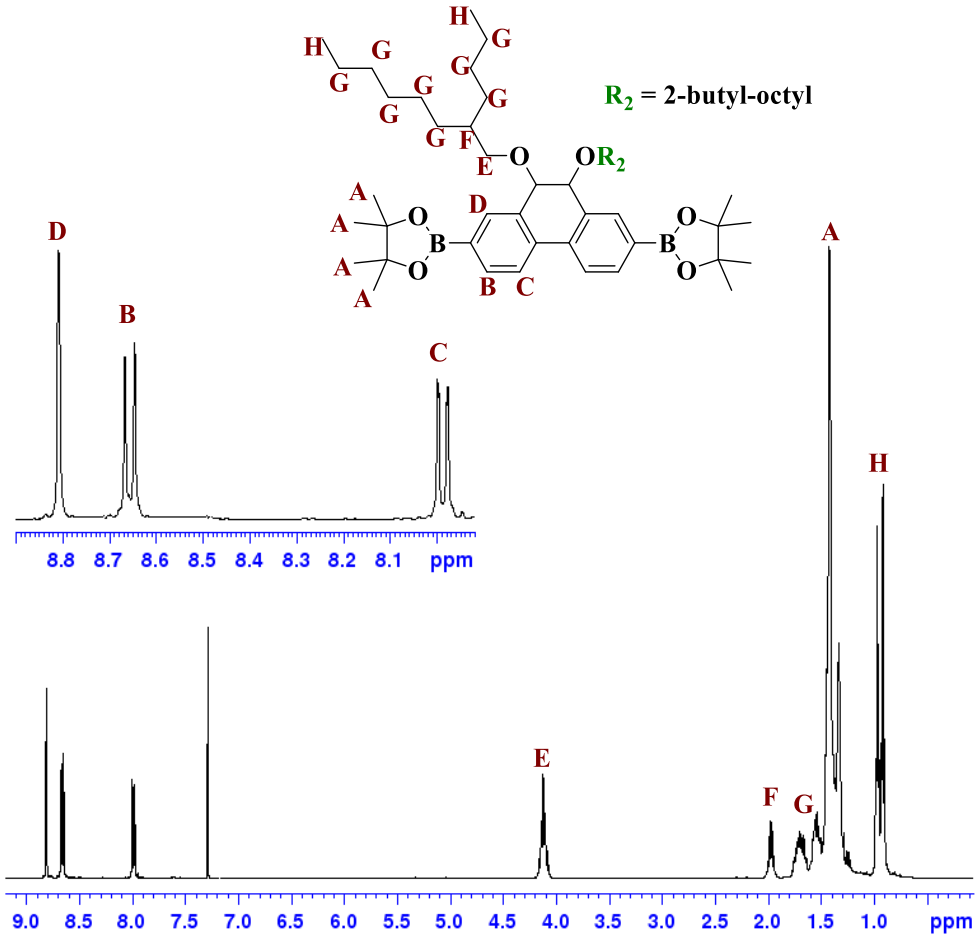

Figure 2.7. ^{1}H-NMR spectrum of compound (19) in $CDCl_3$.

2.2.2. Synthesis of Fluorinated Quinoxaline-based Alternating Copolymers P1, P2, P3 and P4

All four alternating D-A copolymers discussed in this chapter were synthesised through the use of Suzuki cross-coupling between the boronic ester monomers **(16)** and **(19)** as electron donors (Schemes 2.11 and 2.15), and the dibrominated monomers **(9)** and **(21)** as electron acceptors (Schemes 2.3 and 2.10). The polymerisations of the monomers were carried out by using a catalyst comprising palladium (II) acetate ($Pd(OAc)_2$), and tri(*o*-tolyl)phosphine

((P(o-tol)$_3$) with catalyst ratio 1:2. Sodium hydrogen carbonate was used as a base in anhydrous tetrahydrofuran at 90 °C. The polymerisation reactions to produce **P1** and **P2** were stopped after 24 hours, as large amounts of polymer precipitation were observed. Polymerisations of **P3** and **P4** were continued for 72 hours. All polymerisation reactions followed the mechanism of the Suzuki cross-coupling reaction, which was described in Chapter 1.[38]

All reactions were suspended to add the end-capping reagents (bromobenzene and phenyl boronic acid) to the polymer solutions. This also increased the stability of the polymers during fabrication of solar cell devices. All polymers were dissolved in chloroform and then ammonium hydroxide solution was added to remove traces of the palladium catalyst by stirring overnight to form soluble palladium complexes $Pd(NH_3)_4(OH)_2$. Any trace of palladium nanoparticle impurities could affect the efficiency of the OPV devices.[39,40]

The polymers were purified by Soxhlet extraction, which also separated the polymers into fractions to remove unreacted monomers, smaller molecules and oligomers. The following solvents were used: methanol, acetone, hexane toluene and chloroform. The solvents methanol, acetone and hexane removed small molecules, low molecular weight polymer fractions and palladium catalyst residues. Polymers **P1** and **P2** were collected from the toluene fractions, while polymers **P3** and **P4** were collected from the chloroform fractions. The chemical structures of all polymers were verified by ^{1}H-NMR and elemental analysis. Gel permeation chromatography (GPC) was used to determine the number-average molecular weight (M_n) and weight-average molecular weight (M_w) using 1,2,4-trichlorobenzene as an eluent at 140^{o}C (Table 2.1).

All polymers exhibited good solubility in many types of organic solvents at room temperature. The yields of all polymers were higher than 60 per cent. As expected, **P2** showed the highest M_w and M_n, with values of 33,000 Daltons (Da) and 16,000 Da respectively, of all polymers that were synthesised in this chapter. This was a consequence of the presence of the two large solubilising 2-butyl-octyl chains, which were attached to the highly planar phenanthrene-donor moiety, as well as the octyloxy groups that were attached to the quinoxaline-acceptor moiety. It was speculated that these chains were large enough to overcome the rigidity of the polymer **P2**, since it was the most flexible polymer of the group. The large solubilising groups increased the solubility of the polymer to enable further polymerisation, and they

facilitated the formation of higher molecular weight polymers by hindering π-π stacking of polymer backbones.

Polymers **P1**, **P3** and **P4** exhibited lower molecular weights compared with **P2**, with values of 21,300 Da, 21,500 Da and 25,600 Da, respectively. Previous studies have proposed that incorporation of fluorine atoms in the polymer backbone chains enhances π-π stacking and aggregation of polymer chains. Therefore, the polymer quickly precipitates out of solution during the polymerisation, and this impedes the increase of molecular weight of polymers.[41,42,43] In addition, the effect of introducing two or more thiophene units to the backbone of **P1**, **P3** and **P4** can be clearly seen through the reduced M_n and M_w of these polymers. This is owing to the addition of aromatic ring units, which is known to increase the conjugation system and hence increase the rigidity of these polymers.[43]

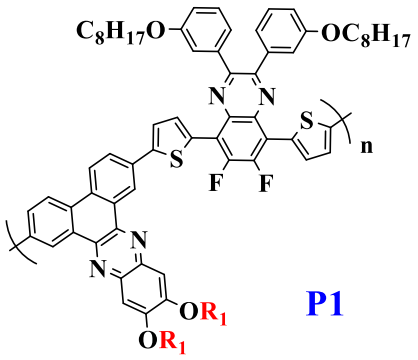

P1

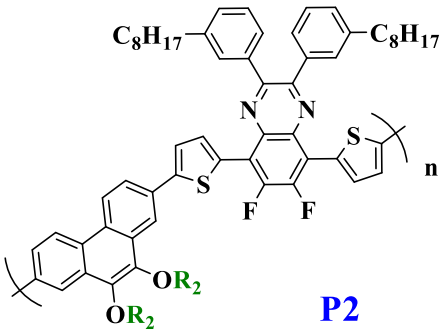

P2

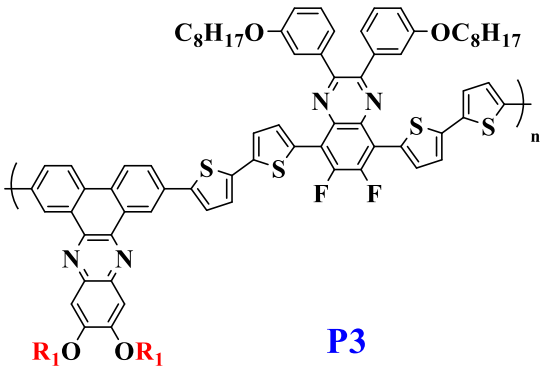

P3

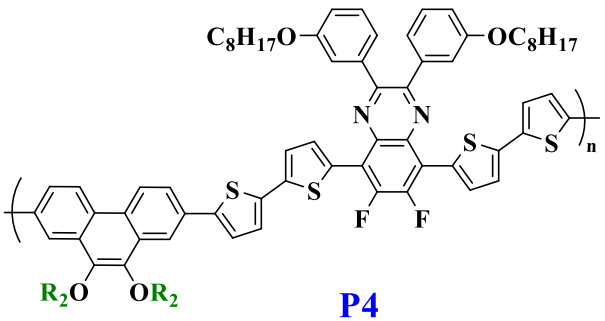

P4

R_1 = 2-hexyldecyl **R_2 = 2-butyl-octyl**

Scheme 2.18. Polymers P1, P2, P3 and P4. Explanations of their synthesis are included in this chapter.

Table 2.1. GPC analysis of P1, P2, P3 and P4

Polymer	Mn (Da) [c]	Mw (Da) [c]	PDI	Yield (%)
P1 [a]	9,900	21,300	1.88	61
P2 [a]	16,000	33,000	2.06	69
P3 [b]	8,200	21,500	2.59	93
P4 [b]	8,600	25,600	2.97	77

[a] Measurements conducted on the toluene fraction of the polymers. [b] Measurements conducted on the chloroform fraction of the polymers. [c] GPC conducted in 1,2,4-trichlorobenzene at 140 °C using a differential refractive index (DRI) detection method. PDI = Polydispersity Index.

2.2.3. Analysis by UV-Visible absorption spectroscopy

The optical properties of the normalised UV-visible absorption spectra of the polymers **P1**, **P2**, **P3** and **P4** were investigated by UV-Vis. The spectra were taken in dilute chloroform solutions (Figure 2.8(a)) and in the solid state as drop-cast thin films on quartz substrates (Figure 2.8(b)). The optical band gaps for all polymers were measured through the onset of absorption of the polymers in the solid state. The optical properties of all polymers are summarised in Table 2.2.

Table 2.2. Optical data of polymers P1, P2, P3 and P4

Polymer	ε (M^{-1} cm^{-1})	Solution λ_{max} (nm)	Thin Film λmax (nm)	Thin Film λ_{onset} (nm)	Optical E_g (eV)
P1	50383	518	522	627	1.97 ± 0.012
P2	41785	504	517	626	1.98 ± 0.009
P3	74599	556	566	688	1.80 ± 0.004
P4	47863	544	552	675	1.83 ± 0.032

The UV-vis spectra of all the polymers showed two main absorption bands. The absorption bands at shorter wavelengths corresponded to π-π* transitions, while the absorption bands at longer wavelengths could be ascribed to ICT between the electron-deficient quinoxaline acceptor unit and the electron-rich phenanthrene-quinoxaline and phenanthrene donor moieties.

The ICT absorption maxima in chloroform solutions for polymers **P1** and **P2** were situated at 518nm and 504nm, respectively. When cast into a thin film, the ICT absorption maxima for polymers **P1** and **P2** were red-shifted, compared with those in solution, to 522nm and 517nm, respectively. The polymer backbones have comparable conformations in solution and solid state, but possess higher planarity in the solid state, which leads to stronger π-π interchain stacking, and this accounts for the red shift in the solid state. **P1** and **P2** showed similar optical band gaps, estimated to be 1.97 eV and 1.98 eV respectively. They were determined from the onset of absorption in solid state.

Polymers **P3** and **P4** displayed ICT absorption maxima in chloroform solutions at 556 nm and 544nm, respectively. When cast into a thin film, the ICT absorption maxima for polymers **P3** and **P4** were red-shifted, relative to their absorption in solution, to 556nm and 552nm, respectively. The optical band gap of **P3** and **P4** were also similar but lower than those of **P1** and **P2** and were estimated to be 1.80 eV and 1.83 eV, respectively. This is due to the increased conjugation system through the addition of thiophene units in **P3** and **P4** relative to their analogues **P1** and **P2** respectively.

Additionally, **P1** showed enhanced resolution of its ICT absorption maximum when cast into a thin film by displaying a shoulder peak at approximately 560nm. This might be attributed to the electronic transition property of the polymer, resulting in an improved molecular arrangement in the solid state. However, this shoulder peak was not present in the spectra of the other polymers. Previous studies have suggested that the introduction of fluorine substituents can result in more intermolecular interactions between fluorine atoms and neighbouring aromatic chains. Therefore, the polymer adopts a more planar conformation and π-π stacking is enhanced between polymer chains.[43]

Furthermore, although **P1** had a larger and different donor unit compared with **P2**, both polymers showed a similar optical band gap. This could be due to the quinoxaline moiety in electron donor **(16)**, which has a pair of hetero (nitrogen) atoms in its structure that act as an electron-dense withdrawing group. This may reduce its electron-donating propensity to the same level as that of the other electron donor **(19)**. Additionally, although the donating alkoxy groups attached to electron donor **(16)** are larger than those in electron donor **(19)**,

their effects are eliminated by the pair of nitrogen atoms in the quinoxaline moiety in the electron donor **(16)**. The same reason may explain the similarity of the optical band gaps of **P3** and **P4**.

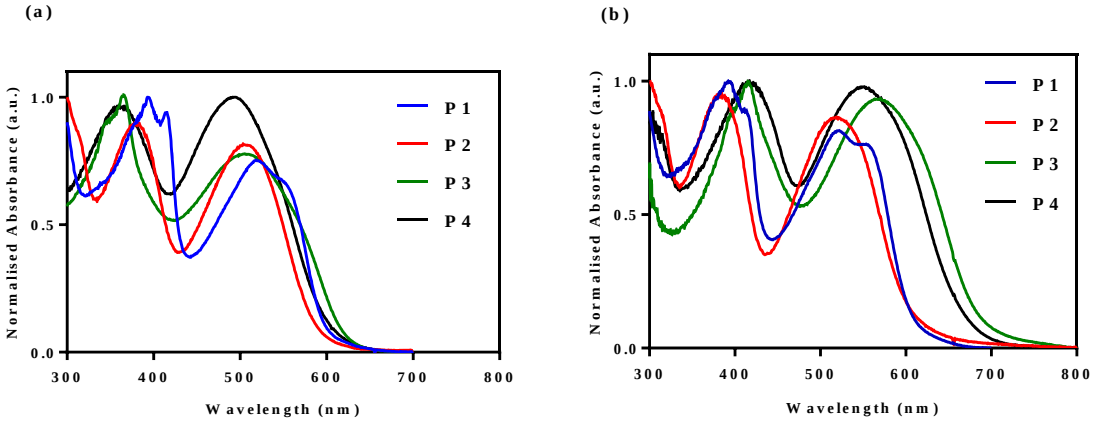

Figure 2.8. Normalised absorption spectra of P1, P2, P3 and P4 in: (a) chloroform solutions; and (b) thin films.

2.2.4. Analysis by Cyclic Voltammetry

CV was used to study and characterise the electrochemical properties of polymers **P1**, **P2**, **P3** and **P4** (Figure 2.9). The onset of oxidation was used to determine the HOMO energy levels for each polymer (*vs*. *vacuum*), whereas the onset of reduction was used to determine the LUMO energy levels (*vs*. *vacuum*), by the use of the following equation:

$$HOMO/LUMO = -\left[\left(E^{onset}_{(ox./red.)} - E_{foc}\right) + E_{ref.}\right] \quad (eV)$$

Equation 2.5. Formula used to determine HOMO and LUMO energy levels.

E_{foc} is the potential of the ferrocene/ferrocenium ion; E_{ref} is the reference energy level of ferrocene (4.8 eV below the *vacuum* level; the *vacuum* level is defined as zero).

The studies were performed on drop-cast polymer films on a platinum disc electrode as the working electrode in acetonitrile with tetrabutylammonium perchlorate as the electrolyte (0.1M) and silver nitrate (Ag/Ag+) as a reference electrode at a scan rate of 100 mV s^{-1} min. The electrochemical band gaps were estimated from the difference of HOMO and LUMO levels, as summarised in Table 2.3.

Table 2.3. Electrochemical properties of P1, P2, P3 and P4

Polymers	HOMO (eV)[a]	LUMO (eV)[b]	E_g^{elect} (eV)[c]
P1	-5.49	-3.50	1.99 ± 0.008
P2	-5.57	-3.58	1.99 ± 0.007
P3	-5.48	-3.55	1.93 ± 0.011
P4	-5.47	-3.57	1.92 ± 0.014

[a] HOMO energy levels determined from the onset of oxidation. [b] LUMO energy levels determined from the onset of reduction. [c] Electrochemical band gap.

All polymers showed low HOMO energy levels. The findings were consistent with previous literature, which reported that incorporation of fluorine atoms on the acceptor moiety was effective in deepening HOMO energy levels of the resulting polymers. Moreover, of all polymers synthesised in this chapter, **P2** exhibited the deepest HOMO level with a value of -5.57 eV. This is due to the effect of fluorine incorporation and because **P2** has fewer aromatic units than the other polymers, with no additional spacer thiophene units. Therefore, the conjugation is reduced, leading to a wider band gap, as has been recorded for **P2.**

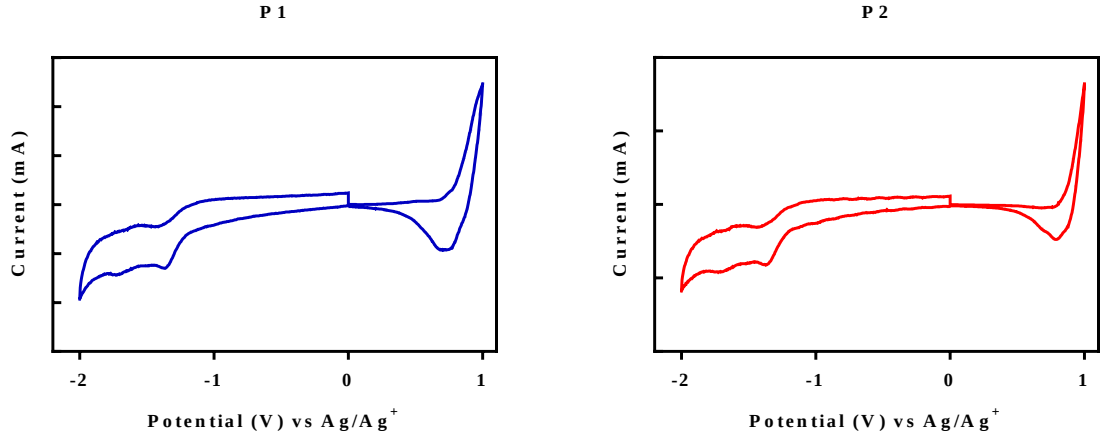

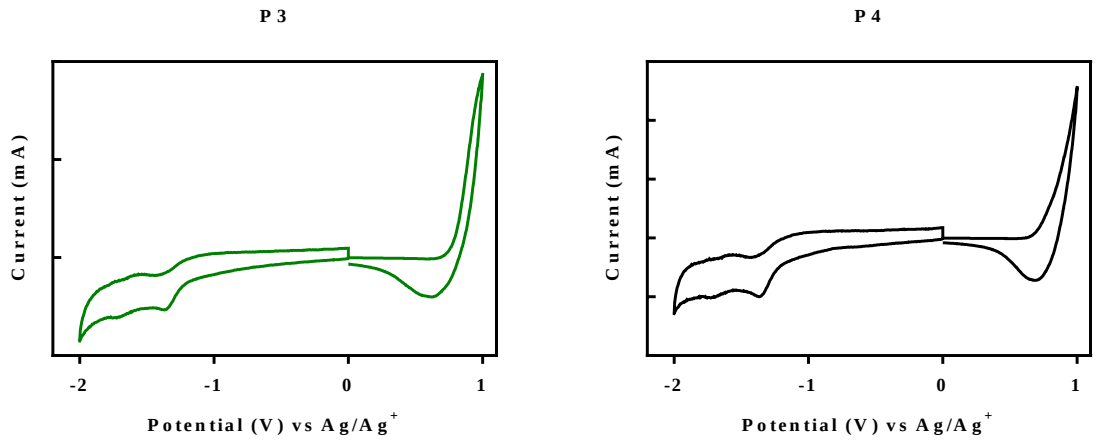

Figure 2.9. Cyclic voltammograms of P1, P2, P3 and P4

Deeper HOMO energy levels were observed in polymers **P1** and **P2,** which possessed single spacer units (thiophene units), compared with polymers **P3** and **P4,** which possessed bithiophene units. The shallower HOMO energy levels of **P3** and **P4** were caused by the increased conjugation, leading to an increase of ICT along the backbone of the polymers. This is consistent with the narrower optical band gaps of **P3** and **P4** when compared with **P1** and **P2**.

Polymers **P1**, **P2**, **P3** and **P4** are comparable to the polymers synthesised by Dang *et al*, **PBDTT-TQ** and **PBDTT-BTQ** (Figure 2.10).[6] The donor moieties in both **PBDTT-TQ** and **PBDTT-BTQ** are the benzo[1,2-b:4,5-b′]dithiophene unit. Dang *et al.* reported that both **PBDTT-TQ and PBDTT-BTQ** exhibited HOMO energy levels estimated at -5.45 eV and -5.33 eV respectively.[6]

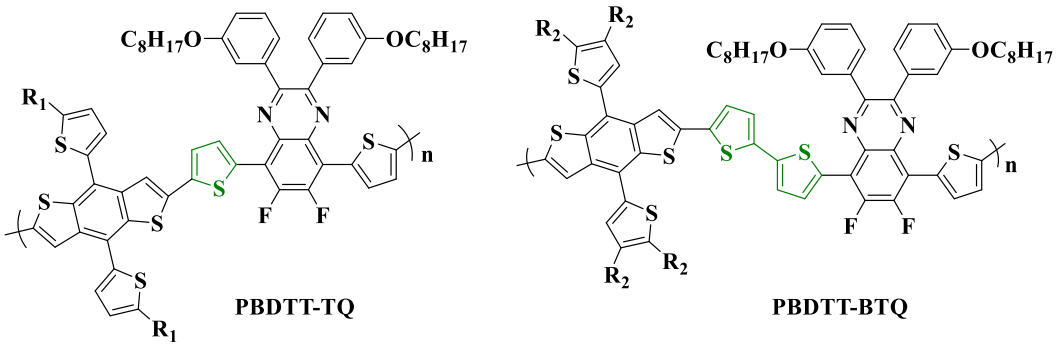

Figure 2.10. Polymer structures of PBDTT-TQ and PBDTT-BTQ synthesised by Dang and co-workers.[6]

Both **PBDTT-TQ** and **PBDTT-BTQ** have slightly shallower HOMO energy levels than **P1**, **P2**, **P3** and **P4**. This can be attributed to the higher strength of the donor moieties in both

PBDTT-TQ and **PBDTT-BTQ** compared with those in **P1**, **P2**, **P3** and **P4**. Therefore, according to theory, polymers **P1**, **P2**, **P3** and **P4** should exhibit higher V_{oc} values when employed to fabricate PV devices compared with devices fabricated from **PBDTT-TQ** or **PBDTT-BTQ**.

The LUMO energy levels of polymers **P2**, **P3** and **P4** were very similar, since all the polymers had the same quinoxaline units as electron acceptors. These units can manipulate the LUMO levels in these polymers. However, the LUMO level of **P1** was shallower than those of the other polymers as a result of the different molecular weights.

2.2.5. Study of Thermal Properties

The thermal stability of all the polymers was measured through TGA. The thermal degradation curves of the polymers are shown in Figure 2.11. The temperatures of onset of decomposition are shown in Table 2.4. The studies were conducted at a heating rate of 10 °C min^{-1} in an inert nitrogen atmosphere.

Table 2.4. Thermal Properties of P1, P2, P3 and P4

Polymer	T_d (˚C)[a]
P1	388
P2	337
P3	397
P4	339

[a] Degradation onset of polymers determined by using thermogravimetric analysis with a heating rate of 10˚C min^{-1} under an inert nitrogen atmosphere.

All polymers displayed good thermal stability. All degradation temperatures exceeded 330˚C. This is sufficient thermal stability for the requirements of OSCs.

P1 and **P3** exhibited similar properties. Each showed one decomposition phase, and both had the highest onset of degradation temperatures, at 388˚C and 397˚C, respectively. This can be attributed to the presence in **P1** and **P3** of larger alkyl chains (2-hexyldecyl) anchored to their

donor moieties compared with **P2** and **P4**, and a larger conjugated polymer backbone. Both of these polymer groups require more thermal energy to break them.

Both **P2** and **P4** showed two decomposition phases. The first occurred at lower temperatures of 337˚C and 339˚C, respectively, owing to the cleavage of the alkoxy groups (2-butyl octyl) attached to their donor moieties. The second decomposition phase marked the onset of degradation of the residual conjugated polymer backbone, at temperatures of 441˚C and 443˚C, respectively.

All polymers decomposed until 50 per cent of their weight was lost. After that the curves remained constant until the limit of the measurement method was reached at 800˚C. It is hypothesised that polymers with large alkyl chains become less volatile during combustion. Therefore, during combustion of **P1**, **P2**, **P3** and **P4**, a thick charred layer formed on the virgin polymer, which insulated the virgin polymer from the heat flux due to its low thermal conductivity. This process would delay the thermal decomposition of the polymers.[44]

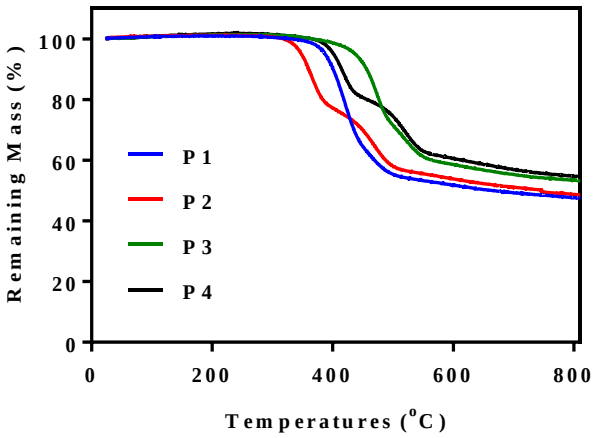

Figure 2.11. Thermogravimetric analysis of P1, P2, P3 and P4 carried out at a heating rate of 10°C min^{-1} and under an inert nitrogen atmosphere.

2.2.6. Studies of the Molecular Structures

The order of the molecular structures of polymers **P1**, **P2**, **P3** and **P4** were studied by powder X-ray diffraction (PXRD) in the solid state. As illustrated in Figure 2.12, broad diffuse peaks were observed from the amorphous part of the PXRD curve of **P1**, **P2**, **P3** and **P4** located at 2θ values of 20.0°, 20.4°, 20.25° and 20.3°. These findings are equivalent to the π-π stacking distance of 4.43 Angstroms (Å), 4.35Å, 4.38Å and 4.37Å respectively. The lack of peaks in the low angle area indicates that all the polymers prepared in this chapter do not exhibit long-range order in thin films. It is speculated that this is a result of attaching large, sterically

demanding alkoxy groups to the donor moieties, leading to greater stacking distances, which suggest that all the polymers exhibit amorphous structures. Furthermore, previous studies have reported that fluorination of the electron-acceptor unit results in a reduction of the π-π stacking distance.[43,42] The PXRD patterns of the polymers synthesised for this study are consistent with previous studies. It is hypothesised that the introduction of bulky alkoxy groups reduces the effects of fluorination on the stacking properties of the polymers in thin films.

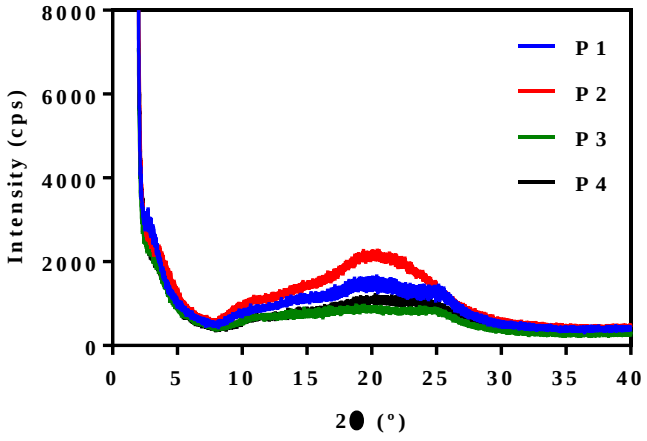

Figure 2.12. PXRD patterns of polymers P1, P2, P3 and P4.

2.3. Conclusion

A series of fluorinated quinoxaline-based copolymers **P1**, **P2**, **P3** and **P4** were synthesised *via* Suzuki cross coupling reactions, and their optical, electrochemical and thermal properties were investigated. All polymers displayed good solubility in many types of organic solvents at room temperature, which was a consequence of incorporating alkoxy groups on to the electron acceptor and donor moieties. The yields of all polymers were greater than 60 per cent. GPC data revealed that **P2** showed the highest M_w and M_n values of all polymers that were synthesised in this chapter.

Polymers **P1**, **P3** and **P4** exhibited lower molecular weights compared with that of **P2**. It was speculated that the large solubilising groups (2-butyl-octyl chains) attached to the highly planar phenanthrene-donor moiety were large enough to overcome the rigidity of the polymer **P2**, since it was the least rigid polymer of those studied in this chapter. Hence, **P2** showed the highest M_w and M_n values. **P1** and **P2** exhibited similar optical band gaps with values of 1.97 eV and 1.98 eV respectively. **P3** and **P4** displayed band gaps that were similar to each other but narrower than those of **P1** and **P2**, owing to the extension of their conjugation system by the addition of two more thiophene units to **P3** and **P4**.

All the polymers demonstrated red shifts in thin films, which could be ascribed to the polymer backbones possessing higher planarity in the solid state, leading to stronger π-π interchain stacking.

CV analysis of all the polymers showed low HOMO energy levels. This was a consequence of the incorporation of fluorine atoms on the acceptor moieties, which helped to lower the HOMO energy levels. **P2** exhibited the deepest HOMO level with a value of -5.57 eV. It has less conjugation, leading to a wider electrochemical band gap with a value of 1.99 eV. The LUMO energy levels of polymers **P1**, **P2**, **P3** and **P4** were positioned in a suitable range from -3.50 eV to -3.58 eV. These values were higher than the LUMO energy level of $PC_{71}BM$. Thus, efficient separation and charge transfer could be anticipated in their corresponding BHJ solar cells.[6]

The PXRD patterns of the polymers showed no peaks in the low-angle region, which indicated that the polymers did not have long-range order in the solid state. Also, the greater π-π stacking distance in the wide-angle region suggested that all the polymers exhibited an amorphous nature. All the polymers showed good thermal stability, with decomposition temperatures in excess of 330˚C, which is high enough for the requirements of OSC

applications. **P1** and **P3** exhibited similar properties. Each showed one decomposition phase, and both had the highest onset of degradation temperatures, at 388˚C and 397˚C, respectively. This is owing to the presence of larger alkyl chains (2-hexyldecyl) in **P1** and **P3** anchored to their donor moieties compared with **P2** and **P4**, in addition to a larger conjugated polymer backbone. Both of these polymer groups require more thermal energy to break them.

The PV properties of polymers **P1**, **P2**, **P3** and **P4** will be analysed through cooperation with the Department of Physics at the University of Sheffield. The PCE will be measured by fabricating BHJ photovoltaic devices with fullerene derivatives.

2.4. References

(1) Xu, Y.; Zhang, F.; Feng, X. Patterning of conjugated polymers for organic optoelectronic devices. *Small* 2011, *7* (10), 1338.

(2) Liu, Y.; Zhao, J.; Li, Z.; Mu, C.; Ma, W.; Hu, H.; Jiang, K.; Lin, H.; Ade, H.; Yan, H. Aggregation and morphology control enables multiple cases of high-efficiency polymer solar cells. *Nature communications* 2014, *5*, 5293.

(3) Guo, X.; Baumgarten, M.; Müllen, K. Designing π-conjugated polymers for organic electronics. *Progress in Polymer Science* 2013, *38* (12), 1832.

(4) Amb, C. M.; Chen, S.; Graham, K. R.; Subbiah, J.; Small, C. E.; So, F.; Reynolds, J. R. Dithienogermole as a fused electron donor in bulk heterojunction solar cells. *Journal of the American Chemical Society* 2011, *133* (26), 10062.

(5) Cheng, Y.-J.; Yang, S.-H.; Hsu, C.-S. Synthesis of conjugated polymers for organic solar cell applications. *Chemical reviews* 2009, *109* (11), 5868.

(6) Dang, D.; Xiao, M.; Zhou, P.; Shi, J.; Tao, Q.; Tan, H.; Wang, Y.; Bao, X.; Liu, Y.; Wang, E. Manipulating backbone structure with various conjugated spacers to enhance photovoltaic performance of D–A-type two-dimensional copolymers. *Organic Electronics* 2014, *15* (11), 2876.

(7) Zhao, B.; Wu, H.; Liu, S.; Luo, G.; Wang, W.; Guo, Z.; Wei, W.; Gao, C.; An, Z. Efficient alternating polymer based on benzodithiophene and di-fluorinated quinoxaline derivatives for bulk heterojunction photovoltaic cells. *Polymer* 2017, *116*, 35.

(8) Chang, D. W.; Lee, H. J.; Kim, J. H.; Park, S. Y.; Park, S.-M.; Dai, L.; Baek, J.-B. Novel quinoxaline-based organic sensitizers for dye-sensitized solar cells. *Organic letters* 2011, *13* (15), 3880.

(9) Wang, E.; Hou, L.; Wang, Z.; Hellström, S.; Zhang, F.; Inganäs, O.; Andersson, M. R. An easily synthesized blue polymer for high-performance polymer solar cells. *Advanced Materials* 2010, *22* (46), 5240.

(10) Chen, C.-H.; Hsieh, C.-H.; Dubosc, M.; Cheng, Y.-J.; Hsu, C.-S. Synthesis and characterization of bridged bithiophene-based conjugated polymers for photovoltaic applications: acceptor strength and ternary blends. *Macromolecules* 2009, *43* (2), 697.

(11) Chen, C.-P.; Chen, Y.-C.; Yu, C.-Y. Increased open circuit voltage in a fluorinated quinoxaline-based alternating conjugated polymer. *Polymer Chemistry* 2013, *4* (4), 1161.

(12) Shi, C.; Yao, Y.; Yang, Y.; Pei, Q. Regioregular copolymers of 3-alkoxythiophene and their photovoltaic application. *Journal of the American Chemical Society* 2006, *128* (27), 8980.

(13) Park, S. M.; Yoon, Y.; Jeon, C. W.; Kim, H.; Ko, M. J.; Lee, D. K.; Kim, J. Y.; Son, H. J.; Kwon, S. K.; Kim, Y. H. Synthesis of phenanthro [1, 10, 9, 8-cdefg] carbazole-based conjugated polymers for organic solar cell applications. *Journal of Polymer Science Part A: Polymer Chemistry* 2014, *52* (6), 796.

(14) Lai, M. H.; Chueh, C. C.; Chen, W. C.; Wu, J. L.; Chen, F. C. Synthesis and properties of new dialkoxyphenylene quinoxaline-based donor-acceptor conjugated polymers and their applications on thin film transistors and solar cells. *Journal of Polymer Science Part A: Polymer Chemistry* 2009, *47* (3), 973.

(15) Dang, D.; Chen, W.; Yang, R.; Zhu, W.; Mammo, W.; Wang, E. Fluorine substitution enhanced photovoltaic performance of a D–A 1–D–A 2 copolymer. *Chemical Communications* 2013, *49* (81), 9335.

(16) Mueller-Westerhoff, U. T.; Zhou, M. Synthesis of Symmetrically and Unsymmetrically Substituted .alpha.-Diones from Organometallic Reagents and 1,4-Dialkylpiperazine-2,3-diones. *The Journal of Organic Chemistry* 1994, *59* (17), 4988.

(17) Zhang, D.; Tessier, C. A.; Youngs, W. J. Synthesis of Tris (2, 5-dialkynylthieno) cyclotriynes, Tris (4, 5-dialkoxyphenyl) cyclotriynes, and Tetrakis (4, 5-dialkoxyphenyl) cyclotetraynes with Long-Chain Alkyl Substituents, and the Nickel and Cobalt Complexes of Tris [4, 5-(didodecyloxy) phenyl] cyclotriyne. *Chemistry of materials* 1999, *11* (11), 3050.
(18) Mammo, W.; Admassie, S.; Gadisa, A.; Zhang, F.; Inganäs, O.; Andersson, M. R. New low band gap alternating polyfluorene copolymer-based photovoltaic cells. *Solar Energy Materials and Solar Cells* 2007, *91* (11), 1010.
(19) Wang, N.; Chen, Z.; Wei, W.; Jiang, Z. Fluorinated benzothiadiazole-based conjugated polymers for high-performance polymer solar cells without any processing additives or post-treatments. *Journal of the American Chemical Society* 2013, *135* (45), 17060.
(20) Oliveira, P. *The Elements*; PediaPress, 2011.
(21) Casado, A. L.; Espinet, P.; Gallego, A. M. Mechanism of the Stille Reaction. 2. Couplings of Aryl Triflates with Vinyltributyltin. Observation of Intermediates. A More Comprehensive Scheme. *Journal of the American Chemical Society* 2000, *122* (48), 11771.
(22) Zhou, E.; Yamakawa, S.; Zhang, Y.; Tajima, K.; Yang, C.; Hashimoto, K. Indolo [3, 2-b] carbazole-based alternating donor–acceptor copolymers: synthesis, properties and photovoltaic application. *Journal of Materials Chemistry* 2009, *19* (41), 7730.
(23) Santos, L. S.; Rosso, G. B.; Pilli, R. A.; Eberlin, M. N. The mechanism of the Stille reaction investigated by electrospray ionization mass spectrometry. *The Journal of organic chemistry* 2007, *72* (15), 5809.
(24) Tsubata, Y.; Suzuki, T.; Miyashi, T.; Yamashita, Y. Single-component organic conductors based on neutral radicals containing the pyrazino-TCNQ skeleton. *The Journal of Organic Chemistry* 1992, *57* (25), 6749.
(25) Robinson, R. S.; Taylor, R. J. Quinoxaline synthesis from α-hydroxy ketones via a tandem oxidation process using catalysed aerobic oxidation. *Synlett* 2005, *2005* (06), 1003.
(26) Takahashi, M.; Masui, K.; Sekiguchi, H.; Kobayashi, N.; Mori, A.; Funahashi, M.; Tamaoki, N. Palladium-Catalyzed C− H Homocoupling of Bromothiophene Derivatives and Synthetic Application to Well-Defined Oligothiophenes. *Journal of the American Chemical Society* 2006, *128* (33), 10930.
(27) Lee, J.; Nolan, T. Sugars with potential antiviral activity—I: A new method for the preparation of glycorufanoyl chlorides and the synthesis of a mannosyl nucleoside. *Tetrahedron* 1967, *23* (6), 2789.
(28) Denton, R. M.; An, J.; Adeniran, B.; Blake, A. J.; Lewis, W.; Poulton, A. M. Catalytic phosphorus (v)-mediated nucleophilic substitution reactions: Development of a catalytic Appel reaction. *The Journal of organic chemistry* 2011, *76* (16), 6749.
(29) Sessler, J. L.; Callaway, W. B.; Dudek, S. P.; Date, R. W.; Bruce, D. W. Synthesis and characterization of a discotic uranium-containing liquid crystal. *Inorganic chemistry* 2004, *43* (21), 6650.
(30) Ram, S.; Ehrenkaufer, R. E. Ammonium formate in organic synthesis: a versatile agent in catalytic hydrogen transfer reductions. *Synthesis* 1988, *1988* (2), 91.
(31) Anwer, M. K.; Sherman, D.; Roney, J. G.; Spatola, A. F. Applications of ammonium formate catalytic transfer hydrogenation. 6. Analysis of catalyst, donor quantity, and solvent effects upon the efficacy of dechlorination. *The Journal of Organic Chemistry* 1989, *54* (6), 1284.

(32) Anwer, M. K.; Spatola, A. F. Applications of ammonium formate catalytic transfer hydrogenolysis--IV1: a facile method for dehalogenation of aromatic chlorocarbons. *Tetrahedron letters* 1985, *26* (11), 1381.
(33) Dobrovolná, Z.; Červený, L. Ammonium formate decomposition using palladium catalyst. *Research on Chemical Intermediates* 2000, *26* (5), 489.
(34) Sharma, U.; Kumar, P.; Kumar, N.; Kumar, V.; Singh, B. Highly Chemo-and Regioselective Reduction of Aromatic Nitro Compounds Catalyzed by Recyclable Copper (II) as well as Cobalt (II) Phthalocyanines. *Advanced Synthesis and Catalysis* 2010, *352* (11-12), 1834.
(35) Brunner, K.; van Dijken, A.; Börner, H.; Bastiaansen, J. J.; Kiggen, N. M.; Langeveld, B. M. Carbazole compounds as host materials for triplet emitters in organic light-emitting diodes: tuning the HOMO level without influencing the triplet energy in small molecules. *Journal of the American Chemical Society* 2004, *126* (19), 6035.
(36) Chen, W.; Yan, L.; Bangal, P. Chemical reduction of graphene oxide to graphene by sulfur-containing compounds. *The Journal of Physical Chemistry C* 2010, *114* (47), 19885.
(37) Chen, Z.; Cai, P.; Zhang, L.; Zhu, Y.; Xu, X.; Sun, J.; Huang, J.; Liu, X.; Chen, J.; Chen, H. Donor–acceptor copolymers based on phenanthrene as electron-donating unit: Synthesis and photovoltaic performances. *Journal of Polymer Science Part A: Polymer Chemistry* 2013, *51* (23), 4966.
(38) Suzuki, A. Organoboron compounds in new synthetic reactions. *Pure and applied chemistry* 1985, *57* (12), 1749.
(39) Krebs, F. C.; Nyberg, R. B.; Jørgensen, M. Influence of residual catalyst on the properties of conjugated polyphenylenevinylene materials: palladium nanoparticles and poor electrical performance. *Chemistry of materials* 2004, *16* (7), 1313.
(40) Nielsen, K. T.; Bechgaard, K.; Krebs, F. C. Removal of palladium nanoparticles from polymer materials. *Macromolecules* 2005, *38* (3), 658.
(41) Shen, P.; Bin, H.; Zhang, Y.; Li, Y. Synthesis and optoelectronic properties of new D–A copolymers based on fluorinated benzothiadiazole and benzoselenadiazole. *Polymer Chemistry* 2014, *5* (2), 567.
(42) Cartwright, L.; Yi, H.; Iraqi, A. Effect of fluorination pattern and extent on the properties of PCDTBT derivatives. *New Journal of Chemistry* 2016, *40* (2), 1655.
(43) Cartwright, L.; Iraqi, A.; Zhang, Y.; Wang, T.; Lidzey, D. G. Impact of fluorine substitution upon the photovoltaic properties of benzothiadiazole-fluorene alternate copolymers. *RSC Advances* 2015, *5* (57), 46386.
(44) Patel, P.; Hull, T. R.; Lyon, R. E.; Stoliarov, S. I.; Walters, R. N.; Crowley, S.; Safronava, N. Investigation of the thermal decomposition and flammability of PEEK and its carbon and glass-fibre composites. *Polymer degradation and stability* 2011, *96* (1), 12.

Chapter 3: Phenanthrene-Thieno[3,4-C]Pyrrole-4,6-Dione Based Polymers for OPV applications

Abstract

A series of narrow band-gap copolymers of thieno[3,4-c]pyrrole-4,6-dione (TPD) as an acceptor, alternating with either electron donors of phenanthro[9,10-b]quinoxaline to give **P5** and **P7**, or 9,10-dialkoxy-phenanthreneto give **P6** and **P8**, are all synthesised *via* Suzuki cross-coupling. Moreover, these copolymers are designed by taking into consideration some parameters that affect the electrical and optical properties of conjugated polymers. The acceptor has a substituent of solubilising group (3,7-dimethyloctyl) on the nitrogen of the imide group in the TPD unit, to enhance solubility of the resulting polymers. In addition, two different alkoxyl substituents are incorporated to donor moieties, and consequently they display good solubility in many organic solvents at room temperature. Furthermore, a number of thienyl units are attached between the donor-acceptor units along the polymer chains to promote conjugation. The report also demonstrates the results of the synthesis of the monomers and copolymers, as well as the data from UV-Vis, CV analysis and TGA for the synthesised copolymers. **P5** and **P6** reveal similar optical band gaps with values of 2.05 eV and 2.03 eV respectively. In contrast, **P7** and **P8** exhibit optical band gaps that are similar to each other but narrower than those for **P7** and **P8,** with values of 1.93 eV and 1.94 eV respectively. This is due to the extension of the conjugation system by the addition of thiophene units flanking **P7** and **P8**. **P7** and **P8** show slightly higher-lying HOMO energy levels than **P5** and **P6**, due to the extension of the conjugation, which leads to an increase in ICT along the backbone of the polymers. Hence, **P7** and **P8** display narrower electrochemical band gaps than **P5** and **P6,** with values of 1.96 eV and 1.95 eV respectively. All polymers show good thermal stability with decomposition temperatures in excess of 300˚C, which is sufficient for the requirements of OSC applications.

3.1. Introduction

As explained in Chapter 1, the high demand for alternative energy resources to replace fossil fuels has led researchers to focus on the exploration of the use of solar energy, which is the only renewable source with the potential to satisfy the world's large and increasing energy demand.[1] Currently, inorganic solar cells dominate commercially available PV technologies. They are based on materials such as wafer-sized single-junction crystalline silicon. These solar cells exhibit a reasonably high PCE of approximately 25 per cent.[2] However, there are drawbacks such as environmental issues, the high cost of manufacturing, and poor performance at low light levels.[1]

Therefore, OPV cells have drawn attention, since organic semiconductors can offer improved performances over their inorganic equivalents: for instance, they offer high absorption coefficients, light weight, large active layers, low-cost production processes and ease of fabrication.[3, 4]

BHJ solar cells employ the most common architecture for the active layer. They utilise conjugated polymers as the electron donor (p-type material) and a fullerene derivative as the electron acceptor (n-type material). They are mixed together to form bicontinuous interpenetrating networks that provide a large interfacial area for favoured charge-separation and transport characteristics.[4] Device efficiencies can be improved by the adjustment of morphology and the blending ratio between the donor and acceptor. Some OPV devices offer PCEs of more than 10 per cent.[5]

High efficiencies in OPV cells can also be achieved through the synthesis and design of conjugated polymers that exhibit low band gaps, extended absorption in the visible and infrared regions, high molecular weights and high charge-carrier mobilities suitable for PV applications. In addition, the solubility of these conjugated polymers can be determined by the length of the side chains attached to their rigid backbones. The design of conjugated polymers that consist of alternating D-A groups is a promising strategy to produce high-efficiency BHJ solar cells. Through this approach, the band gap can be modified and the HOMO and LUMO energy levels can be tuned to desired positions.[1] The alteration of the electron-rich donor unit with an electron-deficient acceptor group can also improve ICT along the polymer backbone chain and therefore enhance charge-carrier mobility. In addition, this arrangement enables the conjugated polymers to harvest many photons efficiently from the whole solar spectrum.[6]

Thieno[3,4-c]pyrrole-4,6-dione (TPD) has drawn much attention within the research community and has been investigated for use in OPV cells.[7] Previous studies demonstrated that TPD had a highly compact planar structure with a high degree of symmetry and strong electron-withdrawing characteristics. This improves electron delocalisation along polymer chains, which reduces the band gap between the HOMO and LUMO levels of the resulting copolymers and promotes their hole mobility.[8] The strong electron-withdrawing nature of TPD leads to electron-seeking characteristics, so copolymerisation with a strong electron-rich unit produces a favourable D-A arrangement. This improves ICT along the polymer backbone chain. Polymers based on TPD as an electron acceptor have shown efficiencies of more than nine per cent when fabricated into a BHJ solar cell.[9,10] Moreover, the nitrogen of the imide group in the TPD unit can be functionalised by the introduction of various solubilising groups, to enhance solubility of the resulting polymers.[11]

Leclerc *et al.* initiated the investigation of the TPD unit when they copolymerised it with benzodithiophene (BDT), producing the copolymer **PBDT-TPD.** This copolymer displayed a PCE of 5.5 per cent. Its structure is shown in Figure 3.1.[8]

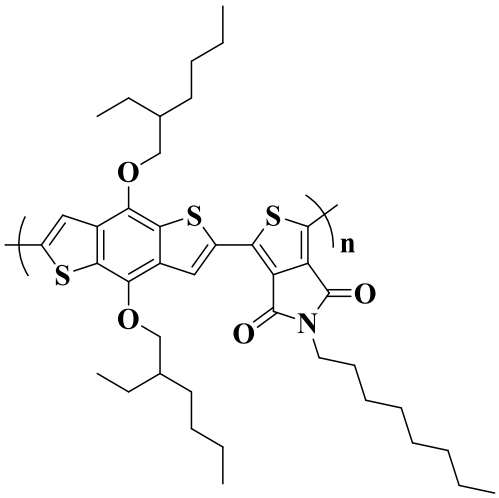

Figure 3.1. Polymer structure of PBDT-TPD synthesised by Leclerc and co-workers.[8]

Another study performed by Chu *et al.* synthesised the copolymer **PDTS-TPD-C8,** which showed high molecular weight and a PCE of 7.5 per cent when fabricated into BHJ solar cells. This polymer is shown in Figure 3.2.[12]

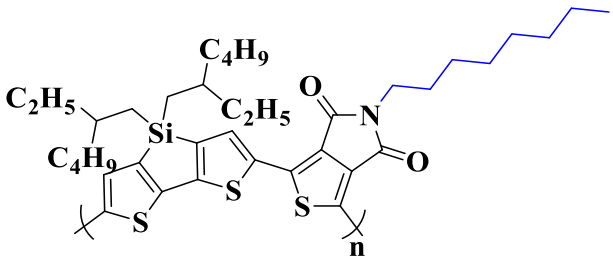

Figure 3.2. Polymer structure of PDTS-TPD-C8 synthesised by Chu *et al.* and co-workers.[12]

Clément *et al.* demonstrated the effect of various side chains on **PBDT-TPD** and the impact of these side chains on the efficiency of OPV devices when fabricated into BHJ solar cells. The study revealed that, when the nitrogen of the imide group in the TPD unit was functionalised by the attachment of an n-heptyl group, the fabricated devices displayed an improved PCE of 8.5 per cent with V_{oc} of 0.97V. The polymer's structure is displayed in Figure 3.3.[9]

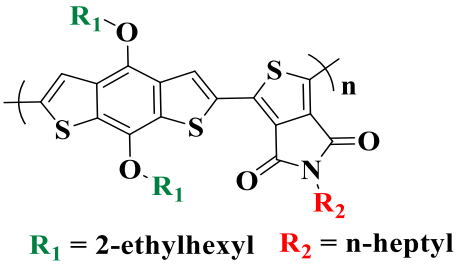

Figure 3. 3. Polymer structure of PBDT-TPD synthesised by Clément and co-workers.[9]

The current study reports the synthesis of a series of conjugated polymers consisting of TPD units in an alternate arrangement with two frequently used donor segments: phenanthro[9,10-b]quinoxaline and 9,10-dialkoxy-phenanthreneunits. The two resulting copolymers produced are poly[[11,12-bis-(2-hexyldecyloxy)-phenanthro[9,10-b]quinoxaline]-(2,7-di-yl)-alt-[1,3-bis(thiophen-2-yl)-5-(3,7-dimethyloctyl)-4H-thieno[3,4-c]pyrrole-4,6(5H)-dione]-5,5-(di-yl)], (**P5**), and poly[9,10-bis(2-hexyldecyloxy)-2,7-phenanthrene-alt-[1,3-bis(thiophen-2-yl)-5-(3,7-dimethyloctyl)-4H-thieno[3,4-c]pyrrole-4,6(5H)-dione]-5,5-(di-yl)], (**P6**). The preparation method for these polymers is shown in Scheme 3.1.

In addition, the conjugation system can be extended by the introduction of a bithiophene unit to the electron acceptor group, which reduces the optical band gap and any steric hindrance. This produces poly[[11,12-bis-(2-hexyldecyloxy)-phenanthro[9,10-b]quinoxaline]-(2,7-di-

yl)-alt-[1,3-bis([2,2'-bithiophen]-5-yl)-5-(3,7-dimethyloctyl)-4H-thieno[3,4-c]pyrrole-4,6(5H)-dione]-5,5-(di-yl)], (**P7**), and poly [9,10-bis(2-hexyldecyloxy)-2,7-phenanthrene-alt-[1,3-bis([2,2'-bithiophen]-5-yl)-5-(3,7-dimethyloctyl)-4H-thieno[3,4-c]pyrrole-4,6(5H)-dione]-5,5-(di-yl)], (**P8**). The methods of preparation of these polymers are shown in Scheme 3.2.

3.2. Results and Discussion

3.2.1. Synthesis of Monomers for the Thienopyrroledione- based Copolymers P5, P6, P7 and P8

Scheme 3.1 shows the monomers required to prepare polymers **P5** and **P6**. The 1,3-bis(5-bromo-thiophen-2-yl)-5-(3,7-dimethyloctyl)-4H-thieno[3,4-c]pyrrole-4,6(5H)-dione, **(31)**, 2,7-bis-(4,4,5,5-tetramethyl-1,3,2-dioxaborolan-2-yl)-11,12-bis-(2-hexyldecyloxy)-phenanthro[9,10-b]quinoxaline, **(16)**, and 2,7-bis-(4,4,5,5-tetramethyl-1,3,2-dioxaborolan-2-yl)-9,10-bis-(2-butyl-octyloxy)-phenanthrene, **(19)**, were prepared in good yields. Their purities and structures were confirmed by mass spectrometry analysis, ^{1}H-NMR, ^{13}C-NMR and elemental analysis. Compound **(31)** was used as an electron acceptor, with compounds **(16)** and **(19)** as electron-donor units to prepare polymers **P5** and **P6** respectively.

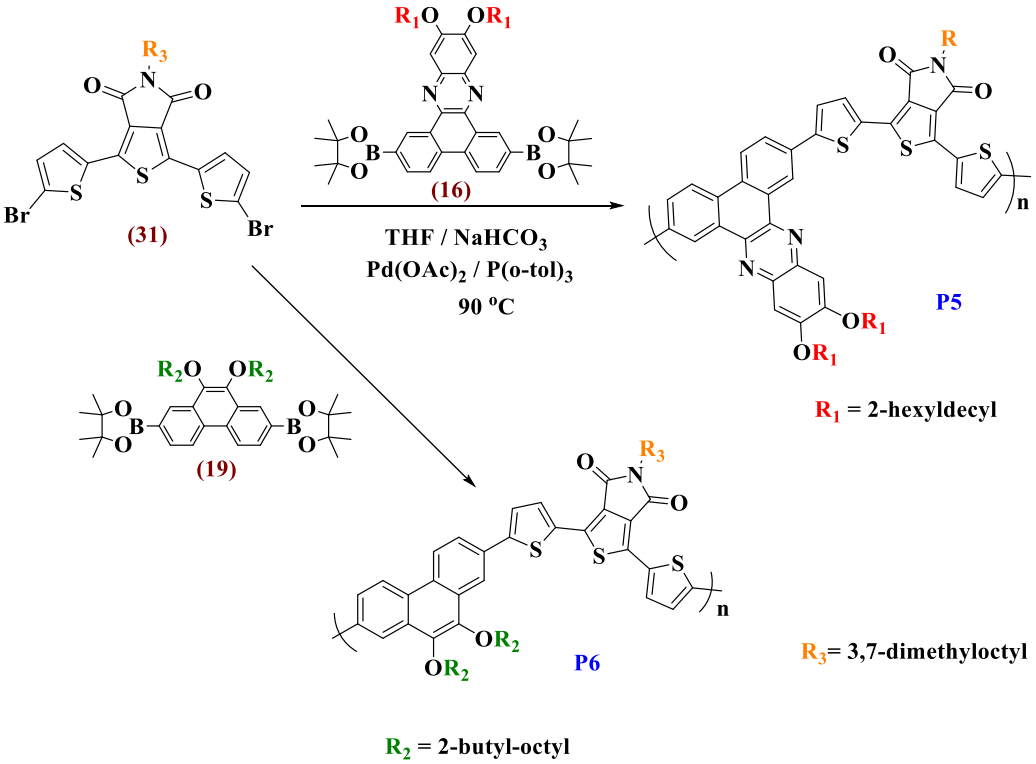

Scheme 3.1. The preparation of P5 and P6 from monomers (31), (16) and (19).

Scheme 3.2 shows which monomers were required to prepare polymers **P7** and **P8**. The 1,3-bis(5'-bromo-[2,2'-bithiophen]-5-yl)-5-(3,7-dimethyloctyl)-4H-thieno[3,4-c]pyrrole-4,6(5H)-dione, **(33)**, compound **(16)** and compound **(19)** were synthesised in good yields. The monomer purities and structures were confirmed as before. Compound **(33)** was used as an electron acceptor, and compounds **(16)** and **(19)** were used as electron-donor units to prepare polymers **P7** and **P8** respectively.

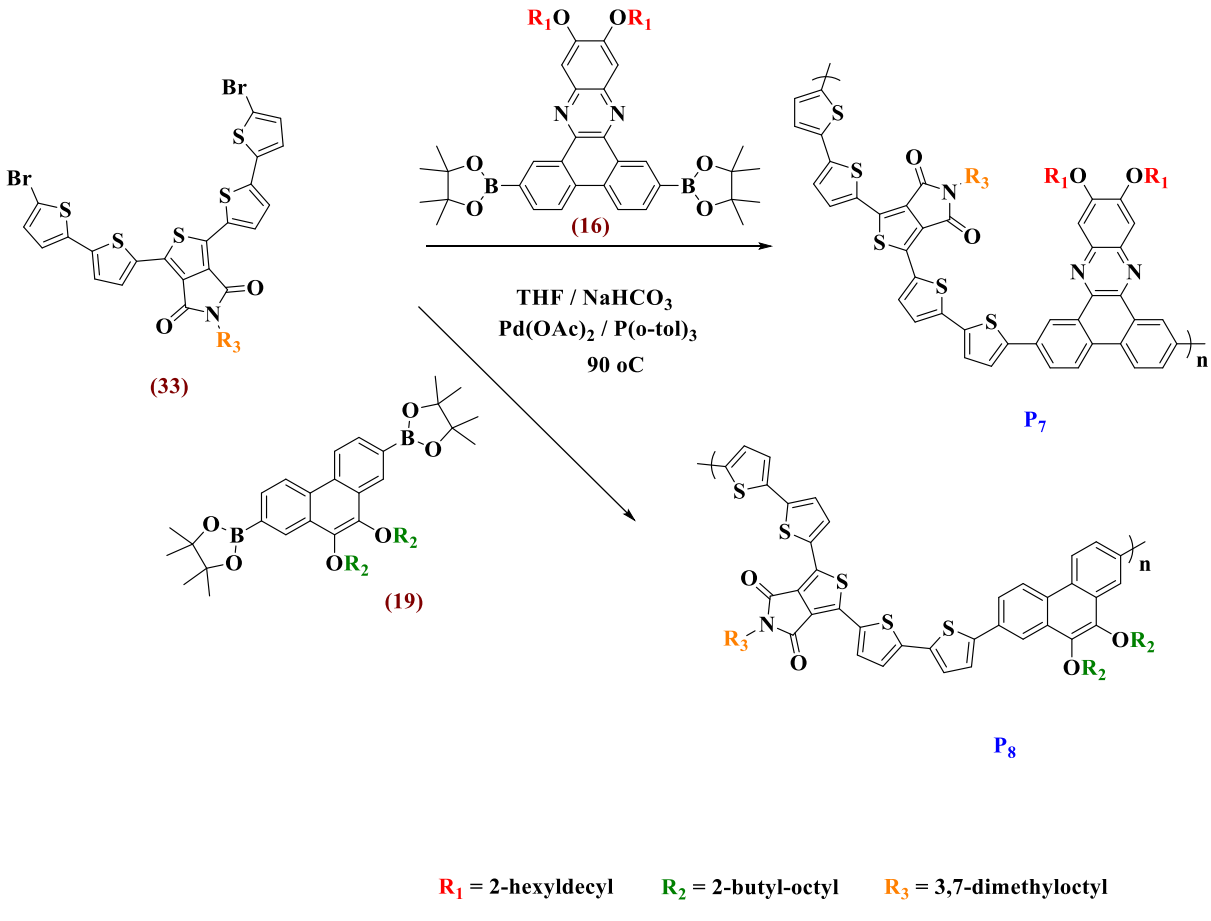

Scheme 3.2. Preparation method for P7 and P8 from monomers (33), (16) and (19)

The synthetic route for the preparation of compound **(31)** is shown in Scheme 3.3. The synthetic route for the preparation of compounds **(16)** and **(19)** were previously shown in Scheme 2.11 and Scheme 2.15 respectively, in Chapter 2.

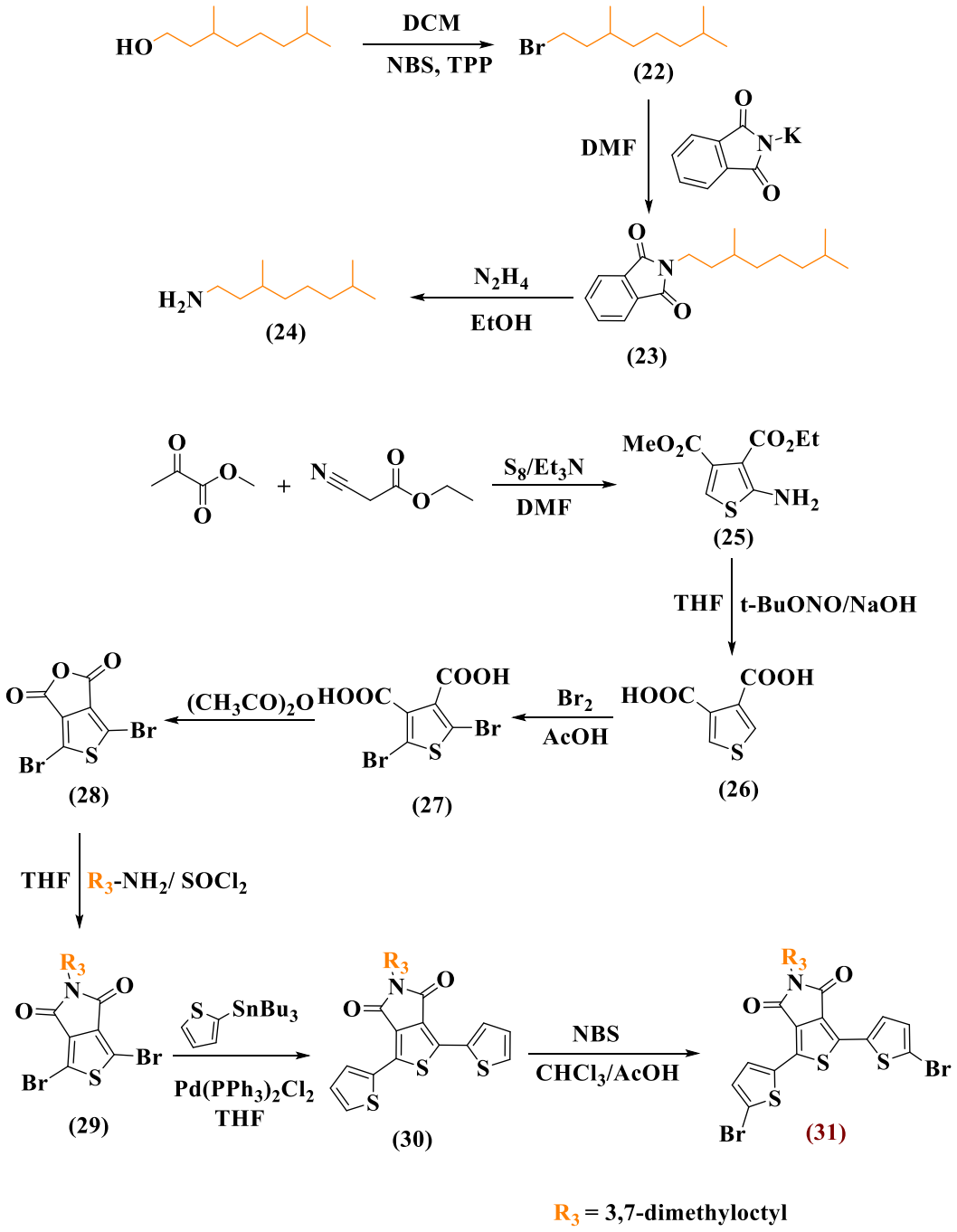

Scheme 3.3. The synthetic route for production of monomer 1,3-bis(5-bromo-thiophen-2-yl)-5-(3,7-dimethyloctyl)-4H-thieno[3,4-c]pyrrole-4,6(5H)-dione (31)

The synthetic route for the preparation of compound **(33)** is shown in Scheme 3.4.

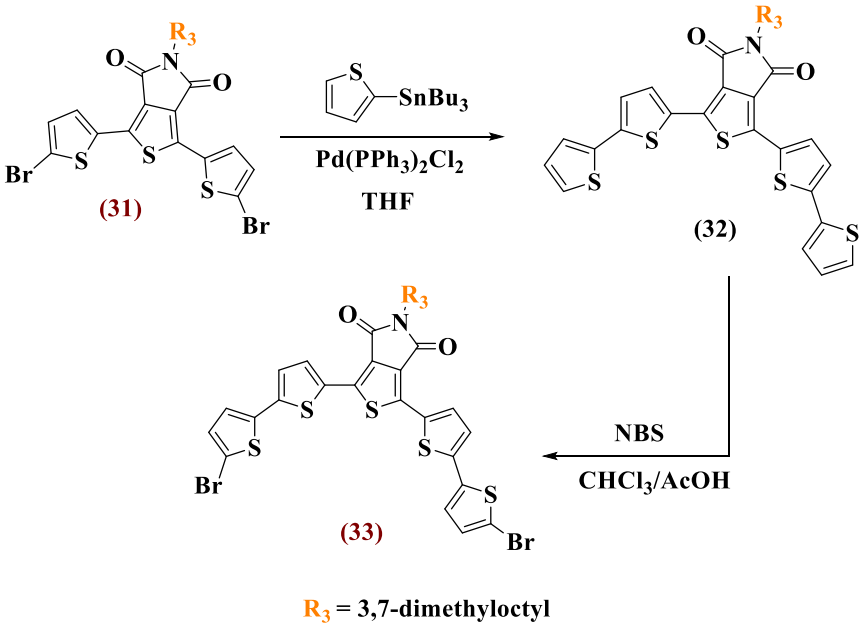

Scheme 3.4. The synthetic route for production of monomer 1,3-bis(5'-bromo-[2,2'-bithiophen]-5-yl)-5-(3,7-dimethyloctyl)-4H-thieno[3,4-c]pyrrole-4,6(5H)-dione (33).

3.2.1.1. Synthesis of the electron acceptor monomers (31) and (33).

The first reaction in the synthetic route towards the preparation of monomers **(31)** and **(33)** was the preparation of 3-ethyl-4-methyl-2-aminothiophene-3,4-dicarboxylate **(25)**. This compound was synthesised according to the procedure by Gewald.[13]

The suggested mechanism of ring closure of compound **(25)** is shown below.

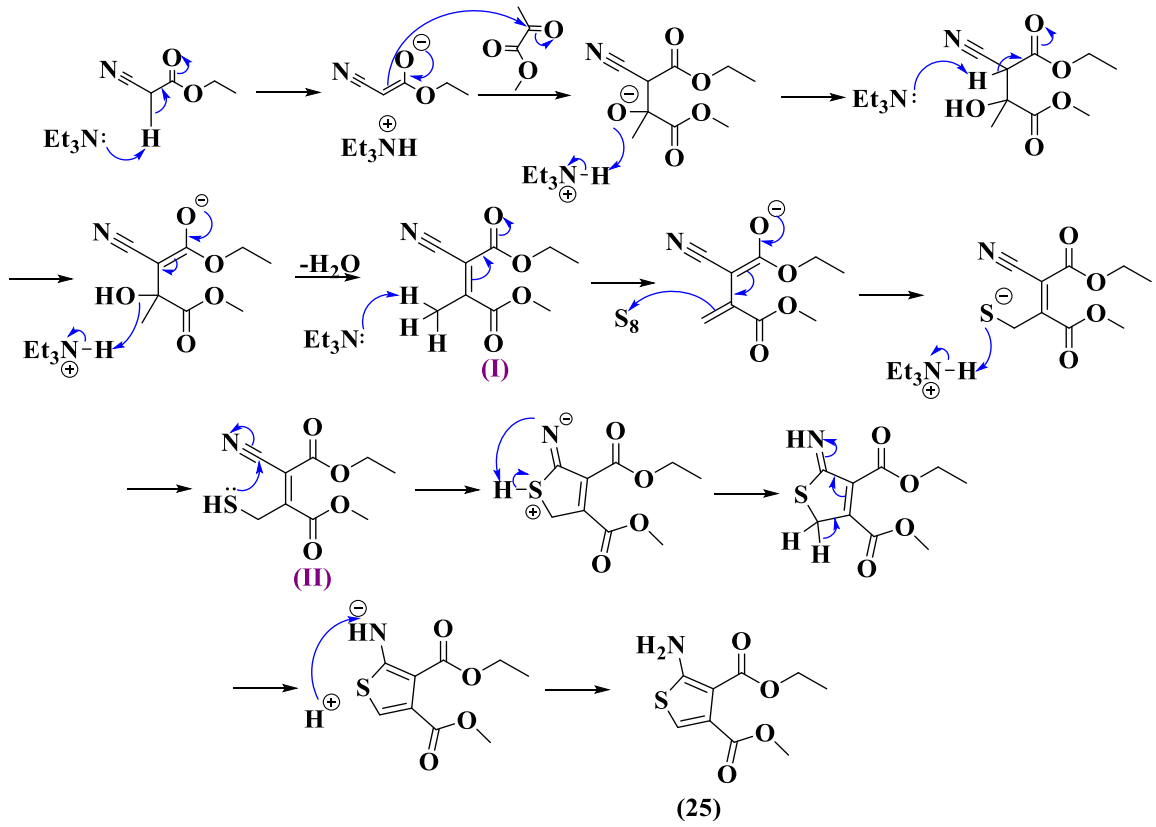

Scheme 3.5. Suggested mechanism for the formation of compound (25).

An α-activated cyanoester (ethyl cyanoacetate in this case) was reacted with a ketone (in this case methyl pyruvate) in a basic solvent such as trimethylamine and in the presence of sulphur. The first step is known as a Knoevenagel condensation between an α-activated cyanoester and a ketone. Then water was eliminated to produce a stable intermediate labelled **(I)** in Scheme 3.5. The mechanism of the sulphur addition steps is not clearly known. It is hypothesised that an intermediate known as an ylidene-sulphur adduct **(II)** is formed. In the case of this study, ring closure and tautomerisation of intermediate **(II)** followed to produce the target compound **(25)**.[14]

Compound **(26)** was synthesised according to a procedure modified from that developed by Sandmeyer.[7]

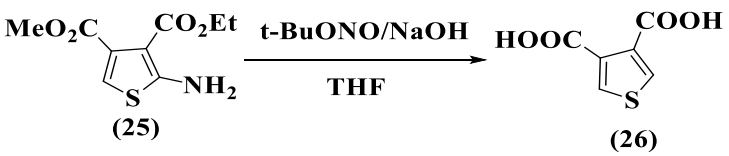

The tertiary amine group in compound **(25)** was removed through use of t-butyl nitrite, after which the ester was hydrolysed to produce compound **(26)**. The mechanism of the deamination and hydrolysis of compound **(25)** is shown below.

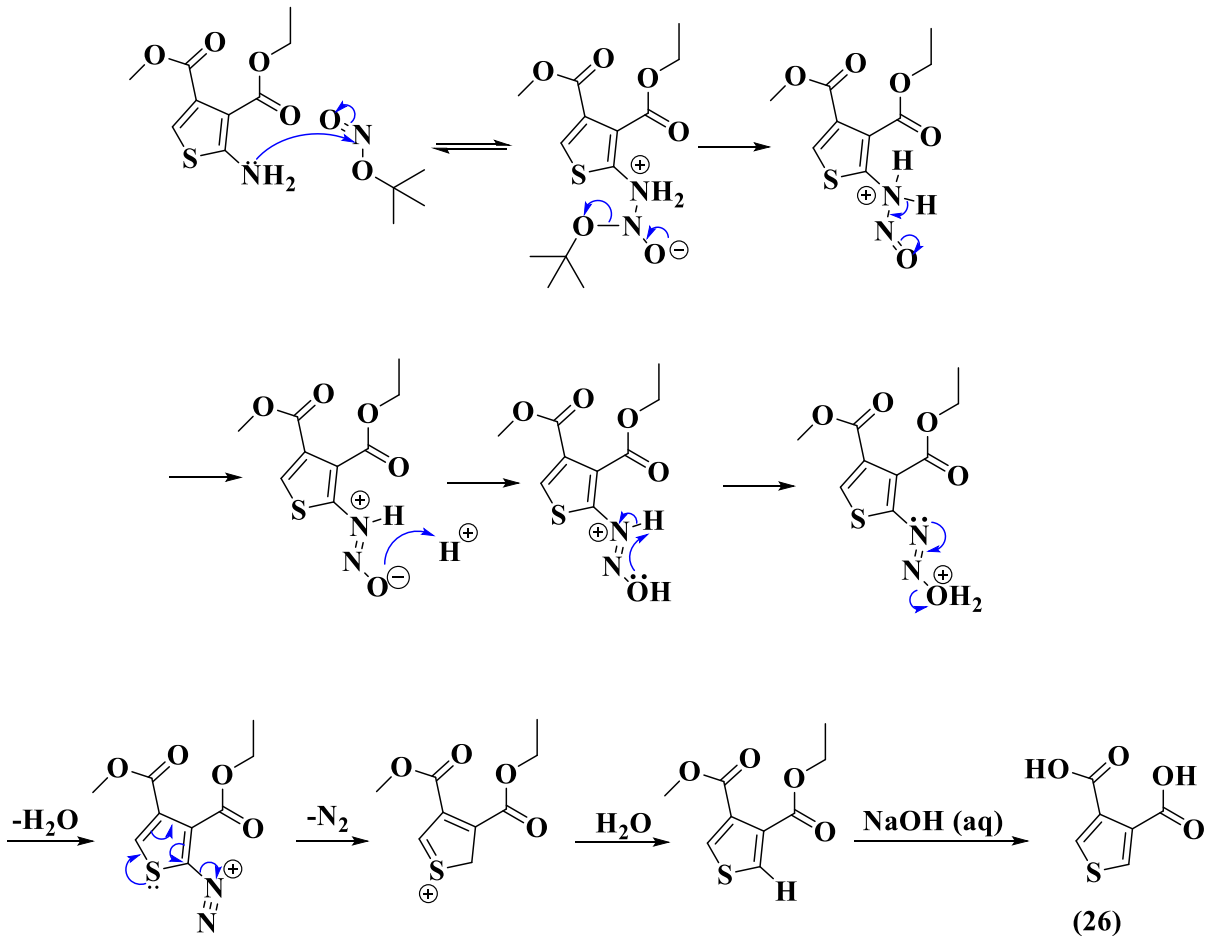

Scheme 3.6. Mechanism of production of compound (26).

Bromination of compound **(26)** at positions 2 and 5 on the thiophene ring through the use of bromine in the presence of acetic acid produced compound **(27)**.[15]

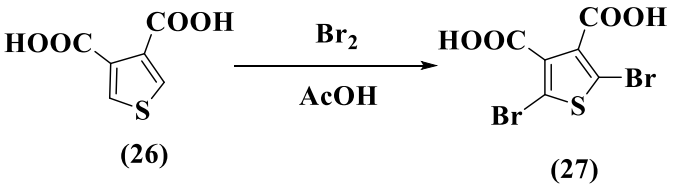

Acetic acid was used as a polar solvent to facilitate the bromination due to the moderately deactivating effect of carboxylic acid groups on the thiophene ring. Acetic acid also stabilised the ionic intermediate.[15]

Compound **(28)** was obtained through the heating of compound **(27)** in acetic anhydride,[16] which operated as a dehydrating agent. The elimination of water produced the cyclic anhydride group within compound **(28)**.

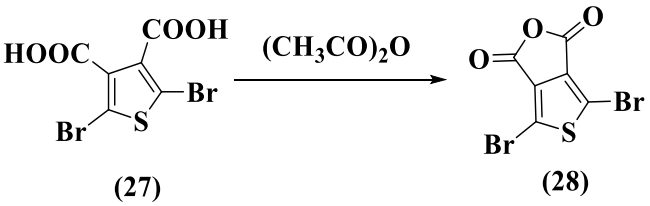

The next step featured a reaction of compound **(28)** with a primary amine (3,7-dimethyloctan-1-amine in this case) to convert the cyclic anhydride to a cyclic imide. Reaction intermediate **(I)** was then reacted with thionyl chloride to yield compound **(29)**.[11] The suggested mechanism of formation of compound **(29)** is shown below in Scheme 3.7.

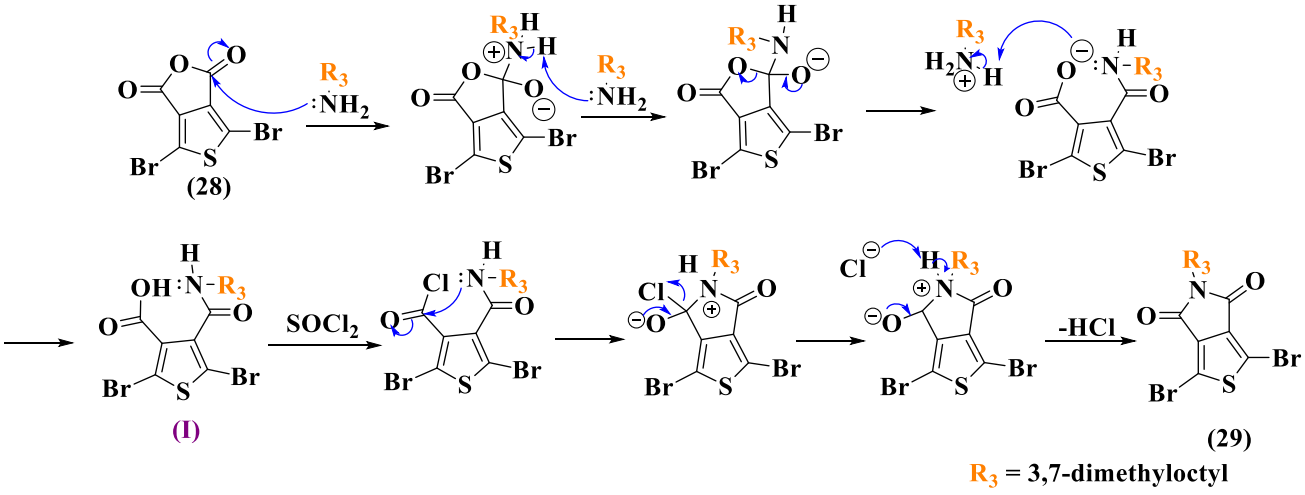

Scheme 3.7. Mechanism of production of compound (29).

Compound **(30)** was then synthesised from compound **(29)** *via* Stille cross-coupling.[17] Bromination of compound **(30)** at both positions 5 on the thiophene rings through the use of NBS in the presence of acetic acid yielded monomer **(31)**.[18]

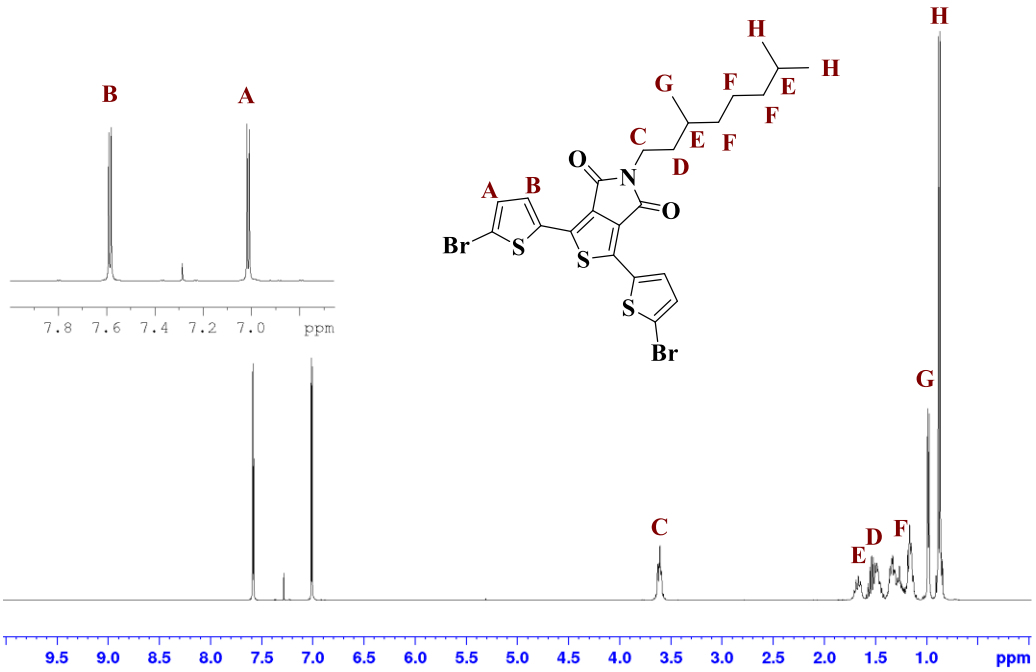

Figure 3.4. ^{1}H-NMR spectrum of compound (31) in $CDCl_3$.

Monomer **(33)** was obtained through a Stille coupling reaction of compound **(31)**, followed by bromination of both positions 5 on the thiophene rings**.**

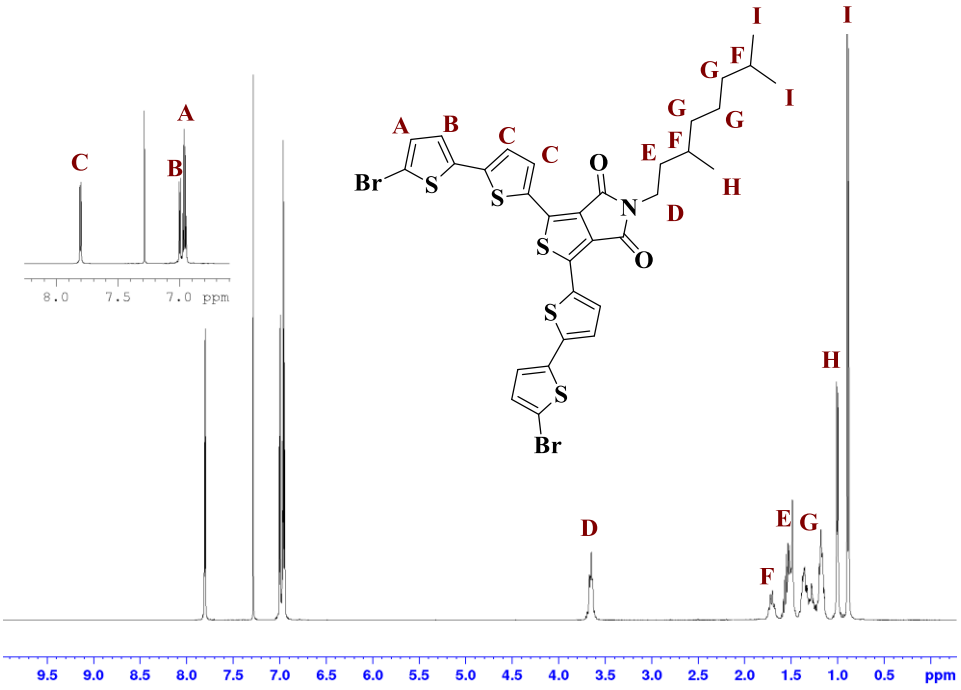

Figure 3. 5. ^{1}H-NMR spectrum of compound (33) in $CDCl_3$.

Monomers **(31)** and **(33)** were prepared *via* a procedure modified from that carried out by Takahashi *et al.*[18] The product was purified by column chromatography using petroleum ether:

dichloromethane as the eluent. The purity of the product was confirmed by gas chromatography-mass spectrometry and elemental analysis. The structure of the product was identified by ^{1}H NMR and ^{13}C NMR. The mass spectra for **(31)** and **(33)** showed peaks at 615 and 779 respectively. Compared with the ^{1}H NMR spectra of compounds **(30)** and **(32)**, the ^{1}H NMR spectra of **(31)** and **(33)** respectively displayed no peaks in the aromatic region that corresponded to the two protons on the thiophene rings. This suggested that bromination had been successful.

3.2.2. Synthesis of the series of TPD-based-alternating copolymers P5, P6, P7 and P8

Four alternating D-A copolymers discussed in this chapter were prepared *via* Suzuki cross-coupling between the boronic ester monomers **(16)** and **(19)** as electron donors (Schemes 3.1 and 3.2), and the dibrominated monomers **(31)** and **(33)** as electron acceptors (Schemes 3.3 and 3.4). The polymerisation procedure was carried out through a similar method to that used in Chapter 2. Polymerisation reactions to produce **P5** and **P6** were stopped after 72 hours. The polymerisation reactions to synthesise **P7** and **P8** were stopped after 24 hours, after which time a large quantity of polymer precipitate had formed.

All polymerisations followed the mechanism of the Suzuki cross-coupling reaction, which was described in Chapter 1.[19] All reactions were stopped temporarily to add the end-capping reagents to the polymer solutions. This would also increase the stability of the polymers during fabrication of solar cell devices. The polymers were fractionated by Soxhlet extraction, with the use of the following solvents: methanol, acetone, hexane toluene and chloroform. The chemical structures of all the polymers were verified by ^{1}H-NMR and elemental analysis. GPC was used to determine the M_n and M_w using 1,2,4-trichlorobenzene as an eluent at 140^{o}C, and polystyrene as the internal standard (Table 3.1).

All polymers showed good solubility in organic solvents at room temperature. The yields of all polymers were higher than 65 per cent. **P7** showed the highest M_w and M_n compared with all polymers whose synthesis is discussed in this chapter, with values of 49,700Da and 43,500Da respectively. Its analogous polymer **P5** showed significantly lower M_w and M_n values of 12,300 Da and 7,200 Da respectively. This is a consequence of the presence of bithiophene spacer units flanked by the acceptor moiety, which leads to a reduction in the steric repulsion between the bulky groups attached to the donor and acceptor moieties during

the coupling reaction. It is hypothesised that this reduced steric hindrance enabled polymerisation to continue further and hence the formation of a polymer with high molecular weight.

In addition, three bulky solubilising groups were thought to decrease the planarity of **P7** and impede its π-π stacking, thereby reducing intermolecular interaction and leading to a polymer of high molecular weight. These solubilising groups were: the 3,7-dimethyloctyl chain that was attached to the TPD moiety, and the two 2-hexyldecyl groups attached to the highly planar phenanthrene-quinoxaline donor moiety.

In contrast, **P8** displayed lower M_w of 17,200Da compared with its counterpart **P6**, which showed M_w of 26,200Da. It is speculated that the incorporation of bithiophene spacer units in the TPD moiety in polymer **P8** extends the π-conjugation and enhances the rigidity of polymer backbones, and therefore hinders the formation of polymers with high molecular weight.[20]

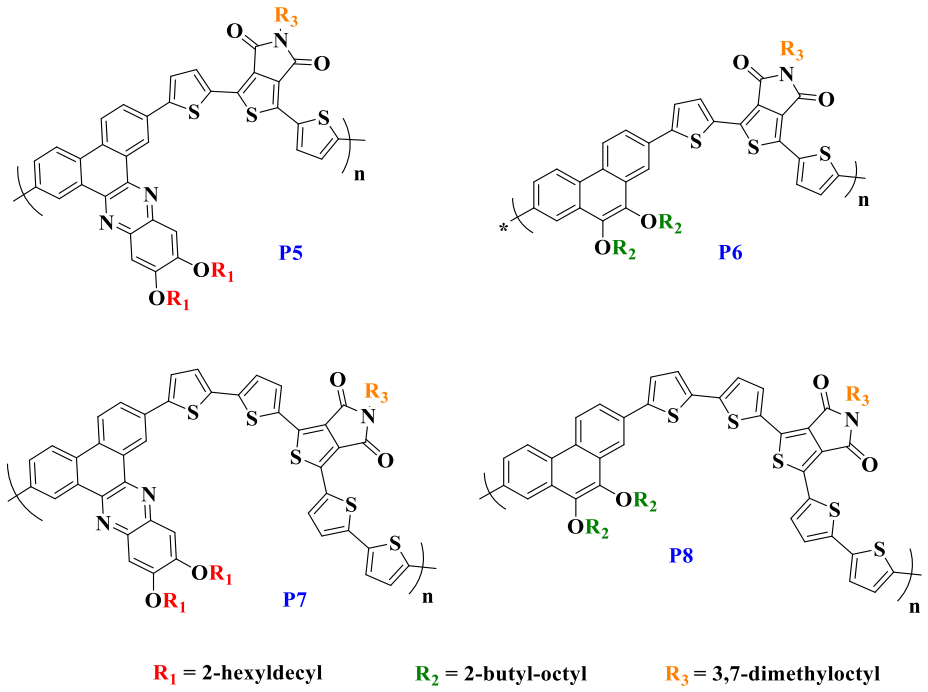

Scheme 3.8. Polymers P5, P6, P7 and P8 whose synthesis is discussed in this chapter.

Table 3.1 GPC analysis of P5, P6, P7 and P8

Polymer	M_n (Da) [a]	M_w (Da) [a]	PDI	Yield (%)
P5	7,200	12,300	1.71	88
P6	9,700	26,200	2.68	84
P7	43,500	49,700	1.14	80
P8	11,800	17,200	1.46	67

Measurements conducted on the chloroform fraction of the polymers. [a] GPC conducted in 1,2,4-trichlorobenzene at 140 °C using a differential refractive index (DRI) detection method. PDI = Polydispersity Index.

3.2.3. Analysis by UV-Visible absorption spectroscopy

UV-Vis was employed to study the optical properties of polymers **P5**, **P6**, **P7** and **P8** in dilute chloroform solutions (Figure 3.7.(a)) and in the solid state as drop-cast thin films on quartz substrates (Figure 3.7.(b)). The optical band gaps of all polymers were determined *via* the onset of optical absorption by the polymers in the solid state. The measured optical properties of all the polymers are summarised in Table 3.2.

Table 3.2. Optical data of polymers P5, P6, P7 and P8

Polymer	ε (M^{-1} cm^{-1})	Solution λ_{max} (nm)	Thin Film λ_{max} (nm)	Thin Film λ_{onset} (nm)	Optical E_g (eV)
P5	48488	494	508	605	2.05 ± 0.031
P6	78162	474	492	610	2.03 ± 0.004
P7	79599	520	533	643	1.93 ± 0.022
P8	68148	507	514	634	1.94 ± 0.006

In chloroform solution, **P5**, **P6**, **P7** and **P8** displayed absorption bands at long wavelengths located at 494nm, 474nm, 520nm and 507nm respectively. These corresponded to ICT between the electron-deficient TPD acceptor units and the electron-rich donor moieties. After drop-casting into thin films, the ICT absorption maxima of **P5**, **P6**, **P7** and **P8** were red-shifted to 508nm, 492nm, 533nm and 514nm, respectively. The red shifts could be ascribed to the conformations of the polymer backbones. These were similar in both solution and in thin films, yet possessed greater planarity in the solid state, which led to stronger π-π

interchain stacking in the solid state. Absorption bands at shorter wavelengths were observed for **P5**, **P7** and **P8** but not for **P6**. These were attributed to π-π* transitions in both solution and in the solid state. **P5** and **P7** showed more pronounced peaks than did **P8**, due to the presence in **P5** and **P7** of the large phenanthrene-quinoxaline donor moiety. The π-π* transitions were observed in **P8** due to the additional bithiophene unit in the **P8** backbone structure when compared with **P6**, which has a single thiophene unit in its backbone structure. **P5** and **P6** showed similar optical band gaps, which were determined from the onset of absorption in the solid state and were estimated to be 2.05 eV and 2.03 eV respectively. **P7** and **P8** also exhibited similar optical band gaps but narrower than those of **P5** and **P6.** They were estimated to be 1.93 eV and 1.94 eV, respectively. The ICT was improved in **P7** and **P8** relative to their analogues **P5** and **P6,** due to the increased conjugation in **P7** and **P8** by the incorporation of additional thiophene units, which led to increased delocalisation of electrons along the polymer backbone and therefore reduced band gaps.

Polymers **P5**, **P6**, **P7** and **P8** were comparable with copolymers synthesised by Cartwright *et al:* **PTA-TPD(O)**, **PTA-TPD(DMO)** and **PTA-TPD(BP)** (Figure 3.6).[21] Their donor moieties were **(triisopropylsilylacetylene or TIPS)**-functionalised anthracene units. Cartwright *et al.* reported that the optical band gaps of **PTA-TPD(O)**, **PTA-TPD(DMO)** and **PTA-TPD(BP)** were estimated to be 2.16 eV, 2.14 eV and 2.12 eV respectively.[21] These polymers contained no spacer units between the electron donor and TPD acceptor units. The authors suggested that the intramolecular steric repulsion between the bulky TIPS groups attached to the donor and acceptor moieties during the coupling reaction was sufficient to disrupt the planarity of the resulting polymer and therefore reduce the electronic conjugation.[21]

However, the study explained in this chapter demonstrates that thiophene spacer units flanked by the acceptor moiety result in reduced steric repulsion between the bulky groups attached to the donor and acceptor moieties during the coupling reaction. This could be deduced from decreases in the optical band gaps. Nevertheless, when conjugated polymers are enriched by the incorporation of spacer units such as thiophene or bithiophene groups, the optical band gaps decrease only to a certain level. If organic semiconductors reached an effective conjugation length, the optical band gaps would not be affected.[22]

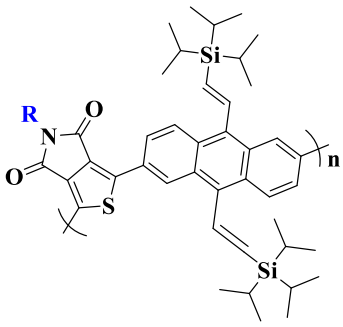

R = n-octyl = PTATPD(O)
R = 4-n-butylphenyl = PTATPD(BP)
R = 3,7-dimethyloctyl = PTATPD(DMO)

Figure 3.6. Polymer structures of PTA-TPD(O), PTA-TPD(DMO) and PTA-TPD(BP), synthesised by Cartwright and co-workers.[21]

The optical band gaps of the polymers discussed in this chapter show a similar trend to that observed for the polymers discussed in Chapter 2. **P1**, **P2**, **P3** and **P4** contain the quinoxaline unit as electron acceptor, whereas **P5, P6, P7** and **P8** incorporate the TPD-acceptor unit, yet polymers **P1**, **P2**, **P5** and **P6** give similar results. In addition, extension of the conjugation systems due to the introduction of additional thiophene produces similar optical band gaps for polymers **P3**, **P4**, **P7** and **P8,** but these are narrower than the band gaps observed in **P1**, **P2**, **P5** and **P6**. This is thought to be due to the quinoxaline-moiety in the electron-donor **(16)**, which contains a pair of nitrogen atoms in its structure that reduces electron density. This reduces its propensity to donate electrons to the same level as that of the other electron donor, which is compound **(19)**. Thus, the electron donors **(16)** and **(19)** show nearly identical donating properties.

However, **P1**, **P2**, **P3** and **P4** exhibit slightly narrower optical band gaps than polymers **P5, P6, P7** and **P8,** owing to the greater electron-deficiency of the quinoxaline-acceptor unit compared with the TPD-acceptor unit. This is due to the presence in the quinoxaline-acceptor unit of the two nitrogen atoms and two fluorine atoms that withdraw electrons and therefore increase its propensity to accept electrons compared with the TPD unit.

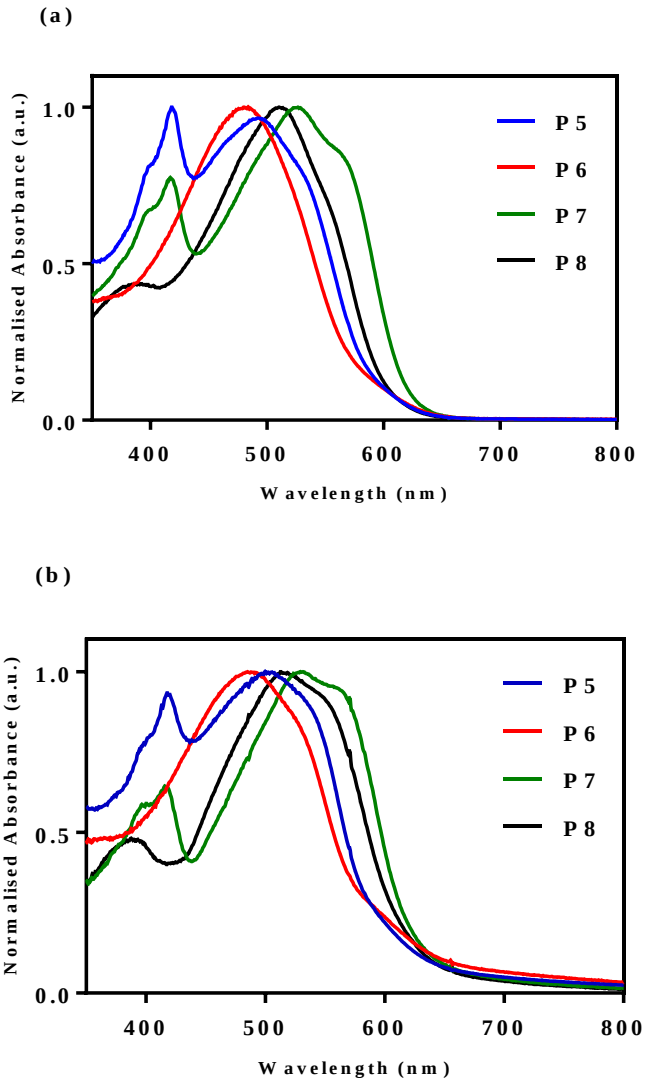

Figure 3.7. Normalised absorption spectra of P5, P6, P7 and P8 in (*a*) chloroform solution; and (*b*) thin films.

3.2.4. Analysis by Cyclic Voltammetry

The results of the study of the electrochemical properties of polymers **P5**, **P6**, **P7** and **P8** by CV are shown in Figure 3.8. The onsets of oxidation and reduction were used to determine the HOMO and LUMO energy levels respectively, compared with *vacuum*.

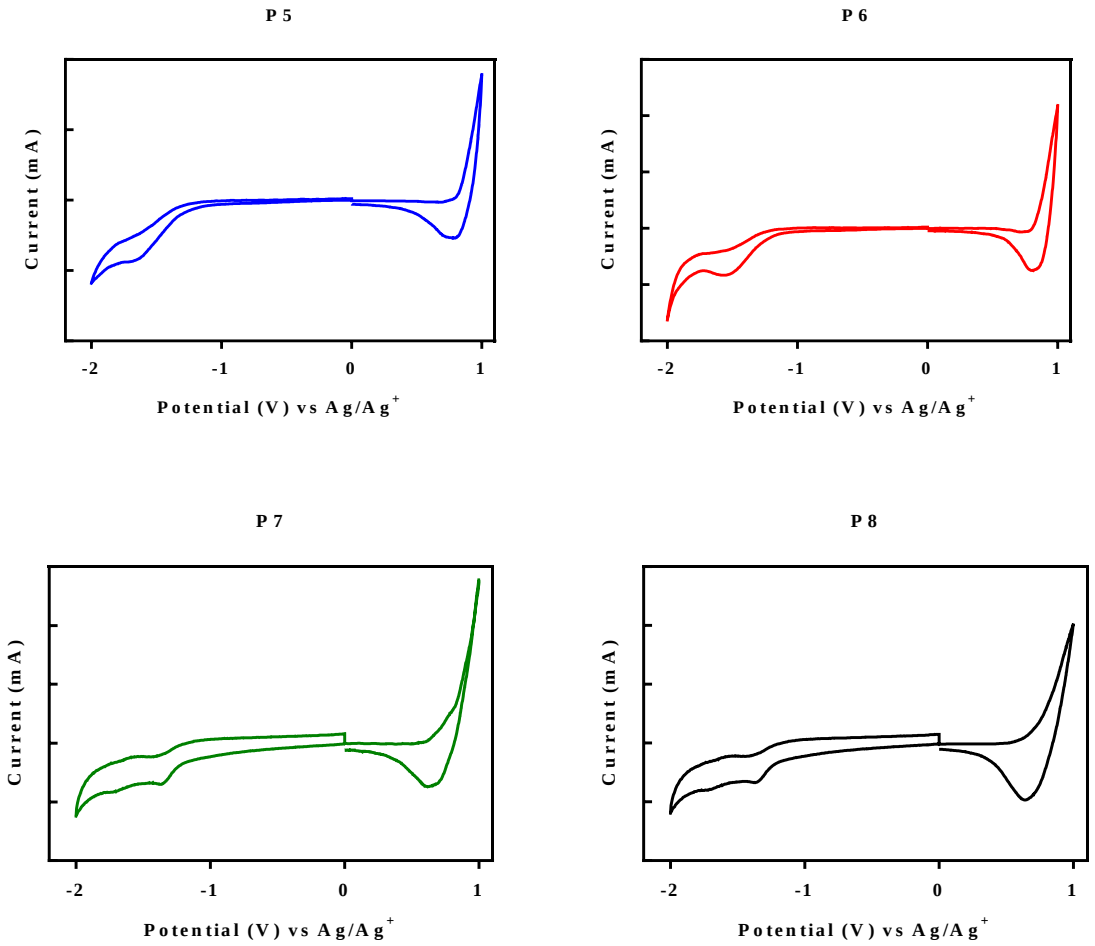

Figure 3.8. Cyclic voltammograms of P5, P6, P7 and P8.

The studies were performed on drop-cast polymer films on a platinum-disc electrode as the working electrode in acetonitrile with tetrabutylammonium perchlorate as the electrolyte (0.1M) and using silver nitrate (Ag/Ag+) as a reference electrode, at a scan rate of 100mV s^{-1} min. The electrochemical band gaps were estimated from the difference of HOMO and LUMO levels, as summarised in Table 3.3.

Table 3.3. Electrochemical properties of P5, P6, P7 and P8

Polymer	HOMO (eV)[a]	LUMO (eV)[b]	E_g^{elect} (eV)[c]
P5	-5.55	-3.46	2.09 ± 0.009
P6	-5.55	-3.51	2.04 ± 0.003
P7	-5.50	-3.54	1.96 ± 0.011
P8	-5.45	-3.50	1.95 ± 0.001

[a] HOMO energy levels determined from the onset of oxidation. [b.] LUMO energy levels determined from the onset of reduction. [c.] Electrochemical band gap.

All polymers displayed very similar low HOMO energy levels. The HOMO levels of both **P5** and **P6,** which contained single thiophene units in their backbone structure, were estimated to be -5.55 eV, whereas **P7** and **P8** that contained bithiophene flanking their donor and acceptor units showed HOMO energy levels calculated to be -5.50 eV and -5.45 eV, respectively. **P7** and **P8** exhibited slightly higher-lying HOMO energy levels than **P5** and **P6**, due to longer conjugation which led to increased ICT along the backbone of the polymers, and hence narrower band gaps. These findings were consistent with the results obtained regarding the optical band gaps.

The electrochemical band gaps of **P5**, **P6**, **P7** and **P8** were estimated to be 2.09 eV, 2.04 eV, 1.96 eV and 1.95 eV, respectively. Polymers **P5** and **P6** showed similar electrochemical band gaps, whereas the increased conjugation of polymers **P7** and **P8** due to additional thiophene led to them exhibiting similar electrochemical band gaps but reduced relative to **P5** and **P6**. It is proposed that this is due to the very similar electron-donating properties of **(16)** and **(19)**. These findings were consistent with the findings regarding optical band gaps, which were lower for **P7** and **P8** when compared with those of their counterparts **P5** and **P6**. The electrochemical band gaps were marginally larger than the optical band gaps. This was because of the interface barrier between the surface of the electrode and the polymers cast as films, which caused the electrochemical band gap to be made up of an optical band gap combined with the interface barrier.[23]

In a previous study, the HOMO energy levels of poly(3-hexylthiophene) (P3HT) was estimated to be -5.00 eV.[24] In contrast, all polymers studied in this chapter exhibited lower-lying HOMO energy levels than P3HT. Lower HOMO levels increase the stability of polymers against oxidisation, which should translate to improved device stability.[25]

P5 exhibited the shallowest LUMO energy levels relative to those of the other polymers whose synthesis is discussed in this chapter. This is a consequence of the strong steric repulsion between the bulky groups attached to the donor and acceptor moieties during the coupling reaction. It is hypothesised that this increased steric repulsion impedes production of long polymers and leads therefore to production of a polymer with low molecular weight. Previous studies have reported that LUMO energy levels are affected by the molecular weight of the polymers. LUMO levels fall more quickly as the polymer chain lengthens.[26] This is consistent with the molecular weights of polymers **P6**, **P7** and **P8**.

3.2.5. Study of Thermal Properties

The thermal stability of the polymers was examined through TGA. The results are shown in Figure 3.9. The temperatures at which decomposition started (T_d) are shown in Table 3.4.

Table 3.4. Thermal Properties of P5, P6, P7 and P8

Polymer	T_d (˚C)[a]
P5	389
P6	343
P7	391
P8	330

[a] Onset of decomposition of polymers determined by using thermogravimetric analysis with a heating rate of 10˚C min^{-1} under an inert nitrogen atmosphere.

P5, **P6**, **P7** and **P8** exhibited good thermal stability with degradation temperatures in excess of 300˚C, which would meet the requirements of OSC applications. **P5** and **P7** each underwent one decomposition phase, and their degradation temperatures were the highest for the four polymers, occurring at 389˚C and 391˚C respectively. **P5** and **P7** have larger aromatic conjugated backbones than **P6** and **P8.** These backbones make the polymers more rigid than **P5** and **P7,** and they therefore require more thermal energy to force breakage. The initial weight loss of **P5** and **P7** corresponded to the loss of both the alkyl chains (2-hexyldecyl) anchored to their donor moieties. In contrast, **P6** and **P8** each displayed two decomposition stages. The first occurred at noticeably lower onset of degradation temperatures of 343˚C and 330˚C, respectively, due to the cleavage of the alkoxy groups (2-

butyloctyl) attached to their donor moieties. The second decomposition phase corresponded to the degradation of the residual conjugated polymer backbone, at onset of degradation temperatures of 455˚C and 463˚C, respectively. As had been observed with **P1**, **P2**, **P3** and **P4**, all the polymers degraded until 50 per cent of the mass remained, and then the curves levelled off until the equipment limit was reached at 800˚C. It is hypothesised that during combustion, polymers with large alkyl chains become less volatile. Hence, during decomposition of **P5**, **P6**, **P7** and **P8**, a thick charred layer formed on the virgin polymer, which insulated the virgin polymer from the heat flux due to its low thermal conductivity. This process would delay the thermal decomposition of the polymers.[27]

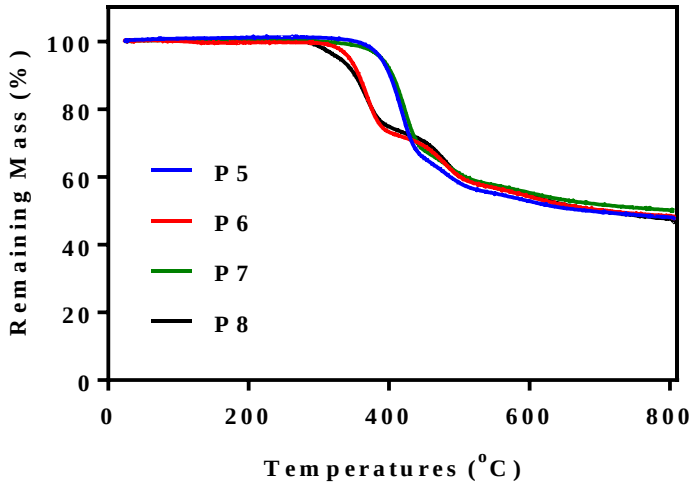

Figure 3.9. Thermogravimetric analysis of P5, P6, P7 and P8 carried out at a heating rate of 10°C min^{-1} under an inert nitrogen atmosphere.

3.2.6. Studies of the Polymers' Molecular Structures

The molecular order studies of polymers **P5**, **P6**, **P7** and **P8** were carried out *via* PXRD in the solid state (Figure 3.10). The PXRD curves for **P5** and **P7** demonstrate broad diffuse peaks in the region of wide-angle scattering located at 2θ values of 19.7° and 20.6°, which correspond to the π-π stacking distance of 4.50Å and 4.31Å, respectively. The lack of peaks in the low-angle region provides evidence that all the synthesised conjugated polymers reported in this chapter do not exhibit long-range order in thin films. It is speculated that this is a result of the attachment of large, sterically demanding alkoxy groups to the donor moieties. The results indicate that **P5** and **P7** exhibit amorphous nature.

The PXRD patterns of **P6** and **P8** display small but pronounced peaks in the low-angle region, positioned at 2θ values of 4.01° and 3.72° respectively. These peaks represent lamellar stacking distances of 22.01Å and 23.72Å for **P6** and **P8** respectively. In addition, **P6** and **P8** show weak, broad diffraction peaks in the wide-angle area located at 2θ values of 19.9° and 20.11°, which are equivalent to the π-π stacking distance of 4.46Å and 4.41Å respectively. Pronounced peaks in the low-angle region of the PXRD patterns for conjugated polymers correspond to backbones of polymers separated by solubilising groups that are attached to electron-donor and acceptor units along the polymer chains.[28] Therefore, the greater stacking distance suggests that all the polymers exhibit amorphous nature.

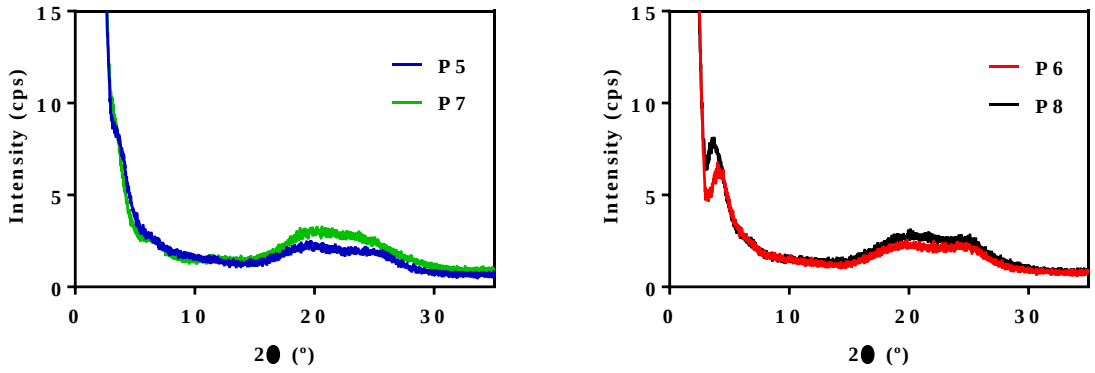

Figure 3.10. PXRD patterns of polymers P5, P6, P7 and P8.

3.3. Conclusion

A series of TPD-based copolymers **P5**, **P6**, **P7** and **P8** were synthesised by Suzuki cross-coupling. Their optical, electrochemical and thermal properties in the solid state were investigated. All the polymers showed good solubility in many organic solvents at room temperature, which was a consequence of the incorporation of solubilising groups on to the electron-acceptor and donor units. The yields of all polymers were greater than 65 per cent. GPC data revealed that **P7** had the highest M_w and M_n values of all the polymers whose synthesis was explained in this chapter. This can be attributed to the effect of bithiophene spacer units flanked by the acceptor unit. These spacer units reduced the severity of steric repulsion between the bulky groups attached to the donor and acceptor moieties during the coupling reaction, which enabled polymerisation to continue until a polymer with high molecular weight was produced.

P5 and **P6** displayed similar optical band gaps with values of 2.05 eV and 2.03 eV respectively. **P3** and **P4** also exhibited similar but lower optical band gaps of 1.93 eV and 1.94 eV respectively, due to the extension of the conjugation system by the addition of two more thiophene units to **P7** and **P8**. All polymers exhibited red shifts when studied as thin films, which could be ascribed to the greater planarity of the polymer backbones in the solid state, leading to stronger π-π interchain stacking.

CV analysis of all the polymers showed very similar low HOMO energy levels. **P7** and **P8** exhibited slightly higher-lying HOMO energy levels with values of -5.50 eV and -5.45 eV respectively, owing to the extension of the conjugation length which resulted in increased ICT along the backbones, and therefore, narrower electrochemical band gaps. All the LUMO energy levels of the polymers lay at higher energies than the LUMO energy level of $PC_{71}BM$.[29] Therefore, efficient separation and charge transfer could be anticipated in their corresponding devices.[30]

All the polymers showed good thermal stability, with decomposition temperatures in excess of 300˚C, which satisfied the requirements of OSC applications. The PXRD studies of **P6** and **P8** showed broad and weak peaks in the low-angle region, which indicated that the polymers had more order in the solid state than **P5** and **P7**. Also, the large π-π stacking distance in the wide-angle region suggested that all the polymers possessed an amorphous nature. The PV properties of polymers **P5**, **P6**, **P7** and **P8** will be examined through cooperation with the

Department of Physics at the University of Sheffield. The PCE will be measured by the fabrication of BHJ photovoltaic devices with fullerene derivatives.

3.4. References

(1) Lu, L.; Zheng, T.; Wu, Q.; Schneider, A. M.; Zhao, D.; Yu, L. Recent advances in bulk heterojunction polymer solar cells. *Chemical reviews* 2015, *115* (23), 12666.

(2) Wang, E.; Wang, L.; Lan, L.; Luo, C.; Zhuang, W.; Peng, J.; Cao, Y. High-performance polymer heterojunction solar cells of a polysilafluorene derivative. *Applied Physics Letters* 2008, *92* (3), 23.

(3) Henson, Z. B.; Müllen, K.; Bazan, G. C. Design strategies for organic semiconductors beyond the molecular formula. *Nature chemistry* 2012, *4* (9), 699.

(4) Dennler, G.; Scharber, M. C.; Brabec, C. J. Polymer-fullerene bulk-heterojunction solar cells. *Advanced materials* 2009, *21* (13), 1323.

(5) Ameri, T.; Khoram, P.; Min, J.; Brabec, C. J. Organic ternary solar cells: a review. *Advanced Materials* 2013, *25* (31), 4245.

(6) Cheng, Y.-J.; Yang, S.-H.; Hsu, C.-S. Synthesis of conjugated polymers for organic solar cell applications. *Chemical reviews* 2009, *109* (11), 5868.

(7) Berrouard, P.; Dufresne, S. p.; Pron, A.; Veilleux, J.; Leclerc, M. Low-cost synthesis and physical characterization of thieno [3, 4-c] pyrrole-4, 6-dione-based polymers. *The Journal of organic chemistry* 2012, *77* (18), 8167.

(8) Zou, Y.; Najari, A.; Berrouard, P.; Beaupré, S.; Réda Aïch, B.; Tao, Y.; Leclerc, M. A thieno [3, 4-c] pyrrole-4, 6-dione-based copolymer for efficient solar cells. *Journal of the American Chemical Society* 2010, *132* (15), 5330.

(9) Cabanetos, C.; El Labban, A.; Bartelt, J. A.; Douglas, J. D.; Mateker, W. R.; Fréchet, J. M.; McGehee, M. D.; Beaujuge, P. M. Linear side chains in benzo [1, 2-b: 4, 5-b′] dithiophene–thieno [3, 4-c] pyrrole-4, 6-dione polymers direct self-assembly and solar cell performance. *Journal of the American Chemical Society* 2013, *135* (12), 4656.

(10) Kim, J.-H.; Park, J. B.; Jung, I. H.; Grimsdale, A. C.; Yoon, S. C.; Yang, H.; Hwang, D.-H. J. E.; Science, E. Well-controlled thieno [3, 4-c] pyrrole-4, 6-(5 H)-dione based conjugated polymers for high performance organic photovoltaic cells with the power conversion efficiency exceeding 9%. 2015, *8* (8), 2352.

(11) Piliego, C.; Holcombe, T. W.; Douglas, J. D.; Woo, C. H.; Beaujuge, P. M.; Fréchet, J. M. Synthetic control of structural order in N-alkylthieno [3, 4-c] pyrrole-4, 6-dione-based polymers for efficient solar cells. *Journal of the American Chemical Society* 2010, *132* (22), 7595.

(12) Chu, T. Y.; Lu, J.; Beaupré, S.; Zhang, Y.; Pouliot, J. R.; Zhou, J.; Najari, A.; Leclerc, M.; Tao, Y. Effects of the molecular weight and the side-chain length on the photovoltaic performance of dithienosilole/thienopyrrolodione copolymers. *Advanced functional materials* 2012, *22* (11), 2345.

(13) Sabnis, R.; Rangnekar, D.; Sonawane, N. 2-Aminothiophenes by the Gewald reaction. *Journal of heterocyclic chemistry* 1999, *36* (2), 333.

(14) Puterová, Z.; Krutošíková, A.; Végh, D. Gewald reaction: synthesis, properties and applications of substituted 2-aminothiophenes. *ARKIVOC: Online Journal of Organic Chemistry* 2010.

(15) Cui, C.; Fan, H.; Guo, X.; Zhang, M.; He, Y.; Zhan, X.; Li, Y. Synthesis and photovoltaic properties of D–A copolymers of benzodithiophene and naphtho [2, 3-c] thiophene-4, 9-dione. *Polymer Chemistry* 2012, *3* (1), 99.

(16) Cornelis, D.; Peeters, H.; Zrig, S.; Andrioletti, B.; Rose, E.; Verbiest, T.; Koeckelberghs, G. A chiroptical study of chiral Λ-and X-type oligothiophenes toward modelling the interchain interactions of chiral conjugated polymers. *Chemistry of Materials* 2008, *20* (6), 2133.

(17) Zhou, E.; Yamakawa, S.; Zhang, Y.; Tajima, K.; Yang, C.; Hashimoto, K. Indolo [3, 2-b] carbazole-based alternating donor–acceptor copolymers: synthesis, properties and photovoltaic application. *Journal of Materials Chemistry* 2009, *19* (41), 7730.
(18) Takahashi, M.; Masui, K.; Sekiguchi, H.; Kobayashi, N.; Mori, A.; Funahashi, M.; Tamaoki, N. Palladium-Catalyzed C− H Homocoupling of Bromothiophene Derivatives and Synthetic Application to Well-Defined Oligothiophenes. *Journal of the American Chemical Society* 2006, *128* (33), 10930.
(19) Suzuki, A. Organoboron compounds in new synthetic reactions. *Pure and applied chemistry* 1985, *57* (12), 1749.
(20) Alqurashy, B. A.; Iraqi, A.; Zhang, Y.; Lidzey, D. G. Preparation and photovoltaic properties of pyrene-thieno [3, 4-c] pyrrole-4, 6-dione-based donor-acceptor polymers. *European Polymer Journal* 2016, *85*, 225.
(21) Cartwright, L.; Neal, T. J.; Rutland, N. J.; Iraqi, A. Anthracene-thieno [3, 4-c] pyrrole-4, 6-dione based donor–acceptor conjugated copolymers for applications in optoelectronic devices. *Polymers for Advanced Technologies* 2016, *27* (4), 525.
(22) Li, Z. H.; Wong, M. S.; Tao, Y.; Lu, J. Diphenylamino End-Capped Oligofluorenes with Enhanced Functional Properties for Blue Light Emission: Synthesis and Structure–Property Relationships. *Chemistry–A European Journal* 2005, *11* (11), 3285.
(23) Misra, A.; Kumar, P.; Srivastava, R.; Dhawan, S.; Kamalasanan, M.; Chandra, S. Electrochemical and optical studies of conjugated polymers for three primary colours. 2005.
(24) Li, Y.; Wu, Y.; Liu, P.; Birau, M.; Pan, H.; Ong, B. S. Poly (2, 5-bis (2-thienyl)-3, 6-dialkylthieno [3, 2-b] thiophene) s—High-Mobility Semiconductors for Thin-Film Transistors. *Advanced Materials* 2006, *18* (22), 3029.
(25) Zhang, Y.; Hau, S. K.; Yip, H.-L.; Sun, Y.; Acton, O.; Jen, A. K.-Y. Efficient polymer solar cells based on the copolymers of benzodithiophene and thienopyrroledione. *Chemistry of Materials* 2010, *22* (9), 2696.
(26) Kim, B. G.; Ma, X.; Chen, C.; Ie, Y.; Coir, E. W.; Hashemi, H.; Aso, Y.; Green, P. F.; Kieffer, J.; Kim, J. Energy Level Modulation of HOMO, LUMO, and Band-Gap in Conjugated Polymers for Organic Photovoltaic Applications. *Advanced Functional Materials* 2013, *23* (4), 439.
(27) Patel, P.; Hull, T. R.; Lyon, R. E.; Stoliarov, S. I.; Walters, R. N.; Crowley, S.; Safronava, N. Investigation of the thermal decomposition and flammability of PEEK and its carbon and glass-fibre composites. *Polymer degradation and stability* 2011, *96* (1), 12.
(28) Du, C.; Li, W.; Duan, Y.; Li, C.; Dong, H.; Zhu, J.; Hu, W.; Bo, Z. Conjugated polymers with 2, 7-linked 3, 6-difluorocarbazole as donor unit for high efficiency polymer solar cells. *Polymer Chemistry* 2013, *4* (9), 2773.
(29) He, Y.; You, J.; Dou, L.; Chen, C.-C.; Richard, E.; Cha, K. C.; Wu, Y.; Li, G.; Yang, Y. High performance low band gap polymer solar cells with a non-conventional acceptor. *Chemical Communications* 2012, *48* (61), 7616.
(30) Dang, D.; Xiao, M.; Zhou, P.; Shi, J.; Tao, Q.; Tan, H.; Wang, Y.; Bao, X.; Liu, Y.; Wang, E. Manipulating backbone structure with various conjugated spacers to enhance photovoltaic performance of D–A-type two-dimensional copolymers. *Organic Electronics* 2014, *15* (11), 2876.

Chapter 4: Phenanthrene-2,1,3-Benzothiadiazole-5,6-Dicarboxylic Imide, Donor-Acceptor Polymers for OPV applications

Abstract

This chapter reports the synthesis of two new narrow band-gap copolymers comprising 2,1,3-benzothiadiazole-5,6-dicarboxylic imide (BDI) as an acceptor, alternating with either electron donors of phenanthro[9,10-b]quinoxaline to produce **P9**, or 9,10-dialkoxy-phenanthreneto produce **P10**, which were both synthesised *via* Suzuki cross-coupling. These copolymers were designed by taking into consideration some factors that affect the optical and electrical properties of prepared conjugated polymers. The acceptor has a substituent solubilising group on the nitrogen of the imide group in the BDI unit. In addition, two different alkoxyl substituents are incorporated on to the donor moieties. Consequently they display good solubility in many types of organic solvents at room temperature. Both polymers show good thermal stability, with decomposition temperatures in excess of 300˚C. The report also demonstrates the data collected from UV-Vis and CV analysis for the synthesised copolymers. **P9** and **P10** reveal narrow optical band gaps with values of 1.74 eV and 1.68 eV, respectively. **P9** and **P10** showed low HOMO energy levels with values of -5.38 eV and -5.37 eV, respectively. This can be ascribed to improved ICT along the conjugated backbones.

4.1 Introduction

An appealing solution to the high demand for renewable, clean energy sources that does not harm the environment is the conversion of solar energy to produce electricity. Still, only a small amount of solar energy is utilised, mostly due to the cost of solar cells based on silicon.[1] Therefore, OPVs show promising potential as they have many advantages over their inorganic counterparts, including high absorption coefficients, improved operation at lower light intensities, flexible substrates and low-cost production.[2,3]

BHJ architecture has been widely applied for the fabrication of the active layer in polymer-based solar devices.[4] The photoactive layer consists of a conjugated polymer as electron donor blended with a fullerene derivative as electron acceptor to form a bicontinuous interpenetrating network, which offers an enlarged interfacial area between the electron donor and acceptor.[5] It is important to adjust the blending ratio of the donor to acceptor to improve the device efficiency.[6]

In addition, OPV cells with high efficiencies can be fabricated by tuning the properties of the conjugated polymers in the active layer. This can be achieved by the manipulation of the HOMO and LUMO energy levels of D-A polymers. For instance, a strongly electron-deficient acceptor unit can be copolymerised with a strongly electron-rich donor monomer to yield a low band-gap conjugated polymer.[7] This approach leads to increased ICT along the backbone of the resulting polymer, which consequently enhances charge-carrier mobility.[8] Moreover, this arrangement of D-A polymers enables the conjugated polymers not only to absorb sunlight efficiently but also to provide deeper HOMO energy levels.[8,9] The use of this arrangement enables several types of D-A polymers to break the barrier of 10 per cent PCE in OSCs.[10]

Numerous studies have reported study of efficient donor units, such as bithiophene, benzodithiophene, carbazole and fluorine.[8] However, the construction of copolymers with an effective acceptor unit is also important. Therefore, research is needed to find strong acceptor units to incorporate into D-A copolymers.[11] One of the most extensively investigated types of strong electron-deficient (acceptor) units to construct push-pull conjugated polymers with low band gaps is 2,1,3-benzothiadiazole (BT). An example of its use is **PBnDT-DTffBT**, which is shown in Figure 4.1. The PCEs of D-A copolymers based on this acceptor unit have exceeded 7.2 per cent when fabricated into PSCs.[12,13,14] In addition, the introduction of two thienyl units between the electron-donor and the BT units decreases steric hindrance and

enables the resulting D-A copolymers to adopt greater planarity in their conformations.[15,16,17,18] Furthermore, these copolymers have good charge-carrier mobility.[19]

However, BT-based copolymers show poor solubility, and therefore, low molecular weights. The attachment of solubilising groups in the 5- and 6-positions of the BT unit, as indicated in Figure 4.2, improves the solubility, and hence, increases the molecular weights of the resulting copolymers.[20,21] The 5- and 6-positions of the BT unit can also be functionalised through the addition of electron-withdrawing substituents to fine-tune the HOMO and LUMO energy levels of the synthesised copolymers. For example, incorporation of highly electronegative substituents such as fluorine atoms in the 5- and 6-positions of the BT unit has been shown to produce a stronger electron-accepting unit. The fluorinated BT moiety deepens the HOMO energy levels and thus improves the V_{oc} when fabricated into solar devices.[12] High-performing PSCs have been reported based on **DTffBT**.[12]

Another unit widely used as a strong acceptor moiety is thieno[3,4-c]pyrrole-4,6-dione (TPD), as in **(PDTG-TPD)** (Figure 4.1). D-A copolymers based on this acceptor unit have exhibited PCEs of 7.3 per cent when fabricated into solar cells.[22] Aside from low optical band gaps, the dicarboxylic imide moiety is a strong electron-withdrawing unit in the D-A copolymers of TPD, leading to a reduction of the HOMO energy levels and therefore larger V_{oc} in the fabricated solar cells.[22]

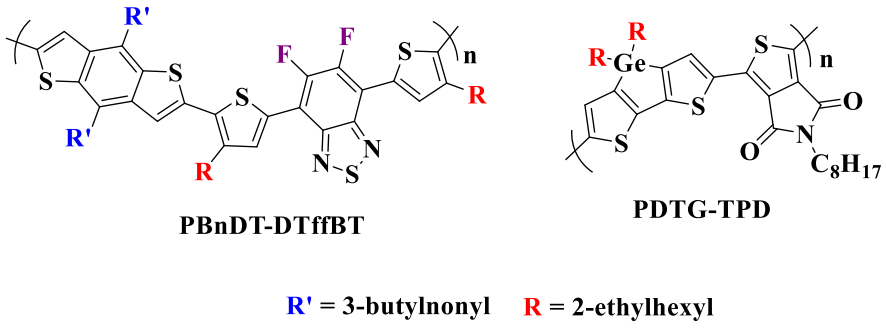

Figure 4.1. Polymer structures of PBnDT-DTffBT (PCEs of 7.2 per cent) and PDTG-TPD (PCEs of 7.3 per cent).[12,22]

Therefore, the incorporation of a dicarboxylic imide moiety at the 5- and 6-positions of the 2,1,3-benzothiadiazole unit results in the formation of a stronger accepting unit, because there is a larger electron-withdrawing substituent in its structure. This newly prepared electron-acceptor 2,1,3-benzothiadiazole-5,6-dicarboxylic imide (**BDI**) shows the advantageous

properties of both the dicarboxylic imide group and the planar BT unit, and is a more electron-deficient unit than its analogues benzothiadiazole (BT) and difluoro-benzothiadiazole (ffBT), as shown in Figure 4.2.[20] The exploitation of these characteristics enables the synthesis of narrow band-gap copolymers with deep HOMO energy levels. Previous studies have shown that PCEs of D-A copolymers based on BDI as an acceptor unit are in excess of eight per cent when fabricated into solar cells.[20] Moreover, the nitrogen of the imide group can be functionalised through the introduction of various solubilising groups, to enhance solubility of the resulting polymers.[23]

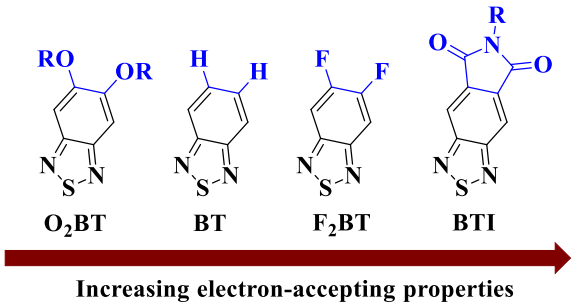

Figure 4.2. Examples of various 2,1,3-benzothiadiazole derivatives, with the alterations in the 5- and 6-positions.[20]

In a study conducted by Wang *et al.*, two novel copolymers were synthesised, based on BDI flanked by two thiophene units as the electron-acceptor and benzodithiophene as the electron-donor unit, for solar cell applications. The reported copolymers **PDI-BDTT** and **PDI-BDTO** were anchored with the same solubilising group on the electron-acceptor unit, but different ones on the donor (Figure 4.3). In film, the UV-vis spectrum of **PDI-BDTT** displayed more bathochromic absorption at the longer wavelength of 692nm compared with its counterpart **PDI-BDTO**, which displayed an absorption band at 654nm. This was attributed to the extended conjugation system of **PDI-BDTT,** caused by the two thienyl groups incorporated into its backbone chains. Consequently, the optical band gaps of **PDI-BDTT** and **PDI-BDTO** were1.55 eV and 1.54 eV respectively. **PDI-BDTT** exhibited deeper HOMO energy levels with a value of -5.51 eV, compared with the HOMO energy levels of **PDI-BDTO,** which showed a value of -5.44 eV. The presence of such narrow band gaps and lower-lying HOMO levels in the fabricated PSCs can be favourable to obtain a higher V_{oc}. The resulting copolymer **PDI-BDTT** achieved a PCE of 5.19 per cent when fabricated into BHJ solar cells. However, under the same fabrication conditions, **PDI-BDTO** exhibited a PCE of 2.10 per cent.[9]

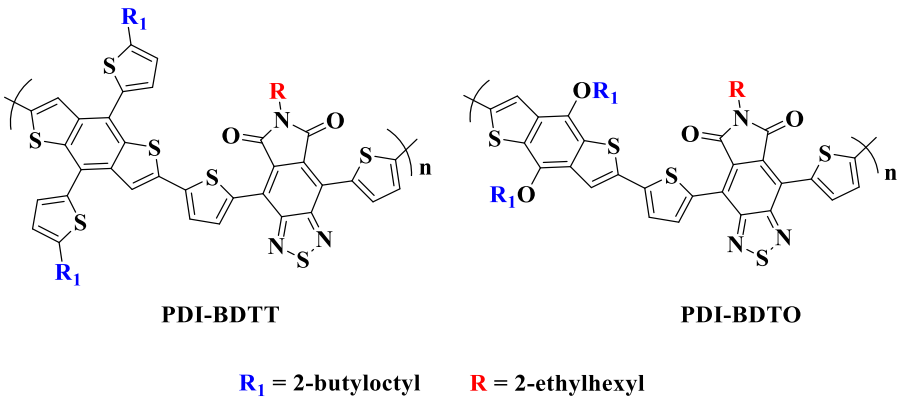

Figure 4.3. Polymer structures of PDI-BDTT and PDI-BDTO synthesised by Wang and co-workers.[9]

Another study by Li *et al.* reported the synthesis of two other copolymers with high molecular weight, based on **BDI** as the electron-acceptor. The resulting polymers **P(BTI-F)** and **P(BTI-B)** exhibited narrow band gaps with values of 1.86 eV and 1.68 eV respectively. In addition, **P(BTI-F)** and **P(BTI-B)** demonstrated deep HOMO energy levels positioned at -5.60 eV and -5.36 eV respectively. The difference in HOMO energy levels between **P(BTI-F)** and **P(BTI-B)** can be ascribed to the benzodithiophene unit in **P(BTI-B)** that has stronger electron-donating properties than the fluorine unit in **P(BTI-F)**. However, **P(BTI-F)** and **P(BTI-B)** achieved PCEs of only 1.61 per cent and 3.42 per cent respectively, when fabricated into BHJ photovoltaic cells. Their chemical structure is shown in Figure 4.4.[24]

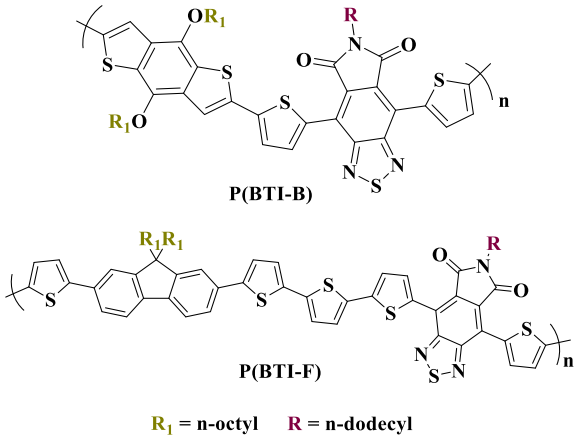

Figure 4.4. Polymer structures of P(BTI-F) and P(BTI-B) synthesised by Li and co-workers.[24]

Nielsen and co-workers copolymerised the strongly electron-deficient BDI unit with two different benzotrithiophene (BTT**)** groups as donor units attached through either a linear *n* -hexadecyl or a branched 1-nonyldecyl side-chain. These experiments yielded two novel

copolymers, **BBTI-1** and **BBTI-2**, respectively, both with high molecular weight (Figure 4.5). The band gaps of both polymers were about 1.5 eV, which were encouraging characteristics for an OPV donor material. Moreover, **BBTI-1** and **BBTI-2** displayed HOMO energy levels at –5.2 eV and –5.3 eV, respectively. Accordingly, the BHJ PV cells designed with **BBTI-1** and **BBTI-2** revealed improved PCEs of 8.3 per cent and six per cent, respectively.[20]

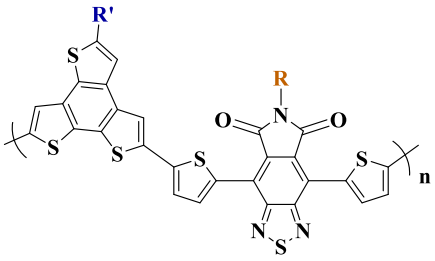

BBTI-1 **R' = n -hexadecyl** **R = 2-decyl-1-tetradecyl**

BBTI-2 **R' = 1-nonyldecyl** **R = 2-decyl-1-tetradecyl**

Figure 4.5. Polymer structures of BBTI-1 and BBTI-2 synthesised by Nielsen and co-workers.[20]

In this study, we report the synthesis of a series of conjugated polymers consisting of alternating BDI units and two frequently used donor segments: phenanthro[9,10-b]quinoxaline and 9,10-dialkoxy-phenanthreneunits. The two resulting copolymers are poly[[11,12-bis-(2-hexyldecyloxy)-phenanthro[9,10-b]quinoxaline](2,7-di-yl)-alt-[4',7'-bis(2-thienyl)-2',1',3'-benzothiadiazole-5,6-N-octyl-dicarboxylic imide]-5,5-(di-yl)] **(P9)** and poly[9,10-bis(2-butyl-octyloxy)-2,7-phenanthrene-alt-[4',7'-bis(2-thienyl)-2',1',3'-benzothiadiazole-5,6-N-octyl-dicarboxylic imide]-5,5-(di-yl)] **(P10).** Their preparation is shown in Scheme 4.1.

4.2. Results and Discussion

4.2.1. Synthesis of Monomers for the BDI based Copolymers P9 and P10

Scheme 4.1 shows the monomers required to prepare polymers **P9** and **P10**. The 4,7-di(5-bromo-thien-2-yl)-2,1,3-benzothiadiazole-5,6-*N*-octyl-dicarboxylic imide **(A)** was synthesised by co-workers in Iraqi's group at the University of Sheffield. The 2,7-bis-(4,4,5,5-tetramethyl-1,3,2-dioxaborolan-2-yl)-11,12-bis-(2-hexyldecyloxy)-phenanthro[9,10-b]quinoxaline **(16)** and 2,7-bis-(4,4,5,5-tetramethyl-1,3,2-dioxaborolan-2-yl)-9,10-bis-(2-butyl-octyloxy)-phenanthrene **(19)** were synthesised in good yields. Their purities and structures were confirmed by ^{1}H NMR, ^{13}C NMR, elemental analysis and mass spectrometry

analysis. Compound **(A)** was used as an electron acceptor and compounds **(16)** and **(19)** were used as electron-donor units to prepare polymers **P9** and **P10** respectively. The synthetic route for the preparation of compounds **(16)** and **(19)** were previously shown in Scheme 2.11 and Scheme 2.15 respectively, in Chapter 2.

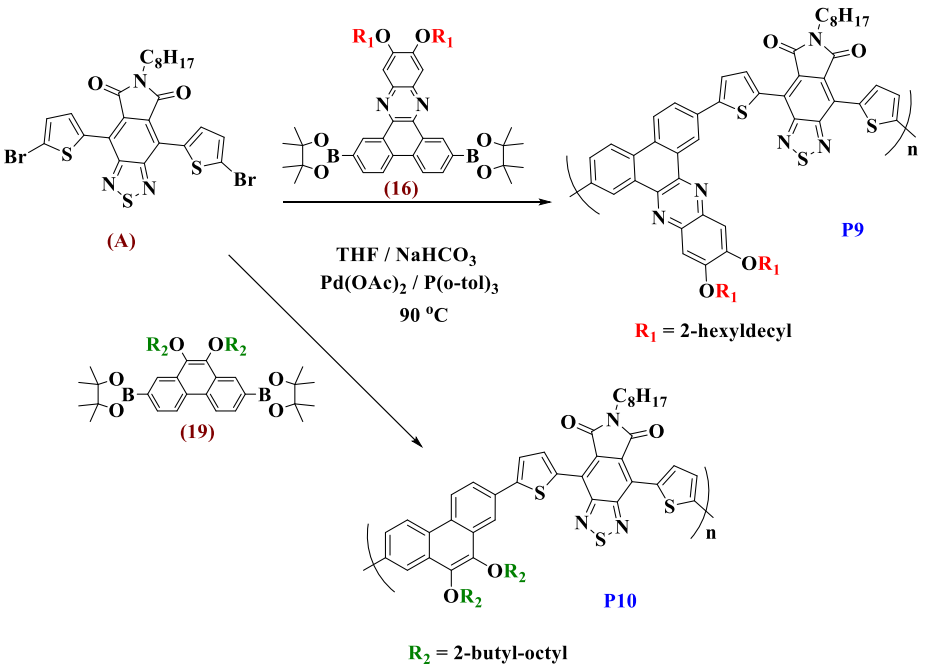

Scheme 4.1. Monomers (A), (16) and (19) used to prepare P9 and P10.

4.2.2. Synthesis of BDI-based alternating copolymers P9 and P10

This chapter describes the preparation of two alternating D-A copolymers *via* Suzuki cross-coupling between the boronic ester monomers **(16)** and **(19)** as electron-donors, and the dibrominated monomer **(A)** as an electron-acceptor (Scheme 4.1). The polymerisation procedure was carried out by using a similar method as that employed in Chapters 2 and 3. Polymerisations of **P9** and **P10** were stopped after 48 hours, as large quantities of polymer precipitate had been formed. Both polymerisation reactions followed the mechanism of Suzuki cross-coupling reaction, which was described in Chapter 1.[25] Both polymerisations were stopped temporarily to add the end capping reagents to the polymer solutions, and this would also increase the stability of the polymers during the fabrication of solar cell devices.

The polymers were fractionated through Soxhlet extraction using the following solvents: methanol, acetone, hexane toluene and chloroform. The chemical structures of both polymers were verified by ^{1}H-NMR and elemental analysis. GPC was used to determine M_n and M_w, using 1,2,4-trichlorobenzene as an eluent at 140^{o}C, and polystyrene as the internal standard.

The results are shown in Table 4.1. Both polymers exhibited good solubility in organic solvents at room temperature. The yields of both polymers were higher than 70 per cent. **P10** displayed higher M_w and M_n than its analogous polymer **P9,** with values of 79,700Da and 23,000Da respectively. **P9** showed significantly lower M_w and M_n values of 15,700Da and 8,800Da respectively. It is speculated that the structure of **P9** involves strong steric repulsion between the bulky solubilising chain 2-hexyl-decyloxy attached to the phenanthro[9,10-b]quinoxaline donor moiety, and the octyl group on the BDI unit during the coupling reaction. This is likely to impede further polymerisation, so a polymer with low molecular weight is formed. The polymer structures are shown in Figure 4.6.

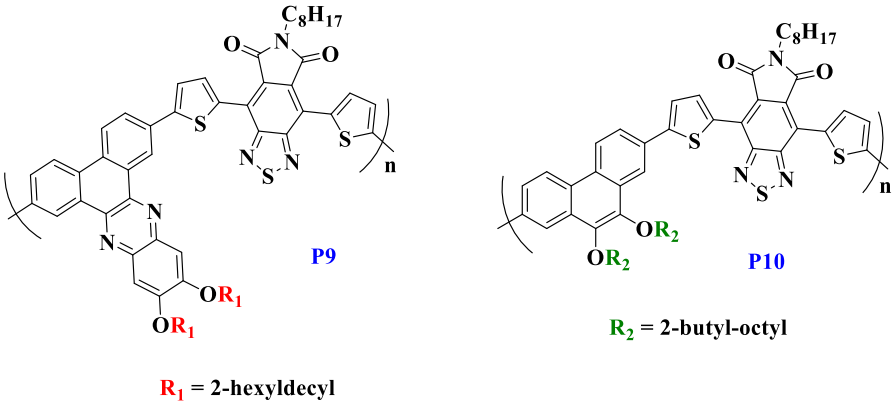

Figure 4.6. Polymers P9 and P10.

Table 4.1. GPC analysis of P9 and P10

Polymer	M_n (Da) [a]	M_w (Da) [a]	PDI	Yield (%)
P9	8,800	15,700	1.79	71
P10	23,000	79,700	2.86	74

Measurements conducted on the chloroform fraction of the polymers. [a]GPC conducted in 1,2,4-trichlorobenzene at 140 °C using a differential refractive index (DRI) detection method. PDI = Polydispersity Index.

4.2.3. UV-Visible absorption spectroscopy analysis

The absorption spectra of the polymers were recorded by UV-vis spectrophotometer to study the optical properties of polymers **P9** and **P10** in dilute chloroform solutions (Figure 4.7.(**a**)) and in the solid state as drop-cast thin films on quartz substrates (Figure 4.7.(**b**)). The optical

band gaps for the polymers were calculated from the absorption onset of the polymers in the solid state. The measured optical properties of both polymers are summarised in Table 4.2.

Table 4.2. Optical data of polymers P9 and P10

Polymer	ε (M^{-1} cm^{-1})	Solution λ_{max} (nm)	Thin Film λ_{max} (nm)	Thin Film λ_{onset} (nm)	Optical E_g (eV)
P9	39019	562	578	714	1.74 ± 0.029
P10	68349	551	592	737	1.68 ± 0.041

The UV-vis spectra of the polymers illustrated two main absorption bands at both short and long wavelengths. The absorption peaks at short wavelengths corresponded to π-π* transitions, whereas the absorption bands at long wavelengths could be ascribed to ICT between the electron-deficient BDI-acceptor unit and the electron-rich phenanthro[9,10-b]quinoxaline and phenanthrene donor moieties.

In dilute chloroform solutions, the ICT bands of **P9** and **P10** displayed absorption bands at longer wavelengths, located at 562nm and 551nm respectively. After drop casting into a thin film, the ICT absorption maxima of **P9** and **P10** were red-shifted to 578nm and 592nm, respectively. In thin films, the absorption spectra of the polymers displayed bathochromic shifts by 16nm to 41nm, relative to their absorption in solution. This could be ascribed to the adoption by the polymer backbones of more planar conformations in the thin films, which led to stronger intermolecular π-π interactions, relative to their absorption in solution. **P9** and **P10** exhibited similar yet narrower optical band gaps which were estimated to be 1.74 eV and 1.68 eV, respectively. However, **P10** was more red-shifted when compared with **P9**. This can be explained by the fact that **P10** has a higher molecular weight than **P9**, which has the effect of reducing the optical band gap of **P10** relative to **P9**.

P9 and **P10** showed narrower optical band gaps than **P(BTI-F)** (Figure 4.4), which was flanked by bithiophene units between its electron-donor and BDI-acceptor unit and therefore exhibited less red-shift than **P9** and **P10.** In contrast, **P(BTI-B)** (Figure 4.4) displayed a lower

optical band gap than **P9** and **P10,** because **P(BTI-B)** had a more electron-rich donating unit than the donor units used in **P9** and **P10**.[24]

All the polymers synthesised showed a similar trend regarding optical band gaps. The polymers contain different electron acceptors: those whose synthesis was discussed in Chapter 2 (**P1, P2, P3** and **P4)** contained a difluoroquinoxaline-acceptor unit; those discussed in Chapter 3 (**P5, P6, P7,** and **P8)** employed a TPD-acceptor unit; and those in this chapter (**P9** and **P10)** contained a BDI-acceptor unit. Yet polymers **P1, P2, P5** and **P6** give similar results. The extension of the conjugation system through the introduction of additional thiophene units produced polymers **P3, P4, P7,** and **P8,** which also show similar optical band gaps but narrower than those of **P1, P2, P5** and **P6**. The same behaviour can be observed in polymers **P9** and **P10**. It is suggested that the pair of hetero (nitrogen) atoms in the quinoxaline moiety in the electron-donor **(16)** acts as an electron-dense withdrawing group, and this affects and reduces the donor group's donating property to the same level as that of the other electron donor **(19)**. However, polymers **P9** and **P10** exhibit the lowest optical band gaps compared with the polymers discussed in the previous chapters. This can be attributed to the greater electron deficiency of the BDI-acceptor unit compared with both the quinoxaline-acceptor unit and the TPD-acceptor unit, due to the merged properties of both the withdrawing electron-dense dicarboxylic imide group and the highly planar BT unit in the BDI structure.

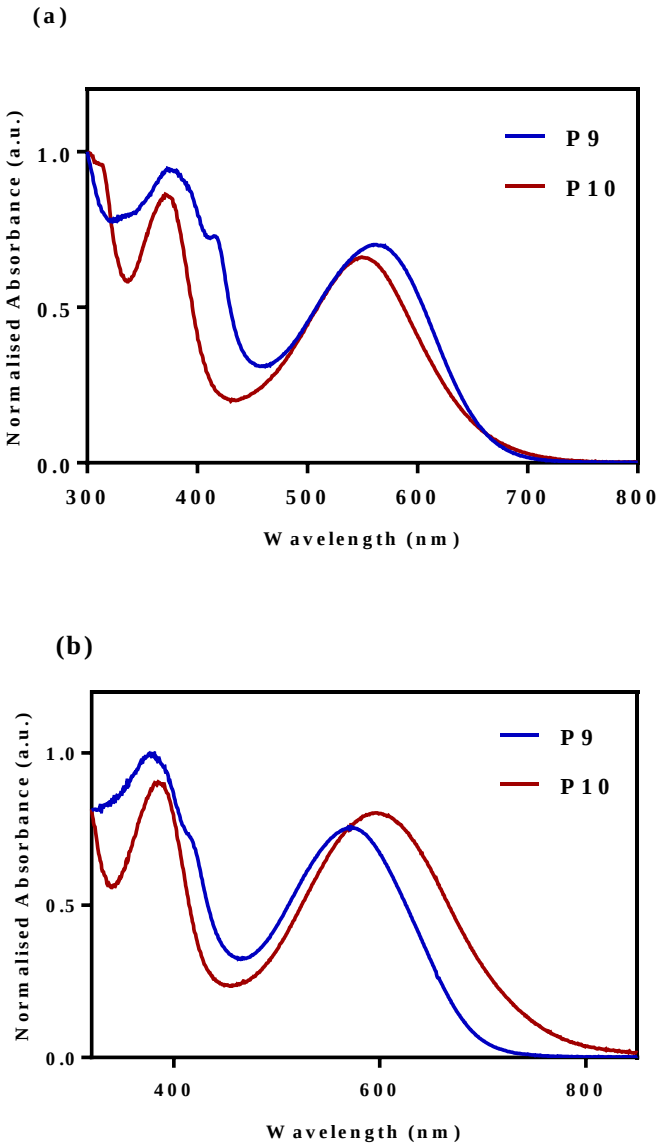

Figure 4.7. Normalised absorption spectra of P9 and P10 in:

(a) chloroform solution; and (b) thin films.

4.2.4. Cyclic Voltammetry analysis

The electrochemical properties of polymers **P9** and **P10** were studied and characterised *via* CV, and the results are shown in Figure 4.8. The onsets of oxidation and reduction were used to determine the HOMO and LUMO energy levels respectively (*vs. vacuum*).

The studies were performed on drop-cast polymer films on a platinum-disc electrode as working electrode in acetonitrile with tetrabutylammonium perchlorate as the electrolyte (0.1M) and silver nitrate (Ag/Ag+) as a reference electrode, at a scan rate of 100 mV s^{-1} min.

The electrochemical band gaps were estimated from the difference between HOMO and LUMO levels, as summarised in Table 4.3.

Table 4.3. Electrochemical properties of P9 and P10

Polymer	HOMO (eV)[a]	LUMO (eV)[b]	E_g^{elect} (eV)[c]
P9	-5.38	-3.58	1.80 ± 0.002
P10	-5.37	-3.62	1.75 ± 0.014

[a] HOMO energy levels determined from the onset of oxidation. [b] LUMO energy levels determined from the onset of reduction. [c] Electrochemical band gap.

P9 and **P10** displayed equally low-lying HOMO energy levels, with values of -5.38eV and -5.37 eV, respectively. The HOMO energy levels are dominated by the nature of the donor moiety.[19, 26] The electrochemical band gaps of **P9** and **P10** were estimated to be 1.80eV and 1.75 eV, respectively. The electrochemical band gaps are slightly larger than the optical band gaps due to the interface barrier between the surface of the electrode and polymers cast as films, which results in the electrochemical band gap being formed of an optical band gap combined with the interface barrier.[27]

P9 and **P10** displayed similar HOMO energy levels when compared with levels reported for **P(BTI-B)** in previous literature (Figure 4.4). However, **P9** and **P10** showed deeper-positioned HOMO energy levels relative to that of **BBTI-1** (Figure 4.4). This could be attributed to the weakness of phenanthro[9,10-b]quinoxaline and phenanthrene units as electron donors compared with the benzotrithiophene unit.[20, 24] The LUMO levels of **P9** and **P10** are low at values of -3.58 eV and -3.62 eV, respectively. This can be ascribed to the fact that both polymers have the same strong electron-withdrawing ability of BDI as an electron-acceptor unit, which controls the LUMO energy levels in these materials. The LUMO level of **P10** is marginally deeper than that of **P9,** which is a consequence of the differing molecular weights.

The HOMO energy levels of **P9** and **P10** are comparable with those whose synthesis was discussed in previous chapters. **P9** and **P10** exhibited the shallowest HOMO energy levels of all the polymers synthesised for this thesis. This is a consequence of improved ICT along the polymer backbone, due to the greater electron deficiency of the BDI-acceptor moiety

compared with the quinoxaline-acceptor unit used in **P1**, **P2, P3** and **P4,** and the TPD-acceptor unit used in **P5, P6, P7,** and **P8.** Moreover, **P9** and **P10** revealed equally low-lying HOMO energy levels. Clearly, switching from the electron-donor **(16)** to electron-donor **(19)** made little impact on the resulting energy levels, since both donors were shown to display the same donating properties. The results agree with the previous findings in Chapters 2 and 3.

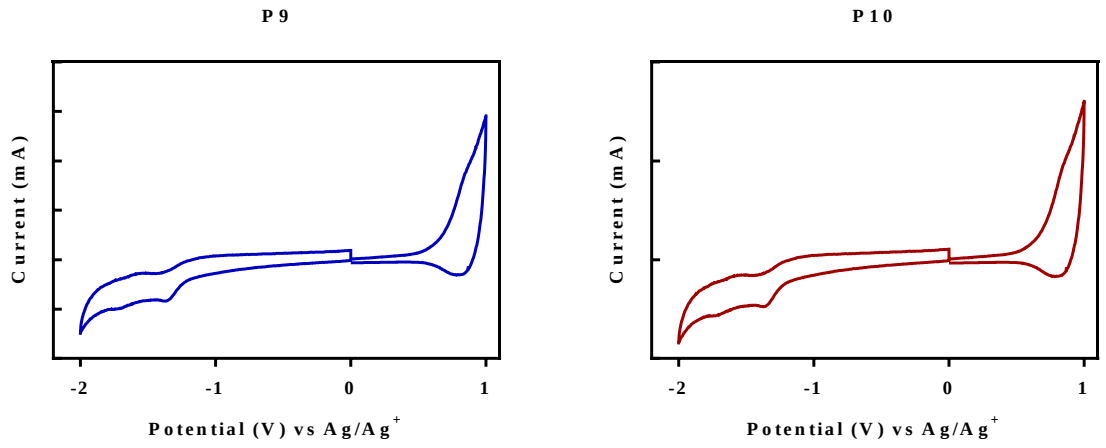

Figure 4.8. Cyclic voltammograms of P9 and P10.

4.2.5. Study of Thermal Properties

TGA was carried out to study the thermal stability of the polymers. The results are shown in Figure 4.9. The onset of decomposition temperatures (T_d) are shown in Table 4.4.

Table 4.4. Thermal properties of P9 and P10.

Polymer	T_d (˚C)[a]
P9	390
P10	338

[a] Degradation onset of polymers determined by using thermogravimetric analysis with a heating rate of 10˚C min^{-1} under an inert nitrogen atmosphere.

P9 and **P10** revealed good thermal stability with degradation temperatures above 300˚C, which is satisfactory for OSC applications. **P9** and **P10** displayed degradation temperatures of 390˚C and 338˚C. It is clear that **P9** has much more thermal stability than **P10**. **P9** has

large, aromatic, conjugated backbones that make the polymer more rigid and require more thermal energy to cause breakage. **P9** showed a single degradation phase, which occurred at 390˚C. The initial weight loss of **P9** corresponds to the loss of both alkyl chains (2-hexyldecyl) anchored to their donor moieties. In contrast, **P10** displayed two decomposition stages. The first one occurred at a noticeably lower onset of degradation with temperatures of 338˚C, due to the cleavage of alkoxy groups (2-butyl octyl) attached to their donor moieties. The second decomposition phase corresponded to the degradation of the residual conjugated polymer backbone, at the onset of degradation temperature of 462˚C. Both polymers degraded until around 50 per cent of the mass remained, and then the curves gradually levelled off to about 800˚C. It is hypothesised that polymers with large alkyl chains become less volatile during combustion. Therefore, while **P9** and **P10** decomposed, a thick-charring layer was formed on the virgin polymer, which insulated the heat flux reaching the virgin polymer, as a consequence of its low thermal conductivity. This process would delay the thermal decomposition of the polymers.[28]

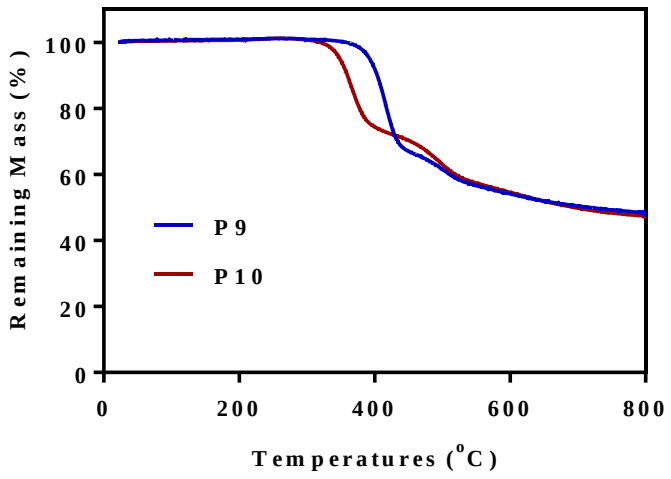

Figure 4.9. Thermogravimetric analysis of P9 and P10 carried out at a heating rate of 10 °C min^{-1} and under an inert nitrogen atmosphere.

4.2.6. Studies of Molecular Structure

The structural properties of **P9** and **P10** were examined in the solid state by PXRD (Figure 4.10). The PXRD curve for **P9** displayed a broad diffraction peak in the wide-angle area situated at a 2θ value of 21.8°, which corresponds to the π-π stacking distance of 4.07Å. There are no peaks in the low-angle region, which indicates that **P9** does not show long-range order in thin films. It is speculated that the attachment of large, sterically demanding alkoxy

groups to the donor moieties can cause steric hindrance to polymer-chain packing. The result indicates that **P9** has an amorphous nature. In contrast, the PXRD graph for **P10** shows a small pronounced peak in the low-angle region, at a 2θ value of 3.72°. This peak represents a lamellar stacking distance of 23.72Å. Pronounced peaks in the low-angle region for conjugated polymers correspond to ordered packing of polymer backbones separated by solubilising groups that are attached to electron-donor and acceptor units along the polymer chains.[29] Moreover, **P10** displayed weak and broad diffraction in the region of wide-angle scattering, at a 2θ value of 20.62°, which reflected the π-π stacking distance of 4.30Å. These stacking distances suggest that both polymers exhibit amorphous characteristics.

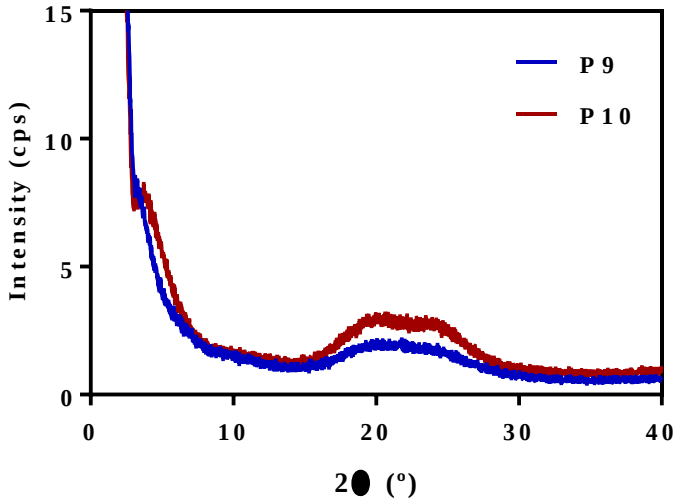

Figure 4.10. PXRD patterns for polymers P9 and P10.

4.3. Conclusion

In summary, the preparation was reported of two alternating copolymers, **P9** and **P10,** which consisted of BDI functionalised units and phenanthro[9,10-b]quinoxaline and 9,10-dialkoxy-phenanthreneunits as electron donors, through Suzuki cross-coupling reactions. Both polymers exhibited good solubility in many organic solvents at room temperature, which was due to the presence of solubilising groups anchored on to the electron acceptor and donor moieties. The yields of both polymers were higher than 70 per cent. GPC data revealed that **P10** showed higher M_w and M_n values than **P9** in chloroform fractions. **P9** and **P10** revealed low optical band gaps with values of 1.74 eV and 1.68 eV respectively. These values would be beneficial to obtain high J_{sc} values after fabrication into BHJ solar cells. Both polymers demonstrated red shifts in thin films, which can be ascribed to the high planarity of the polymer backbones in the solid state, leading to strong π-π interchain stacking. However, **P10** was more red-shifted than **P9,** which could be due to the fact that **P10** had a higher molecular weight than **P9**. CV analysis of **P9** and **P10** exhibited low HOMO energy levels with values of -5.38 eV and -5.37 eV. Thus they could offer superior V_{oc} when fabricated into BHJ solar devices. The LUMO energy levels of **P9** and **P10** were positioned in a suitable range at -3.58 eV to -3.62 eV, which were higher than the LUMO energy levels of $PC_{71}BM$. Thus, efficient separation and charge transfer could be anticipated in their corresponding BHJ solar cells.[30] Both polymers showed good thermal stability, with decomposition temperatures in excess of 330˚C, which is sufficient for the requirements of OSCs. The PXRD patterns of the polymers showed long π-π stacking distances in the wide-angle region, which suggested that both polymers exhibited an amorphous nature. The photovoltaic properties of polymers **P9** and **P10** will be studied in cooperation with the Department of Physics at the University of Sheffield. The PCE will be measured by the fabrication of BHJ PV devices with fullerene derivatives.

4.4. References

(1) Beaupré, S.; Boudreault, P. L. T.; Leclerc, M. Solar-Energy Production and Energy-Efficient Lighting: Photovoltaic Devices and White-Light-Emitting Diodes Using Poly (2, 7-fluorene), Poly (2, 7-carbazole), and Poly (2, 7-dibenzosilole) Derivatives. *Advanced Materials* 2010, *22* (8), E6.

(2) Hoppe, H.; Sariciftci, N. S. Organic solar cells: An overview. *Journal of materials research* 2004, *19* (7), 1924.

(3) Thompson, B. C.; Fréchet, J. M. Polymer–fullerene composite solar cells. *Angewandte chemie international edition* 2008, *47* (1), 58.

(4) Winder, C.; Sariciftci, N. S. Low bandgap polymers for photon harvesting in bulk heterojunction solar cells. *Journal of Materials Chemistry* 2004, *14* (7), 1077.

(5) Yu, G.; Gao, J.; Hummelen, J. C.; Wudl, F.; Heeger, A. J. Polymer photovoltaic cells: enhanced efficiencies via a network of internal donor-acceptor heterojunctions. *Science* 1995, *270* (5243), 1789.

(6) Ameri, T.; Khoram, P.; Min, J.; Brabec, C. J. Organic ternary solar cells: a review. *Advanced Materials* 2013, *25* (31), 4245.

(7) Lu, L.; Zheng, T.; Wu, Q.; Schneider, A. M.; Zhao, D.; Yu, L. Recent advances in bulk heterojunction polymer solar cells. *Chemical reviews* 2015, *115* (23), 12666.

(8) Cheng, Y.-J.; Yang, S.-H.; Hsu, C.-S. Synthesis of conjugated polymers for organic solar cell applications. *Chemical reviews* 2009, *109* (11), 5868.

(9) Wang, L.; Cai, D.; Zheng, Q.; Tang, C.; Chen, S.-C.; Yin, Z. Low band gap polymers incorporating a dicarboxylic imide-derived acceptor moiety for efficient polymer solar cells. *Acs Macro Letters* 2013, *2* (7), 605.

(10) Zhang, S.; Ye, L.; Hou, J. Breaking the 10% Efficiency Barrier in Organic Photovoltaics: Morphology and Device Optimization of Well-Known PBDTTT Polymers. *Advanced Energy Materials* 2016, *6* (11), 1502529.

(11) Park, S. H.; Roy, A.; Beaupré, S.; Cho, S.; Coates, N.; Moon, J. S.; Moses, D.; Leclerc, M.; Lee, K.; Heeger, A. J. Bulk heterojunction solar cells with internal quantum efficiency approaching 100%. *Nature photonics* 2009, *3* (5), 297.

(12) Zhou, H.; Yang, L.; Stuart, A. C.; Price, S. C.; Liu, S.; You, W. Development of fluorinated benzothiadiazole as a structural unit for a polymer solar cell of 7% efficiency. *Angewandte Chemie International Edition* 2011, *50* (13), 2995.

(13) Hou, J.; Chen, H.-Y.; Zhang, S.; Li, G.; Yang, Y. Synthesis, characterization, and photovoltaic properties of a low band gap polymer based on silole-containing polythiophenes and 2, 1, 3-benzothiadiazole. *Journal of the American Chemical Society* 2008, *130* (48), 16144.

(14) Zhu, Z.; Waller, D.; Gaudiana, R.; Morana, M.; Mühlbacher, D.; Scharber, M.; Brabec, C. Panchromatic conjugated polymers containing alternating donor/acceptor units for photovoltaic applications. *Macromolecules* 2007, *40* (6), 1981.

(15) Huo, L.; Chen, H.-Y.; Hou, J.; Chen, T. L.; Yang, Y. Low band gap dithieno [3, 2-b: 2′, 3′-d] silole-containing polymers, synthesis, characterization and photovoltaic application. *Chemical Communications* 2009, (37), 5570.

(16) Chen, M. H.; Hou, J.; Hong, Z.; Yang, G.; Sista, S.; Chen, L. M.; Yang, Y. Efficient polymer solar cells with thin active layers based on alternating polyfluorene copolymer/fullerene bulk heterojunctions. *Advanced Materials* 2009, *21* (42), 4238.

(17) Slooff, L.; Veenstra, S.; Kroon, J.; Moet, D.; Sweelssen, J.; Koetse, M. Determining the internal quantum efficiency of highly efficient polymer solar cells through optical modeling. *Applied Physics Letters* 2007, *90* (14), 143506.

(18) Boudreault, P.-L. T.; Najari, A.; Leclerc, M. Processable low-bandgap polymers for photovoltaic applications. *Chemistry of Materials* 2010, *23* (3), 456.

(19) Zhou, H.; Yang, L.; You, W. Rational design of high performance conjugated polymers for organic solar cells. *Macromolecules* 2012, *45* (2), 607.
(20) Nielsen, C. B.; Ashraf, R. S.; Treat, N. D.; Schroeder, B. C.; Donaghey, J. E.; White, A. J.; Stingelin, N.; McCulloch, I. 2, 1, 3-Benzothiadiazole-5, 6-Dicarboxylic Imide–A Versatile Building Block for Additive-and Annealing-Free Processing of Organic Solar Cells with Efficiencies Exceeding 8%. *Advanced Materials* 2015, *27* (5), 948.
(21) Zhou, P.; Zhang, Z.-G.; Li, Y.; Chen, X.; Qin, J. Thiophene-fused benzothiadiazole: a strong electron-acceptor unit to build D–A copolymer for highly efficient polymer solar cells. *Chemistry of Materials* 2014, *26* (11), 3495.
(22) Amb, C. M.; Chen, S.; Graham, K. R.; Subbiah, J.; Small, C. E.; So, F.; Reynolds, J. R. Dithienogermole as a fused electron donor in bulk heterojunction solar cells. *Journal of the American Chemical Society* 2011, *133* (26), 10062.
(23) Piliego, C.; Holcombe, T. W.; Douglas, J. D.; Woo, C. H.; Beaujuge, P. M.; Fréchet, J. M. Synthetic control of structural order in N-alkylthieno [3, 4-c] pyrrole-4, 6-dione-based polymers for efficient solar cells. *Journal of the American Chemical Society* 2010, *132* (22), 7595.
(24) Li, H.; Sun, S.; Mhaisalkar, S.; Zin, M. T.; Lam, Y. M.; Grimsdale, A. C. A high voltage solar cell using a donor–acceptor conjugated polymer based on pyrrolo [3, 4-f]-2, 1, 3-benzothiadiazole-5, 7-dione. *Journal of Materials Chemistry A* 2014, *2* (42), 17925.
(25) Shaheen, S. E.; Ginley, D. S.; Jabbour, G. E. Organic-based photovoltaics: toward low-cost power generation. *MRS bulletin* 2005, *30* (1), 10.
(26) Zhou, H.; Yang, L.; Stoneking, S.; You, W. A weak donor− strong acceptor strategy to design ideal polymers for organic solar cells. *ACS applied materials and interfaces* 2010, *2* (5), 1377.
(27) Misra, A.; Kumar, P.; Srivastava, R.; Dhawan, S.; Kamalasanan, M.; Chandra, S. Electrochemical and optical studies of conjugated polymers for three primary colours. 2005.
(28) Patel, P.; Hull, T. R.; Lyon, R. E.; Stoliarov, S. I.; Walters, R. N.; Crowley, S.; Safronava, N. Investigation of the thermal decomposition and flammability of PEEK and its carbon and glass-fibre composites. *Polymer degradation and stability* 2011, *96* (1), 12.
(29) Du, C.; Li, W.; Duan, Y.; Li, C.; Dong, H.; Zhu, J.; Hu, W.; Bo, Z. Conjugated polymers with 2, 7-linked 3, 6-difluorocarbazole as donor unit for high efficiency polymer solar cells. *Polymer Chemistry* 2013, *4* (9), 2773.
(30) Dang, D.; Xiao, M.; Zhou, P.; Shi, J.; Tao, Q.; Tan, H.; Wang, Y.; Bao, X.; Liu, Y.; Wang, E. Manipulating backbone structure with various conjugated spacers to enhance photovoltaic performance of D–A-type two-dimensional copolymers. *Organic Electronics* 2014, *15* (11), 2876.

Chapter 5: Conclusions and Future Work

5.1. Conclusions

The main purposes of the research were to synthesise and design a range of D-A conjugated polymers which offered narrow band gaps, extended absorption in the visible and infrared regions, and high molecular weights suitable for PV applications. The donor-acceptor, or push-pull, method was used for the synthesis of a new series of conjugated polymers *via* palladium-catalysed Suzuki cross-coupling reactions. A large part of this thesis has focused on 9,10-dialkoxy-phenanthreneand its derivative, phenanthro[9,10-b]quinoxaline, as electron donors in the D-A copolymers, and the exploitation of the 2,7-positions as linkage positions along the conjugated polymer backbones. Various solubilising groups were attached in the donor and acceptor units to assess their effect on the optical and electronic properties of the resultant conjugated polymers. The main outcomes of this project were investigated and discussed in each chapter, findings were summarised and, where appropriate, polymers were compared with each other.

Chapter 2 discussed the preparation of a series of fluorinated quinoxaline-based copolymers **P1**, **P2**, **P3,** and **P4**. Their optical, electrochemical and thermal properties were investigated. All polymers displayed good solubility in many types of organic solvents at room temperature. GPC data revealed that **P2** showed the highest M_w and M_n values of all the polymers discussed in Chapter 2. The optical band gaps of **P1** and **P2** exhibited similar values of 1.97 eV and 1.98 eV respectively. **P3** and **P4** displayed similar optical band gaps to each other, but narrower band gaps than those of **P1** and **P2**, owing to the extension of the conjugation system through the addition of two more thiophene units to **P3** and **P4**. All polymers discussed in Chapter 2 demonstrated red shifts in thin films, which could be ascribed to the high planarity of the polymer backbones in the solid state, leading to strong π-π interchain stacking. **P1** and **P3** had the highest onset of degradation temperatures, at 388 ˚C and 397 ˚C, respectively, compared with **P2** and **P4**. Overall, all the polymers showed good thermal stability with decomposition temperatures in excess of 330 ˚C, which was sufficient for the requirements of OSCs. CV analysis of all these polymers showed low HOMO energy levels. The LUMO energy levels of polymers **P1**, **P2**, **P3** and **P4** were positioned in a suitable range for the requirements of OSCs. These values are higher than the LUMO energy level of $PC_{71}BM$. Thus, efficient separation and charge transfer could be anticipated in their corresponding BHJ solar cells. The PXRD studies suggested that all these polymers in this chapter exhibited an amorphous nature.

Chapter 3 demonstrated the synthesis and characterisation of a series of TPD-based copolymers **P5**, **P6**, **P7** and **P8**. Their optical, electrochemical and thermal properties in the solid state were investigated. All polymers showed sufficient thermal stability, with decomposition temperatures in excess of 300 ˚C, and good solubility in many types of organic solvents at room temperature, which is a requirement for OSC applications. GPC data revealed that **P7** showed the highest M_w and M_n values of all polymers whose synthesis was explained in Chapter 3. The optical band gaps of **P5** and **P6** displayed similar values of 2.05 eV and 2.03 eV respectively. **P7** and **P8** exhibited similar band gaps to each other but lower band gaps than those of **P5** and **P6,** at 1.93 eV and 1.94 eV respectively. This was owing to the extension of the conjugation system in **P7** and **P8** through the addition of two extra thiophene units. The CV analysis of all polymers showed very similar low HOMO energy levels, owing to the extended conjugation and therefore narrowed the electrochemical band gaps. All the polymers discussed in this section showed LUMO energy levels at higher values than that of $PC_{71}BM$. The PXRD studies proposed that all these polymers possessed amorphous characteristics.

Chapter 4 discussed the preparation of two alternating copolymers that consisted of BDI-functionalised units and phenanthrene-quinoxaline and 9,10-dialkoxy-phenanthreneunits as electron donors, to yield polymers **P9** and **P10**. Both polymers showed good thermal stability, with decomposition temperatures in excess of 330 ˚C. This is sufficient for OSC applications. GPC data revealed that **P10** showed higher M_w and M_n values than **P9** in chloroform fractions. **P9** and **P10** revealed low optical band gaps with values of 1.74 eV and 1.68 eV respectively. These values would be beneficial to obtain high J_{sc} values in BHJ solar cells. CV analysis of **P9** and **P10** exhibited low-lying HOMO energy levels with values of -5.38 eV and -5.37 eV, which should improve V_{oc} when these polymers are fabricated to BHJ solar devices. The LUMO energy levels of **P9** and **P10** were positioned in a suitable range of -3.58 eV to -3.62 eV, which were higher than the LUMO energy level of $PC_{71}BM$. The PXRD patterns of the polymers exhibited amorphous nature.

The PV properties of polymers **P1** to **P10** will be examined in cooperation with the Department of Physics at the University of Sheffield. The PCEs will be measured through the fabrication of BHJ photovoltaic devices with fullerene derivatives.

5.2. Future work

Several conjugated polymers synthesised and discussed for this thesis demonstrate optical and electronic properties that encourage further study regarding their use as electron donors in active layers and as blends with various ratios of fullerene derivatives for applications in BHJ solar cells. Thus, future work should include studies of their physical properties in BHJ solar devices. Furthermore, the polymer backbones can be structurally modified to tune the energy band gap. Modifications of flanking spacer units such as thieno[3,2-b]thiophene or 2,2'-bithiophene between the donor and acceptor moieties should also be studied. These have been shown to possess the ability to reduce steric hindrance caused by the incorporation of large alkyl groups in the polymer backbones. For example, **P9** and **P10** based on BDI exhibited the lowest band gaps (1.74 eV and 1.68 eV, respectively) of all the polymers synthesised for this project. However, the band gaps could be further reduced by the addition of an extra thiophene unit or by the attachment of thieno[3,2-b]thiophene between the donor and acceptor moieties in the conjugated polymers. Some suggested modifications are illustrated in Figure 5.1.

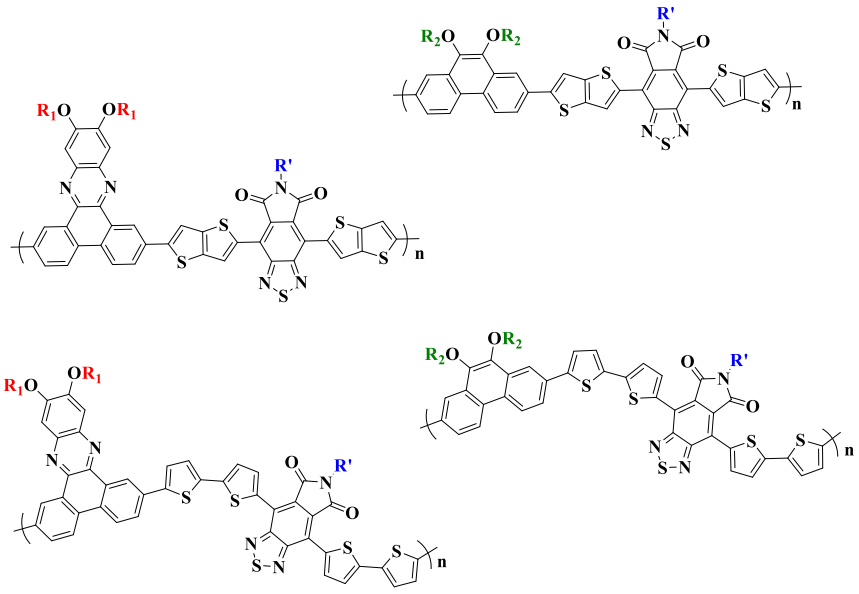

Figure 5.1. Schematic representations of modified P9 and P10 that should be investigated.

Other structural modifications could be made by anchoring various types of solubilising groups to the donor and acceptor units. This would address the solubility issue and increase the polymer molecular weights, leading to improved optical and electronic properties of the resultant conjugated polymers and therefore lower energy band gaps, owing to the improvement of charge-carrier mobility. Moreover, all polymers synthesised for this study

were based on phenanthrene and its derivative phenanthroquinoxaline units as electron donors. These could be substituted with other donor units that exhibit stronger electron-donating properties, such as benzo[1,2-b:4,5-b′]dithiophene, in order to obtain conjugated polymers with enhanced optical and electronic properties. Some suggested modifications are shown in Figure 5.2.

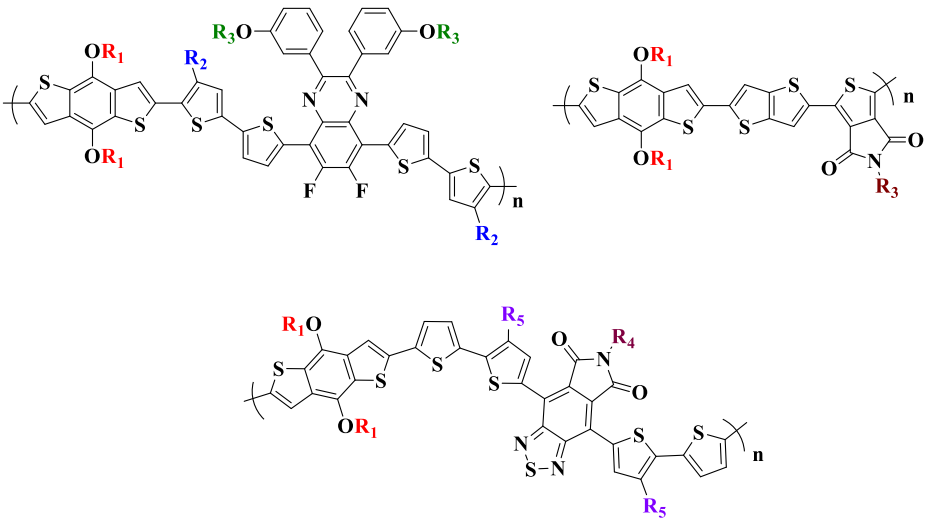

Figure 5.2 Schematic representations of suggested conjugated polymers with different types of alkyl chains.

This project also included the investigation of some copolymers based on fluorinated quinoxaline as the electron acceptor, and examined the impact of the fluorine atoms on HOMO and LUMO energy levels of D-A conjugated polymers. The presence of fluorine lowered these energy levels, because fluorine atoms can increase planarity *via* non-covalent interactions, and thus improve π-π stacking of polymer chains. Further study should be conducted into the incorporation of more fluorine atoms to polymer backbones, since this can achieve more effective morphology, which can lead to higher PCEs when the polymers are fabricated into BHJ photovoltaic devices. It would be interesting to synthesise analogous polymers to study and evaluate their impact on the energy band gaps and the PCEs of BHJ solar cells. The PV properties of polymers **P5**, **P6**, **P7** and **P8** will be examined through cooperation with the Department of Physics at the University of Sheffield. The PCE will be measured by the fabrication of BHJ photovoltaic devices with fullerene derivatives.

Chapter 6: Experimental

6.1. Materials

All chemical and starting materials were acquired from commercial suppliers and were used as received without further purification. Anhydrous solvents were obtained from a Grubbs solvent purification system. Reagent grade solvents, deuterated solutions, reagents, and drying agents were bought from internal stores. Reactions and polymerisations were conducted in dried glassware, utilising Schlenk line techniques and using Argon gas as an inert atmosphere.

6.2. Analytical Techniques Used for Measurements

6.2.1. Nuclear magnetic resonance spectra (NMR)

NMR spectra of all monomers were recorded on Bruker Avance 400 (400 MHz) at 22˚C and ^{1}H-NMR spectra of all polymers were performed on Bruker Avance III HD 500 (500 MHz) at 100 °C, dissolved in deuterated solutions such as chloroform-d_1, DMSO-d_6 and 1,1,2,2-tetrachloroethane-d_2 solvents, which were ordered from Sigma-Aldrich and used as received. Tetramethylsilane (TMS) was used as the internal standard for the calibration of chemical shifts (δ). NMR spectra were measured in parts per million (ppm) and the coupling constant (*J*) was calculated in Hertz (Hz). Spectra were analysed using TopSpin 3.2 software.

6.2.2. Thin layer chromatography (TLC)

TLCs were run on silica-coated aluminium plates. The chromophores were detected using an ultraviolet (UV) light lamp. In the case of inactive UV compounds, TLCs were sprayed with a solution of *p*-anisaldehyde and developed by heating using a heat gun. The anisaldehyde solution consisted of 9.3 ml *p*-anisaldehyde, 340 ml ethanol, 3.8 ml acetic acid, and 12.5 ml sulphuric acid.

6.2.3. Elemental analysis

A Perkin Elmer 2400 series II Analyser was employed to obtain the elemental analysis of carbon, hydrogen, nitrogen and sulphur content. Halide anions were measured using the Schoniger oxygen-flask combustion technique. The amount required for analysis was 5mg for CHNS analysis and 5mg for the halide anions.

6.2.4. Melting point

Melting points were obtained using a Gallenkamp Melting Point Apparatus. Samples were inserted in open-ended capillary tubes and positioned in the dedicated place on the apparatus.

6.2.5. Gel permeation chromatography analysis

GPC data was performed on a Viscotek GPCmax VE2001 GPC solvent/sample module and a Waters 410 Differential Refractometer using a RI-detection method. A series of polystyrene narrow standards (Polymer Laboratories) were used to calibrate the GPC curves. All polymers were dissolved in 1,2,4-trichlorobenzene, which was also used as the eluent at 140^{o}C. The prepared polymer samples were spiked with toluene as a reference. The equation below was used to calculate the polydispersity index (PDI).

$$\boldsymbol{PDI = M_w/M_n}$$

Where:

M_w is the weight-average molecular weight of the polymer; and

M_n is the number-average molecular weight of the polymer.

6.2.6. Cyclic voltammetry

Cyclic voltammograms were taken using a Princeton Applied Research Model 263A Potentiostat/Galvanostat. All measurements were performed in an electrolyte solution of tetrabutylammonium perchlorate dissolved in acetonitrile to give a 0.1M solution. The system set-up involved three electrodes: Ag/Ag^{+} as a reference electrode, a platinum wire as a counter electrode, and a platinum disc as a working electrode. Thin films of all polymers were prepared by drop-casting solution from $CHCl_3$. All the electrodes were submerged in the prepared electrolyte during the measurements. According to IUPAC's recommendations, ferrocene was used as the reference redox system.

6.2.7. UV-Visible absorption spectroscopy analysis

A Hitachi U-2010 Double Beam UV/Visible Spectrophotometer was employed to record the UV-visible absorption spectra, in dilute chloroform solutions which were measured using quartz cuvettes with a path length of 1cm, and in a solid state as drop-cast thin films on quartz substrates using approximately 1mg of polymer dissolved in chloroform.

6.2.8. Thermogravimetric analysis

TGA curves were collected using a Perkin Elmer TGA-1 Thermogravimetric Analyser. The analysis of samples was carried out under an inert atmosphere of nitrogen at a scan rate of 10˚C min^{-1}, with 3mg of each sample.

6.2.9. Powder X-ray diffraction analysis

A Bruker D8 advance diffractometer with a Cu Kα radiation source (1.5418Å, rated as 1.6kW) was employed to measure the molecular structural order of polymer samples. All measurements were carried out at scattering angles ranging from 2^o to 40^o 2θ.

6.3. Preparation of Monomers

6.3.1. Synthesis of 1,4-dimethylpiperazine-2,3-dione (1)[1]

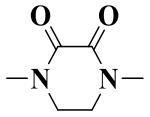

(1)

In a 500 ml round-bottomed flask, a solution of N,N'-dimethylethylene-diamine (10.27 g, 116.5 mmol) and diethyl oxalate (17.94 g, 122.8 mmol) in anhydrous diethyl ether (250 ml) was stirred for 19 hours under argon atmosphere at room temperature. A pale-yellow solution with a white precipitate formed. The mixture was filtered and washed with diethyl ether. Recrystallisation in toluene yielded the product as white needle-shaped crystals, (10.50 g, 73.894 mmol, 92 %).

^{1}H NMR (400 MHz; $CDCl_3$) δ (ppm): 3.58 (s, 4H), 3.10 (s, 6H).

^{13}C NMR (250 MHz, $CDCl_3$) δ (ppm): 157.5, 46.10, 35.

Calculated elemental analysis (%): C, 50.69; H, 7.09; N, 19.71; O, 22.51. Found: C, 50.63; H, 7.06; N, 19.61.

EI-MS (*m/z*): [M^+] calculated: 142.16; found: 142.

M.P. 178 ^{o}C.

6.3.2. Synthesis of 1-Bromo-3-(octyloxy) benzene (2)[2]

(2)

In a 500 ml round-bottomed flask, a solution of m-bromophenol (20.05 g, 115.7 mmol) and 1-bromooctane (24.09 g, 124.7 mmol) in dimethylformamide (130 ml) was prepared.

Potassium carbonate (40.05 g, 289.8 mmol) was added and the mixture was stirred at 70˚C for 18 hours. Distilled water (400 ml) was added. Upon completion, the mixture was extracted with diethyl ether (7 x 100 ml), washed with brine (4 x 100 ml) and water (4 x 100 ml), and dried over magnesium sulphate. The solvent was removed *in vacuo* to yield a golden oil, which was purified by column chromatography using 40-60 petroleum ether as an eluent to yield the product as a colourless oil (21.24 g, 74.73 mmol, 65 %).

^{1}H NMR (400 MHz; $CDCl_3$) δ (ppm): 7.15 (t, *J* = 8.2 Hz, 1H), 7.09 (m, 2H), 6.86 (dd, *J* = 2.4 and 8.1 Hz, 1H), 3.95 (t, *J* = 6.5 Hz, 2H), 1.80 (quintet, *J* = 7.1 Hz, 2H), 1.46 (quintet, *J*= 7.2 Hz , 2H), 1.33 (m, 8H), 0.91 (t, *J*= 6.8 Hz, 3H)

^{13}C NMR (250 MHz, $CDCl_3$) δ 159.9, 130.5, 123.5, 122.8, 117.7, 113.6, 68.3, 31.8, 29.3, 29.2, 29.1, 26.0, 22.7, 14.1.

Calculated elemental analysis (%): C, 58.95; H, 7.42; Br, 28.01; O, 5.61. Found: C, 59.01; H, 7.47; Br, 28.19.

EI-MS (*m/z*): [M^+] calculated: 284.22; found: 284.

6.3.3. Synthesis of 1,2-bis(3-(octyloxy)phenyl)ethane-1,2-dione (3)[3]

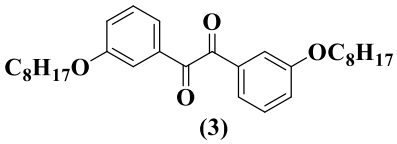

(3)

In a 500 ml, three-necked, round-bottomed flask, a solution of compound **(2)** (21.24 g, 74.73 mmol) in anhydrous tetrahydrofuran (143 ml) was cooled to -78˚C. A solution of n-butyllithium (33 ml, 82.5 mmol, 2.5 M in hexanes) was added dropwise and the mixture was stirred for a full hour. Compound **(1)** (5.26 g, 37 mmol) was added and the mixture was stirred for additional hour. After that, it was left to warm to room temperature and stirred for a further 16 hours. Distilled water (100 ml) was added, and the mixture was extracted with diethyl ether (3 x 300 ml), dried over magnesium sulphate, and the solvent removed *in vacuo* to form a yellow residue. Precipitation in cold methanol (50 ml) yielded the product as a white solid (10 g, 21.66 mmol, 60 %).

^{1}H NMR (400 MHz; $CDCl_3$) δ (ppm): 7.53 (t, *J* = 8.3 Hz, 2H,), 7.42 (m, 4H), 7.22 (dd, *J* = 8.1 and 2.4 Hz, 2H), 4.03 (t, *J* = 6.5 Hz, 4.0H), 1.81 (quintet, *J* = 7.1 Hz, 4H), 1.48 (quintet, *J* = 7.2 Hz, 4H), 1.34 (m, 16H), 0.91 (t, *J* = 6.9 Hz, 6H).

^{13}C NMR (250 MHz, $CDCl_3$) δ (ppm): 194.6, 159.6, 134.2, 129.9, 122.9, 122.2, 113.6, 68.37, 31.8, 29.3, 29.2, 29.1, 26.0, 22. 7, 14.1.

Calculated elemental analysis (%): C, 77.21; H, 9.07. Found: C, 77.20; H, 8.97.

EI-MS (*m/z*): [M^+] calculated: 466.31; found: 466.

M.P. 158-160 ºC.

6.3.4. Synthesis of 5,6-difluoro[c][1,2,5]thiadiazole (4)[4]

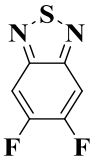

(4)

In a 1000 ml, round-bottomed, three-necked flask, under a protective atmosphere of argon, a solution of 1,2-diamino-5,6-difluoro-benzene (5 g, 34.7 mmol), in $CHCl_3$ (500 ml) and triethylamine (14.25 ml) was prepared. The solution was stirred until the diamine was totally dissolved. Thionyl chloride (9 g, 5.5 ml, 76.3 mmol) was added dropwise and the mixture heated to reflux overnight. The mixture was then cooled to room temperature and quenched with distilled water (300 ml). The mixture was transferred to a separation funnel and the product was extracted with DCM (3 x 300 ml). The organic layer was dried over $MgSO_4$ and the solvent removed *in vacuo*. The crude product was purified *via* column chromatography using petroleum ether: DCM (5:1) as an eluent. The product was obtained as an ivory white solid (3.58 g, 20.81 mmol, 60 %).

^{1}H NMR (400 MHz, $CDCl_3$) δ (ppm): 7.78 (t, 2H, J = 8.7 Hz).
^{13}C NMR (250 MHz, $CDCl_3$) δ (ppm): 154.2, 153.9, 152.3, 151.6, 151.4, 149.8, 105.2, 105.2, 105.1, 105.0.
^{19}F NMR (400 MHz, $CDCl_3$) δ (ppm): -127.91.
Calculated elemental analysis (%): C, 41.86; H, 1.17; N, 16.27; S, 18.62. Found: C, 42.06; H, 1.19; N, 16.54; S, 18.54.

EI-MS (*m/z*): [M^+] calculated: 171.99; found: 172.

M.P. 67-70 ºC.

6.3.5. Synthesis of 5,6-difluoro-4,7-diiodo-benzo[1,2,5]thiadiazole (5)[4]

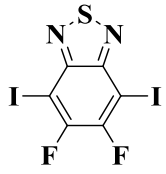

(5)

In a 500 ml, two-necked, round-bottomed flask, a mixture of 5,6-difluoro-benzo[1,2,5]thiadiazole (1 g, 5.8 mmol), I_2 (2.74 g, 10.78 mmol) was prepared. Fuming sulphuric acid (22 ml) was added dropwise and stirred at 60 ^oC for 24 hours. After cooling to room temperature, the reaction was poured onto crushed ice to quench the effect of the remaining fuming sulphuric acid. Chloroform was added, and the mixture was transferred into a separating funnel and washed with distilled water (3 x 100 ml), followed by 1 M NaOH solution to remove excess iodine, and lastly washed with $NaHCO_3$ (3 x 100 ml). The organic layer was dried over $MgSO_4$ and the solvent removed *in vacuo* to yield the product as cream crystals (1.74 g, 4.1 mmol, 92 %).

^{19}F NMR (400 MHz, $CDCl_3$) δ (ppm): -105.01.

^{13}C NMR (250 MHz, $CDCl_3$) δ (ppm): 154.2, 153.9, 152.3, 151.6, 151.4, 149.8, 105.2, 105.2, 105.1, 105.0.

Calculated elemental analysis (%): C, 17.00; F, 8.96; I, 59.87; N, 6.61; S, 7.56, found: C, 16.89; I, 59.67; N, 6.56; S, 7.47.

EI-MS (*m/z*): [M^+] calculated: 423.78; found: 423, 424 and 425;

M.P. 154-157 ^oC.

6.3.6. Synthesis of 5,6-difluoro-4,7-bis(4,2-thienyl)-2,1,3-benzothaidiazole (6)[5]

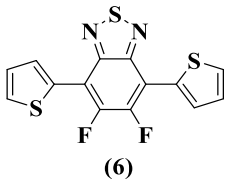

(6)

To a 100 ml, round-bottomed flask was added 5,6-difluoro-4,7-diiodo-benzo[1,2,5]thiadiazole **(5)** (1.4 g, 3.3 mmol), (2-tributylstannyl)thiophene (3.18 g, 7.26 mmol) and anhydrous toluene (15 ml). The mixture was under an inert atmosphere of argon. $Pd(PPh_3)_2Cl_2$ (40 mg) was then added and the reaction mixture was degassed four times and set under an argon atmosphere. The reaction mixture was heated to reflux and left for 48

hours. After that, the reaction mixture was cooled to room temperature and the solvent was removed *in vacuo*. The crude product was purified by precipitation in methanol (35 ml) and filtered, yielding orange crystals (1g, 3 mmol, 90 %).

^{1}H NMR (400 MHz, $CDCl_3$) δ (ppm): 8.32 (d, 2H, *J* = 3.7 Hz), 7.63 (dd, 2H, *J* = 5.2 and 1.1 Hz), 7.29 (d, 2H, *J* = 4.1 Hz).

^{19}F NMR (400 MHz, $CDCl_3$) δ (ppm): -127.98.

^{13}C NMR (250 MHz, $CDCl_3$) δ (ppm): 131.5, 130.9, 128.9, 127.4.

Calculated elemental analysis (%): C, 49.99; H, 1.80; F, 11.30; N, 8.33; S, 28.59, found: C, 50.06; H, 2.19; N, 8.28; S, 28.64.

EI-MS (*m/z*): [M^+] calculated: 335.97; found: 336.

M.P. 125-127 °C.

6.3.7. Synthesis of 1,2-diamino-3,6-di(2-thienyl)-4,5-difluorobenzene (7) and 2,3-Bis(3-(octyloxy)phenyl)-5,8-di(2-thienyl)-6,7-difluoroquinoxaline (8)[3,6]

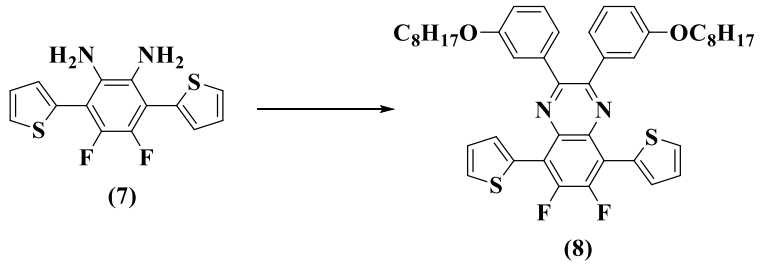

In a 100 ml, round-bottomed flask, a mixture of 5,6-difluoro-4,7-bis(4,2-thienyl)-2,1,3-benzothaidiazole (0.60 g, 1.8 mmol), zinc powder (2.63 g, 40.23 mmol) and acetic acid (30 ml, glacial) was heated under reflux (120 °C) for 90 minutes. The mixture was cooled to room temperature. Excess zinc was removed *via* filtration and the solid washed thoroughly with diethyl ether. The filtrate was washed with aqueous sodium hydroxide 10 % (5 x 200 ml,) and brine (5 x 200 ml), dried over magnesium sulphate and the solvent removed *in vacuo* to leave a crude orange solid (1,2-diamino-3,6-di(2-thienyl)-4,5-difluorobenzene, **(7)**), (~0.44g, 1.43 mmol, ~80 %). (Product **(7)** was unstable to oxidation and needed to be used directly);

In a 100 ml, round-bottomed flask, a mixture of the orange solid (1,2-diamino-3,6-di(2-thienyl)-4,5-difluorobenzene) and compound 3 (1,2-Bis(3-(octyloxy)phenyl)ethane-1,2-dione) (0.833 g, 1.86 mmol) in methanol (60 ml) was prepared and stirred for 5 mins. Acetic acid

(5.5 ml, glacial) was added and the mixture was heated under reflux at 80 °C and left overnight. The mixture was left to cool to room temperature and the solvent removed *in vacuo* to produce a yellow sludge. After addition of water (400 ml), the mixture was extracted with chloroform (8 x100 ml), washed with brine (5 x 100 ml), dried over magnesium sulphate and the solvent removed *in vacuo* to produce a yellow residue. Purification *via* column chromatography, using 40-60 petroleum ether/dichloromethane (1:1) as an eluent, yielded the product as a bright yellow solid (0.60 g, 0.79 mmol, 50 %).

^{1}H NMR ($CDCl_3$, 400 MHz) δ (ppm): 8.03 (d, *J* = 3.9 Hz, 2H), 7.65 (dd, *J* = 5.2, 1.0 Hz, 2H), 7.39 (s, 2H), 7.27-7.23 (m, 6H), 6.98-6.95 (m, 2H), 3.93 (t, *J* = 6.6 Hz, 4H), 1.79-1.74 (m, 4H), 1.47-1.42 (m, 4H), 1.35-1.32 (m, 8H), 0.92 (t, *J* = 6.9 Hz, 6H);

^{13}C NMR (250 MHz, $CDCl_3$) δ (ppm): 159.1, 151.3, 139.3, 134.7, 130.9, 130.8, 129.9, 129.2, 126.5, 122.8, 117.9, 116.6, 115.7, 68.2, 31.5, 29.1, 25.7, 22.6, 14.0;

Calculated elemental analysis (%): C, 71.51; H, 6.55; F, 5.14; N, 3.79; O, 4.33; S, 8.68.
Found: C, 71.04; H, 6.50; N, 3.65; S, 8.53;

EI-MS (*m/z*): [M^+] calculated: 738.31; found: 738;

M.P. 147-149 °C.

6.3.8. Synthesis of 2,3-bis(3-(octyloxy)phenyl)-6,7-difluoro-5,8-bis(5-bromo-2-thienyl)quinoxaline (9)[3]

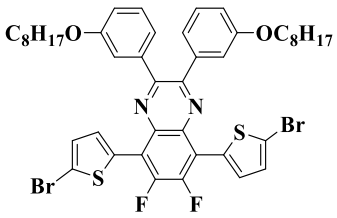

(9)

In a 100 ml, round-bottomed flask, a solution of 2,3-bis(3-(octyloxy)phenyl)-5,8-di(2-thienyl)-6,7-difluoroquinoxaline (0.50 g, 0.61 mmol) in chloroform (30 ml) and acetic acid (3 ml) was protected from light and cooled to 0 ˚C. N-bromosuccinimide (0.23 g, 1.3 mmol) was added in small portions, after which the solution was stirred for 15 minutes at 0 ˚C. The mixture was then stirred for 21 hours at room temperature. Distilled water (100ml) was added and the mixture was extracted with chloroform (5 x 100 ml), dried over magnesium sulphate, filtered and the solvent removed *in vacuo* to produce an orange solid. Purification by

recrystallisation in isopropanol yielded the product as an orange solid (0.46 g, 51 mmol, 85 %).

^{1}H NMR ($CDCl_3$, 400 MHz) δ (ppm): 7.82 (d, *J* = 4.1 Hz, 2H), 7.54 (S, 2H), 7.23 (t, *J* = 7.9 Hz, 2H), 7.20 (d, *J* = 4.2 Hz, 2H), 7.11 (d, *J* = 7.6 Hz ,2H), 7.01 (dd, *J* = 8.1, 2.2 Hz, 2H), 4.06 (t, *J* = 6.4 Hz, 4H), 1.86-1.79 (m, 4H), 1.53-1.48 (m, 4H), 1.38-1.33 (m, 8H), 0.92 (t, *J* = 6.6 Hz, 6H);

^{13}C NMR (250 MHz, $CDCl_3$) δ (ppm): 159.4, 151.6, 138.7, 133.8, 132.4, 130.9, 130.8, 130.8, 129.3, 129.1, 122.9, 118.9, 117.4, 117.0, 115.1, 68.3, 31.9, 29.5, 29.4, 29.3, 26.2, 22.7, 14.2;

^{19}F NMR (400 MHz, $CDCl_3$) δ (ppm): -128.59;

Calculated elemental analysis (%): C, 58.93; H, 5.17; Br, 17.82; F, 4.24; N, 3.12; O, 3.57; S, 7.15. Found: C, 58.29; H, 5.28; Br, 17.52; N, 3.06; S, 7.08;

EI-MS (*m/z*): [M^+] calculated: 896.13; found: 894, 896 and 898;

M.P. 135-137 °C.

6.3.9. Synthesis of 2,7-dibromophenanthrene-9,10-dione (10)[7]

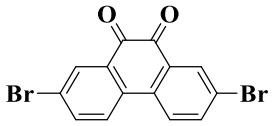

(10)

In a 250 ml, round-bottomed flask, NBS (8.23 g, 0.04 mol) was added to a well-stirred viscous solution of phenanthrene-9,10-dione (4.60 g, 0.02 mol) in 98 % H_2SO_4 (80 ml), then stirred at room temperature overnight. The mixture was poured on to crushed ice. The orange product was filtered and washed with cold distilled water. It was recrystallised in DMSO (80 ml) to produce orange needle-shaped crystals (4.8 g, 13.11 mmol, 60 %).

^{1}H NMR (400 MHz, DMSO-d_6) δ (ppm): 8.25 (d, *J* = 8.7 Hz, 2H), 8.07 (d, *J* = 2.3 Hz, 2H), 7.96 (dd, *J* = 8.7, 2.3 Hz, 2H);

^{13}C NMR (250 MHz, $CDCl_3$) δ (ppm): 176.8, 137.4, 133.6, 133.2, 131.1, 126.9, 122.9;

Calculated elemental analysis (%): C, 45.94; H, 1.65; Br, 43.66. Found: C, 46.01; H, 1.82; Br, 43.49;

EI-MS (*m/z*): [M^+] calculated: 365.87; found: (m/z) 366;

M.P. 336-339 ºC.

6.3.10. Synthesis of bromo-2-hexyldecane (11)[8]

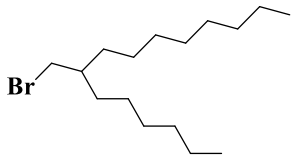

(11)

In a 1000 ml, round-bottomed flask, a solution of 7-hydroxymethylpentadecane (24.24 g, 100 mmol) in DCM (800 ml) was prepared, triphenylphosphine (TPP) (31.47 gm, 120 mmol) was added, followed by NBS (21.36 gm, 120 mmol) in small portions. The solution was stirred for 15 min at room temperature, and then the solvent was removed *in vacuo* to produce a dark-brown residue. This was washed with saturated $NaHCO_3$ aqueous solution (200 ml) and dried with $MgSO_4$, after which 500 ml of petroleum ether was added and the mixture stirred for 1 hour and filtered. The solvent in the filtrate was removed *in vacuo*. The crude product was purified by column chromatography with petroleum ether as eluent. The solvent was removed *in vacuo* to obtain a colourless liquid (29.75 g, 97.55 mmol, 98 %), which was pure product as the first spot.

^{1}H NMR (400 MHz, $CDCl_3$) δ (ppm): 3.60 (d, 2H, J = 4.69 Hz), 1.58 (m, 1H), 1.29 (m, 24H), 0.90 (6H);

^{13}C NMR (250 MHz, $CDCl_3$) δ (ppm): 39.8, 39.5, 32.6, 31.9, 31.8, 29.8, 29.6, 29.5, 29.3, 26.6, 26.5, 22.7, 22.7, 14.0;

Calculated elemental analysis (%): C, 62.94; H, 10.89; Br, 26.17. Found: C, 63.32; H, 10.58; Br, 26.00;

EI-MS (*m/z*): [M^+] calculated: 304.18; found: (m/z) 304 and 306.

6.3.11. Synthesis of 1,2 bis-(2-hexyldecyloxy) benzene (12)[9]

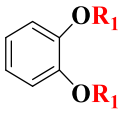

R_1 = 2-hexyldecyl

(12)

In a 250 ml, round-bottomed flask, a mixture of catechol (3.34 g, 30.00 mmol), 7-bromoethylpentadecane (21.27 g, 69.00 mmol) and K_2CO_3 (12.67 g, 91.00 mmol) was added. The system was closed and degassed four times. After the addition of dry DMF (50 ml, 630 mmol), the mixture was stirred at 100 ^oC under argon atmosphere for 40 hours. After cooling the mixture to room temperature, 500 ml of distilled water were added. The organic layer was separated, and the aqueous layer was extracted with DCM (5 x 200 ml). The combined organic layer was dried over $MgSO_4$. After filtration, the filtrate was concentrated under a *vacuum*. The product was purified using column chromatography, passing first petroleum ether to eliminate the residue of the alkyl group, and then petroleum ether: dichloromethane, (10:2), as an eluent to obtain a pure colourless liquid as first spot (11.38 g, 20 mmol, 67 %).

^1H NMR (400 MHz, $CDCl_3$) δ (ppm): 6.89 (s, 4H), 3.88 (d, 4H, *J*=5.7), 1.56 (m, 1H), 1.28 (m, 24H), 0.90 (m, 6H);

^{13}C NMR (250 MHz, $CDCl_3$) δ (ppm): 149.7, 120.8, 113.9, 71.9, 38.2, 31.9, 31.4, 30.2, 29.8, 29.7, 29.4, 26.9, 26.9, 22.7, 14.1;

Calculated elemental analysis (%): C, 81.65; H, 12.62; O, 5.72; found: C, 79.97; H, 12.28;

EI-MS (*m/z*): [M^+] calculated: 558.54; found: (m/z) 558.

6.3.12. Synthesis of 1,2-dinitro-4,5-bis(2-hexyldecyloxy)benzene (13)[9]

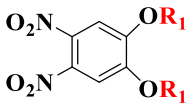

R_1 = 2-hexyldecyl

(13)

In a 500 ml, round-bottomed flask, 1,2 bis(2-hexyldecyloxy)benzene (5 g, 8.5 mmol) was dissolved in DCM (70 ml) and acetic acid (70 ml), and the mixture was stirred for 10 mins. The solution was cooled to 0 °C, and HNO_3 (65 %, 10ml) was added dropwise. The mixture was allowed to warm to room temperature and stirred for 1 hour. The mixture was cooled again to 0 °C, then fuming nitric acid (25 ml) was added dropwise. The reaction was stirred

for 40 hours, and a yellow liquid formed. The mixture was poured into ice. The DCM layer was separated, and the aqueous phase was extracted with DCM again. The combined organic layer was washed with water, with saturated $NaHCO_3$ (aq), and with brine, and then the organic layer was dried over $MgSO_4$ and filtered. The product was concentrated under *vacuum* to produce a yellow oil (5.32 g, 8.2 mmol, 96 %).

^{1}H NMR (400 MHz, $CDCl_3$) δ (ppm): 7.30 (s, 2H), 3.99 (d, 4H, *J*= 5.4), 1.87 (m, 1H), 1.30 (24H, m), 0.90 (6H);

^{13}C NMR (250 MHz, $CDCl_3$) δ (ppm): 152.1, 136.4, 107.5, 72.7, 37.8, 31.9, 31.8, 31.2, 30.01, 29.8, 29.6, 29.4, 26.8, 26.8, 22.7, 14.1;

Calculated elemental analysis (%): C, 70.33; H, 10.56; N, 4.32; O, 14.79. Found: C, 69.11; H, 10.39; N, 3.83;

EI-MS (*m/z*): [M^+] calculated: 648.51; found: (m/z) 648.

6.3.13. Synthesis of 1,2-diamine-4,5-bis(2-hexyldecyloxy)benzene (14)[10]

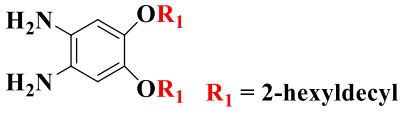

(14)

In a 250 ml, round-bottomed flask, a mixture of 1,2-dinitro-4,5-bis(2-hexyldecyloxy)benzene (2 g, 3.08 mmol), ammonium formate (1.656 g, 26.26 mmol) in the presence of 10 % Pd/C (0.20 g) in methanol (80 ml) was prepared. After degassing, dry THF (40 ml) was added and the mixture left to stir under argon for 10 mins at room temperature, and then heated to 70 °C for 2 hours. Upon completion, the mixture was left to cool to room temperature, the catalyst was removed by filtration under a stream of argon in a dry condition, and a pale-yellow solution was produced. The solvent was removed under reduced pressure to give a colourless, air-sensitive oil compound of 1,2-diamine-4,5-bis(2-hexyldecyloxy)benzene. (The product was unstable to oxidation and needed to be used straight after filtration).

6.3.14. Synthesis of 2,7-dibromo-11,12-bis-(2-hexyldecyloxy)-phenanthro[9,10-b]quinoxaline(15)[11]

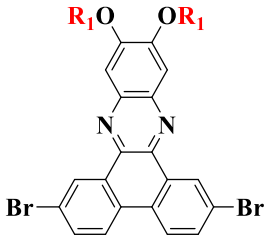

R_1 = 2-hexyldecyl

(15)

A 500 ml, two-necked, round-bottomed flask was charged with 1,2-diamine-4,5-bis(2-hexyldecyloxy) benzene (1.64 g, 2.78 mmol), 2,7 dibromophenanthrene-9,10-dione (1.01 g, 2.76 mmol), p-toluenesulphonic acid (PTSA) (0.811 g, 4.71 mmol) and toluene (375 ml). The mixture was stirred under argon and heated at 120 °C under reflux for 24 hours. The resulting dark solution was evaporated to dryness. The crude was purified by column chromatography using petroleum ether and toluene (10:2) as an eluent, to produce, as second spot, a yellow thick oil (1.41 g, 1.54 mmol, 61 %).

^{1}H NMR (400 MHz, $CDCl_3$) δ (ppm): 9.42 (d, *J*=2.2 Hz, 2H), 8.27 (d, *J*=8.8 Hz, 2H), 7.78 (dd, *J*=2.2, 8.7 Hz, 2H), 7.44 (s, 2H), 4.16 (d, *J*=5.5 Hz, 4H), 2.05-1.94 (m, 2H), 1.69-1.23 (m, 48H), 0.90 (t, *J*= 7.0 Hz, 12H);

^{13}C NMR (250 MHz, $CDCl_3$) δ (ppm): 154.4, 140.3, 138.2, 132.1, 129.1, 128.2, 128.1, 125.31, 124.3, 122.4, 106.2, 71.8, 37.9, 31.9, 31.5, 30.1, 29.8, 29.7, 29.4, 26.9, 26.9, 22.8, 22.7, 14.1;

Calculated elemental analysis (%): C, 67.96; H, 8.12; Br, 17.39; N, 3.05; O, 3.48. Found: C, 68.38; H, 7.90; Br, 17.46; N, 2.85;

EI-MS (*m/z*): [M^+] calculated: 918.41; found: (m/z) 916, 918 and 920.

6.3.15. Synthesis of 2,7- bis-(4,4,5,5-tetramethyl-1,3,2-dioxaborolan-2-yl)-11,12-bis-(2-hexyldecyloxy)-phenanthro[9,10-b]quinoxaline (16)[12]

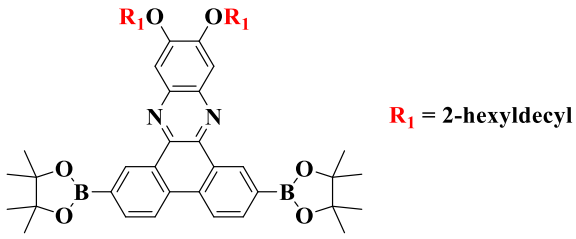

(16)

A 25 ml, round-bottomed flask was charged with compound **(15)** (0.245 g, 0.266 mmol), bis(pinacolato)diboron (0.231 g, 0.91 mmol), potassium acetate (0.153 g, 1.56 mmol), and $PdCl_2$(DPPF) (0.011 g, 5.54 mol %), then degassed under an argon atmosphere. Dry DMF (7 ml) was added to the mixture, which was stirred and degassed again, then heated at 100 °C for 48 h. Upon completion, the reaction mixture was allowed to cool to room temperature, then poured into 100ml of distilled water. It was extracted with diethyl ether (5 x 150 ml) and the organic layer washed with H_2O (3 x 200 ml), dried over $MgSO_4$, filtered and the solvent was removed under *vacuum* to give a dark-brown solid as a crude product. The crude product was precipitated from methanol to obtain a dark-green dense oil (0.210 g, 0.207 mmol, 78 %).

^{1}H NMR (400 MHz, $CDCl_3$) δ (ppm): 9.84 (s, 2H), 8.64 (d, *J* = 8.2 Hz, 2H), 8.18 (d, *J* = 8.1 Hz, 2H), 7.61 (s, 2H), 4.18 (d, *J*=5.5 Hz, 4H), 2.06-1.94 (m, 2H), 1.75-1.57 (m, 8H), 1.47 (s, 24H) 1.39-1.19 (m, 40H), 0.90 (t, *J*= 7.1 Hz, 12H);

^{13}C NMR (250 MHz, $CDCl_3$) δ (ppm): 153.7, 140.0, 139.8, 134.9, 133.3, 132.5, 130.3, 122.4, 106.6, 84.1, 71.7, 37.9, 31.9, 31.9, 31.5, 30.1, 29.8, 29.7, 29.4, 26.9, 26.9, 25.0, 22.7, 22.7, 14.1;

Calculated elemental analysis (%): C, 75.88; H, 9.75; B, 2.13; N, 2.77; O, 9.48. Found: C, 75.67; H, 9.47; N, 2.64;

EI-MS (*m/z*): [M^+] calculated: 1012.76; found: (m/z) 1011, 1012 and 1013.

6.3.16. Synthesis of 5-bromomethylundecane (17)[8]

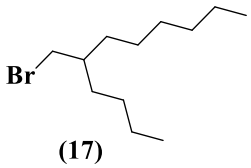

(17)

In a 1000 ml round-bottomed flask, a solution of 2-butyl-1-octanol (12.26 g, 65.84 mmol) in DCM (400 ml) was prepared. Triphenylphosphine (TPP) (15.78 g, 60.16 mmol) was added, and then NBS (10.68 g, 60.01 mmol) in small portions. The solution was stirred for 20 mins at room temperature to give a brown solution, then the solvent was removed *in vacuo* to produce a dark-brown residue. This was washed with saturated $NaHCO_3$ aqueous solution (200 ml) and dried with $MgSO_4$. After that, 500 ml of petroleum ether was added and the mixture stirred for 1h and filtered. The solvent in the filtrate was removed *in vacuo*, then the crude was purified by column chromatography with petroleum ether as an eluent. The solvent was removed by *vacuum* to obtain the product as a colourless liquid (13.79 g, 55.58 mmol, 84.5 %).

^{1}H NMR (400 MHz, $CDCl_3$) δ (ppm): 3.48 (d, J = 4.8 Hz, 2H), 1.62 (m, 1H), 1.30 (m, 24H), 0.91 (6H);

^{13}C NMR (250 MHz, $CDCl_3$) δ (ppm): 39.7, 39.5, 32.6, 32.3, 31.8, 29.5, 28.8, 26.5, 22.9, 22.7, 14.1, 14.1;

Calculated elemental analysis (%): C, 57.83; H, 10.11; Br, 32.06. Found: C, 58.63; H, 9.66; Br, 32.13;

EI-MS (*m/z*): [M^+] calculated: 248.11; found: (m/z) 248 and 250.

6.3.17. Synthesis of 2,7-dibromo-9,10-bis-(2-butyl-octyloxy) phenanthrene (18)[13]

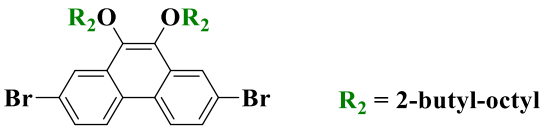

(18)

In a 50 ml, round-bottomed flask, a mixture of 2,7-dibromophenanthrene-9,10-dione (0.5 g, 1.37 mmol), $Na_2S_2O_4$ (1.43 g, 8.2 mmol), n-BuNBr (0.55 g, 1.7 mmol), H_2O (5 ml) and THF (10 ml) were added together and stirred for 1 h at 25 °C. After that, an aqueous solution of

KOH (1.23 g in 5 ml H_2O) and 5-bromomethylundecane (1.36 g, 5.48 mmol) were added and the mixture stirred for 5 hours at 70 °C. After that, the reaction mixture was extracted with EtOAc (5 x 100 ml). The organic layer was washed with brine three times, dried with anhydrous $MgSO_4$, and finally the solvent was removed *in vacuo*. The resultant product was purified *via* column chromatography by passing petroleum ether first to eliminate any residue of unreacted alkoxy, and then petroleum ether: dichloromethane, (100:1), as an eluent to obtain pure-yellow oil as the third spot (0.58 g, 0.82 mmol, 60.4 %).

^{1}H NMR (400 MHz, $CDCl_3$) δ (ppm): 8.41 (m, 4H), 7.69 (dd, *J*= 2.1, 8.8 Hz, 2H), 4.08 (d, *J*= 6.0 Hz, 4H), 1.94 (m, 2H), 1.66-1.46 (m, 8H), 1.42-1.33 (br, 24H), 0.94 (m, 12H);

^{13}C NMR ($CDCl_3$) δ (ppm): 143.1, 131.1, 129.0, 126.7, 125.0, 124.2, 121.5, 39.2, 31.9, 31.4, 31.1, 29.8, 29.1, 26.9, 23.2, 22.7, 14.2;

Calculated elemental analysis (%): C, 64.77; H, 8.01; Br, 22.68; O, 4.54. Found: C, 65.01; H, 8.19; Br, 23.08;

EI-MS (*m/z*): [M^+] calculated: 704.26; found: (m/z) 702, 704 and 706.

6.3.18. Synthesis of 2,7- bis-(4,4,5,5-tetramethyl-1,3,2-dioxaborolan-2-yl)-9,10-bis-(2-butyl-octyloxy)-phenanthrene (19)[12]

(19)

R_2 = 2-butyl-octyl

A 25 ml, round-bottomed flask was charged with 2,7-dibromo-9,10-bis-(2-butyl-octyloxy) phenanthrene **(**0.406 g, 0.58 mmol), bis(pinacolato)diboron (0.512 g, 1.99 mmol), potassium acetate (0.339 g, 3.41 mmol), and $PdCl_2$(DPPF) (0.026 g, 6 mol %), and then degassed under argon atmosphere. Dry DMF (7 ml,) was added to the mixture, which was stirred and degassed again, then heated at 100 °C for 48 h. Upon completion, the reaction mixture was allowed to cool to room temperature, then poured into 100 ml of distilled water. It was extracted with diethyl ether (5 x 100 ml) and the organic layer washed with H_2O (5 x 100 ml), dried over $MgSO_4$, filtered and the solvent removed under *vacuum* to give a dark-brown oil as a crude product. This was precipitated from methanol to obtain a brown dense oil (0.344 g, 0.43 mmol, 75 %).

^{1}H NMR (400 MHz, $CDCl_3$) δ (ppm): 8.80 (s, 2H), 8.66 (d, *J*= 8.2 Hz, 2H), 7.99 (d, *J*= 8.2 Hz, 2H), 4.12 (m, 4H), 1.97 (m, 2H), 1.76–1.5 (m, 8H), 1.41(s, 24H), 0.94 (m, 12H);

^{13}C NMR ($CDCl_3$) δ (ppm): 143.5, 130.7, 130.4, 129.9, 129.4, 122.0, 83.8, 39.3, 31.9, 31.5, 31.2, 29.9, 29.3, 27.1, 24.9, 23.2, 22.7, 14.2, 14.2;

Calculated elemental analysis (%): C, 75.18; H, 10.10; B, 2.71; O, 12.02. Found: C, 66.61; H, 8.65;

EI-MS (*m/z*): [M^+] calculated: 798.61; found: (m/z) 796, 798 and 800.

6.3.19. Synthesis of 2,3-Bis(3-(octyloxy)phenyl)-6,7-difluoro-5,8-bis((2,2′-bithiophene)-5-yl)quinoxaline (20)[5]

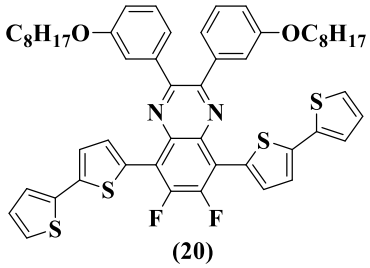

(20)

To a 100 ml, round-bottomed flask was added 2,3-bis(3-(octyloxy)phenyl)-6,7-difluoro-5,8-bis(5-bromo-2-thienyl)quinoxaline **(9)** (0.100g, 0.112mmol), (2-tributylstannyl) thiophene (0.15 g, 0.392 mmol) and anhydrous THF (5 ml). The mixture was under an inert atmosphere of argon. $Pd(PPh_3)_2Cl_2$ (13 mg) was then added and the reaction mixture was degassed four times and set under an argon atmosphere. The reaction mixture was heated to reflux and left for 48 hours. Then, the reaction mixture was cooled to room temperature and the solvent was removed *in vacuo*. The crude was purified by precipitation in methanol (35 ml) and filtered to yield dark-orange crystals (0.074 g, 0.082 mmol, 73 %)**.**

^{1}H NMR (400 MHz, $CDCl_3$) δ (ppm): 7.99 (d, J = 4 Hz, 2H), 7.55 (s, 2H), 7.32-7.22 (m, 10H), 7.09-7.07 (m, 2H), 6.99 (m, 2H), 3.94 (t, *J* = 6.5 Hz, 4H), 1.75-1.69 (m, 4H), 1.39-1.31 (br, 20H), 0.92 (t, *J* = 6.8 Hz, 3H).

^{19}F NMR (400 MHz, $CDCl_3$) δ (ppm): -128.78.

^{13}C NMR (250 MHz, $CDCl_3$) δ (ppm): 159.3, 139.1, 129.2, 127.9, 124.9, 123.9, 123.3, 122.9, 116.5, 115.8, 68.2, 31.9, 29.4, 29.3, 26.1, 22.7, 14.1;
Calculated elemental analysis (%): C, 69.15; H, 5.80; F, 4.21; N, 3.10; S, 14.20. Found: C, 69.24; H, 5.78; N, 2.95; S, 14.11;

EI-MS (*m/z*): [M^+] calculated: 902.29; found: 902;

M.P. 152-154 °C.

6.3.20. Synthesis of 2,3-bis(3-(octyloxy)phenyl)-6,7-difluoro-5,8-bis(5-bromo-(2,2'-bithiophene)-5-yl)quinoxaline (21)[3]

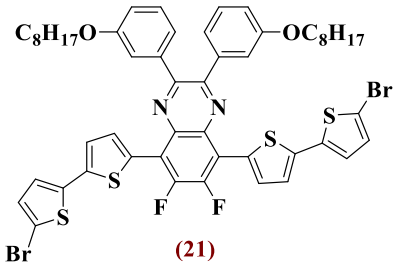

(21)

In a 100 ml, round-bottomed flask, a solution of 2,3-bis(3-(octyloxy)phenyl)-6,7-difluoro-5,8-bis((2,2′-bithiophene)-5-yl)quinoxaline (0.232 g, 0.257 mmol) in THF (10 ml) was produced while the flask was protected from light and placed under an argon atmosphere. N-bromosuccinimide (0.098 g, 0.553 mmol) was added in small portions. The mixture was then stirred overnight at room temperature. Distilled water (100 ml) was added and the mixture was extracted with DCM (5 x 100 ml), dried over magnesium sulphate, filtered and the solvent removed *in vacuo* to produce an orange solid. This was purified by recrystallisation in methanol to yield the product as a red solid (0.253 g, 0.238 mmol, 93 %).

^{1}H NMR (400 MHz, $CDCl_3$) δ (ppm): 7.96 (d, *J* = 4.0 Hz, 2H), 7.55 (t, *J* = 2.0 Hz, 2H), 7.27-7.21 (m, 4H), 7.19-7.15 (m, 2H), 7.05-6.98 (m, 6H), 3.96 (t, *J* = 6.6 Hz, 4H), 1.77- 1.72 (m, 4H), 1.40-1.33 (br, 20H), 0.92 (t, *J* = 6.8 Hz, 6H);

^{13}C NMR (250 MHz, $CDCl_3$) δ (ppm): 159.3, 151.1, 148.4, 148.2, 140.6, 138.9, 133.9, 131.5, 131.5, 130.8, 130.2, 129.0, 123.8, 123.3, 122.9, 117.1, 116.3, 116.0, 115.1, 111.5, 68.3, 53.4, 31.9, 29.5, 29.4, 26.2, 26.1, 22.7, 14.2;

^{19}F NMR (400 MHz, $CDCl_3$) δ (ppm): -128.35;

Calculated elemental analysis (%): C, 58.86; H, 4.75; Br, 15.06; N, 2.64; S, 12.09. Found: C, 58.08; H, 4.81; Br, 15.06; N, 2.57; S, 12.01;

EI-MS (*m/z*): [M^+] calculated: 1060.11; found: 1058, 1060 and 1062;

M.P. 142-144 °C.

6.3.21. Synthesis of 1-bromo-3,7-dimethyloctane (22)[8]

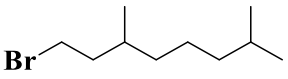

(22)

In a 1000 ml, round-bottomed flask, a solution of 3,7-dimethyl-1-octanol (6 g, 37.92 mmol) in DCM (150 ml) was prepared, and triphenylphosphine (TPP) (11.68 g, 45.20 mmol) was added. Then NBS (10.68 g, 60.01 mmol) was added in small portions. The solution was stirred for 2 h, under protection from light at room temperature, to give a yellow solution, then the solvent was removed *in vacuo* to produce a brown residue. This was washed with saturated $NaHCO_3$ aqueous solution (200 ml) and dried with $MgSO_4$. After that, 500 ml of petroleum ether was added, and the mixture stirred for 1h and filtered. The solvent in the filtrate was removed *in vacuo*, then the crude was purified by column chromatography with petroleum ether as eluent. The solvent was removed *in vacuo* to obtain a product as a colourless oil (8.09 g, 36.76 mmol, 97 %), which was obtained as a pure product as the first spot.

^{1}H NMR (400 MHz, $CDCl_3$) δ (ppm): 3.44 (m, 2H), 1.89 (m, 2H), 1.68 (m, 2H), 1.55 (m, 1H), 1.30 (m, 3H), 1.16 (m, 3H), 0.90 (t, J = 8.6 Hz, 9H);

^{13}C NMR (250 MHz, $CDCl_3$) δ (ppm): 40.1, 39.2, 36.7, 32.2, 31.7, 27.9, 24.6, 22.7, 22.6, 18.9;

Calculated elemental analysis (%): C, 54.30; H, 9.57; Br, 36.13. Found: C, 54.63; H, 9.38; Br, 35.95;

EI-MS (*m/z*): [M^+] calculated: 220.08; found: 220 and 222.

6.3.22. Synthesis of N-(3,7-dimethyloctyl)phthalimide (23)[14]

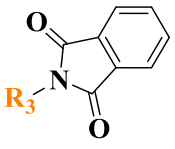

R_3 = 3,7-dimethyloctyl

(23)

In a 250 ml, round-bottomed flask, a solution of 1-bromo-3,7-dimethyloctane (7.86 g, 35.94 mmol) in dry DMF (43 ml) was prepared. Potassium phthalimide (7.15 g, 38.61 mmol) was added to the solution. The reaction was stirred at 90 ^{o}C for 16 hours. Upon completion, the reaction was left to cool to room temperature, then poured into water (100 ml). The crude was

extracted with DCM (5 x 100 ml). The organic layers were combined, then washed with H_2O (3 x 300 ml), and dried over $MgSO_4$. The solvent was removed *in vacuo* to give the title product as a colourless oil (10.11 g, 33 mmol, 98 %).

^{1}H NMR (400 MHz, $CDCl_3$) δ (ppm): 7.84 (m, 2H), 7.73 (m, 2H), 3.71 (t, *J* = 7.1 Hz, 2H), 1.70 (m, 1H), 1.49 (m, 3H), 1.32-1.06 (m, 6H), 0.97 (d, *J* = 6.3 Hz, 3H), 0.86 (d, *J* = 6.5 Hz, 2H);

^{13}C NMR (250 MHz, $CDCl_3$) δ (ppm): 168.5, 133.8, 132.2, 123.1, 39.2, 36.9, 36.4, 35.5, 30.7, 27.9, 24.6, 22.6, 22.6, 19.4;

Calculated elemental analysis (%): C, 75.22; H, 8.77; N, 4.87; O, 11.13. Found: C, 74.90; H, 8.17; N, 4.78;

EI-MS (*m/z*): [M^+] calculated: 287.19; found: 287.

6.3.23. Synthesis of 3,7-dimethyloctan-1-amine (24)[14]

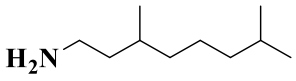

(24)

In a 250 ml, round-bottomed flask, a solution of N-(3,7-dimethyloctyl)phthalimide (8.32 g, 28.97 mmol), hydrazine monohydrate (64 %, 2.75 g, 68 mmol) and ethanol (90 ml) was prepared. The mixture was stirred under reflux for 2 hours. A large amount of white precipitate was formed in the flask. Upon completion, the mixture was cooled to room temperature, then concentrated hydrochloric acid (1 ml) was added and the mixture stirred for a further 15 mins. The precipitate was filtered and washed with ethanol. Sodium hydroxide (20%, 40 ml) was added to the filtrate to neutralise the reaction mixture. Then the amine was extracted with DCM (4 x150 ml) to yield a clear yellow oil (4.46 g, 28.37 mmol, 98 %). The crude was used without any further purification.

6.3.24. Synthesis of 3-ethyl-4-methyl-2-aminothiophene-3,4-dicarboxylate (25)[15]

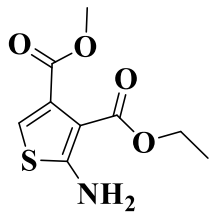

(25)

In a 500 ml, two-necked, round-bottomed flask, a solution of methyl pyruvate (24.33 g, 0.24 mol), ethyl cyanoacetate (24.85 g, 0.23 mol), and sulphur (8.50 g, 0.265 mol) in dry DMF (120 ml) was prepared. Then a solution of triethylamine (60 ml) in dry DMF (120 ml) was added slowly in a dropwise manner and the reactants stirred at room temperature. After addition, the reaction mixture was heated to 50 °C and left overnight. Upon completion, the mixture was cooled to room temperature and water (1000 ml) was added. The product was left for 72 hours to crystallise. The crystals were filtered off and washed with ice-cold water to obtain the product as ivory-coloured crystals (20 g, 0.087 mol, 36 %).

^{1}H NMR (400 MHz, $CDCl_3$) δ (ppm): 6.62 (s, 1H), 6.00 (s, br, 2H), 4.27 (q, *J* = 7.2 Hz, 2H), 3.85 (s, 3H), 1.32 (t, *J* = 7.1 Hz, 3H);

^{13}C NMR (250 MHz, $CDCl_3$) δ (ppm): 165.6, 164.6, 162.8, 132.5, 111.4, 105.0, 60.2, 52.2, 14.2;

Calculated elemental analysis (%): C, 47.15; H, 4.84; N, 6.11; O, 27.92; S, 13.98. Found: C, 47.16; H, 4.89; N, 6.03; S, 14.00;

EI-MS (*m/z*): [M^+] calculated: 229.04; found: 230;

M.P. 110-113 °C.

6.3.25. Synthesis of thiophene-3,4-dicarboxylic acid (26)[16]

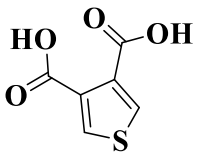

(26)

In a 1000 ml, two-necked, round-bottomed flask, a solution of 3-ethyl-4-methyl-2-aminothiophene-3,4-dicarboxylate (5 g,21.74 mmol) in dry THF (200 ml) was added slowly in a dropwise manner to boiling tert-butyl nitrite (2.38 g, 23.10 mmol) in dry THF (300 ml) under an argon atmosphere. After addition, the reaction mixture was left under reflux to stir for 3 hours. Upon completion, the reaction mixture was left to cool to room temperature, and then the solvent was removed *in vacuo*. A dark-brown oil was formed and purified by column chromatography using hexane:ethyl acetate (7:3) as an eluent. After that, the intermediate product was diluted in NaOH (2M, 100 ml) and stirred at 90 ^{o}C for 24 hours. After completion, the reaction mixture was cooled to room temperature and acidified to pH 1 by adding HCl. The product was extracted with diethyl ether (5 x 150 ml). The organic layers were combined, dried over $MgSO_4$ and at that point, the solvent was removed *in vacuo*. The product was obtained as off-white crystals (2.1 g, 12.21 mmol, 56 %).

^{1}H NMR (400 MHz, DMSO-d_6) δ (ppm): 8.17 (s, 2H);

^{13}C NMR (250 MHz, DMSO-d_6) δ (ppm): 164.9, 134.1, 133.9;

Calculated elemental analysis (%): C, 41.86; H, 2.34; 17; S, 18.62. Found: C, 41.86; H, 2.56; S, 18.77;

EI-MS (*m/z*): [M^+] calculated: 171.98; found: 171;

M.P. 227-230 °C.

6.3.26. Synthesis of 2,5-dibromothiophene-3,4-dicarboxylic acid (27)[17]

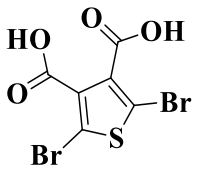

(27)

In a 250 ml, two-necked, round-bottomed flask, a solution of thiophene-3,4-dicarboxylic acid (7.0 g, 41 mmol) and glacial acetic acid (42 ml) was prepared. Bromine (8.5 ml, 163 mmol) was added dropwise at room temperature. The mixture was stirred and heated to 55 ^{o}C for 24 hours. Upon completion, the mixture was cooled to room temperature, and the excess of bromine was quenched with a saturated aqueous solution of $NaHSO_4$ until the mixture was colourless. The mixture was allowed to cool, and crystals precipitated out of solution. The crystals were filtered off and washed with ice-water to yield a beige powder (8.41 g, 25.5 mmol, 63 %).

^{13}C NMR (250 MHz, DMSO-d_6) δ (ppm): 163.0, 135.6, 114.9;

Calculated elemental analysis (%): C, 21.84; H, 0.61; Br, 48.43; S, 9.72. Found: C, 21.97; H, 0.80; Br, 48.67; S, 9.90;

EI-MS (*m/z*): [M^+] calculated: 329.80; found: 327, 329 and 331;

M.P. 236-239 °C.

6.3.27. Synthesis of 4,6-dibromothieno[3,4-c]furan-1,3-dione (28)[18]

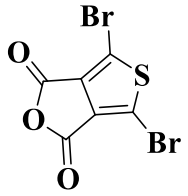

(28)

In a 250 ml, round-bottomed flask, a solution of 2,5-dibromothiophene-3,4-dicarboxylic acid (8.41 g, 25.5 mmol), and acetic anhydride (75 ml) was prepared. The mixture was degassed and placed under argon atmosphere to stir at 120 ^{o}C overnight. After completion, the reaction mixture was allowed to cool to room temperature in order to induce crystallisation. The crystals were filtered and washed with cold hexane to obtain off-white crystals (6.22 g, 12.1 mmol, 78 %).

^{13}C NMR (250 MHz, acetone-d_6) δ (ppm): 153.9, 133.8, 117.1;

Calculated elemental analysis (%): C, 23.10; Br, 51.23; S, 10.28. Found: C, 23.24; Br, 51.37; S, 10.37;

EI-MS (*m/z*): [M^+] calculated: 311.79; found: 309, 311 and 313;

M.P. 167-169 °C.

6.3.28. Synthesis of 1,3-dibromo-5-(3,7-dimethyloctyl)-4H-thieno[3,4-c]pyrrole-4,6(5H)-dione (29)[19]

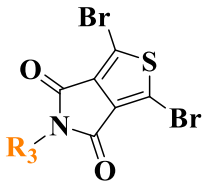

R_3 = 3,7-dimethyloctyl

(29)

In a 100 ml, round-bottomed flask, a solution of 4,6-dibromothieno[3,4-c]furan-1,3-dione (5 g, 16 mmol) and 3,7-dimethyloctamine (3.02 g, 19 mmol) in dry THF (30 ml) was prepared. The reaction mixture was heated to 55 ^oC for 3 hours. After that, the mixture was cooled to room temperature. Thionyl chloride (20 ml) was added dropwise. Upon completion, the reaction was heated up to 60^oC and left to stir overnight. The reaction was allowed to cool to room temperature, and then slowly poured into methanol: water (100 ml:50 ml). The white precipitate was filtered and purified *via* chromatography using PE: DCM (10:7) as the eluent to yield a white solid (4 g, 8.87 mmol, 55 %).

^{1}H NMR (400 MHz, $CDCl_3$) δ (ppm): 3.63 (t, *J* = 7.2 Hz, 2H), 1.61 (m, 1H), 1.55-1.42 (m, 3H), 1.33-1.12 (m, 6H), 0.97 (d, *J* = 6.3 Hz, 3H), 0.89 (d, *J* = 6.6 Hz, 6H);

^{13}C NMR (250 MHz, $CDCl_3$) δ (ppm): 160.4, 134.8, 112.9, 39.2, 37.1, 36.9, 35.2, 30.7, 27.9, 24.5, 22.7, 22.6, 19.4;

Calculated elemental analysis (%): C, 42.59; H, 4.69; Br, 35.42; N, 3.10; S, 7.11. Found: C, 42.25; H, 4.33; Br, 35.65; N, 3.00; S, 7.38;

EI-MS (*m/z*): [M^+] calculated: 450.96; found: 449, 451 and 453;

M.P. 106-110 °C.

6.3.29. Synthesis of 1,3-bis(thiophen-2-yl)-5-(3,7-dimethyloctyl)-4H-thieno[3,4-c]pyrrole-4,6(5H)-dione (30)[20,21]

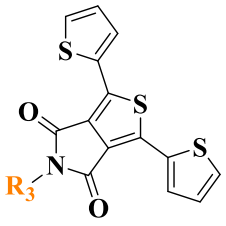

(30)

R_3 = 3,7-dimethyloctyl

A 100 ml, round-bottomed flask containing 1,3-dibromo-5-(3,7-dimethyloctyl)-4H-thieno[3,4-c]pyrrole-4,6(5H)-dione (1.34 g, 2.97 mmol), 2-(tributylstannyl)thiophene (4.43 g, 11.88 mmol), and bis(triphenylphosphine) palladium(II) dichloride (16 mg, 6 %) was degassed and placed under an argon atmosphere, then the mixture was dissolved into dry THF (150 ml). The solution was refluxed for 24 h. Upon completion, the reaction mixture was cooled to room temperature and poured into water. The mixture was extracted with DCM (5 x 100 ml). The organic phases were washed with brine (3 x 100 ml), dried over magnesium sulphate and then filtered. The solvent was removed under reduced pressure and the crude product was purified by column chromatography using petroleum ether: dichloromethane as eluent (10:8). This yielded the product as a bright yellow solid (1.18 g, 2.58 mmol, 87 %).

^{1}H NMR (400 MHz, $CDCl_3$) δ (ppm): 7.92 (d, *J*= 5.1 Hz, 2H); 7.34 (d, *J*= 5.1 Hz, 2H); 7.03 (t, *J* = 4.4 Hz, 2H); 3.59 (t, *J* = 6.9 Hz, 2H); 1.69 (m, 1H), 1.56-1.45 (m, 3H), 1.37-1.12 (m, 6H), 0.98 (d, *J* = 6.3 Hz, 3H), 0.87 (d, *J* = 6.7 Hz, 6H);

^{13}C NMR (250 MHz, $CDCl_3$) δ (ppm): 162.4, 136.4, 132.4, 129.8, 128.5, 128.4, 128.3, 39.3, 37.1, 36.7, 35.5, 30.9, 27.9, 24.6, 22.8, 22.7, 19.4;

Calculated elemental analysis (%): C, 62.99; H, 5.95; N, 3.06; S, 21.02. Found: C, 62.09; H, 5.86; N, 3.00; S, 20.98;

EI-MS (*m/z*): [M^+] calculated: 457.12; found: 457;

M.P. 109-113 °C.

6.3.30. Synthesis of 1,3-bis(5-bromo-thiophen-2-yl)-5-(3,7-dimethyloctyl)-4H-thieno[3,4-c]pyrrole-4,6(5H)-dione (31)[20]

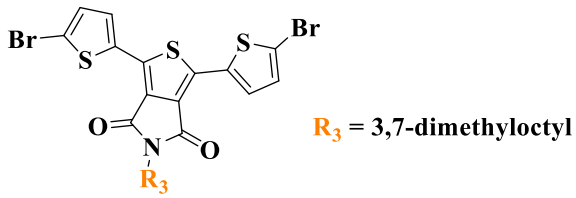

(31)

In a 100 ml, round-bottomed flask, a solution of 1,3-bis(thiophen-2-yl)-5-(3,7-dimethyloctyl)-4H-thieno[3,4-c]pyrrole-4,6(5H)-dione (1.07 g, 2.34 mmol) in chloroform (30 ml) and acetic acid (30 ml) was protected from light and cooled to 0˚C. N-bromosuccinimide (0.83 g, 4.68 mmol) was added in small portions, after which the solution was stirred for 15 minutes at 0˚C. Then the mixture was stirred for 18 hours at room temperature. Distilled water (150 ml) was added and the mixture was extracted with chloroform (5 x 100 ml), dried over magnesium sulphate, filtered and the solvent removed *in vacuo*. The crude was purified by column chromatography using petroleum ether: dichloromethane as an eluent (10:5), after which it was recrystallised in hexane to yield the product as a bright yellow solid (1.2 g, 1.99 mmol, 83%).

^{1}H NMR (400 MHz, $CDCl_3$) δ (ppm): 7.68 (d, *J*= 4.0 Hz, 2H); 7.10 (d, *J*= 4.0 Hz, 2H); 3.68 (t, *J* = 6.7 Hz, 2H); 1.70 (m, 1H), 1.55-1.48 (m, 3H), 1.36-1.14 (m, 6H), 0.99 (d, *J* = 6.2 Hz, 3H), 0.88 (d, *J* = 6.67 Hz, 6H);

^{13}C NMR (250 MHz, $CDCl_3$) δ (ppm): 162.4, 135.2, 133.7, 131.2, 130.0, 129.8, 128.7, 39.2, 37.0, 36.9, 35.4, 30.9, 27.9, 24.6, 22.7, 22.6, 19.4;

Calculated elemental analysis (%): C, 46.84; H, 4.09; Br, 25.97; N, 2.28; S, 15.63. Found: C, 46.76; H, 4.13; Br, 26.03; N, 2.16; S, 15.96;

EI-MS (*m/z*): [M^+] calculated: 614.94; found: 613, 615 and 617;

M.P. 130-133 °C.

6.3.31. Synthesis of 1,3-bis([2,2'-bithiophen]-5-yl)-5-(3,7-dimethyloctyl)-4H-thieno[3,4-c]pyrrole-4,6(5H)-dione (32)[20]

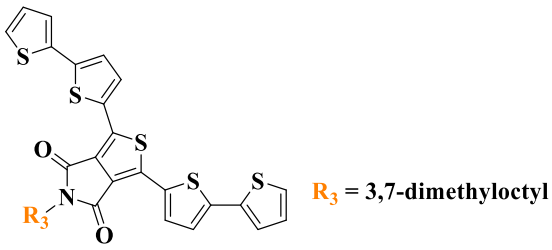

(32)

In a 100 ml, round-bottomed flask, 1,3-bis(5-bromo-thiophen-2-yl)-5-(3,7-dimethyloctyl)-4H-thieno[3,4-c]pyrrole-4,6(5H)-dione (0.50 g, 0.81 mmol), 2-(tributylstannyl)thiophene (1.21 g, 3.25 mmol), and bis(triphenylphosphine) palladium(II) dichloride (40 mg) were degassed and placed under an argon atmosphere, then dissolved into dry THF (36 ml). The solution was refluxed at 70˚C for 24 h. Upon completion, the reaction mixture was cooled to room temperature and poured into water. The mixture was extracted with DCM (4 x 150 ml). The organic phases were combined and washed with brine (3 x 100 ml), dried over magnesium sulphate and filtered. The solvent was removed under reduced pressure and the crude product was purified by column chromatography using petroleum ether: dichloromethane as eluent (10:5) to yield the product as a dark-red solid (0.32 g, 0.52 mmol, 64 %).

^{1}H NMR (400 MHz, $CDCl_3$) δ (ppm): 7.78 (d, *J*= 3.9 Hz, 2H); 7.22 (d, *J*= 5.1 Hz, 2H); 7.16 (d, *J*= 3.6 Hz, 2H); 7.03 (m, 4H); 3.58 (m, 2H); 1.68 (m, 1H), 1.59-1.47 (m, 3H), 1.41-1.14 (m, 6H), 0.99 (d, *J* = 6.2 Hz, 3H), 0.89 (d, *J* = 6.6 Hz, 6H);

^{13}C NMR (250 MHz, $CDCl_3$) δ (ppm): 162.2, 140.6, 136.4, 135.5, 130.9, 130.7, 128.2, 128.0, 125.5, 124.7, 124.5, 39.2, 37.1, 36.9, 35.5, 30.9, 27.9, 24.7, 22.7, 22.6, 19.4;

Calculated elemental analysis (%): C, 61.80; H, 5.02; N, 2.25; S, 25.78. Found: C, 60.98; H, 4.98; N, 2.13; S, 24.88;

EI-MS (*m/z*): [M^+] calculated: 621.10; found: 621;

M.P. 139-143 °C.

6.3.32. Synthesis of 1,3-bis(5'-bromo-[2,2'-bithiophen]-5-yl)-5-(3,7-dimethyloctyl)-4H-thieno[3,4-c]pyrrole-4,6(5H)-dione (33)[20]

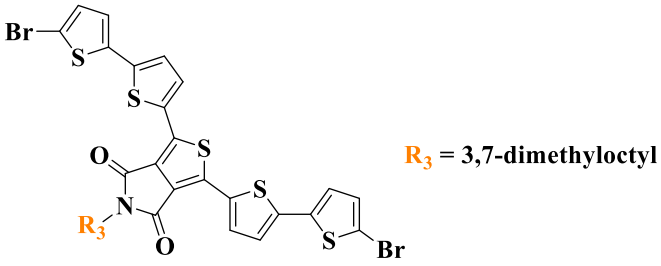

(33)

In a 100 ml, round-bottomed flask protected from light, a solution of 1,3-bis([2,2'-bithiophen]-5-yl)-5-(3,7-dimethyloctyl)-4H-thieno[3,4-c]pyrrole-4,6(5H)-dione (1.00 g, 1.61 mmol) in chloroform (10 ml) and acetic acid (10 ml) was prepared. N-bromosuccinimide (0.57 g, 3.22 mmol) was added in small portions. Then the mixture was stirred for 2 hours at room temperature. Distilled water (100 ml) was added and the mixture was extracted with chloroform (4 x 150 ml), dried over magnesium sulphate, filtered and the solvent removed *in vacuo*. The crude was purified by column chromatography using petroleum ether: dichloromethane as an eluent (10:5) to yield the product as dark-red crystals (1.12 g, 1.44 mmol, 89%);

^{1}H NMR (400 MHz, $CDCl_3$) δ (ppm): 7.81 (d, *J*= 3.9 Hz, 2H); 7.00 (d, *J*= 3.9 Hz, 2H); 6.96 (m, 4H); 3.64 (m, 2H); 1.72 (m, 1H), 1.58-1.49 (m, 3H), 1.39-1.14 (m, 6H), 1.00 (d, *J* = 6.3 Hz, 3H), 0.89 (d, *J* = 6.5 Hz, 6H);

^{13}C NMR (250 MHz, $CDCl_3$) δ (ppm): 162.3, 139.5, 137.8, 135.5, 131.2, 130.9, 130.7, 128.6, 127.5, 124.8, 124.7, 39.3, 37.1, 36.9, 35.5, 30.9, 27.9, 24.7, 22.7, 22.6, 19.4;

Calculated elemental analysis (%): C, C, 49.30; H, 3.75; Br, 20.50; N, 1.80; O, 4.10; S, 20.56. Found: C, 48.96; H, 3.84; Br, 20.59; N, 1.77; S, 20.39;

EI-MS (*m/z*): [M^+] calculated: 778.91; found: 777, 779 and 781;

M.P. 159-164 °C.

6.3.33. 4,7-di(5-bromo-thien-2-yl)-2,1,3-benzothiadiazole-5,6-N-octyl-dicarboxylic imide (A)

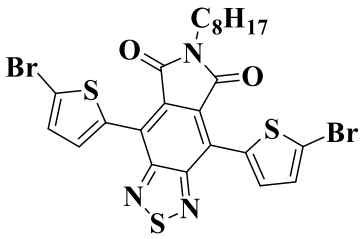

(A)

Prepared by A. Murad in Iraqi's group at the University of Sheffield.

6.4. Preparation of the Polymers

6.4.1. Poly [11,12-bis-(2-hexyl-decyloxy)-phenanthro[9,10-b]quinoxaline-(2,7-di-yl)-alt-(2,3-Bis(3-(octyloxy)phenyl)-6,7-difluoro-5,8-bis(2-thienyl)quinoxaline)-5,5-(di-yl)] (P1)[22]

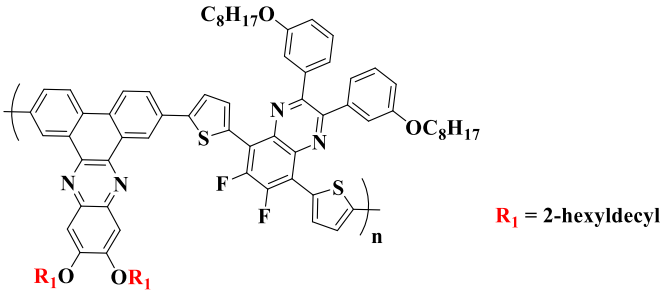

R_1 = 2-hexyldecyl

P1

In a 25 ml, round-bottomed flask, a mixture of **(9)** (0.100 g, 0.112 mmol) and **(16)** (0.113 g, 0.112 mmol), $Pd(AcO)_2$, (2 mg, 0.01 mmol) and tri(o-tolyl)phosphine (6 mg, 0.02 mmol) was prepared. The reaction mixture was degassed and placed under argon atmosphere. Then, a saturated aqueous solution of sodium hydrogen carbonate (2.5 ml), which had been previously degassed and bubbled with argon for 3 hours, was added. After that, dry THF (3 ml) was added to the mixture. The reaction mixture was stirred at room temperature for 10 mins and then refluxed at 80 °C for 24 hours under argon atmosphere. The mixture was cooled to room temperature and bromobenzene (0.10 ml, 0.95 mmol) was added. It was then degassed and refluxed at 90 °C for 2 hours. The mixture was cooled to room temperature again and phenylboronic acid (0.12 g, 0.98 mmol) was added. The mixture was then degassed and refluxed at 90 °C for a further 2 hours. Upon completion, the reaction mixture was allowed to cool to room temperature, and chloroform (200 ml) was added to dissolve the polymer. Ammonium hydroxide solution (50 ml, 30-33 wt. % in H_2O) was added, and the

mixture was stirred vigorously at room temperature and left overnight. The organic layer was separated and then washed with distilled water (4 × 100 ml). It was then concentrated to about 50 ml and precipitated in methanol (200 ml). The mixture was stirred at room temperature overnight and filtered through a membrane filter. The collected solid was purified by Soxhlet extraction in the following order of solvents: with methanol (200 ml, for 12 hours); with acetone (200 ml, for 12 hours); with hexane (200 ml, 24 hours); and with chloroform (200 ml, 12 hours). The toluene fraction was collected and concentrated to about 50 ml. Then it was precipitated in methanol (200 ml). The mixture was stirred at room temperature overnight and filtered through a membrane filter. A dark-purple solid was collected and dried under *vacuum* to give the product (0.102 g, 61 %).

GPC (Toluene fraction): Mw = 21,300 g mol^{-1}, Mn = 9,900 g mol^{-1}, PDI = 2.14.

Calculated elemental analysis (%): C, 77.12; H, 8.32; N, 3.67; S, 4.20. Found: C, 77.69; H, 8.03; N, 3.45; S, 4.18;

6.4.2. Poly[9,10-bis-(2-butyl-octyloxy)-2,7-phenanthrene-alt-[2,3-Bis(3-(octyloxy)phenyl)-6,7-difluoro-5,8-bis(2-thienyl)quinoxaline]-5,5-(di-yl)] (P2)[22]

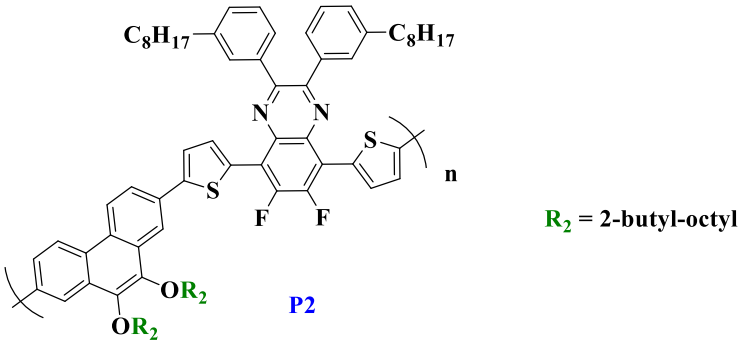

P2 was copolymerised according to the same procedure outlined in **P1**, by using a mixture of **(9)** (0.100 g, 0.112 mmol) and **(19)** (0.090 g, 0.112 mmol) for 24h to give **P2** as a deep-red solid (0.096 g, 69 %).

GPC (toluene fraction): Mw = 33,000 g mol^{-1}, Mn = 16,000 g mol^{-1}, PDI = 2.06;

Calculated elemental analysis (%): C, 78.83; H, 8.51; F, 2.97; N, 2.19; O, 2.50; S, 5.01. Found: C, 78.81; H, 8.29; N, 1.92; S, 4.97.

6.4.3. Poly[[11,12-bis-(2-hexyl-decyloxy)-phenanthro[9,10-b]quinoxaline]-(2,7-di-yl)-alt-[2,3-Bis(3-(octyloxy)phenyl)-6,7-difluoro-5,8-bis-(2,2'-bithiophene)-5-yl)quinoxaline]-5,5-(di-yl)] (P3)[22]

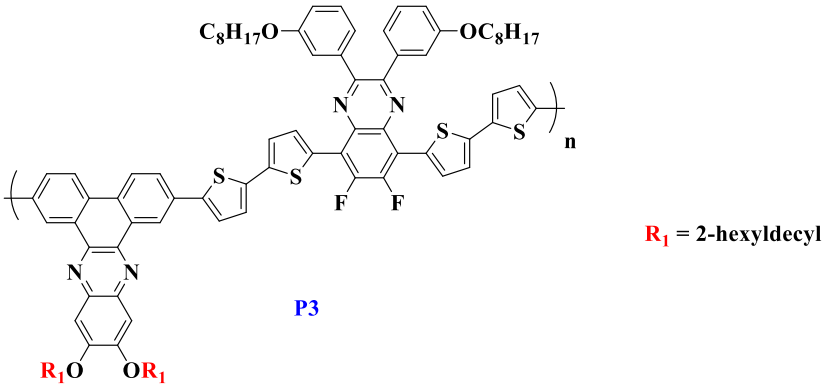

P3

P3 was copolymerised according to the procedure outlined for **P1**, by using a mixture of **(21)** (0.100 g, 0.094 mmol) and **(16)** (0.096 g, 0.094 mmol) for 72h to give **P3** as a deep-red solid (0.146 g, 93 %).

GPC (chloroform fraction): Mw = 21,500 g mol^{-1}, Mn = 8,200 g mol^{-1}, PDI = 2.59;

Calculated elemental analysis (%): C, 75.31; H, 7.75; N, 3.31; S, 7.59. Found: C, 74.81; H, 7.15; N, 3.35; S, 7.30.

6.4.4. Poly[9,10-bis-(2-butyl-octyloxy)-2,7-phenanthrene-alt-[2,3-Bis(3-(octyloxy)phenyl)-6,7-difluoro-5,8-bis-(2,2'-bithiophene)-5-yl)quinoxaline]-5,5-(di-yl)] (P4)[22]

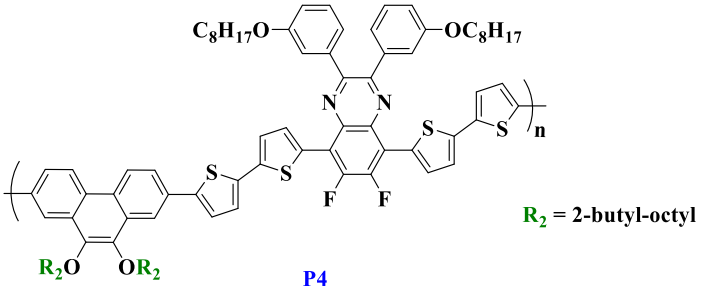

P4

P4 was copolymerised according to the same procedure as that outlined to produce **P1**, by using a mixture of **(21)** (0.100 g, 0.112 mmol) and **(19)** (0.090 g, 0.112 mmol) for 72h to give **P4** as a deep-red solid (0.146 g, 77 % yield).

GPC (chloroform fraction): Mw = 25,600 g mol^{-1}, Mn = 8,600 g mol^{-1}, PDI = 2.97;

Calculated elemental analysis (%): C, 74.86; H, 7.65; N, 1.90; S, 8.69. Found: C, 73.90; H, 7.32; N, 1.73; S, 8.13.

6.4.5. Poly[[11,12-bis-(2-hexyl-decyloxy)-phenanthro[9,10-b]quinoxaline]-(2,7-di-yl)-alt-[1,3-bis(thiophen-2-yl)-5-(3,7-dimethyloctyl)-4H-thieno[3,4-c]pyrrole-4,6(5H)-dione]-5,5-(di-yl)] (P5)[22]

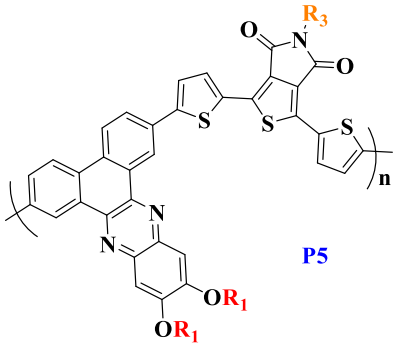

P5

R_3 = 3,7-dimethyloctyl

R_1 = 2-hexyldecyl

P5 was copolymerised according to the procedure outlined for **P1**, by using a mixture of **(31)** (0.061 g, 0.1 mmol) and **(16)** (0.100 g, 0.1 mmol) for 72h to give **P5** as a black solid (0.87 g, 88 % yield).

GPC (chloroform fraction): Mw = 12,300 g mol^{-1}, Mn = 7,200 g mol^{-1}, PDI = 1.71

Calculated elemental analysis (%): C, 75.26; H, 8.50; N, 3.38; S, 7.73. Found: C, 75.14; H, 7.81; N, 3.36; S, 7.53.

6.4.6. Poly[9,10-bis(2-butyl-octyloxy)-2,7-phenanthrene-alt-[1,3-bis(thiophen-2-yl)-5-(3,7-dimethyloctyl)-4H-thieno[3,4-c]pyrrole-4,6(5H)-dione]-5,5-(di-yl)] (P6)[22]

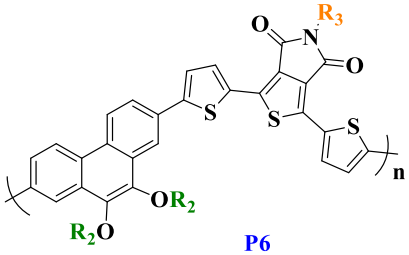

P6

R_3 = 3,7-dimethyloctyl

R_2 = 2-butyl-octyl

P6 was copolymerised according to the procedure outlined for **P1**, by using a mixture of **(31)** (0.077 g, 0.125 mmol) and **(19)** (0.100 g, 0.125 mmol) for 72h to give **P6** as a black solid (0.100 g, 84 % yield).

GPC (chloroform fraction): Mw = 26,200 g mol^{-1}, Mn = 9,700 g mol^{-1}, PDI = 2.68;

Calculated elemental analysis (%): C, 74.59; H, 8.51; N, 1.36; O, 6.21; S, 9.33. Found: C, 73.89; H, 8.01; N, 1.28; O, 6.21; S, 9.23.

6.4.7. Poly[[11,12-bis-(2-hexyl-decyloxy)-phenanthro[9,10-b]quinoxaline]-(2,7-di-yl)-alt-[1,3-bis([2,2'-bithiophen]-5-yl)-5-(3,7-dimethyloctyl)-4H-thieno[3,4-c]pyrrole-4,6(5H)-dione]-5,5-(di-yl)] (P7)[22]

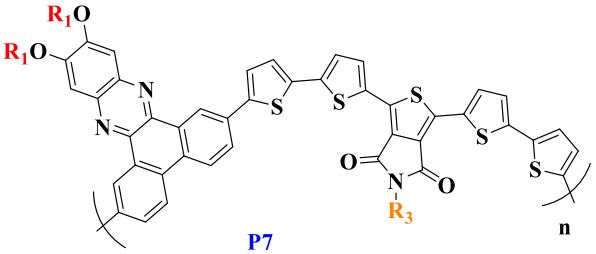

P7

R_1 = 2-hexyldecyl

R_3 = 3,7-dimethyloctyl

P7 was copolymerised according to the procedure outlined for **P1**, by using a mixture of **(33)** (0.077 g, 0.098 mmol) and **(16)** (0.100 g, 0.098 mmol) for 24h to give **P7** as a dark red solid (0.067 g, 80 % yield).

GPC (chloroform fraction): Mw = 49,700 g mol^{-1}, Mn = 43,500 g mol^{-1}, PDI = 1.14;

Calculated elemental analysis (%): C, 73.30; H, 7.80; N, 2.98; S, 11.38. Found: C, 72.68; H, 7.50; N, 2.88; S, 11.08.

6.4.8. Poly[9,10-bis(2-butyl-octyloxy)-2,7-phenanthrene-alt-[1,3-bis([2,2'-bithiophen]-5-yl)-5-(3,7-dimethyloctyl)-4H-thieno[3,4-c]pyrrole-4,6(5H)-dione]-5,5-(di-yl)] (P8)[22]

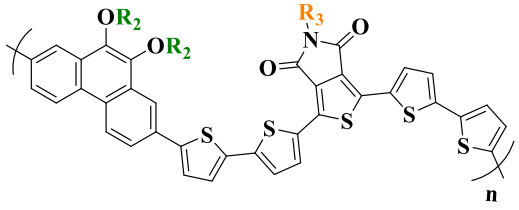

P8

R_2 = 2-butyl-octyl

R_3 = 3,7-dimethyloctyl

P8 was copolymerised according to the procedure outlined for **P1**, by using a mixture of **(33)** (0.077 g, 0.125 mmol) and **(19)** (0.100 g, 0.125 mmol) for 24h to give **P8** as a dark purple solid (0.060 g, 67 % yield).

GPC (chloroform fraction): Mw = 17,200 g mol^{-1}, Mn = 11,800 g mol^{-1}, PDI = 1.46;

Calculated elemental analysis (%): C, 72.38; H, 7.68; N, 1.17; S, 13.42. Found: C, 72.05; H, 7.67; N, 1.10; S, 13.52.

6.4.9. Poly[[11,12-bis-(2-hexyl-decyloxy)-phenanthro[9,10-b]quinoxaline]-(2,7-di-yl)-alt-[4',7'-bis(2-thienyl)-2',1',3'-benzothiadiazole-5,6-N-octyl-dicarboxylic imide]-5,5-(di-yl)] (P9)[22]

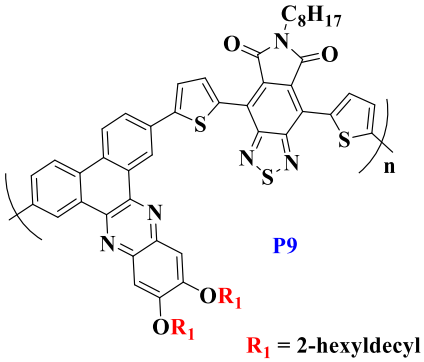

P9

R_1 = 2-hexyldecyl

P9 was copolymerised according to the procedure outlined for **P1**, by using a mixture of **(A)** (0.063 g, 0.099 mmol) and **(16)** (0.100 g, 0.099 mmol) for 48h to give **P9** as a dark-red solid (0.109 g, 71 % yield).

GPC (chloroform fraction): Mw = 15,700 g mol^{-1}, Mn = 8,800 g mol^{-1}, PDI = 1.79;

Calculated elemental analysis (%): C, 73.83; H, 8.02; N, 5.52; S, 7.58. Found: C, 73.33; H, 7.93; N, 5.40; S, 7.59.

6.4.9. Poly[9,10-bis(2-butyl-octyloxy)-2,7-phenanthrene–alt-[4',7'-bis(2-thienyl)-2',1',3'-benzothiadiazole-5,6-N-octyl-dicarboxylic-imide]-5,5-(di-yl)] (P10)[22]

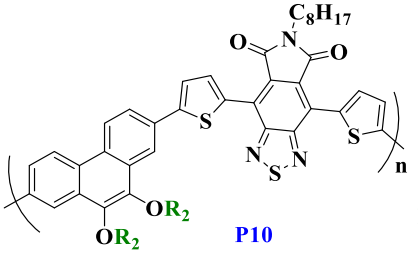

P10

R_2 = 2-butyl-octyl

P10 was copolymerised according to the procedure outlined for **P1**, by using a mixture of **(A)** (0.080 g, 0.125 mmol) and **(19)** (0.100 g, 0.125 mmol) for 48h to give **P10** as a dark purple solid (0.080 g, 74 % yield).

GPC (chloroform fraction): Mw = 79,700 g mol^{-1}, Mn = 23,000 g mol^{-1}, PDI = 3.46;

Calculated elemental analysis (%): C, 72.89; H, 7.93; N, 3.98; S, 9.12. Found: C, 72.12; H, 7.56; N, 3.82; S, 9.00.

6.5. Reference

(1) Mueller-Westerhoff, U. T.; Zhou, M. J. T. J. o. O. C. Synthesis of symmetrically and unsymmetrically substituted. alpha.-diones from organometallic reagents and 1, 4-dialkylpiperazine-2, 3-diones. 1994, *59* (17), 4988.

(2) Wakioka, M.; Ikegami, M.; Ozawa, F. J. M. Stereocontrolled synthesis and photoisomerization behavior of all-cis and all-trans poly (m-phenylenevinylene) s. 2010, *43* (17), 6980.

(3) Park, S. M.; Yoon, Y.; Jeon, C. W.; Kim, H.; Ko, M. J.; Lee, D. K.; Kim, J. Y.; Son, H. J.; Kwon, S. K.; Kim, Y. H. J. J. o. P. S. P. A. P. C. Synthesis of phenanthro [1, 10, 9, 8-cdefg] carbazole-based conjugated polymers for organic solar cell applications. 2014, *52* (6), 796.

(4) Wang, N.; Chen, Z.; Wei, W.; Jiang, Z. J. J. o. t. A. C. S. Fluorinated benzothiadiazole-based conjugated polymers for high-performance polymer solar cells without any processing additives or post-treatments. 2013, *135* (45), 17060.

(5) Cho, N.; Song, K.; Lee, J. K.; Ko, J. J. C. A. E. J. Facile Synthesis of Fluorine-Substituted Benzothiadiazole-Based Organic Semiconductors and Their Use in Solution-Processed Small-Molecule Organic Solar Cells. 2012, *18* (36), 11433.

(6) Kitamura, C.; Tanaka, S.; Yamashita, Y. J. C. o. M. Design of narrow-bandgap polymers. Syntheses and properties of monomers and polymers containing aromatic-donor and o-quinoid-acceptor units. 1996, *8* (2), 570.

(7) Unver, E. K.; Tarkuc, S.; Udum, Y. A.; Tanyeli, C.; Toppare, L. J. J. o. P. S. P. A. P. C. Effect of conjugated core building block dibenzo [a, c] phenazine unit on π-conjugated electrochromic polymers: Red-shifted absorption. 2010, *48* (8), 1714.

(8) Wiley, G.; Hershkowitz, R.; Rein, B.; Chung, B. J. J. o. t. A. C. S. Studies in organophosphorus chemistry. I. Conversion of alcohols and phenols to halides by tertiary phosphine dihalides. 1964, *86* (5), 964.

(9) Helgesen, M.; Gevorgyan, S. A.; Krebs, F. C.; Janssen, R. A. J. C. o. M. Substituted 2, 1, 3-benzothiadiazole-and thiophene-based polymers for solar cells− Introducing a new thermocleavable precursor. 2009, *21* (19), 4669.

(10) Sharma, U.; Kumar, P.; Kumar, N.; Kumar, V.; Singh, B. J. A. S.; Catalysis. Highly Chemo-and Regioselective Reduction of Aromatic Nitro Compounds Catalyzed by Recyclable Copper (II) as well as Cobalt (II) Phthalocyanines. 2010, *352* (11-12), 1834.

(11) Robinson, R. S.; Taylor, R. J. J. S. Quinoxaline synthesis from α-hydroxy ketones via a tandem oxidation process using catalysed aerobic oxidation. 2005, *2005* (06), 1003.

(12) Ishiyama, T.; Ishida, K.; Miyaura, N. J. T. Synthesis of pinacol arylboronates via cross-coupling reaction of bis (pinacolato) diboron with chloroarenes catalyzed by palladium (0)–tricyclohexylphosphine complexes. 2001, *57* (49), 9813.

(13) Chen, Z.; Cai, P.; Zhang, L.; Zhu, Y.; Xu, X.; Sun, J.; Huang, J.; Liu, X.; Chen, J.; Chen, H. J. J. o. P. S. P. A. P. C. Donor–acceptor copolymers based on phenanthrene as electron-donating unit: Synthesis and photovoltaic performances. 2013, *51* (23), 4966.

(14) Liu, S.; Kan, Z.; Thomas, S.; Cruciani, F.; Brédas, J. L.; Beaujuge, P. M. J. A. C. I. E. Thieno [3, 4-c] pyrrole-4, 6-dione-3, 4-difluorothiophene Polymer Acceptors for Efficient All-Polymer Bulk Heterojunction Solar Cells. 2016, *55* (42), 12996.

(15) Berrouard, P.; Grenier, F. o.; Pouliot, J.-R.; Gagnon, E.; Tessier, C.; Leclerc, M. J. O. l. Synthesis and characterization of 5-octylthieno [3, 4-c] pyrrole-4, 6-dione derivatives as new monomers for conjugated copolymers. 2010, *13* (1), 38.

(16) Berrouard, P.; Dufresne, S. p.; Pron, A.; Veilleux, J.; Leclerc, M. J. T. J. o. o. c. Low-cost synthesis and physical characterization of thieno [3, 4-c] pyrrole-4, 6-dione-based polymers. 2012, *77* (18), 8167.
(17) Cui, C.; Fan, H.; Guo, X.; Zhang, M.; He, Y.; Zhan, X.; Li, Y. J. P. C. Synthesis and photovoltaic properties of D–A copolymers of benzodithiophene and naphtho [2, 3-c] thiophene-4, 9-dione. 2012, *3* (1), 99.
(18) Cornelis, D.; Peeters, H.; Zrig, S.; Andrioletti, B.; Rose, E.; Verbiest, T.; Koeckelberghs, G. J. C. o. M. A chiroptical study of chiral Λ-and X-type oligothiophenes toward modelling the interchain interactions of chiral conjugated polymers. 2008, *20* (6), 2133.
(19) Piliego, C.; Holcombe, T. W.; Douglas, J. D.; Woo, C. H.; Beaujuge, P. M.; Fréchet, J. M. J. J. o. t. A. C. S. Synthetic control of structural order in N-alkylthieno [3, 4-c] pyrrole-4, 6-dione-based polymers for efficient solar cells. 2010, *132* (22), 7595.
(20) Liu, S.; Bao, X.; Li, W.; Wu, K.; Xie, G.; Yang, R.; Yang, C. J. M. Benzo [1, 2-b: 4, 5-b′] dithiophene and thieno [3, 4-c] pyrrole-4, 6-dione based donor-π-acceptor conjugated polymers for high performance solar cells by rational structure modulation. 2015, *48* (9), 2948.
(21) Zhou, E.; Yamakawa, S.; Zhang, Y.; Tajima, K.; Yang, C.; Hashimoto, K. J. J. o. M. C. Indolo [3, 2-b] carbazole-based alternating donor–acceptor copolymers: synthesis, properties and photovoltaic application. 2009, *19* (41), 7730.
(22) Yi, H.; Al-Faifi, S.; Iraqi, A.; Watters, D. C.; Kingsley, J.; Lidzey, D. G. J. J. o. M. C. Carbazole and thienyl benzo [1, 2, 5] thiadiazole based polymers with improved open circuit voltages and processability for application in solar cells. 2011, *21* (35), 13649.

Chapter 7: Supplementary Information

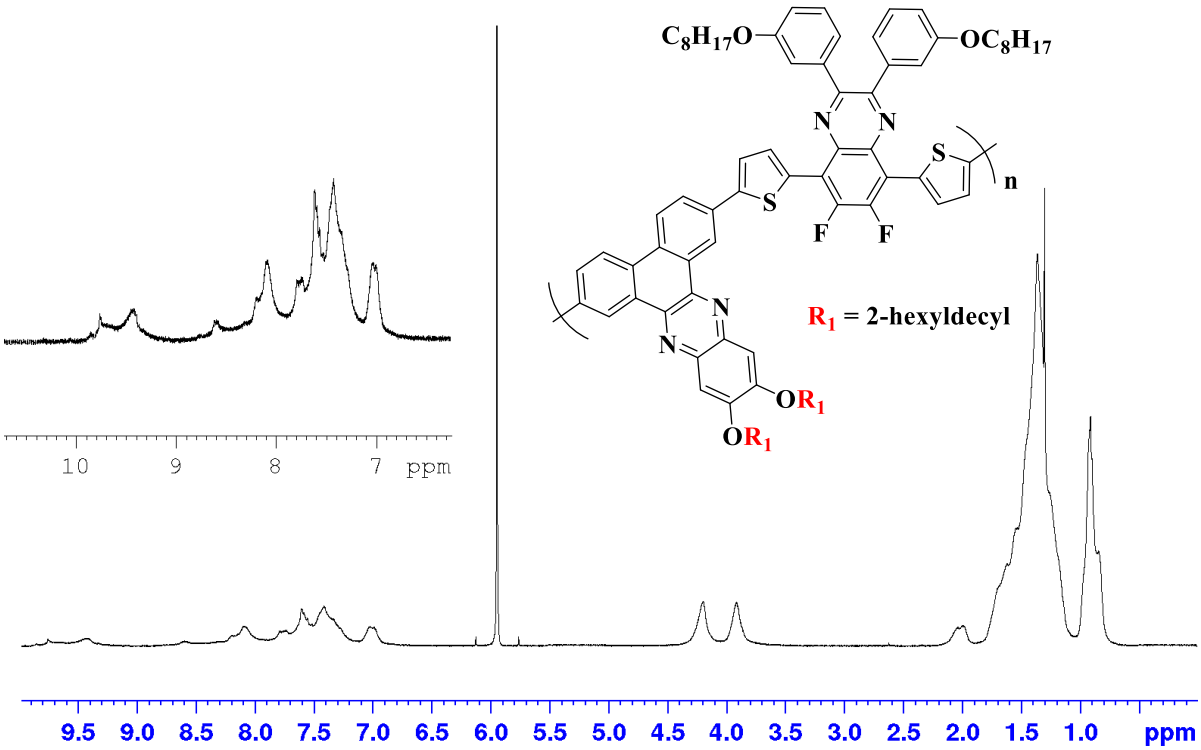

Figure S.1. ^{1}H NMR spectrum of P1 in $C_2D_2Cl_4$ at 100 °C.

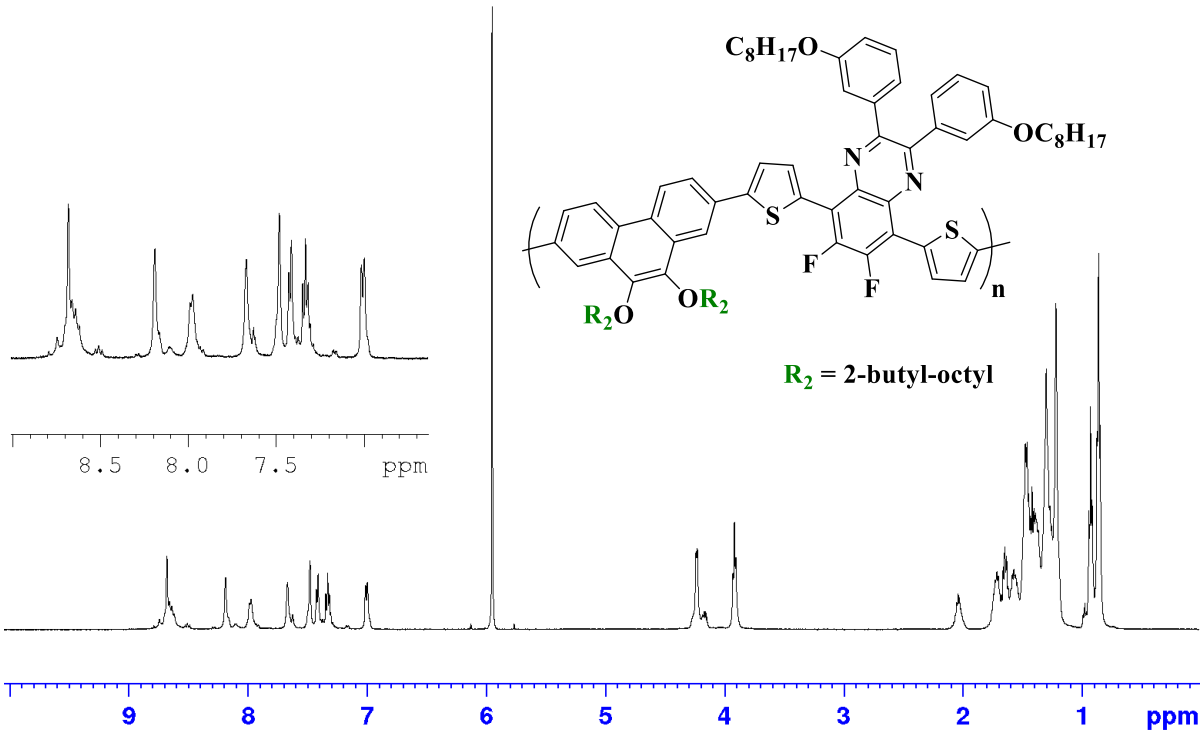

Figure S.2. ^{1}H NMR spectrum of P2 in $C_2D_2Cl_4$ at 100 °C.

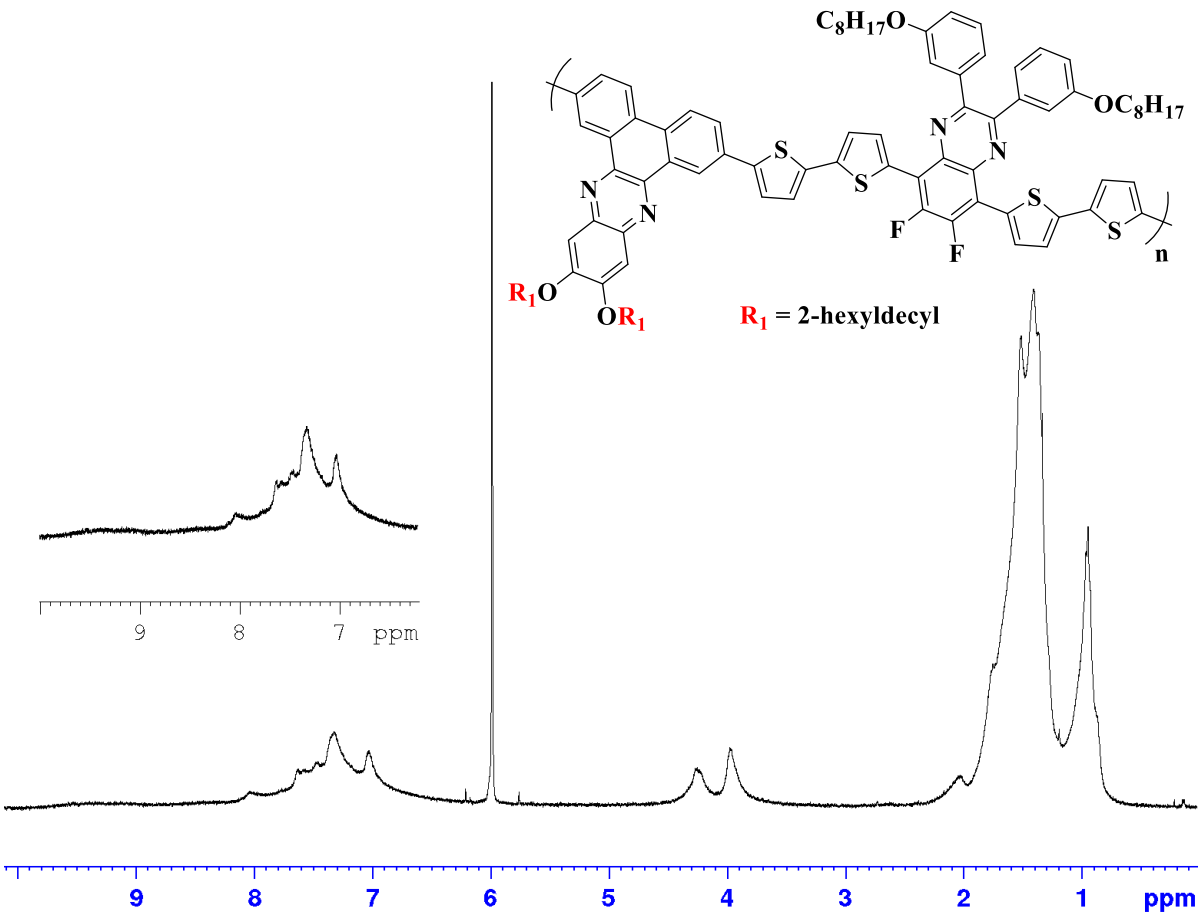

Figure S.3. ^{1}H NMR spectrum of P3 in $C_2D_2Cl_4$ at 100 °C.

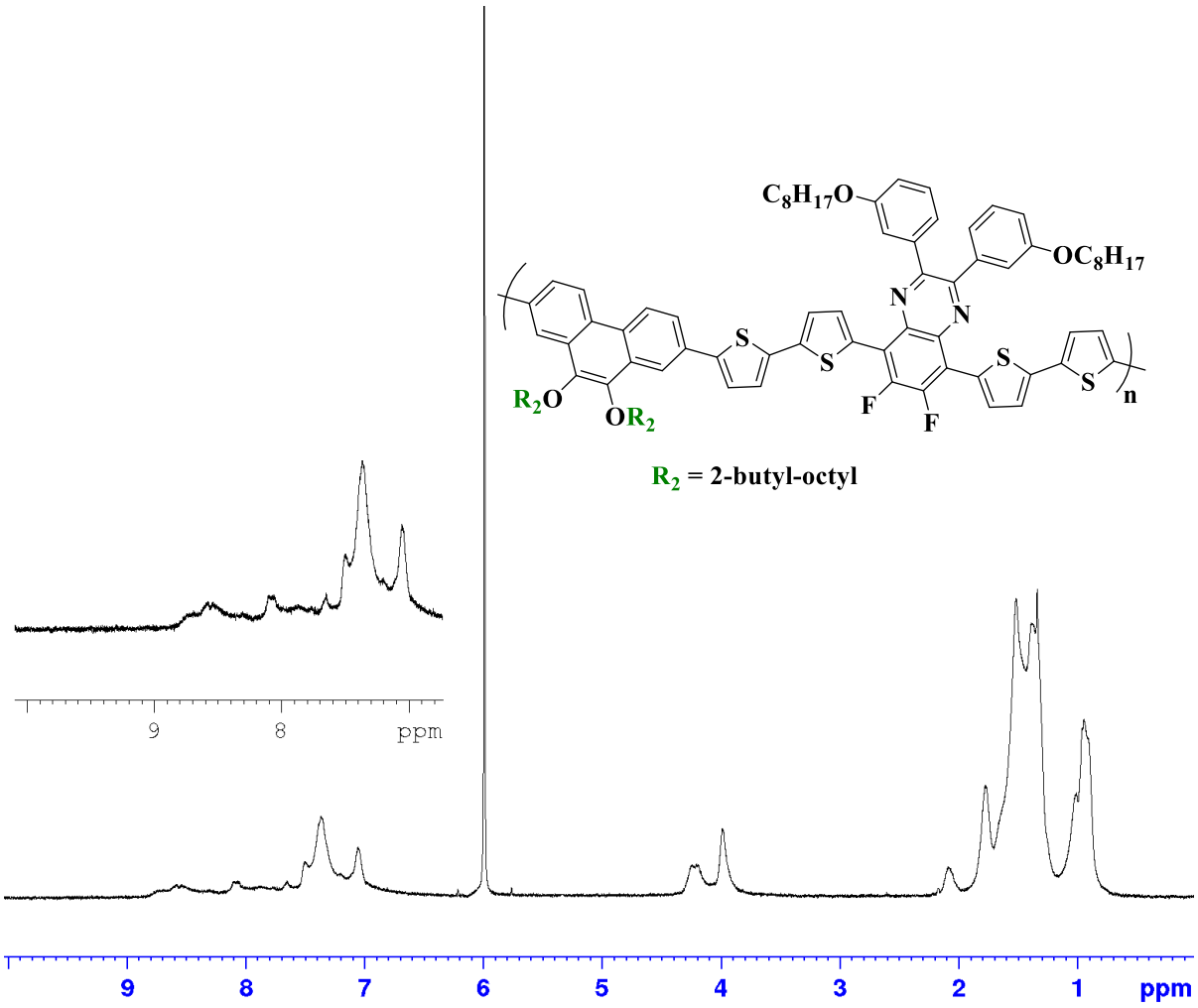

Figure S.4. ^{1}H NMR spectrum of P4 in $C_2D_2Cl_4$ at 100 °C.

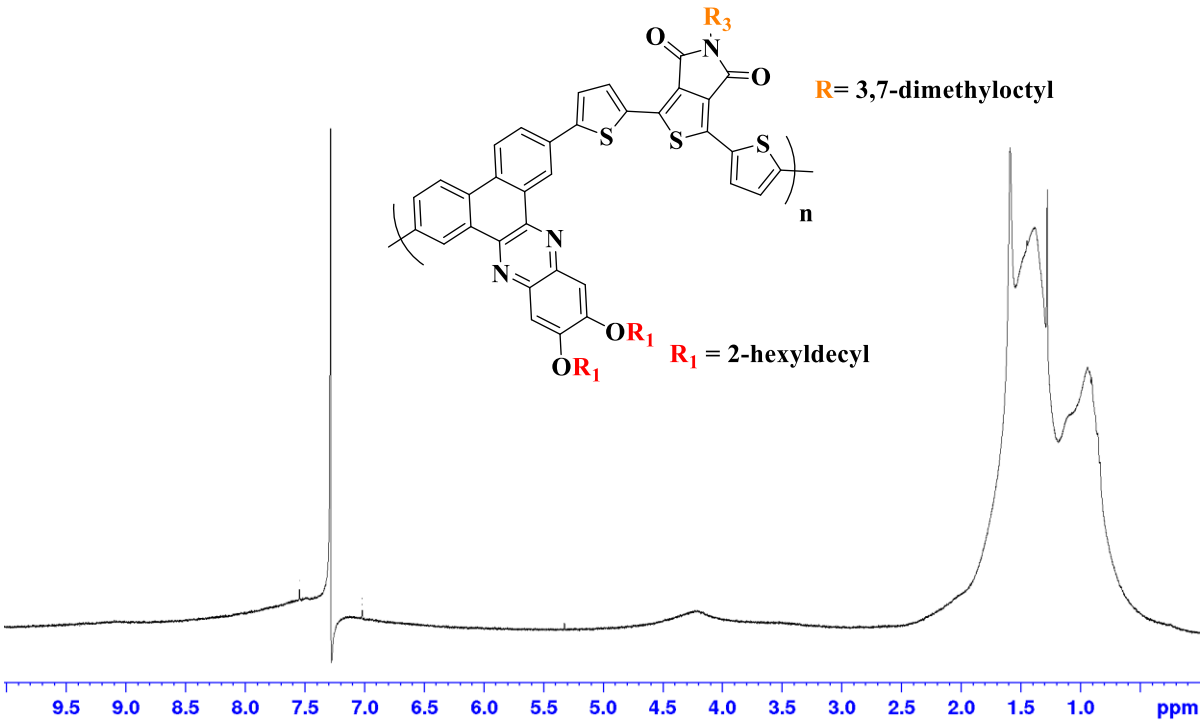

Figure S.5. ^{1}H NMR spectrum of P5 in $CDCl_3$ at RT.

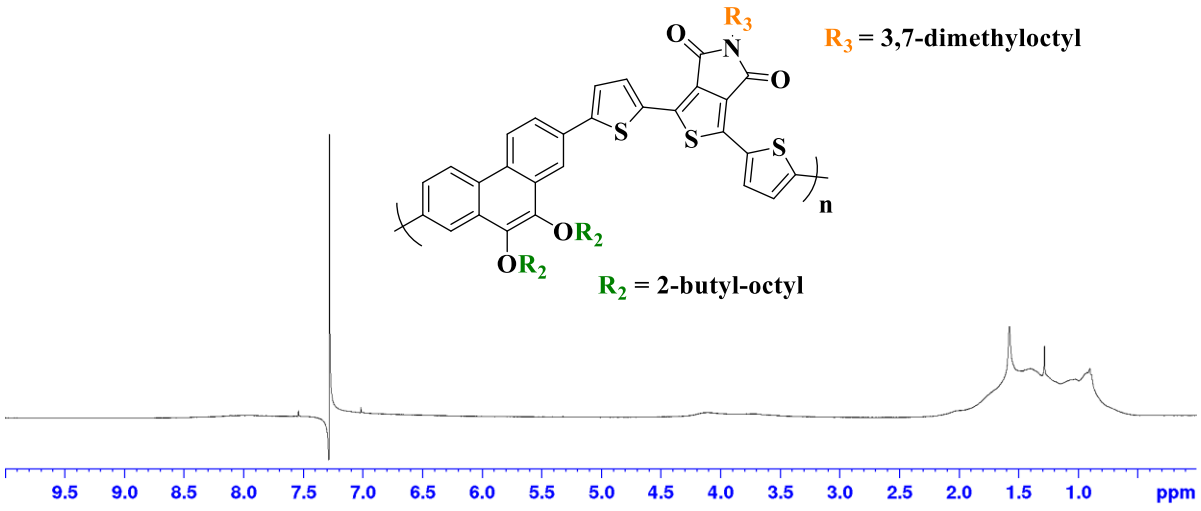

Figure S.6. ^{1}H NMR spectrum of P6 in $CDCl_3$ at RT.

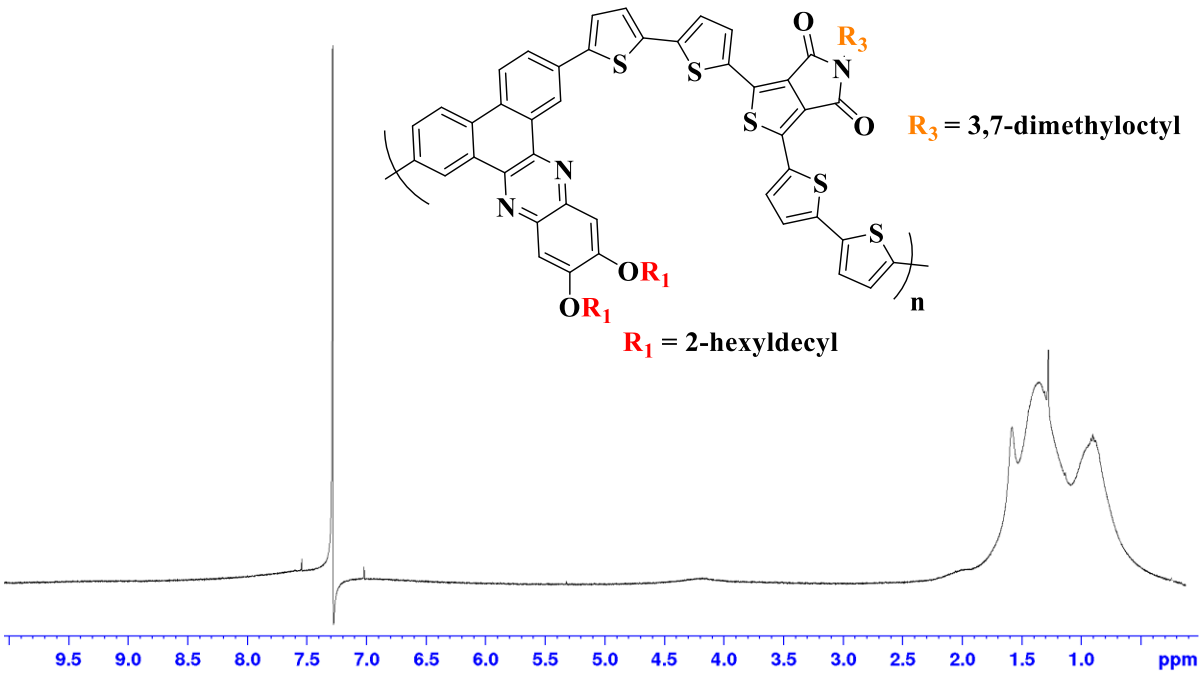

Figure S.7. ^{1}H NMR spectrum of P7 in in $CDCl_3$ at RT.

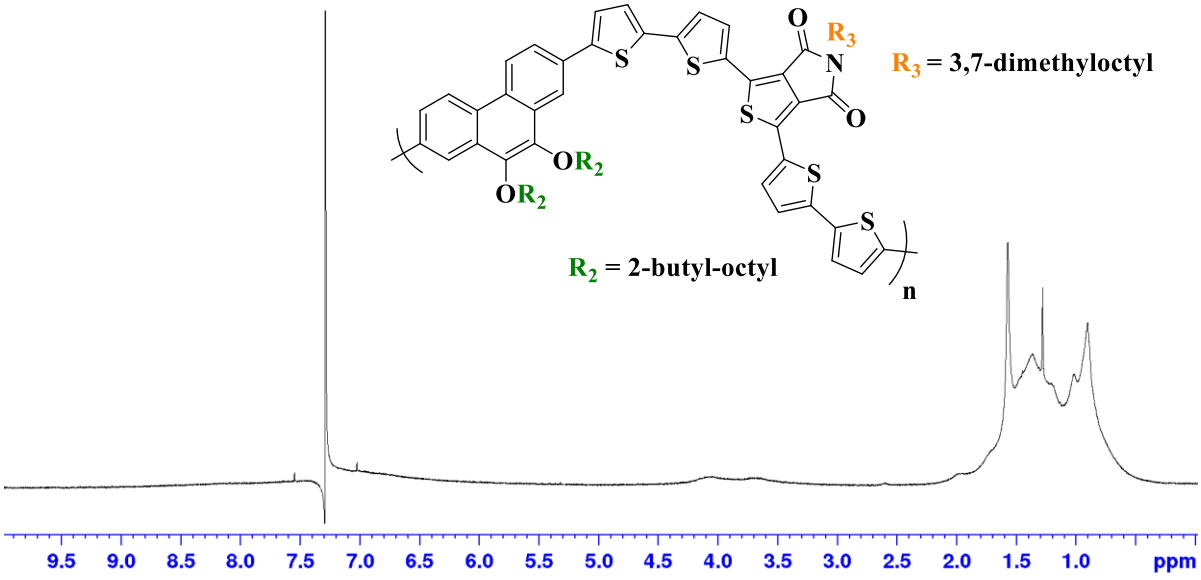

Figure S.8. ^{1}H NMR spectrum of P8 in in $CDCl_3$ at RT.

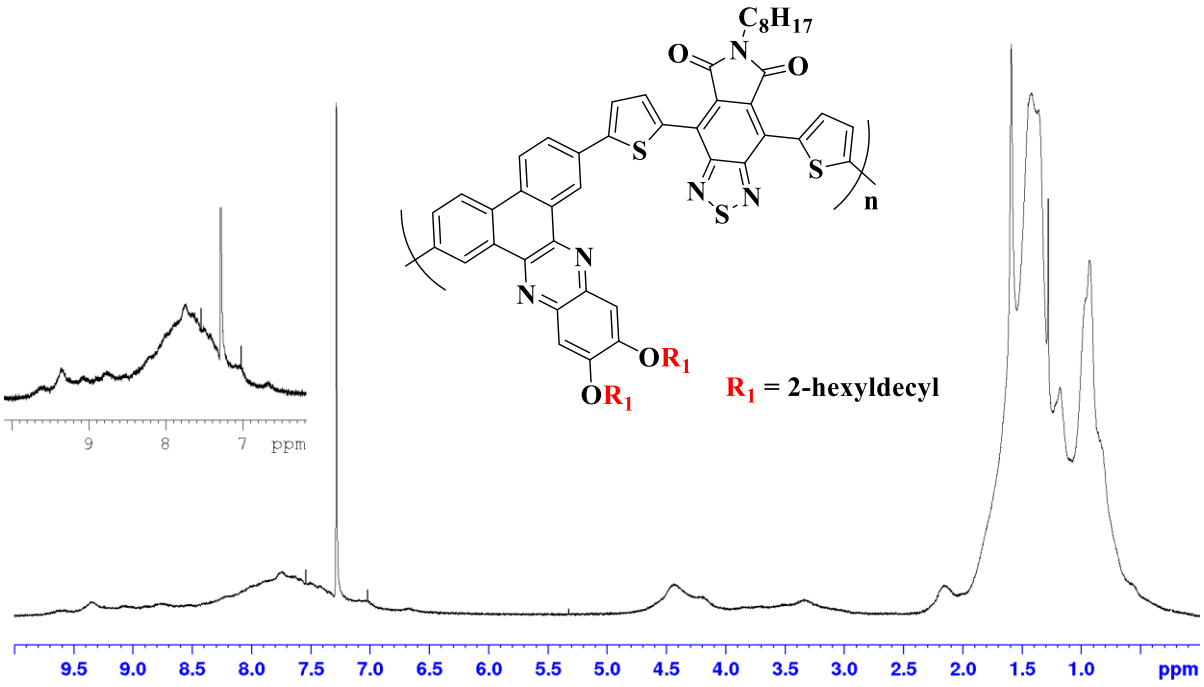

Figure S.9. ^{1}H NMR spectrum of P9 in in $CDCl_3$ at RT.

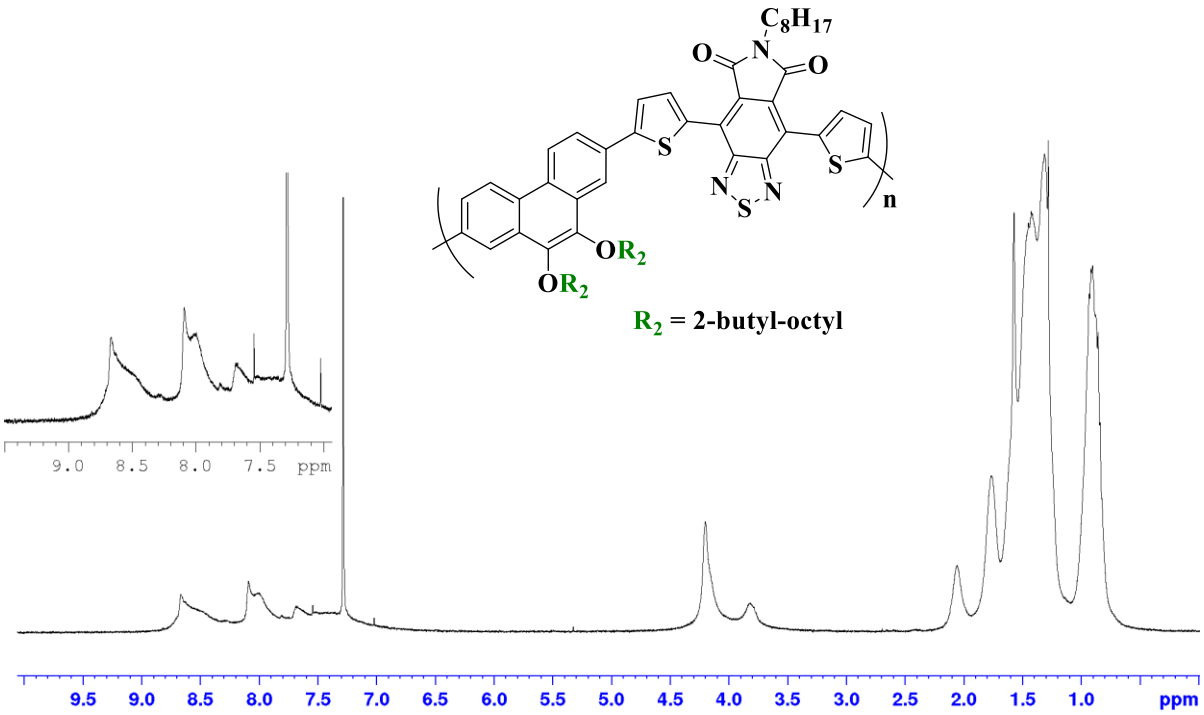

Figure S.10. ^{1}H NMR spectrum of P10 in in $CDCl_3$ at RT.